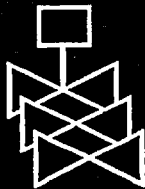
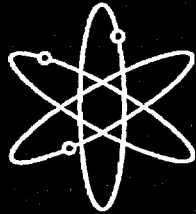
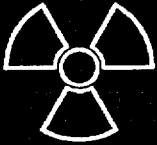


# Proceedings of the 2002 Nuclear Safety Research Conference



Held at  
Marriott Hotel at Metro Center  
Washington, DC  
October 28-30, 2002

**U.S. Nuclear Regulatory Commission  
Office of Nuclear Regulatory Research**

Proceedings prepared by  
Brookhaven National Laboratory



## AVAILABILITY OF REFERENCE MATERIALS IN NRC PUBLICATIONS

### NRC Reference Material

As of November 1999, you may electronically access NUREG-series publications and other NRC records at NRC's Public Electronic Reading Room at <http://www.nrc.gov/reading-rm.html>. Publicly released records include, to name a few, NUREG-series publications; *Federal Register* notices; applicant, licensee, and vendor documents and correspondence; NRC correspondence and internal memoranda; bulletins and information notices; inspection and investigative reports; licensee event reports; and Commission papers and their attachments.

NRC publications in the NUREG series, NRC regulations, and *Title 10, Energy*, in the Code of *Federal Regulations* may also be purchased from one of these two sources.

1. The Superintendent of Documents  
U.S. Government Printing Office  
Mail Stop SSOP  
Washington, DC 20402-0001  
Internet: [bookstore.gpo.gov](mailto:bookstore.gpo.gov)  
Telephone: 202-512-1800  
Fax: 202-512-2250
2. The National Technical Information Service  
Springfield, VA 22161-0002  
[www.ntis.gov](http://www.ntis.gov)  
1-800-553-6847 or, locally, 703-605-6000

A single copy of each NRC draft report for comment is available free, to the extent of supply, upon written request as follows:

Address: Office of the Chief Information Officer,  
Reproduction and Distribution  
Services Section  
U.S. Nuclear Regulatory Commission  
Washington, DC 20555-0001  
E-mail: [DISTRIBUTION@nrc.gov](mailto:DISTRIBUTION@nrc.gov)  
Facsimile: 301-415-2289

Some publications in the NUREG series that are posted at NRC's Web site address <http://www.nrc.gov/reading-rm/doc-collections/nuregs> are updated periodically and may differ from the last printed version. Although references to material found on a Web site bear the date the material was accessed, the material available on the date cited may subsequently be removed from the site.

### Non-NRC Reference Material

Documents available from public and special technical libraries include all open literature items, such as books, journal articles, and transactions, *Federal Register* notices, Federal and State legislation, and congressional reports. Such documents as theses, dissertations, foreign reports and translations, and non-NRC conference proceedings may be purchased from their sponsoring organization.

Copies of industry codes and standards used in a substantive manner in the NRC regulatory process are maintained at—

The NRC Technical Library  
Two White Flint North  
11545 Rockville Pike  
Rockville, MD 20852-2738

These standards are available in the library for reference use by the public. Codes and standards are usually copyrighted and may be purchased from the originating organization or, if they are American National Standards, from—

American National Standards Institute  
11 West 42<sup>nd</sup> Street  
New York, NY 10036-8002  
[www.ansi.org](http://www.ansi.org)  
212-642-4900

Legally binding regulatory requirements are stated only in laws; NRC regulations; licenses, including technical specifications; or orders, not in NUREG-series publications. The views expressed in contractor-prepared publications in this series are not necessarily those of the NRC.

The NUREG series comprises (1) technical and administrative reports and books prepared by the staff (NUREG-XXXX) or agency contractors (NUREG/CR-XXXX), (2) proceedings of conferences (NUREG/CP-XXXX), (3) reports resulting from international agreements (NUREG/IA-XXXX), (4) brochures (NUREG/BR-XXXX), and (5) compilations of legal decisions and orders of the Commission and Atomic and Safety Licensing Boards and of Directors' decisions under Section 2.206 of NRC's regulations (NUREG-0750).

**DISCLAIMER:** Where the papers in these proceedings have been authored by contractors of the U. S. Government, neither the U. S. Government nor any agency thereof, nor any U. S. employee makes any warranty, expressed or implied, or assumes any legal liability or responsibility for any third party's use or the results of such use, of any information, apparatus, product, or process disclosed in these proceedings, or represents that its use by such third party would not infringe privately owned rights. The views expressed in these proceedings are not necessarily those of the U. S. Regulatory Commission

# **Proceedings of the 2002 Nuclear Safety Research Conference**

**Held at  
Marriott Hotel at Metro Center  
Washington, DC  
October 28-30, 2002**

---

---

Manuscript Completed: February 2003  
Date Published: March 2003

Compiled by: S. Monteleone, Meeting Coordinator

S. Nesmith, NRC Project Manager

Office of Nuclear Regulatory Research  
U.S. Nuclear Regulatory Commission  
Washington, DC 20555-0001

Proceedings prepared by  
Brookhaven National Laboratory



---

**NUREG/CP-0180, has been reproduced  
from the best available copy.**

---

## ABSTRACT

This report contains papers presented at the 2002 Nuclear Safety Research Conference at the Marriott Hotel at Metro Center in Washington, DC, October 28-30, 2002. The papers were presented in each of the conference's seven breakout sessions over the course of the three days. They describe progress and results of programs in nuclear safety research conducted in this country and abroad. International participation in the meeting included papers presented by researchers from France, Japan, Norway and Russia.

The titles of the papers and the names of the authors have been updated and may differ from those that appeared in the final program of the meeting.

**PROCEEDINGS OF THE  
2002 NUCLEAR SAFETY RESEARCH CONFERENCE  
OCTOBER 28-30, 2002**

**Contents**

	<u>Page</u>
Abstract .....	iii
Registered Attendees .....	ix

**MONDAY, OCTOBER 28, 2002**

**SESSION 1: DEGRADATION OF REACTOR COOLANT PRESSURE BOUNDARY MATERIALS  
W. Cullen (NRC), L. Mathews (Southern Nuclear Co.), Co-Chairs**

Summary of US NRC's Research to Address Pressure Boundary Degradation Issues . . . . W. Cullen (NRC)	1
Parametric Studies of the Probability of Failure of CRDM Nozzles ..... W. Shack (ANL)	15
EPRI Materials Reliability Program for Alloy 600 ..... L. Mathews (Southern Nuclear Co.)	29
Inservice Inspection of PWSCC in Alloy 600\182\82 Material ..... S. Doctor (PNNL), D. Jackson (NRC)	39

**SESSION 2: ADVANCED REACTORS  
J. Flack, J. Lyons (NRC) Co-Chairs**

Thermal-Hydraulic Research Issues Relevant to Advanced Light Water Reactors ..... S. Bajorek (NRC)	45
Modeling Issues for High Temperature Gas-Cooled Reactor Designs ..... D. Carlson, R. Lee, F. Odar (NRC)	49
Irradiation and Accident Condition Testing of High-Temperature Gas-Cooled Reactor Fuel ..... S. Rubin (NRC)	59
Materials Research Needs for Advanced Reactors ..... C. Greene, J. Muscara, M. Srinivasan (NRC)	85

TUESDAY, OCTOBER 29, 2003

	<u>Page</u>
<b>SESSION 3: FUELS I</b>	
<b>R. Meyer (NRC), R. Yang (EPRI) Co-Chairs</b>	
LOCA Ductility Tests ..... R. Meyer (NRC)	99
Understanding LOCA-Related Ductility in E110 Cladding ..... V. Asmolov, L. Yegorova, K. Lioutov (RRC), V. Smirnov, et al. (State Research Center, RIAR)	109
LOCA Research Results for High-Burnup BWR Fuel ..... Y. Yan, R. Strain, M. Billone (ANL)	127
Characterization of High-Burnup PWR and BWR Rods, and PWR Rods After Extended Dry-Cask Storage ..... H. Tsai, M. Billone (ANL)	157

<b>SESSION 5: FUELS II</b>	
<b>R. Meyer (NRC), R. Yang (EPRI), Co-Chairs</b>	
Oxidation of Zr Alloys in High Pressure Steam and Some Results Under Atmospheric Pressure ..... G. Hache (IRSN)	169
Investigation of the Impact of In-Reactor Short-Term Dry-Out Incidents on Fresh and Pre-Irradiated Fuel Cladding ..... M. McGrath (OECD Halden), B Oberländer (Institut for Energiteknikk), T. Anegawa, T. Hara (TEPCO)	191
Main Outcomes from the PATRICIA Program on Clad to Coolant Heat Transfer During RIAs ..... V. Bessiron (IRSN)	209
NSRR High Burnup Fuel Tests for RIAs and BWR Power Oscillations without Scram .. T. Nakamura, et al. (JAERI)	221
Failure of Zircaloy-4 Sheet Containing Hydride Blisters ..... O. Pierron, D. Koss, A. Motta (Penn State U.), R. Daum (ANL), K. Chan (Southwest Research Institute)	231

**SESSION 6: DRY CASK STORAGE AND TRANSPORTATION OF SPENT NUCLEAR FUEL**  
**A. Hsia (NRC), A. Machiels (EPRI), Co-Chairs**

Thermal Creep of Dry-Cask-Stored Surry PWR Cladding .....	249
H. Tsai, M. Billone (ANL)	
Drop Impact Analyses of Spent Fuel Dry Cask Storage Systems .....	257
J. Braverman, et al. (BNL), S. Shaukat (NRC)	
Evaluation of Seismic Behavior of HI-STORM 100 Casks at Private Fuel Storage Facility .....	271
V. Luk, D. Aube (SNL), S. Shaukat (NRC), I. Lam (Earth Mechanics, Inc.), R. Dameron (ANATECH Corp.)	

**WEDNESDAY, OCTOBER 30, 2002**

**SESSION 7: CONTROL OF SLIGHTLY CONTAMINATED MATERIALS**  
**C. Trottier (NRC), S. Chen (ANL), Co-Chairs**

Finalization of Inventory Report: Materials Having Possibilities for Very Low Levels of Radiation that are Potentially Clearable .....	297
C. Feldman (NRC)	
Surveys of Volumetric Contamination and Difficult Geometries .....	299
G. Powers (NRC)	

**SESSION 8: PRA: METHODS / ANALYSIS AND OPERATIONAL EXPERIENCE**  
**N. Siu (NRC), Chair**

Fire Risk Research Program: Addressing Key Uncertainties .....	303
J. Hyslop (NRC)	
Narrowing the Uncertainties in Human Reliability Analysis .....	311
E. Lois, et al. (NRC)	
Standardized Plant Analysis Risk (SPAR) Model Development Program .....	333
P. O'Reilly (NRC)	

# *Nuclear Safety Research Conference*

October 28-30, 2002 - Washington, DC USA

Organized by the U.S. Nuclear Regulatory Commission

Office of Nuclear Regulatory Research

## Registered Attendees

---

John Alvis  
ANATECH  
5435 Oberlin Dr.  
San Diego, CA 92121 USA  
Phone: 858 455 6350  
Fax:  
E-mail: john@anatech.com

---

Todd Angerhofer  
U.S. Department of Energy NR1  
1240 Isaac Hull Ave., SE  
Washington, DC 20376-8041 USA  
Phone: 202 781 6117  
Fax:  
E-mail: angerhoferte@navsea.navy.

---

Samim Anghaie  
University of Florida  
202 NSC  
Gainesville, FL 32611 USA  
Phone: 352 392 8653  
Fax: 352 392 8656  
E-mail: anghaie@ufl.edu

---

Alvin Ankrum  
Pacific Northwest National Laboratory  
PO Box 999 K8-60  
Richland, WA 99352 USA  
Phone: 509 372 4095  
Fax: 509 372 6485  
E-mail: alvin.ankrum@pnl.gov

---

George Apostolakis  
MIT  
Room 24-221  
Cambridge, MA 02139-4307 USA  
Phone: 617 252 1570  
Fax: 617 258 8863  
E-mail: apostola@mit.edu

---

William Arcien  
Information Systems Laboratories  
11140 Rockville Pike, Ste 500  
Rockville, MD 20852 USA  
Phone: 301 255 2275  
Fax:  
E-mail: billa@islinc.com

---

Geun-Sun Auh  
KINS  
PO Box 114, Yuseong  
Taejon, 305-600 Korea  
Phone: 82 42 868 0466  
Fax:  
E-mail: k332ags@kins.re.kr

---

Koo-Hyun Bae  
KINS  
PO Box 114, Yuseong  
Daejon, 305-600 Korea  
Phone: 82 42 868 0210  
Fax: 82 42 861 4046  
E-mail: bae@kins.re.kr

---

Kenneth Barry  
EPRI  
1300 Harris Blvd  
Charlotte, NC 28262 USA  
Phone: 704 547 6040  
Fax: 704 547 6128  
E-mail: kbarry@epri.com

---

# Registered Attendees

---

Viktor Belikov  
IBRAE RAS  
B. Tulskaaya 52  
Moscow, 113191 Russia  
Phone: 7 095 9552259  
Fax:  
E-mail: bel@ibrae.ac.ru

---

Remy Bertrand  
IRSN  
France  
Phone: 33 1 5835 9105  
Fax: 33 1 5835 8989  
E-mail: remy.bertrand@irsn.fr

---

Vincent Besson  
IRSN  
Centre d' Etudes de Cadarache  
St Paul lez Durance, 13115 France  
Phone: 33 4 4225 6619  
Fax: 33 4 4225 6143  
E-mail: vincent.besson@irsn.fr

---

Ralph Best  
JAI Corp.  
2750 Prosperity Ave, #B220  
Fairfax, VA 22031-4312 USA  
Phone: 703 645 0440  
Fax:  
E-mail: rbest@JAICorp.com

---

Michael Billone  
Argonne National Laboratory  
9700 S. Cass Ave.  
Argonne, IL 60439 USA  
Phone: 630 252 7146  
Fax: 630 252 9232  
E-mail: billone@anl.gov

---

Nathan Bixler  
Sandia National Laboratories  
PO Box 5800, Dept 6415, MS 0739  
Albuquerque, NM 87185-0739 USA  
Phone: 505 845 3144  
Fax: 505 844 8719  
E-mail: nbixler@sandia.gov

---

Henning Born  
TUV Nord  
Grobe Bahnstr 31  
Hamburg, 22525 Germany  
Phone: 49 40 8557 2494  
Fax: 49 40 8557 2429  
E-mail: hbom@tuev-nord.de

---

Joseph Braverman  
Brookhaven National Laboratory  
PO Box 5000, Bldg. 130  
Upton, NY 11973-5000 USA  
Phone: 631 344 2186  
Fax: 631 344 4255  
E-mail: braverman@bnl.gov

---

Charles Brnkman  
Westinghouse Electric Company  
12300 Twinbrook Parkway  
Rockville, MD 20852 USA  
Phone: (301) 881-7040  
Fax: 301-881-7043  
E-mail: brnkmcb@westinghouse.co

---

Geoffrey Brown  
Serco Assurance  
Thomson House, Risley  
Warrington, Cheshire WA3 1HW  
United Kingdom  
Phone: 44 00 1925 254473  
Fax: 44 00 1925 254536  
E-mail: geoff.brown@sercoassuranc

---

Edward Burns  
Washington Group Int'l  
2345 Crystal Dr, Ste 708  
Crystal City, VA 22202 USA  
Phone: 703 236 2752  
Fax: 703 236 1930  
E-mail: ed.burns@wgint.com

---

Keith Bussey  
Bechtel  
122 Orchard Dr  
Manor, PA 157665 USA  
Phone: 412 476 5543  
Fax:  
E-mail:

---

# Registered Attendees

---

John Butler  
Nuclear Energy Institute  
1776 I St, NW  
Washington, DC 20006 USA  
Phone: (202) 739-8108  
Fax:  
E-mail: jcb@nei.org

---

Jose Butragueno  
CSN  
Justo Dorado, 11  
Madrid, 28040 Spain  
Phone: 34 1 3460407  
Fax: 34 1 3460588  
E-mail: jlb@csn.es

---

Jose Calvo  
CSN  
Justo Dorado, 11  
Madrid, 28008 Spain  
Phone: 34 91 3460 240  
Fax: 34 91 3460 496  
E-mail: jicm@csn.es

---

Allen Camp  
Sandia National Laboratories  
PO Box 5800  
Albuquerque, NM 87185-0747 USA  
Phone: 505 844 5960  
Fax: 505 844 1648  
E-mail: alcamp@sandia.gov

---

S Y. Chen  
Argonne National Laboratory  
9700 So Cass Ave.  
Argonne, IL 60439 USA  
Phone: 630 252 4611  
Fax:  
E-mail: sychen@anl.gov

---

Chang Cho  
Kepco Nuclear Fuel Co.  
493 Deogjin-Dong, Yusung-Gu  
Daejeon, 305-353 Korea  
Phone: 82 42 868 1840  
Fax: 82 42 863 4430  
E-mail: cscho@mail.knfc.co.kr

---

Whee Choe  
TXU Energy  
1601 Bryan St.  
Dallas, Texas 75201-3411 USA  
Phone: 214 812 4371  
Fax: 214 812 8687  
E-mail: whee.choe@txu.com

---

Dong-Uk Choi  
KNFC  
493 Deogjin-Dong  
Daejeon, 305-353 Korea  
Phone: 82 42 868 1838  
Fax: 82 42 863 4430  
E-mail: duchoi@mail.knfc.co.kr

---

T.Y. Chu  
SNL/DOE  
1000 Independence Ave.,  
Washington, DC 20585 USA  
Phone: 202 586 5883  
Fax: 202 586 1057  
E-mail: tychu@sandia.gov

---

Dae Wook Chung  
Korea Institute of Nuclear Safety  
P.O. Box 114, Yusung-gu  
Taejeon, Korea  
Phone: 82-42-868-0220  
Fax:  
E-mail: dwchung@kins.re.kr

---

Jean-Pierre Clausner  
DGSNR  
6 Pl du Colonel Bourgoin  
Paris, 75572 France  
Phone: 33 1 4319 7151  
Fax: 33 1 4319 7069  
E-mail: jean-pierre.clausner@asn.mi

---

Jose Conde  
CSN  
Justo Dorado, 11  
Madrid, 28040 Spain  
Phone: 34 91 3460253  
Fax: 34 91 3460588  
E-mail: jmc@csn.es

---

# Registered Attendees

---

Bernie Copsey  
Framatome ANP  
3315 Old Forest Rd.  
Lynchburg, VA 24501 USA  
Phone: 434 832 2545  
Fax: 434 832 2968  
E-mail: [bernie.copsey@framatome-a](mailto:bernie.copsey@framatome-a)

---

Mitchell Cunningham  
Pacific Northwest National Laboratory  
PO Box 999  
Richland, WA 99352 USA  
Phone: 509 372 4987  
Fax: 509 372 4989  
E-mail: [mitch.cunningham@pnl.gov](mailto:mitch.cunningham@pnl.gov)

---

Diane D'Amgo  
NIRS  
1424 16th St NW, Ste 404  
Washington, DC 20036 USA  
Phone: 202 328 0002  
Fax: 202 462 2183  
E-mail: [dianed@nirs.org](mailto:dianed@nirs.org)

---

Les Davies  
HM NII  
  
United Kingdom  
Phone: 44 151 951 3742  
Fax:  
E-mail: [les.davies@hse.gsi.gov.uk](mailto:les.davies@hse.gsi.gov.uk)

---

Benoit DeBoeck  
AVN  
Rue Walcourt 148  
Brussels, B-1070 Belgium  
Phone: 32 2 5280121  
Fax: 32 2 5280101  
E-mail: [bdg@avn.be](mailto:bdg@avn.be)

---

David Diamond  
Brookhaven National Laboratory  
Bldg. 130  
Upton, NY 11973-5000 USA  
Phone: 631 344 2604  
Fax: 631 344 3957  
E-mail: [diamond@bnl.gov](mailto:diamond@bnl.gov)

---

Paul Dietershagen  
Lockheed Martin, KAPL  
River Rd  
Niskayuna, NY 12309 USA  
Phone: 518 395 4795  
Fax: 518 395 5291  
E-mail: [kieters@kapl.gov](mailto:kieters@kapl.gov)

---

Bert Dunn  
Framatome ANP  
3315 Old Forest Rd., PO Box 10935  
Lynchburg, VA 24506-0935 USA  
Phone: 434 832 2427  
Fax: 434 832 2431  
E-mail: [bert.dunn@framatome-anp.c](mailto:bert.dunn@framatome-anp.c)

---

Raymond Durante  
Durante Assocs , Inc.  
4641 Montgomery Ave  
Bethesda, MD 20814 USA  
Phone: 301 718 2995  
Fax: 301 718 0606  
E-mail: [durantes@aol.com](mailto:durantes@aol.com)

---

David Ebert  
Consultant  
5611 35th Ave.  
Hyattsville, MD 20782 USA  
Phone: 301 779 1039  
Fax:  
E-mail: [DavyDeanE@aol.com](mailto:DavyDeanE@aol.com)

---

Behzad Edalat  
GRS-Koeln  
Schwertnergasse 1  
Koeln, 50667 Germany  
Phone: 49 221 2068 617  
Fax: 49 221 2068 629  
E-mail: [eda@grs.de](mailto:eda@grs.de)

---

Thecla Fabian  
Nuclear Waste News  
8737 Colesville Rd, Ste 1100  
Silver Spring, MD 20910 USA  
Phone: 301 587 6300  
Fax: 301 587 1081  
E-mail: [tfabian@bpinews.com](mailto:tfabian@bpinews.com)

---

# Registered Attendees

---

Mana Faury  
IRSN  
Cen Cadarache, Bat 245, DRS/PECSA  
St Paul lez Durance, 13108 France  
Phone: 33 4 4225 4124  
Fax 33 4 4225 7315  
E-mail: mana.fauy@irsn.fr

---

Stephen Floyd  
NEI  
1776 Eye St., NW  
Washington, DC 20006 USA  
Phone: (202) 739-8078  
Fax. 202 785 1898  
E-mail sdf@nei.org

---

John Forester  
Sandia National Laboratories  
PO Box 5800, MS 0748  
Albuquerque, NM 87185-0748 USA  
Phone: 505 844 0578  
Fax. 505 844 2829  
E-mail: jafores@sandia.gov

---

Steve Frankl  
Stoller Nuclear Fuel  
485 Washington Ave.  
Pleasantville, NY 10570 USA  
Phone: 914 741 1200  
Fax: 914 741 2093  
E-mail: ifrankl@nacintl.com

---

Gianni Frescura  
NEA / OECD  
12, Blvd des Iles  
Issy-les-Moulineaux, 92130 France  
Phone: 33 1 4524 1050  
Fax: 33 1 4524 1129  
E-mail: gianni.frescura@oecd.org

---

John Funk  
Cleveland Plain Dealer  
1801 Superior Ave.  
Cleveland, OH 44236 USA  
Phone: 216 999 4800  
Fax: 216 999 6355  
E-mail: jfunk@plained.com

---

John Galembush  
Westinghouse Electric Company  
PO Box 355  
Pittsburgh, PA 15230 USA  
Phone. 412 374 5036  
Fax: 412 374 4011  
E-mail: galem1js@westinghouse.co

---

Pablo Garcia  
Iberdrola Ingeniera  
Avenida de Burgos 8-B  
Madrid, 28036 Spain  
Phone: 34 91 3833180  
Fax: 34 91 3833311  
E-mail. pgs@iberdrolaingenieria.es

---

Eugene Grecheck  
Dominion Energy, Inc.  
5000 Dominion Blvd.  
Glen Allen, VA 23060 USA  
Phone: (804) 273-2442  
Fax: 804-273-3471  
E-mail: Eugene.Grecheck@dom.com

---

Paul Gunter  
Nuclear Information and Resource  
Service  
1424 16th St, NW, Ste 404  
Washington, DC 20036 USA  
Phone: (202) 328-0002  
Fax:  
E-mail: pgunter@nirs.org

---

Jaejoo Ha  
Korea Atomic Energy Research  
Institute  
Dukjim 150  
Yuseong, Daejeon Korea  
Phone: 82 42 868 2755  
Fax. 82 42 868 8256  
E-mail. jjha@kaeri.re.kr

---

Georges Hache  
IRSN  
DRS Batiment 250, Cadarache  
St Paul lez Durance, 13115 France  
Phone: 33 44 2252055  
Fax. 33 442256346  
E-mail: georges.hache@irsn.fr

---

# Registered Attendees

---

Richard Hannon  
U.S. Department of Transportation  
400 Seventh St. SW  
Washington, DC 20590-0001 USA  
Phone: 202 366 4484  
Fax: 202 366 8700  
E-mail: rchard.hannon@rspa dot.gov

---

Philippe Hessel  
Canadian Nuclear Safety Commission  
280 Slalen, P.O. Box 1046, Station B  
Ottawa, Ontario K1P559 Canada  
Phone: 1-613-947-2367  
Fax: 1-613-943-1292  
E-mail: hesselp@cnsccan.gc.ca

---

Paul Highberger  
JAI Corp.  
2750 Prosperity Ave  
Fairfax, VA 22031 USA  
Phone: 703 645 0440  
Fax: 703 645 0445  
E-mail:

---

Masao Hirose  
NUPEC  
17-1, 3-Chome Toranomon, Minato-Ku  
Tokyo, 105-0001 Japan  
Phone: 81 3 4512 2750  
Fax: 81 3 4512 2799  
E-mail: m-hirose@nupec.or.jp

---

Elaine Hiruo  
Platts Nuclear Publications  
1200 G St., NW, Ste. 1100  
Washington, DC 20005 USA  
Phone: (202) 383-2163  
Fax: 202-383-2125  
E-mail: hiruo@platts.com

---

Lawrence Hochreiter  
Penn State University  
233 Reber Bldg  
University Park, PA 16802 USA  
Phone: 814 865 6198  
Fax: 814 865 8499  
E-mail: lehnuc@engr.psu.edu

---

Jerald Holm  
Framatome ANP  
2101 Horn Rapids Road  
Richland, WA 99352 USA  
Phone: (509) 375-8142  
Fax:  
E-mail: jerald.holm@framatome-anp

---

Heikki Holmstrom  
VTT Processes  
Tekniikantie 4 C  
Espoo, 02150 Finland  
Phone: 358 9 4565050  
Fax: 358 9 4565000  
E-mail: Heikki.Holmstrom@vtt.fi

---

William Horak  
Brookhaven National Laboratory  
PO Box 5000, Bldg. 475B  
Upton, NY 11973-5000 USA  
Phone: 631 344 2627  
Fax: 631 344 7650  
E-mail: horak@bnl.gov

---

Steve Hunt  
Dominion Engineering  
11730 Plaza America Dr., Ste 310  
Reston, VA 20190 USA  
Phone: 703 437 1155  
Fax: 703 437 0780  
E-mail: shunt@domeng.com

---

Hamilton Hunter  
Oak Ridge National Laboratory  
P.O. Box 2008  
Oak Ridge, TN 378316362 USA  
Phone: (865) 574-6297  
Fax: 865-574-6182  
E-mail: hunterht@ornl.gov

---

Takahiro Imamura  
MHIA  
PO Box 355, Ste 268 E  
Pittsburgh, PA 15230-0355 USA  
Phone: 412 374 7395  
Fax: 412 374 7377  
E-mail: imamurt@outlands.westingh

---

# Registered Attendees

---

Kunio Ito  
NUPEC  
3-17-1 Chome Toranomom Bldg 6F  
Minato-ku, Tokyo 105-0001 Japan  
Phone: 81 3 4512 2673  
Fax: 81 3 4512 2699  
E-mail: K-ITO@nupec.or.jp

---

Jose Izquierdo  
CSN  
11 Justo Dorado St.  
Madrid, 28040 Spain  
Phone: 34 9134 60237  
Fax: 34 9134 60496  
E-mail: jmir@csn.es

---

Rich Janati  
PADEP/BRP Nuclear Safety Program  
PO Box 8469  
Harrisburg, PA 17105 USA  
Phone: 717 787 2163  
Fax: 717 783 8965  
E-mail: rjanati@state.pa.us

---

Josef Jansky  
BTB Jansky GMBH  
Gerlinger St. 151  
Leonberg, 71229 Germany  
Phone: 07152 41058  
Fax: 07152 73868  
E-mail: btb@btbjansky.com

---

Andrew Kadak  
MIT  
253 Rumstick Point Rd  
Barnington, RI 02806 USA  
Phone: 617 253 0166  
Fax: 617 258 8863  
E-mail: kadak@mit.edu

---

Suk-Chull Kang  
KINS  
PO Box 114, Yuseong  
Taejon, 305-600 Korea  
Phone: 82 42 868 0185  
Fax: 82 42 861 9945  
E-mail: kang@kins.re.kr

---

Storm Kauffman  
U.S. Department of Energy  
NR-1 NNSA  
Washington, DC 20585 USA  
Phone: 202 781 6225  
Fax:  
E-mail: kauffmansr1@navsea.navy.

---

Paul Kersting  
KW Consulting, Inc.  
P.O. Box 101567  
Pittsburgh, PA 152378567 USA  
Phone: (412) 635-7333  
Fax: 412-367-2195  
E-mail: paul@kwconsulting.com

---

Hussein Khalil  
Argonne National Laboratory  
9700 S Cass Ave  
Argonne, IL 60441 USA  
Phone: 630 252 7266  
Fax: 630 252 4780  
E-mail: hkhalil@anl.gov

---

Peter Kiang  
Link Technologies, Inc.  
20030 Century Blvd., Ste 210  
Germantown, MD 20874 USA  
Phone: 301 515 9654  
Fax: 301 515 9658  
E-mail: peter.kiang@linksolutions.co

---

Hee-Dong Kim  
Korea Atomic Energy Research  
Institute  
150 Duckjindong Yusong  
Daejeon, Korea  
Phone: 82 42 868-2664  
Fax: 82 42 868-8256  
E-mail: hdkim@kaeri.re.kr

---

Hho Jung Kim  
KINS  
PO Box 114 Yusong  
Taejeon, Korea  
Phone: 82 42 868 0230  
Fax: 82 42 861 9945  
E-mail: kimhj@kins.re.kr

---

# Registered Attendees

---

In-Goo Kim  
KINS  
PO Box 114, Yuseong  
Taejon, 305-600 Korea  
Phone: 82 42 868 0151  
Fax:  
E-mail: igkim@kins.re.kr

---

Woong Sik Kim  
KINS  
PO Box 114, Yusong  
Taejon, 305-338 Korea  
Phone: 82 42 868 0327  
Fax: 82 42 861 9945  
E-mail: wskim@kins.re.kr

---

Bernadette Kirk  
Oak Ridge National Laboratory  
PO Box 2008  
Oak Ridge, TN 37831-6362 USA  
Phone: 865 574 6176  
Fax: 865 574 6182  
E-mail: kirkbl@ornl.gov

---

Kazuhiko Kishioka  
JEPIC, Inc.  
1120 Connecticut Ave NW, Ste 1070  
Washington, DC 20036 USA  
Phone: 202 955 5610  
Fax: 202 955 5612  
E-mail: genden@jepic.com

---

Michael Knapik  
McGraw-Hill Companies  
1200 G St., NW, Ste. 1100  
Washington, DC 200053802 USA  
Phone: (202) 383-2167  
Fax: (202) 383-2125  
E-mail: mike\_knapik@platts.com

---

Klaus Koeberlein  
GRS  
Forschungsgelaende  
Garching, Bavaria 85748 Germany  
Phone: 49 89 3200 4445  
Fax: 49 89 3200 4301  
E-mail: koe@grs.de

---

Stephen Koff  
Cleveland Plain Dealer  
  
, USA  
Phone: 202 638 1366  
Fax:  
E-mail: skoff@plains.com

---

Zdenek Krz  
Nuclear Research Institute  
  
Rez, 250 68 Czech Republic  
Phone: 420 26617 3428  
Fax: 420 26617 3468  
E-mail: krz@ujv.cz

---

Junichi Kurakami  
Japan Nuclear Fuel Cycle  
Development Institution  
2600 Virginia Ave., NW, Ste. 715  
Washington, DC USA  
Phone: (202) 338-3770  
Fax:  
E-mail: kurakami@jnc-dc.org

---

Karl Kussmaul  
MPA - U. of Stuttgart  
32 Pfaffenwaldring  
Stuttgart, D70569 Germany  
Phone:  
Fax:  
E-mail: kussmaul@mpa.uni-stuttgart.

---

Kee-Choon Kwon  
KAERI  
150 DeokJin-Dong, YuSeong-Gu  
Daejeon, 305-600 Korea  
Phone: 82 42 868 2926  
Fax: 82 42 868 8916  
E-mail: kckwon@kaeri.re.kr

---

Jukka Laaksonen  
STUK  
P O. Box 14, 00881 Helsinki  
Helsinki, 02810 Finland  
Phone: 358 9 75988200  
Fax:  
E-mail: jukka.laaksonen@stuk.fi

---

# Registered Attendees

---

James Lang  
EPRI  
1300 WT Harris Blvd  
Charlotte, NC 28262 USA  
Phone: 704 547 6100  
Fax: 704 547 6168  
E-mail: jlang@epri.com

---

Jeanne Marie Lanore  
IRSN  
BP 17 Fontenay aux Roses Cedex  
, 92262 France  
Phone: 158 35 7648  
Fax: 158 35 8385  
E-mail: jeanne\_marie.lanore@irsn.fr

---

Nanci Laroche  
Canadian Nuclear Safety Commission  
280 Slater St., POB 1046, Sta. B  
Ottawa, Ontario K1P 5S9 Canada  
Phone: 613 995 2609  
Fax: 613 995 5086  
E-mail: laroche@cnsccs.gc.ca

---

Catherine Lecomte  
IRSN  
BP17  
Fontenay aux Roses Cedex, 92262  
France  
Phone: 01 58 357736  
Fax: 01 58357971  
E-mail: catherine.lecomte@irsn.fr

---

James Lee  
Los Alamos National Laboratory  
MS K575, D-10  
Los Alamos, NM 87545 USA  
Phone: (505) 667-4097  
Fax: 505-665-2897  
E-mail: JHL@lanl.gov

---

Jeong Bae Lee  
KINS  
19 Gusong-dong Yusong-gu  
Daejeon, 305-338 Korea  
Phone: 82 42 868 0162  
Fax: 82 42 861 2535  
E-mail: lee jb@kins.re.kr

---

Sang Yong Lee  
Korea Electric Power Company  
150 Dukjim-Dong Paeduck Danja  
Daejeon, Korea  
Phone: (42 ) 868-4015  
Fax:  
E-mail: sanglee@kopec.co.kr

---

Seung Lee  
KINS  
PO Box 114, Yusong  
Daejeon, 305-338 Korea  
Phone: 82 42 868 0132  
Fax: 82 42 868 0457  
E-mail: k0351sh@kins.re.kr

---

Sol Levy  
Levy & Associates  
, USA  
Phone:  
Fax  
E-mail:

---

Kirill Lioutov  
RRC "Kurchatov Institute"  
Kurchatov Square, 1  
Moscow, 123182 Russia  
Phone: 095 196 9635  
Fax: 095 196 1702  
E-mail: kinll@nsi.kiae.ru

---

Yung Liu  
Argonne National Laboratory  
9700 S Cass Ave., MS 308  
Argonne, IL 60439 USA  
Phone: 630 252 5127  
Fax: 630 252 3250  
E-mail: ylliu@anl.gov

---

David Lochbaum  
Union of Concerned Scientists  
1707 H St., NW, Ste 600  
Washington, DC 20006 USA  
Phone: 202 223 6133  
Fax: 202 223 6162  
E-mail: dlochbaum@ucsusa.org

---

# Registered Attendees

---

Gustaf Loewenhielm  
SKI  
  
Stockholm, SE10568 Sweden  
Phone: 46 8 698 8496  
Fax: 46 8 661 9086  
E-mail: gustaf.loewenhielm@ski.se

---

Vincent Luk  
Sandia National Laboratories  
PO Box 5800, MS 0744  
Albuquerque, NM 87185-0744 USA  
Phone: 505 844 5498  
Fax: 505 844 1648  
E-mail: vkluk@sandia.gov

---

Edwin Lyman  
Nuclear Control Institute  
1000 Connecticut Ave NW  
Washington, DC 20036 USA  
Phone: (202) 822-6594  
Fax: 202 452 0892  
E-mail: lyman@nci.org

---

Melanie Lyons  
Nuclear Energy Institute  
1776 I St NW  
Washington, DC 20004 USA  
Phone: 202 739 8010  
Fax:  
E-mail:

---

Albert Machiels  
EPRI  
3412 Hillview Ave  
Palo Alto, CA 94304 USA  
Phone: 650 855 2054  
Fax: 650 855 2002  
E-mail: amachiel@epri.com

---

Geza Macsuga  
Hungarian Atomic Energy Authority  
Fenyves A., 4  
Budapest, H1036 Hungary  
Phone: 37 1 436 4910  
Fax: 36 1 436 4909  
E-mail: macsuga@haea.gov.hu

---

Robert Maiers  
PADEP/BRP Nuclear Safety Program  
PO Box 8469  
Harrisburg, PA 17105-8469 USA  
Phone: 717 783 8979  
Fax:  
E-mail: rmaiers@state.pa.us

---

Alain Mailliat  
IRSN  
Bldg 250 - BP 3  
St Paul lez Durance, Bouches du  
Rhone 13118 France  
Phone: 33 4 42 253637  
Fax: 33 4 42 252971  
E-mail: alain.mailliat@irsn.fr

---

John Mangels  
Cleveland Plain Dealer  
1801 Superior Ave  
Cleveland, OH 44236 USA  
Phone: 216 999 4842  
Fax: 216 999 6354  
E-mail: jmangels@plains.com

---

Ted Marston  
EPRI  
PO Box 10412, 3412 Hillview Ave.  
Palo Alto, CA 94303 USA  
Phone: 650 855 2997  
Fax: 650 855 1026  
E-mail: tmarston@epri.com

---

Chiwata Masanori  
NUPEC  
17-1, 3-Chome Toranomom, Minato-ku  
Tokyo, 105-0001 Japan  
Phone: 81 3 4512 2856  
Fax: 81 3 4512 2889  
E-mail: chiwata@nupec.or.jp

---

Mahmoud Massoud  
Calvert Cliffs Nuclear Power Plant  
1650 Calvert Cliffs Pkwy.  
Lusby, MD 20716 USA  
Phone: 410 495 6522  
Fax: 410 495 4498  
E-mail: mahmoud.massoud@ccnppi.

---

# Registered Attendees

---

Larry Mathews  
Southern Nuclear  
PO Box 1295  
Birmingham, AL 35201 USA  
Phone: 205 992 7729  
Fax: 205 992 5793  
E-mail: lmathew@southernco.com

---

Borut Mavko  
J. Stefan Institute  
Jamova 39  
Ljubljana, 1111 Slovenia  
Phone: 386 1 5885 330  
Fax:  
E-mail: borut.mavko@ijs.si

---

Robin McCollum  
Bettis Laboratory  
PO Box 79  
West Mifflin, PA 15122 USA  
Phone: 412 476 6356  
Fax: 412 476 6364  
E-mail: mccollum@zbzoom.net

---

Margaret McGrath  
OECD Halden Reactor Project  
Postboks 173  
Halden, Ostfold N1751 Norway  
Phone: 476 9212338  
Fax: 476 9212201  
E-mail: margaret.mcgrath.hrp.no

---

Michael McKloskey  
Transport Logistics Int'l  
4000 Blackburn LA, Ste 250  
Burtonsville, MD 20866 USA  
Phone: 301 421 4324  
Fax: 301 421 4326  
E-mail: mmckloskey@tliusa.com

---

Jean-Claude Melis  
IRSN  
Bldg. 250 - BP 3  
St Paul lez Durance, Bouches du  
Rhône 13118 France  
Phone: 33 4 4225 3722  
Fax: 33 4 4225 2971  
E-mail: jean-claude melis@irsn.fr

---

James Meyer  
ISL, Inc.  
11140 Rockville Pike, Suite 500  
Rockville, MD 20852 USA  
Phone: (301) 468-6425  
Fax: 301-468-0883  
E-mail: jmeyer@islinc.com

---

Gordon Michaels  
Oak Ridge National Laboratory  
PO Box 2008  
Oak Ridge, TN 37831 USA  
Phone: 865 574 4187  
Fax: 865 574 7879  
E-mail: michaelsge@ornl.gov

---

Tom Miller  
U S Department of Energy  
  
, USA  
Phone:  
Fax:  
E-mail:

---

Toshihiko Miyamoto  
NUPEC  
17-1, 3-Chome Toranomon, Minato-ku  
Tokyo, 105-0001 Japan  
Phone: 81 3 4512 2424  
Fax: 81 3 4512 2439  
E-mail: miyamoto@nupec.or.jp

---

Shotaro Mori  
KEPCO  
2001 L St., NW, Ste 801  
Washington, DC 20036 USA  
Phone: 202 659 1138  
Fax: 202 457 0272  
E-mail: mori@kansai.com

---

Arthur Motta  
Penn State University  
227 Reber  
University Park, PA 16802 USA  
Phone: (814) 865-0036  
Fax: 814-865-8499  
E-mail: atm2@psu.edu

---

# Registered Attendees

---

Takehiko Nakamura  
JAERI

Tokai-mura, Ibaraki-ken 319-1195  
Japan  
Phone: 81 29 282 6386  
Fax: 81 29 282 5429  
E-mail: take@fsrl.tokai.jaeri.go.jp

---

Randy Nanstad  
Oak Ridge National Laboratory  
P.O. Box 2008, MS-6151  
Oak Ridge, TN 37831 USA  
Phone: (865) 574-4471  
Fax: 865-574-0641  
E-mail: nanstadrk@ornl.gov

---

Mamoru Nishiyama  
JEPIC, Inc.  
1120 Connecticut Ave NW, Ste 1070  
Washington, DC 20036 USA  
Phone: 202 955 5610  
Fax: 202 955 5612  
E-mail: kyuden@jepic.com

---

Timo Okkonen  
STUK, Radiation & Nuclear Safety  
Authority  
PO Box 14  
Helsinki, 00881 Finland  
Phone: 358 9 759 88 299  
Fax: 358 9 759 88 382  
E-mail: timo.okkonen@stuk.fi

---

Larry Ott  
Oak Ridge National Laboratory  
1099 Commerce Park  
Oak Ridge, TN 37831-8057 USA  
Phone: 865 574 0324  
Fax: 865 574 8216  
E-mail: ottlj@ornl.gov

---

Odell Ozer  
EPRI  
PO Box 10412  
Palo Alto, CA 94303 USA  
Phone: 650 855 2089  
Fax: 650 855 1026  
E-mail: oozer@epri.com

---

Cecil Parks  
Oak Ridge National Laboratory  
P.O. Box 2008  
Oak Ridge, TN 378316370 USA  
Phone: (865) 574-5280  
Fax: 865-574-3527  
E-mail: paruscvc@ornl.gov

---

Jean-Louis Petitclerc  
IRSN  
78-83 Ave du General de Gaulle  
Clamart, 92140 France  
Phone: 33 1 5835 8177  
Fax: 33 1 5835 8925  
E-mail: jean-louis.petitclerc@irsn.fr

---

Larry Phillips  
Consultant  
118 Monroe St. #705  
Rockville, MD 20850 USA  
Phone: 301 294 3069  
Fax:  
E-mail: larryephillips55@cs.com

---

Olivier Pierron  
Penn State University  
  
, PA USA  
Phone:  
Fax:  
E-mail: olivier-pierron@psu.edu

---

Tony Pietrangelo  
Nuclear Energy Institute  
1776 Eye St , NW, Ste 400  
Washington, DC 20006 USA  
Phone: 202 739 8081  
Fax: 202 533 0182  
E-mail: arp@nei.org

---

Etienne Pochon  
CEA - Nuclear Energy Division  
CEA/Saclay Bat 121  
, 91191 Gif/Yvettes France  
Phone: 33 0169086204  
Fax: 33 0169085859  
E-mail: etienne.pochon@cea.fr

---

# Registered Attendees

---

Alain Porraccia  
CEA - Nuclear Energy Division  
CEA/Saclay Bat 121  
, 91191 Gif/Yvettes France  
Phone. 33 01 9086215  
Fax: 33 01 69085870  
E-mail. alain.porracchi@cea.fr

---

Steve Power  
Serco Assurance  
TH5R10, Thomson House, Risley  
Warrington, Cheshire WA3 6AT  
United Kingdom  
Phone: 44 1925 254977  
Fax: 44 1925 254536  
E-mail. steve.power@sercoassuranc

---

Manuel Quecedo  
ENUSA  
Santiago Rusinol 12  
Madrid, 28040 Spain  
Phone: 34 913474264  
Fax: 34 913474215  
E-mail. mqg@enusa.es

---

Nancy Ranek  
Argonne National Laboratory  
955 L'Enfant Plaza N, SW, Ste 6000  
Washington, DC 20024 USA  
Phone: 202 488 2417  
Fax: 202 488 2413  
E-mail. ranekn@anl.gov

---

Joe Rashid  
ANATECH  
5435 Oberlin Dr  
San Diego, CA 92121 USA  
Phone 858 455 6350  
Fax: 858 455 1094  
E-mail: joe@anatech.com

---

Michel Reocreux  
IRSN  
IRSN/DRS/Dir BP3  
St Paul lez Durance, 13115 France  
Phone: 33 4 4225 3148  
Fax: 33 4 4225 6346  
E-mail: michel.reocreux@irsn.fr

---

James Riccio  
Greenpeace  
702 H St. NW, Ste 300  
Washington, DC 20001 USA  
Phone: 202 319 2487  
Fax. 202 462 4507  
E-mail. jim.r4iccio@wdec.greenpeac

---

Kenneth Rogers  
KCR  
6202 Perthshire Ct  
Bethesda, MD 20817 USA  
Phone. 301 530 4489  
Fax: 301 530 4033  
E-mail. kcrogers@aol.com

---

Thomas Rosseel  
Oak Ridge National Laboratory  
P.O. Box 2008  
Oak Ridge, TN 37831 USA  
Phone: (865) 574-5380  
Fax: 865-574-6095  
E-mail:

---

Don Rowland  
Westinghouse Nuclear Fuel  
5801 Bluff Rd , Drawer R  
Columbia, SC 29250 USA  
Phone: 803 647 3641  
Fax: 803 776 2610  
E-mail: rowlandm@westinghouse.co

---

Peter Rudling  
Advanced Nuclear Technology  
Uppsala Science Park  
Uppsala, SE-751 83 Sweden  
Phone: 46 70 669 6681  
Fax: 46 18 506685  
E-mail. peter.rudling@ant.se

---

Marty Sattison  
INEEL  
PO Box 1625, MS 3870  
Idaho Falls, ID 83415-3870 USA  
Phone: 208 526 9626  
Fax: 208 526 2930  
E-mail: sbm@inel.gov

---

# Registered Attendees

---

Pierre Saverot  
JAI Corp.  
2750 Prosperity Ave , Ste 220-B  
Fairfax, VA 22031 USA  
Phone: 703 645 0440  
Fax: 703 645 0445  
E-mail: psaverot@jaicorp.com

---

Martin Schwartz  
Lawrence Livermore National  
Laboratory (Retired)  
2244 University Ave.  
Sacramento, CA 95825 USA  
Phone: 916 489 6672  
Fax: 916 483 8462  
E-mail: mwschwartz@attbi.com

---

Michel Schwarz  
IRSN  
Bldg 250, BP 3  
St Paul lez Durance, Bouches du  
Rhone 13118 France  
Phone: 33 4 4225 7748  
Fax: 33 4 4225 2971  
E-mail: michel.schwarz@irsn.fr

---

Bal Raj Sehgal  
Royal Institute of Technology  
33A Drottning Kristina Vag  
Stockholm, 10044 Sweden  
Phone: 46 8 790 9252  
Fax: 46 8 790 9197  
E-mail: sehgal@ne.kth.se

---

Charles Serpan  
NRC (Retired)  
  
USA  
Phone: 301 656 2268  
Fax:  
E-mail: pcserpan@olg.com

---

William Shack  
Argonne National Laboratory  
Building 212  
Argonne, IL 60439 USA  
Phone: (630) 252-5137  
Fax: 630-252-4798  
E-mail: wjshack@anl.gov

---

Julie Simpson  
Oak Ridge National Laboratory  
1 Bethel Valley Rd.  
Oak Ridge, TN 37831-6210 USA  
Phone: 865 574 0422  
Fax: 865 241 4069  
E-mail: simpsonjj@ornl.gov

---

William Slagel  
Westinghouse Electric Company  
4350 Northern Pike  
Monroeville, PA 15146-2886 USA  
Phone: 412 374 2088  
Fax: 412 374 2045  
E-mail: slaglewh@westinhouse.com

---

Victor Snell  
AECL  
2251 Speakman Dr  
Mississauga, Ontario L5K 1B2 Canada  
Phone: 905 823 9060  
Fax: 905 403 7337  
E-mail: snellv@aecl.ca

---

Donald Spellman  
Oak Ridge National Laboratory  
1099 Commerce Park, MS 8057  
Oak Ridge, TN 37830 USA  
Phone: 865 574 7891  
Fax: 865 574 8216  
E-mail: spellmandj@ornl.gov

---

Arunkumar Sndharan  
Penn State University  
317 Reber Bldg  
University Park, PA 16802 USA  
Phone: 814 865 2289  
Fax:  
E-mail: sxa26@psu.edu

---

Peter Storey  
HSE - NII  
Room 313, St. Peter's House  
Merseyside, L20 3LZ United Kingdom  
Phone: 151 951 4172  
Fax: 151 951 4100  
E-mail: peter.storey@hse.gsi.gov.uk

---

# Registered Attendees

---

Alfred Strasser  
Aquarius Services Corp.  
17 Pokahoe Dr.  
Seepy Hollow, NY 10591 USA  
Phone: 914 366 8875  
Fax: 914 366 8876  
E-mail: stras69@at.net

---

Valeri Stnzhov  
IBRAE RAS  
B. Tulskeya 52  
Moscow, 113191 Russia  
Phone: 7 095 9580873  
Fax: 7 095 9580040  
E-mail: vfs@ibrae.ac.ru

---

Dion Sunderland  
Anatech Corp.  
321 Main Street  
Poughkeepsie, NY 126012919 USA  
Phone: (845) 454-6100  
Fax: 845-454-2292  
E-mail: dion@anatech.com

---

Michael Terry  
Numark Associates  
1220 19th St., NW, Ste. 500  
Washington, DC 20036 USA  
Phone: (202) 466-2700  
Fax:  
E-mail: mterry@numarkassoc.com

---

Victor Teschendorff  
GRS  
Forschungsgelaende  
Garching, 85748 Germany  
Phone: 49 89 32004-423  
Fax: 49 89 32004 9035  
E-mail: TES@GRS.de

---

Spyros Traiforos  
Link Technologies, Inc.  
20030 Century Blvd., Suite 210  
Germantown, MD 20874 USA  
Phone: 301 515 9654  
Fax: 301 515 9658  
E-mail: spyros.traiforos@linksolution

---

Hanchung Tsai  
Argonne National Laboratory  
9700 S. Cass Ave  
Argonne, IL 60439 USA  
Phone: 630 252 6178  
Fax: 630 252 9232  
E-mail: htsai@anl.gov

---

Robert Tsai  
Exelon Nuclear  
4300 Winfield Rd.  
Warrenville, IL 60555 USA  
Phone: 630 657 2162  
Fax: 630 657 4331  
E-mail: robert tsai@exeloncorp.com

---

Thomas Tseng  
TECRO/Science Division  
4201 Wisconsin Ave., NW, MB 09  
Washington, DC 20016 USA  
Phone: 202 895 1932  
Fax: 202 895 1939  
E-mail: dc@tecrosd.org

---

Shizuo Tsurumaki  
NUPEC  
Shuwa-Kamiyacho Bldg. 2F  
Tokyo, T105-0001 Japan  
Phone: 81 3 4514 5600  
Fax: 81 3 4514 5609  
E-mail: tsurumaki@nupec.or.jp

---

Gregory Twachtman  
Inside NRC  
1200 G St., NW, Suite 1100  
Washington, DC 20005 USA  
Phone: (202) 383-2166  
Fax: 202-383-2125  
E-mail: gregory\_twachtman@platts.c

---

Robert Twilley  
Framatome ANP  
3315 Old Forest Rd  
Lynchburg, VA 24056 USA  
Phone: 434 832 4019  
Fax:  
E-mail: bob.twilley@framatome-anp.

---

# Registered Attendees

---

Richard Valentin  
Argonne National Laboratory  
9700 S. Cass Ave., Bldg. 308  
Argonne, IL 60439 USA  
Phone: 630 252 4483  
Fax: 630 252 3250  
E-mail: rchv@anl.gov

---

John Valentino  
International Access Corp.  
1015 18th St., NW, Ste 504  
Washington, DC 20036 USA  
Phone: 202 223 7040  
Fax: 202 296 5373  
E-mail: valentino@iacdc.com

---

Keijo Valtonen  
STUK, Radiation & Nuclear Safety  
Authority  
PO Box 14  
Helsinki, 00881 Finland  
Phone: 358 9 759 88 331  
Fax: 358 9 759 88 382  
E-mail: keijo.valtonen@stuk.fi

---

Willem van Doesburg  
HSK Swiss Federal Nuclear Safety  
Inspectorate  
PO Box 5232  
Villigen, 5232 Switzerland  
Phone: 41 56 3103862  
Fax: 41 56 3104979  
E-mail: willem.vandoesburg@hsk.psi

---

W. VanRenterghem  
SCK-CEN  
Boeretang 200  
Mol, 2400 Belgium  
Phone: 32 14 333098  
Fax: 32 14 332111  
E-mail: wvrenter@sckcen.be

---

Gary Vine  
EPRI  
2000 L St. NW, Suite 805  
Washington, DC 20036 USA  
Phone: (202) 293-6347  
Fax: 202-293-2697  
E-mail: gvine@epri.com

---

Doug Vogt  
Lawrence Livermore National Lab  
PO Box 808, Mail Stop L-632  
Livermore, CA 94551 USA  
Phone: 925 423 7798  
Fax: 925 422 9913  
E-mail: vogt3@llnl.gov

---

Nicolas Waeckel  
EDF  
12-14 Avenue Dutnevoz  
Villeurbanne, 69628 France  
Phone: 33 4 7282 7244  
Fax: 33 4 7282 7711  
E-mail: nicolas.waeckel@edf.fr

---

Robert Waters  
Sandia National Laboratories  
P.O. Box 5800, MS 0748  
Albuquerque, NM 87185 USA  
Phone: (505) 844-4672  
Fax: 505 844 2829  
E-mail: rdwater@sandia.gov

---

Jenny Weil  
McGraw-Hill  
USA  
Phone: 202 383 2161  
Fax:  
E-mail: jenny\_weil@platts.com

---

Andrew White  
AECL, Reactor Safety  
Chalk River Labs  
Chalk River, Ontario K0J 1J0 Canada  
Phone: 613 584 3311 x 3442  
Fax: 613 584 4200  
E-mail: whitea@aecl.ca

---

Glenn White  
Dominion Engineering  
11730 Plaza America Dr., Ste 310  
Reston, VA 20190 USA  
Phone: 703 437 7826  
Fax: 703 437 0780  
E-mail: gwhite@domeng.com

---

# Registered Attendees

---

Eric Wieser  
Nuclear Waste News  
8737 Colesville Rd., Ste. 1100  
Silver Spring, MD 20910 USA  
Phone: (301) 587-6300  
Fax: 301-587-1081  
E-mail. ewieser@bpinews.com

---

Gery Wilkowski  
Engineering Mechanics Corp. of  
Columbus  
3518 Riverside Drive, Suite 202  
Columbus, OH 43026 USA  
Phone: (614) 459-3200  
Fax: 614-459-6800  
E-mail: gwilkows@columbus rr.com

---

Mark Williams  
U.S. Department of Energy  
  
USA  
Phone: 301 903 6892  
Fax:  
E-mail: mark.williams@hq doe.gov

---

Michael Woods  
Pittsburgh Post-Gazette  
National Press Building, Ste. 955  
Washington, DC 20045 USA  
Phone: (202) 662-7070  
Fax: 202-662-7328  
E-mail. mwoods@nationalpress.com

---

Tomofumi Yamamoto  
NUPEC  
4-3-13, Toranomon, Minato-Ku  
Tokyo, 105-0001 Japan  
Phone 81 3 4514 5557  
Fax:  
E-mail: tm-yamamoto@nupec.or.jp

---

Rosa Yang  
EPRI  
3412 Hillview Ave.  
Palo Alto, CA 94304 USA  
Phone 650 855 2481  
Fax: 650 855 1026  
E-mail: ryang@epn.com

---

You-Hsin Yang  
Institute of Nuclear Energy Research  
1000 Wenhua Rd., Chiaan Village  
Lungtan, Taoyuan 325 Taiwan  
Phone: 886 347 11400  
Fax: 886 347 11404  
E-mail: yhyang@iner.gov.tw

---

Lanssa Yegorova  
RRC "Kurchatov Institute"  
Kurchatov Square, 1  
Moscow, 123182 Russia  
Phone: 095 196 7283  
Fax: 095 196 1702  
E-mail: yegorova@nsi.kiae.ru

---

Yuzuru Yoshioka  
International Access Corp  
1015 18th St NW, Ste 504  
Washington, DC 20036 USA  
Phone: 202 223 7040  
Fax: 202 296 5373  
E-mail yuzuru@iacdc.com

---

Robert Youngblood  
ISL / NSAD  
11140 Rockville Pike, Ste 500  
Rockville, MD 20852 USA  
Phone: 301 255 2270  
Fax: 301 468 0883  
E-mail. ryoungblood@islinc.com

---

Won-Young Yun  
KINS  
Gusong-dong 19, Yusong-ku  
Daejeon, 305-338 Korea  
Phone: 82 42 868 0237  
Fax. 82 42 861 2535  
E-mail. k034ywy@kins.re.kr

---

Jinzhao Zhang  
Tractebel  
Ave. Ariane 7  
Brussels, B-1200 Belgium  
Phone. 32 2 7739843  
Fax: 32 2 7738900  
E-mail. jinzhao.zhang@tractebel.co

---

# Registered Attendees

---

Martin Zimmermann  
Paul Scherrer Institut  
  
Villigen, 5232 Switzerland  
Phone: 41 56 310 2733  
Fax: 41 56 310 2327  
E-mail: martin.zimmermann@psi.ch

---

Paul Zmola  
C & P Engineering  
4620 N. Park Ave. #1605E  
Chevy Chase, MD 20815 USA  
Phone. 301 656 5756  
Fax: 301 656 5756  
E-mail: pzmola@attglobal.net

---

## **SUMMARY OF USNRC'S RESEARCH TO ADDRESS PRESSURE BOUNDARY DEGRADATION ISSUES**

William H. Cullen, Jr., Sr. Materials Engineer  
Materials Engineering Branch, Office of Research  
US Nuclear Regulatory Commission  
Washington, DC 20555 USA  
(301) – 415 – 6754  
whc@nrc.gov

### **ABSTRACT**

The NRC Office of Research has funded materials testing programs to address issues of pressure boundary degradation for over 30 years. The aspects of the work that address the effects of the reactor coolant environment specifically are being carried out principally at Argonne National Laboratory. Two aspects of the ongoing program there center on determination of (a) the effects of reactor environments on fatigue life, and (b) stress corrosion crack growth rates in nickel-base alloys, such as Alloy 600 and Alloy 182, principally to define better the variables that affect cracking of vessel head penetrations, and other attachments fabricated from nickel-base alloys, or joined with mixed metal welds.

The largely unanticipated discovery of substantial wastage of the low-alloy steel pressure vessel head at the Davis-Besse plant has resulted in a significant effort on the part of industry and the NRC to understand the root cause of this incident, the corrosion processes involved, and the margin of safety that existed at the time of discovery. NRC/RES immediately set about determining the margin of safety that existed at the plant at the time of shutdown, and has initiated two test and evaluation programs to (a) determine the corrosion processes that were involved, and (b) to evaluate the integrity of the cavity and the cladding. This report summarizes the observations made by the licensee, and details the response on the part of the NRC, especially the Office of Research.

### **I. ENVIRONMENTALLY-ASSISTED CRACKING OF LIGHT WATER REACTOR BOUNDARY COMPONENTS**

Since 1986, the Materials Engineering Branch has funded a program at Argonne National Laboratory (ANL) (and at the Naval Research Laboratory and Materials Engineering Associates, Inc. before that) to address the irradiation sensitivity, thermal aging and environmental degradation of pressure boundary components. The program currently being conducted at ANL consists of elements to address (a) degradation of fatigue life of carbon, low-alloy and stainless steels, (b) irradiation-assisted cracking of reactor internals, and (c) stress-corrosion cracking studies of nickel-base alloys. All three elements include specifically the effects of both BWR and PWR environments, as well as correlative studies of mechanisms and failure modes, and their connection with materials and environmental chemistry, thermomechanical processing and other important variables. The most recent annual report from this program is cited as Reference 1, and the descriptions immediately below are taken from that report.

The program on fatigue life specifically addresses the effects of strain rate and environment on the three classes of materials that dominate pressure boundary structures: carbon steels, low-

alloy steels and stainless steels. For carbon and low-alloy steels, environmental effects on fatigue life are significant in high-DO water (>0.04 ppm DO) and only moderate (less than a factor of 2 decrease in life) in low-DO water. The reduction in fatigue life of carbon and low-alloy steels in LWR environments has been explained by the slip oxidation/dissolution mechanism for crack advance (Ref. 2). The requirements for the model are that a strain increment occur to rupture the protective surface oxide film and thereby expose the underlying matrix to the environment; once the passive oxide film is ruptured, crack extension is controlled by dissolution of freshly exposed surfaces and their oxidation characteristics. Unlike the case of carbon and low-alloy steels, environmental effects on the fatigue lives of austenitic SSs are significant in low-DO (i.e., <0.01 ppm DO) water (Fig. 1); in high-DO water, environmental effects appear to be either comparable (Refs 3, 4) or, in some cases, smaller (Ref. 5) than those in low-DO water. These results are difficult to reconcile in terms of the slip oxidation/dissolution model.

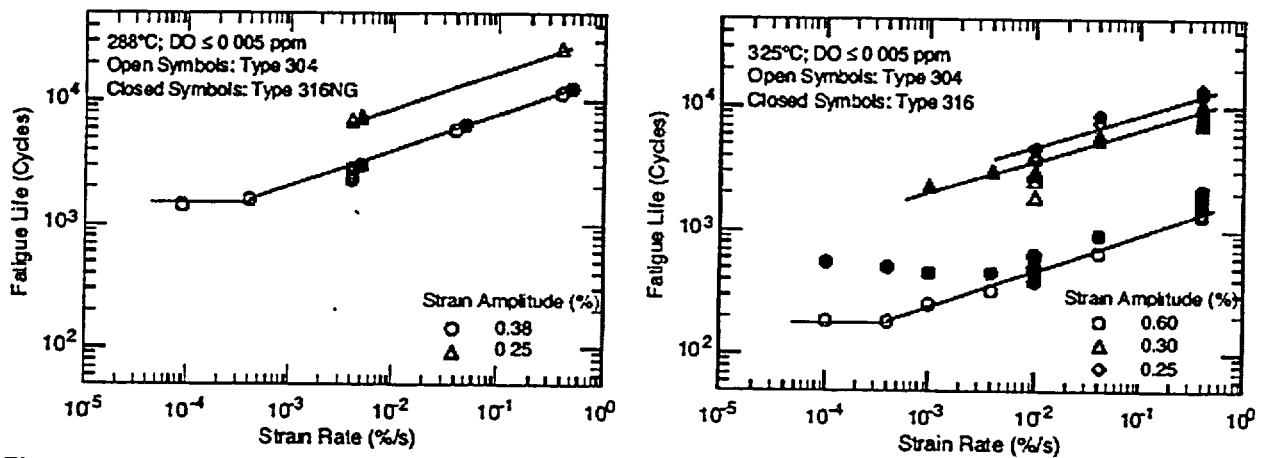


Figure 1. This shows the dependence of fatigue life of austenitic stainless steel on strain rate, for various strain amplitudes in deaerated, PWR-like environments. There does appear to be a saturation effect at low strain rates, corresponding to about one cycle each hour (Data from Reference 1).

Stress-corrosion cracking of Alloy 600 steam generator tubing has been investigated since the 1970s. The work of Coriou (Ref. 6), showed that Alloy 600 was susceptible also to stress corrosion cracking in pure water. However, the issue did not attract much attention until late-1980s with domestic and international discoveries of leaks in several Alloy 600 instrument nozzles, and the 1991 discovery of a small flaw in the control rod drive mechanism (CRDM) housing at Bugey 3, located in east-central France, near Lyon. Reference 7 is an excellent summary of the situation through 1993. At this point, the tendency of Alloy 600 vessel head penetrations and the associated welds to crack throughout a range of time and temperature conditions has resulted in decisions to replace the vessel heads throughout France, and at many plants in the US.

At Argonne, fracture mechanics crack growth rate (CGR) tests are being conducted on compact specimens of Alloys 600 and 690 in either oxygenated high-purity water or deaerated water that contains B, Li, and low concentrations of dissolved H at 289–320°C. Because environmental degradation of the alloys in many cases is very sensitive to processing, the effects of various

thermomechanical treatments are also being evaluated. The fatigue CGRs of Alloy 600 are enhanced in high-DO water; the environmental enhancement of growth rates does not appear to depend on either the C content or heat treatment of the material. Also, in high-DO water, the CGRs at 320°C are comparable to those at 289°C. In contrast to the behavior in high-DO water, environmental enhancement of CGRs of Alloy 600 in low-DO water seems to depend on material conditions such as yield strength and grain boundary coverage of carbides. Materials with high yield strength and/or low grain boundary coverage of carbides exhibit enhanced CGRs. Correlations have been developed for estimating the enhancement of CGRs of Alloy 600 in LWR environments relative to the CGRs in air under the same loading conditions.

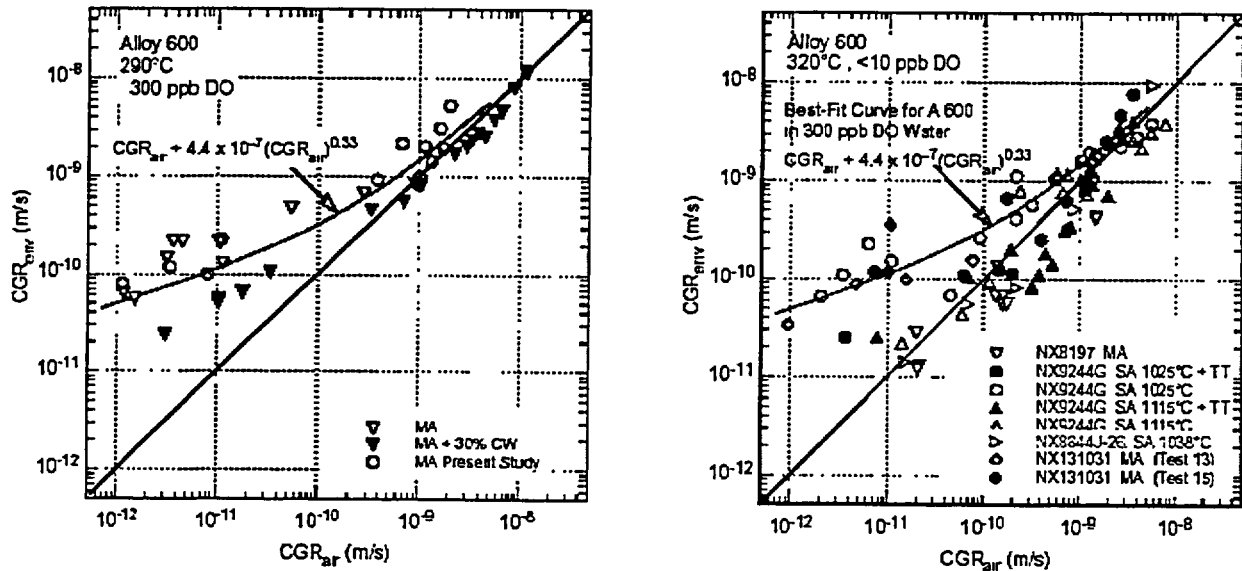


Figure 2. Crack growth rate data under cyclic loading for MA and MA plus 30% cold worked Alloy 600 in high-purity water at 290°C with ~ 300 ppb DO and at 320°C with <5 ppb DO (Data from Reference 1).

During repair work of a CRDM nozzle at the Davis-Besse plant, located on the shores of Lake Erie, a large cavity emanating from an axial crack was discovered in the low alloy steel vessel head. While there have been other much smaller and less potentially damaging incidents of boric acid corrosion of carbon and low-alloy steels, the magnitude of the wastage in this case has resulted in considerable alarm throughout the NRC, other licensees, and the international, reactor safety community.

## II. BACKGROUND OF THE DAVIS-BESSE INCIDENT

In early March, 2002, inspectors at the Davis-Besse plant, located on the shore of Lake Erie near Toledo, Ohio, USA, discovered a large cavity in the reactor head created by boric acid wastage resulting from leaks in CRDM Nozzle #3. Just prior to that finding, the licensee had completed a 100% volumetric inspection of the 69 Control Rod Drive Modules (CRDMs) in the head, and had found five nozzles with cracks that required repair before restarting. In the process of machining out the cracks in Nozzle #3 preparatory to repair, the nozzle came completely loose, boring was stopped, and that area of the head, which had been covered with boric acid residue, was cleaned enough to discover and view the cavity (Fig. 3).



*Figure 3. A view of the corrosion cavity near Nozzle #3. This photo was taken after an 18-inch (~0.5m) diameter dropout had been cut from the head, and the Alloy 600 CRDM nozzle had been removed. The "downhill" direction is to the left. The opening to the right is the former location of Nozzle #3.*

The licensee informed the USNRC of this finding on March 8, 2002. Due to the unprecedented extent of the corrosion that was found, the NRC began to mobilize a substantial fraction of personnel and contractor resources to address the issue. Seven months later, several activities related to this issue are in progress, and some will continue for many more months. This presentation reviews several of those activities, particularly those that are managed by the Materials Engineering Branch of the USNRC's Office of Research.

### **The Augmented Inspection Team**

On March 12, the NRC assembled an on-site, five-person "Augmented Inspection Team" with the responsibility of discovering the facts and circumstances related to the degradation of the reactor head, and to identify any precursor indications of this condition. The AIT, consisting of personnel from the Office of Nuclear Reactor Regulation (NRR), including Region III which is directly responsible for Davis-Besse oversight, and the Office of Research (RES), produced its report (Ref. 8) and presented its findings at a public meeting on April 5.

The AIT report focused on a number of "missed opportunities" that might have been better interpreted as evidence of seriously leaking CRDMs, or serious corrosion of the vessel head itself. The AIT found that both radiation element filters and the containment air cooler (CAC) had experienced an increase in their respective rates of fouling beginning in November 1998 and March 1999 respectively. Examination of the products causing the fouling showed large amounts of crystalline boric acid, together with black, brown and red iron oxide corrosion

products. However, the source of the corrosion products was assumed by the licensee to be from CRDM flanges that were known to be leaking, and not from corrosion of the vessel head.

During this same time period, and earlier (1996 – 2002), the licensee was unable to visually inspect the head near the centermost nozzles because substantial deposits of non-removable boric acid products prevented observation by the video cameras used in this type of inspection. A photo of the boric acid residues and corrosion products that flowed down the head of the reactor is shown in Figure 4. As with the filter deposits, the licensee alleged that these deposits originated from the known, higher-up leakage from the CRDM flanges, rather than leakage from cracks in the CRDM housing itself. The licensee asserted that visual inspection of the centermost nozzles was not important, since the center nozzles were believed to have lower levels of residual stresses, and therefore were less susceptible to initiation and growth of stress-corrosion cracks. However, the NRC regulators, supported by RES contractors with expertise in the inspection area, required the Davis-Besse plant to shut down on February 16, 2002 for a 100% volumetric inspection of the CRDM nozzles, in consideration of the fact that a 100% bare head visual had, for the previous eight years or more, been impossible.



*Figure 4. Photograph taken at the 13<sup>th</sup> Refueling Outage (RFO 13) in 2000. The head bolts are seen at the left, and the service structure, housing the CRDM drive motors, the head insulation package and circulation fans, is shown at the right. The corrosion products flowed from a series of “mouse holes” – the square cutouts around the lower edge of the service structure skirt.*

In parallel with the AIT meetings, the NRC established a link on the public website on which was posted notices of all the public meetings and available documents that pertained to the incident (Ref. 9) On April 15, the licensee delivered the root cause report to the NRC (Ref. 10), and on May 7, the NRC hosted a public meeting to allow the licensee to present their findings, and respond to questions from NRC staff and the general public. RES personnel have been heavily involved in the ongoing activities to evaluate the root cause report and recommend additional tasks that will be necessary to satisfy any open issues that remain.

### Description of the CRDM and Cavity Inspections

The volumetric inspection found four axial cracks in this nozzle, two of them throughwall (TW). One TW crack, extending 1.1 inch (~28 mm) above the J-weld, was facing into the cavity, and was presumably the source of the corroding environment. However, the second throughwall crack (see Fig. 5), extending about 1.0 inch (~25 mm) above the J-weld, was directly opposite the first, and faced directly into the smooth, and completely unattacked region showing in Fig. 3 as the darkened area to the right of the cavity.

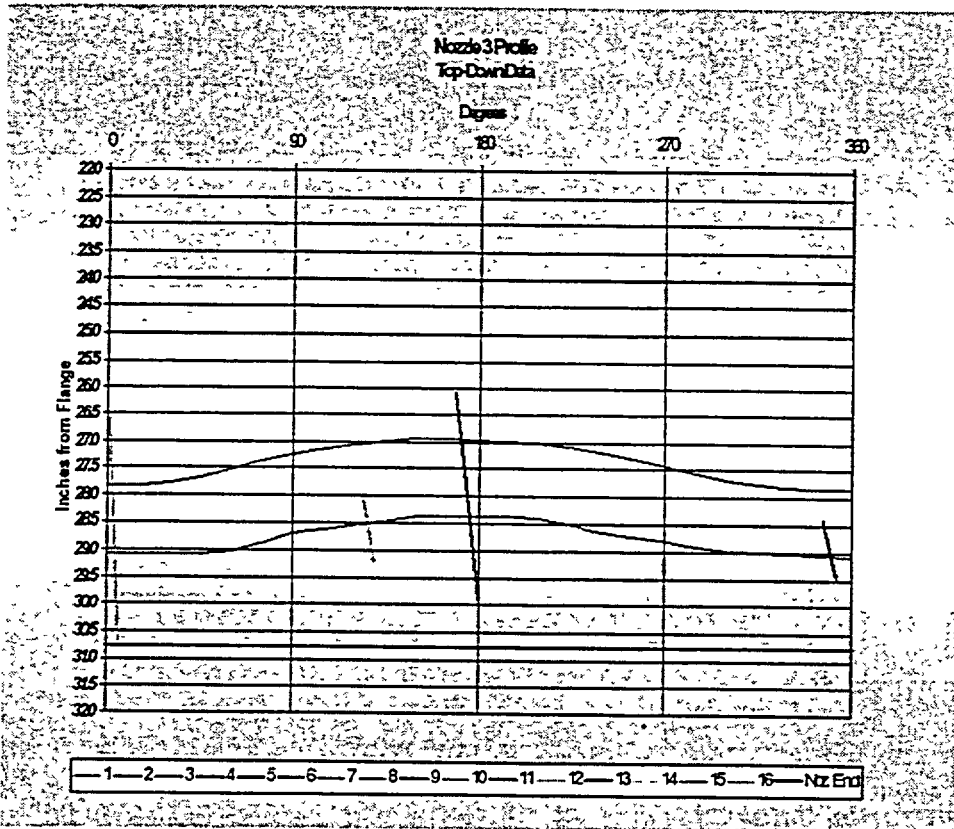
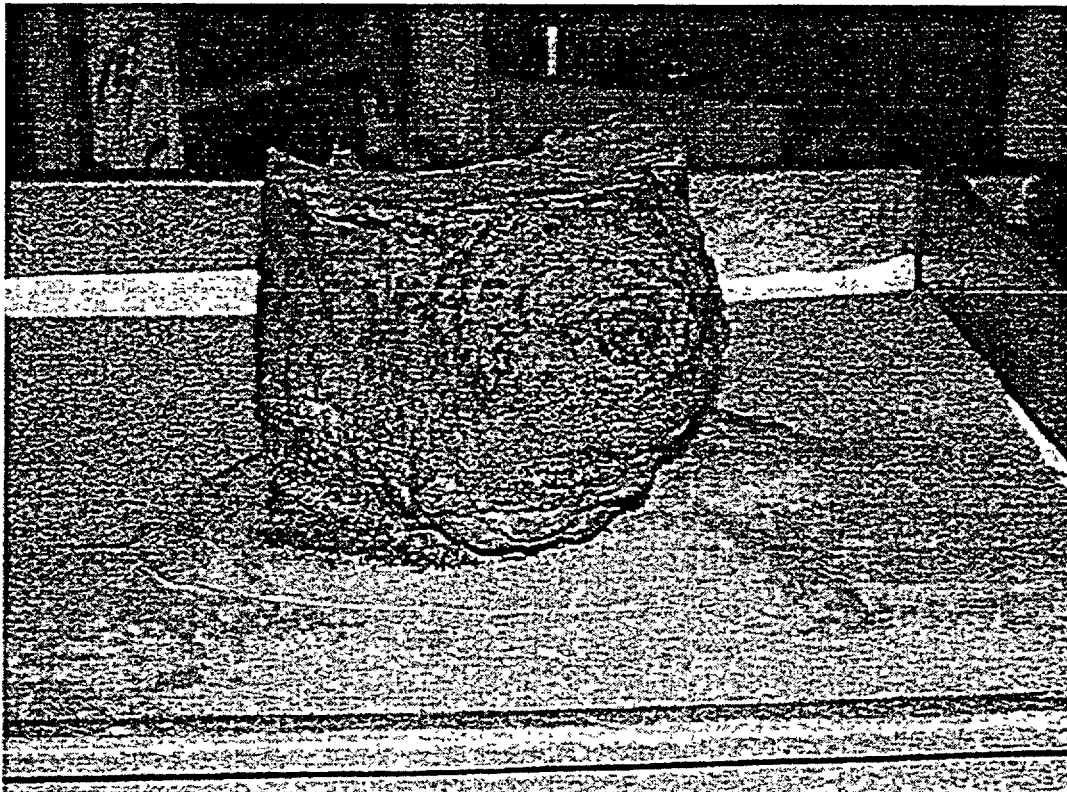


Figure 5. Interpretation of the ultrasonic inspection probe readings from Nozzle #3. Four cracks are coded according to the legend along the bottom of the figure. The parallel, wavy lines designate the upper and lower surfaces of the structural J-weld. The #1 axial crack (close to 0°) faced into the cavity, leaking the coolant that fed the corrosion. The #4 crack (close to 180°) faced the uphill direction, and no leak path was found associated with this flaw.

The licensee agreed to use a waterjet cutting procedure to remove a 18-inch (~0.5m) diameter section from the head, including the areas around Nozzles #3 and #11, and including the entire cavity. This section, together with Nozzles #3 and #11 were shipped to BWX Technologies (BWXT) laboratory for further investigation, including metallography of the low-alloy steel and cladding, fractographic studies of cracks in the cladding, J-welds and CRDM tubes, microhardness measurements of the clad and underlying base metal, and tensile tests of the clad.

As part of the investigative work at BWXT, silicon rubber castings were made of the cavity, in order to determine its true size and shape, and to get an accurate measurement of the area of the exposed clad. Figure 6 shows one such cast replica. From this replica, the exposed clad surface area was measured to be 16.5 sq. inches (~0.011 m<sup>2</sup>); if the exposed J-weld is included, the total is about 21 sq. inches (~0.014 m<sup>2</sup>). The casting shape also depicts the general wastage that occurred on the top of the head beyond the limits of the cavity walls. This corrosion was apparently resulted from the outflow of concentrated boric acid solutions fed by the continued leakage from the CRDM cracks.



*Figure 6. A cast, silicon rubber replica of the cavity and upper head surface wastage near Nozzle #3. The casting is shown upside down, with the "footprint" of the exposed clad at the top, and the molding of the general corrosion on the top surface of the head at the bottom. The downhill direction is to the right. The cavity portion of the green, rubber mold is covered with reddish-brown corrosion products that were extracted, along with the replica itself.*

By mid-summer, the licensee had procured a replacement head from a cancelled reactor, had begun activities to remove the old head from containment, and to modify very slightly and install the replacement head. Concurrent with these activities, an Inspection Manual Chapter 0350 panel was convened to provide oversight to the restarting procedures planned by the licensee. The panel, which is composed primarily of staff from Region III, provides a central focus for the NRC for decision-making and prioritization of the activities that are essential for a safe restart of the reactor. Currently, restart is scheduled for early January, 2003.

### **III. REDIRECTION OF RESEARCH EFFORTS**

The assessment of the remaining margin of safety was among the activities of the Office of Research staff. The Office of Research redirected the efforts of staff at the Oak Ridge National Laboratory (ORNL) to produce a finite element model of the Davis-Besse head, including the details of the cavity, and to calculate the pressure to develop a rupture, leading to a LOCA. A second calculation was completed assessing the maximum dimensions of the cavity and the associated exposed clad that could sustain normal operating pressure of the reactor. Based in part on these results, a probabilistic risk assessment was developed. Office of Research personnel have been instrumental in developing the boundary conditions, determining the relevant data requirements including materials properties and corrosion rates, and coordinating the derivation of these models and their results.

### **IV. ASSESSMENT OF REMAINING MARGINS**

The initial ORNL assessment of the remaining pressure margin of the as-found cavity was completed with the best set of measurements and materials properties that were available early in the discovery process. Among other errors and unknowns, the exposed cladding measurements provided to the NRC were too high by almost 50%. In spite of the uncertainties at that time, and the conservative assumptions that were used in lieu, the calculations showed that more than 5000 psi (>34 MPa), would be required to burst through the exposed clad.

During the last few months, better-established details of the cavity size and shape, and more accurate stress-strain representations of 308 stainless cladding were provided to an improved model. The current representation of the finite element submodel of the sector of the Davis-Besse head, including the cavity and the neighboring nozzles, is shown in Figure 7.

Some of the values required as input to the model are known accurately, some are known with some uncertainty, some need to be modeled conservatively, and some considerations are not yet known. The head design and the internal pressure are known. The dimensions of the irregularly shaped cavity were known (at the time) only approximately. A conservative approximation was used, assuming the walls were straight and placed at the outer limits of the cavity. This produced a value of the exposed cladding of 35.4 sq. inches (0.023 m<sup>2</sup>). – much greater than the actually measured value of about 21 sq. inches (~0.014 m<sup>2</sup> including the area of the exposed J-weld). Similarly, the thickness of the exposed clad is variable, ranging from 0.24 to 0.35 inches (6.1 to 8.9 mm), so a conservative value of 0.24 inches was used in the calculation. [Later work showed that the minimum thickness of the clad was just over 0.20 inches (5 mm)]. The integrity of the J-groove weld was not assured, so its geometry was not included in the model. For the purposes of the calculation, the area of the J-weld was represented as if only clad of nominal thickness was in its place. By adapting the stress-strain

curve for 304SS to conservative values of the yield and ultimate strengths and the work-hardening coefficient for 308SS found in the literature, a surrogate stress-strain curve for 308SS was developed, along with a normal distribution matching that for 304SS. Not included in the calculation at all were considerations such as the thermal gradient across the cladding (a constant temperature of 600°F (315°C) was assumed), and the presence of any residual stresses anywhere in the model.

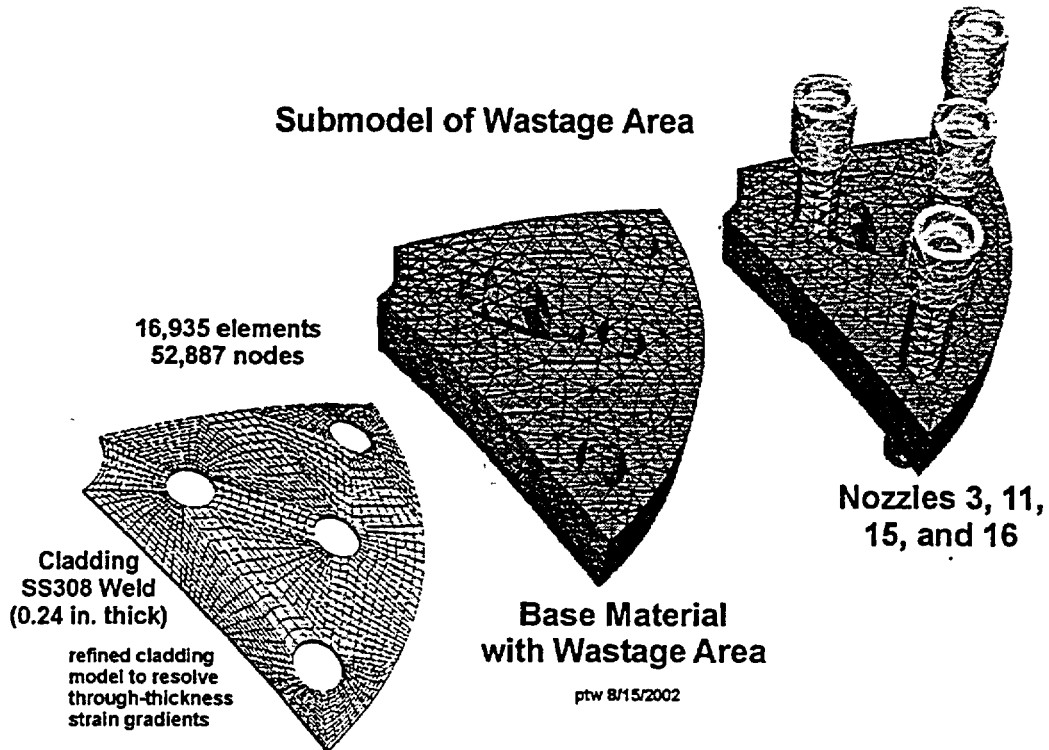


*Figure 7. A submodel of the Davis-Besse head, corrosion cavity and nearby nozzles. A model of the complete head was used to determine boundary values at the edges of the submodel. Burst pressures under various configurations of the cavity, both as-found and with postulated, additional growth, were calculated from the submodel response.*

The failure criterion was established by calibrating the model against literature-based burst test data for 304 stainless steel (304SS) disks of a similar diameter [6.0 inches (150 mm)] (Ref. 11). Using stress strain data for 304SS, the ORNL model “predicted” disk burst pressures that were about 10% below the actual measured burst pressures. The model was “pressurized” in the numerical sense until net section failure occurred, and the predicted burst pressure was established to be that number, less 10%. Based on these assumptions, the mean failure pressure with cladding thickness of 0.24 in. (6.1mm) would be substantially higher than the operating pressure of the reactor system. Coupled with the fact that the assumptions detailed above are either accurate or conservative support the conclusion that failure of the clad membrane in the condition that existed at Davis Besse at shutdown was an exceedingly unlikely event.

The other approach to the safety assessment issue is to compute how much longer the Davis-Besse reactor could have operated under a scenario of continued corrosion and increasing dimensions of the cavity. As required input to that computation, MEB personnel have recently completed a review of the available data on corrosion of stainless and low-alloy steels in concentrated boric acid solutions. Based on an industry document (Ref. 12) that contains a conclusion that the temperature of the concentrated boric acid solution in the cavity at the time of reactor shutdown was about the boiling point of the solution [ $\sim 215^\circ - 220^\circ\text{F}$ , ( $\sim 102^\circ - 104^\circ\text{C}$ ) depending on the concentration of boric acid], a conclusion was reached that the wastage rate of low-alloy steel could have been as high as 5 inches per year ( $\sim 4 \times 10^{-9}$  m/s).

The evolution of the dimensions of the cavity, should it have continued to corrode, are complete speculation. For the purposes of calculation, two assumptions were made: (a) that the cavity continued to grow self-similarly (i.e., with the same shape, achieved computationally by "growing" the walls normal to the centroid of the cavity), or (b) that the cavity morphed into an ellipsoidal shape, which would have been dictated more by the draw of gravity on the cavity contents. This latter assumption is supported in part by the shape of the silicon rubber mold of the top surface of the vessel head (See Figure 6). For either of these assumptions, the area of exposed clad would have to have increased substantially before rupture would have occurred.

A short time before this report was completed, small cracks, or crazing, were discovered on the surface of the exposed clad (i.e., at the (former) interface of the clad with the low-alloy steel. Figure 8 shows an optical micrograph of the exposed clad surface, and the flaws. These cracks appear to follow obvious metallographic features such as weld interpass boundaries, and other topological features of the exposed clad surface.

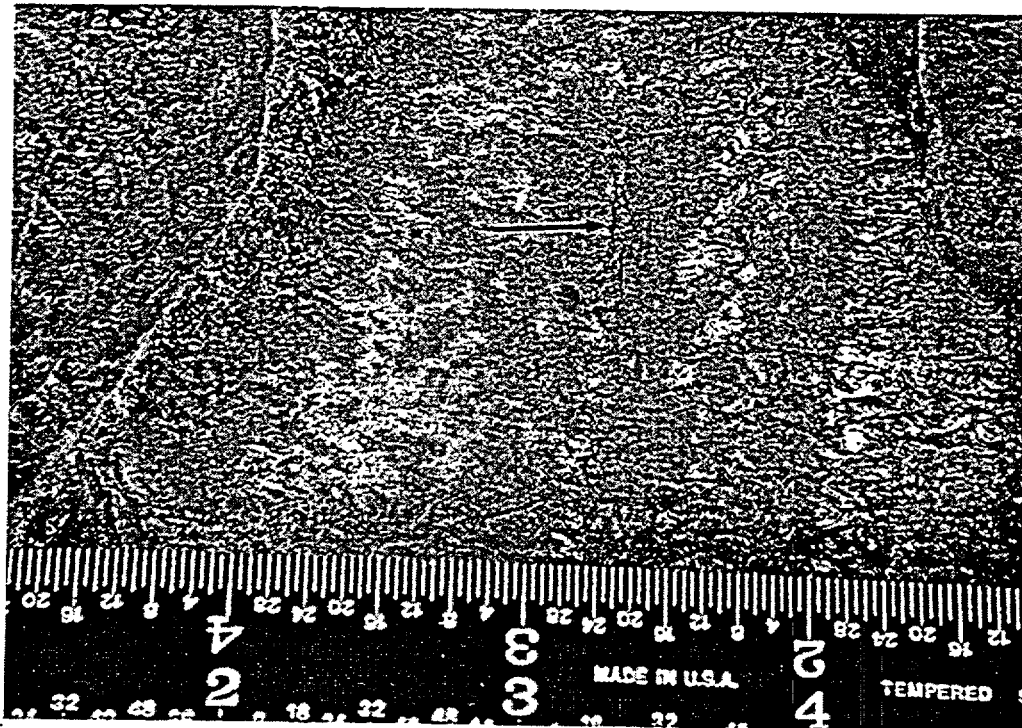


Figure 8. A photograph of the exposed clad surface, showing the small cracks which are most open where the deflection of the clad is a maximum.

These cracks will be characterized much more completely in the future, but their presence compromises the calculations of the remaining margins that were described in the preceding paragraphs. Plans are in place to suitably adjust these calculations once the sizing and distribution of these cracks has been completed. At that time also, a decision will have to be made concerning the failure mode, which might change to a ductile tearing mode, rather than the net section failure criterion that has been used.

## V. INITIATIVES FOR FUTURE RESEARCH

Driven by what was not known at the time of discovery of the corrosion cavity, several newly conceived research programs have been put in place, or will start in the near future. Other NRC activities with a more long term focus on the inspection, leakage and corrosion damage issues include a variety of research programs that have been initiated or refocused recently. As an example, the Program at Pacific Northwest National Laboratory (PNNL) will become more focused on refinement of UT and eddy current techniques for CRDM and J-weld inspection.

A new corrosion program, awarded to Argonne National Laboratory, will establish corrosion characteristics of low-alloy steel, stainless cladding steel and Alloy 600 in concentrated boric acid solutions. This same program also contains a task to develop a probabilistically-based, integrated crack growth rate and inspection frequency determination model. This program consists of several tasks, summarized below:

- (a) Crack Initiation and Growth Rates of Alloys 600 and 182 Removed from Davis-Besse Nozzles and J-weld: The objective of this task is to conduct stress-corrosion crack initiation and crack growth rate tests in simulated PWR coolant of CRDM and J-weld alloys removed from the head of the Davis-Besse plant. The initiation tests will show whether cracks could have formed with little or no incubation period, and give some information about the shape of the cracks, given the particular material characteristics of superficial work hardening, residual stress and grain size. The crack growth rate tests will demonstrate how the materials used in the construction of the original Davis-Besse head compare with the existing SCC data base.
- (b) Development of an Integrated Crack Growth Rate and Inspection Frequency Determination Model: The objective of this task is to invoke a probabilistic approach to the development of a calculational model leading to prediction of appropriate inspection intervals for vessel penetrations. The probabilistic model will incorporate uncertainties in factors, such as: (a) sizing of cracks as determined through non-destructive inspections; (b) probability of detection; (c) variation in crack growth rates, due to microstructural and environmental conditions; (d) variations in stress intensity factor, due principally to residual stresses; (e) variations in leakage rates; and (f) structural integrity evaluations.
- (c) Corrosion of Reactor Steels in Concentrated Boric Acid Solutions: The objective of this task is to measure the wastage rates of A533B pressure vessel steel and 308SS cladding steel in flowing and quiescent boric acid solutions of varying concentrations and at various temperatures. Additionally, corrosion tests will be

conducted in molten boric acid and boric oxide mixtures at two temperatures, to be determined, and under pressure and humidity conditions that provide chemical compound stability for the molten species.

- (d) Measurement of Electrochemical Potential (Corrosion Potential) of Alloy 600, Alloy 182 and A533B in Concentrated Boric Acid Solutions: The objective of this task is to measure the electrochemical corrosion potential of the materials found in the head and nozzles of the Davis Besse reactor, under the same set of temperature, solution concentration and flow/no flow conditions as will be explored in (b), above.

With the discovery of the small cracks in the cladding, the safety assessment took a new turn, departing from a rather straightforward analysis of a stressed membrane, with a complex shape, to an evaluation of whether such a membrane would fail by net section collapse, or by a ductile tearing of a flaw. This phase of work, undertaken by ORNL, consists of several aspects, both analytical and experimental.

The analytical efforts consist of:

- (a) estimations of the cladding residual strains at 600°F (315°C), using finite element methodologies;
- (b) estimations of the crack driving forces as functions of flaw size, and membrane stress by performing elastic-plastic finite element analyses of sharp, surface-breaking flaws; and
- (c) estimation of the plastic collapse stress, as a function of flaw size, assuming the flaws blunt. The flaws assumed will range over 5%, 25% and 50% of the thickness of the clad, with lengths ranging from 0.375 in. through 2.0 in. (9.5 – 51 mm);

Each of these analytical experiments will be conducted first with a flat plate geometry, and then with the geometry of the submodel shown in Figure 7.

The experimental efforts consist of:

- (a) burst tests of flawed and unflawed exposed clad on low-alloy steel plates, with cavity sizes similar to that found at Davis-Besse. The tests are intended to simulate the loading, geometry, thermal and material characteristics of the Davis-Besse reactor pressure vessel head
- (b) Materials characterization tests, including tensile tests of 308SS cladding steel removed from the Davis-Besse head; and
- (c) Microstructural characterization of the stainless clad used in the actual experiments to assure that its properties match credibly well with those known for the Davis-Besse plant.

In March, 2003, the Office of Research plans to hold a workshop to review and exchange information on vessel head penetration inspection and repair procedures, including presentation of recent, nickel-base alloy stress-corrosion cracking test results, corrosion mechanisms model development, and leak-rate calculations.

## **VI ACKNOWLEDGEMENTS**

Most of the information in Section I describing the activities and results of the ANL program was gleaned from monthly and annual (Ref. 1) reports. As indicated, the NRC has assigned a large team of employees and contractors to assist with various aspects of the Davis-Besse issue. In this paper, the photographs of the Davis-Besse reactor and cavity were taken from reports provided by the licensee to the NRC. Those pictures, and a great many more, as well as the root cause report, AIT report, and other relevant reports, may be found at the NRC website: [www.nrc.gov/reactors.html](http://www.nrc.gov/reactors.html). The figures relating to the finite element modeling came from ORNL reports provided to the MEB. These reports will be published in the near future. Reports will also be generated during the conduct of the experimental programs that are described in Sections IV and V.

## **VII REFERENCES**

1. Environmentally Assisted Cracking in Light Water Reactors Annual Report: January—December 2001, NUREG/CR-4667, ANL 02/33 (November, 2002).
2. F. P. Ford, "Prediction of Corrosion-Fatigue Initiation in Low-Alloy Steel and Carbon Steel/Water Systems at 288°C," in Proc. of the Sixth Intl. Symp. on Environmental Degradation of Materials in Nuclear Power Systems-Water Reactors, R. E. Gold and E. P. Simonen, eds., The Minerals, Metals, and Materials Society, Warrendale, PA, pp. 9-17 (1993).
3. H. Kanasaki, R. Umehara, H. Mizuta, and T. Suyama, "Fatigue Lives of Stainless Steels in PWR Primary Water," Trans. 14th Intl. Conf. on Structural Mechanics in Reactor Technology (SMiRT 14), Lyon, France, pp. 473-483 (1997).
4. K. Tsutsumi, H. Kanasaki, T. Umakoshi, T. Nakamura, S. Urata, H. Mizuta, and S. Nomoto, "Fatigue Life Reduction in PWR Water Environment for Stainless Steels," in Assessment Methodologies for Preventing Failure: Service Experience and Environmental Considerations, PVP Vol. 410-2, R. Mohan, ed., American Society of Mechanical Engineers, New York, pp. 23-34 (2000).
5. O. K. Chopra, "Effects of LWR Coolant Environments on Fatigue Design Curves of Austenitic Stainless Steels," NUREG/CR-5704, ANL-98/31 (1999).
6. H. Coriou, et al., "Stress Corrosion Cracking of Inconel in High Temperature Water", Third Symposium on Metallurgical Corrosion, June 29 - July 1, 1959, pub. by the Saclay Center for Nuclear Study (Centre d'Etudes Nucleaires de Saclay), North Holland Publishing Co., Amsterdam, p. 161.

7. PWSCC of Alloy 600 Materials in PWR Primary Penetrations, EPRI TR-103696, Project RP-3223-01, Prepared by Jeff Gorman, Dominion Engineering, Inc., Raj Pathania, EPRI Prog. Manager
8. Davis Besse Nuclear Power Station NRC Augmented Inspection Team - Degradation of the Reactor Pressure Vessel Head - Report No. 50-346/02-03, available from the NRC Website: [www.nrc.gov](http://www.nrc.gov)
9. [www.nrc.gov/reactors/operating/ops-experience/vessel-head-degradation](http://www.nrc.gov/reactors/operating/ops-experience/vessel-head-degradation)
10. Root Cause Analysis Report – Significant Degradation of the Reactor Pressure Vessel Head, CR 2002-0891, available from the NRC Website: [www.nrc.gov](http://www.nrc.gov)
11. P. C. Riccardella, Elasto-Plastic Analysis of Constrained Disk Burst Tests, Petroleum Engrg. Conference, Sept. 1972, Paper 72-PVP-12.
12. PWR Reactor Pressure Vessel (RPV) Upper Head Penetrations Inspection Plan (MRP-75), EPRI TR-1007337, available from the Electric Power Research Institute, Palo Alto, CA 94304

## Parametric Studies of the Probability of Failure of CRDM Nozzles

William J. Shack  
Argonne National Laboratory

### Abstract

Preliminary studies have been conducted with an integrated model for the probability of failure of control rod drive mechanism (CRDM) nozzles by the growth of circumferential cracks leading to net section failure. The model describes initiation through Weibull probability distributions that are fit to plant data on the occurrence of leakage. The model and data show that there is a significant plant-to-plant variability in probabilities of failure or leakage even if different head operating temperatures are taken into account. For many plants the predicted probability of failure will be sensitive to the details of the correlation between the susceptibility of the plant to leakage and the expected crack growth rates in the nozzle material.

### Introduction

The U.S. Nuclear Regulatory Commission (USNRC) Office of Nuclear Reactor Research is sponsoring work to develop an integrated model for the degradation of CRDM nozzles and reactor heads. Such models are also being developed by the Materials Reliability Program (MRP). These models provide input to regulatory decisions on the degree of "credit" for lower head temperatures that can be given when inspection timing and appropriate intervals for inspection are considered. This is work in progress. The current work is focused on CRDM nozzle failure due to stress corrosion cracking (SCC); future studies would also consider the possibilities for failure by wastage of the head. The goal of the parametric studies presented here is to try to understand how model and data uncertainties can impact predictions of CRDM nozzle failure due to SCC.

The overall approach to modeling is similar to that used by the MRP. The failure process initiates with the development of a leak; the leak is associated with the formation of an initial circumferential crack on the outer diameter (OD) of the nozzle. In reality, the formation of the circumferential crack probably involves initiation of multiple surface cracks. These cracks grow through the wall and circumferentially to link and form a primary crack, which continues to grow circumferentially and through the wall. At some stage, the circumferential growth of the primary crack becomes dominant mode of crack progression rather than extension by linking and joining of surface cracks. In the future, the modeling can be extended to consider the extent over the circumference for which it is likely that surface cracks will initiate and the rate that throughwall growth can occur. However, the approach at present is to assume that once leakage to the crevice around the nozzle occurs, a circumferential crack instantaneously forms over an extent that is large enough that further growth is dominated by the circumferential growth of this crack rather than initiation, linkage, and throughwall growth of surface cracks

on the OD of the nozzle. In the MRP model, the initial circumferential crack is assumed to be a half-throughwall 30° crack. In the model considered here, initial throughwall cracks are also considered.

#### Initiation of primary water stress corrosion cracking (PWSCC) in Alloy 600

Despite extensive research on PWSCC of Alloy 600 primarily for steam generator tubing, no consensus has formed on the mechanism of PWSCC initiation, although the phenomenology has been fairly well characterized.<sup>1</sup> There is a strong influence of temperature with an activation energy of 40–52 kcal/mol. Stresses near yield are needed for initiation, and the time to initiation is sensitive to the stress level. The stress dependence of the time to initiation is frequently modeled as a power law  $\sim\sigma^4$ . Cold work has an important accelerating effect. In the case of CRDM nozzles this suggests that fabrication processes such as machining could have important consequences on susceptibility to cracking. Studies with steam generator tubing have shown that carbide morphology plays an important role. Intergranular carbides improve resistance to intergranular SCC. However, because no archival materials exist that could be used to characterize the microstructures, and it is difficult to extract quantitative information on the degree of cold work associated with the fabrication of particular nozzles, the current ranking used by industry and the USNRC to prioritize inspection accounts only for the effect of temperature with an activation energy of 50 kcal/mol.

Currently models for CRDM failure do not attempt to describe the initiation of leakage phenomenologically in terms of cracking in the nozzle or the Alloy 182 J weld and the subsequent growth of the throughwall crack that permits leakage to the crevice between the nozzle and wall of the pressure vessel. Instead, following the work of Gorman, Staelhe and Stavropoulos<sup>2</sup> for steam generator tubes, they describe the process probabilistically using Weibull probability distributions. The effect of temperature, however, is accounted for explicitly through an activation energy that is assumed to be the same as that for initiation of a crack.

The Weibull cumulative probability is

$$F(t) = 1 - \exp\left[-\left(\frac{x}{\theta}\right)^b\right], \quad (1)$$

where  $\theta$  is the time at which the cumulative probability of a leak is 0.63, and  $b$  is the Weibull slope. The Weibull slope  $b$  characterizes the rate at which the chance of failure is increasing with time ( $b = 1$  gives a constant failure rate). Ideally,  $b$  would be determined from the analysis of failure fractions at different times. Because such data are very limited, the MRP has suggested a value of 3, which is consistent with existing PWSCC initiation data (primarily obtained in tests on steam generator tubing). The limited data for repeated inspections that are currently available suggest that a higher value of  $b$  may be appropriate, and some analyses have been performed with  $b = 6$ .

Once a value of  $b$  is selected,  $\theta$  can be determined by fitting to the observed data for leaks. The MRP analysis assumes a triangular distribution for  $\theta$  with values spanning  $15 \pm 6$  years. Although other distributions can be considered for  $\theta$ , these values are representative of the observed range. The values of  $\theta$  determined by the analysis of early leaks are probably somewhat conservative. Most heads will have nozzles from different heats, and not all welds will have the same residual stresses. The early failures are presumably due to the worst heat and the most severe weld geometries, but the analyses of the field data are not done by heat of material and usually assume that all nozzles have the same probability of failure.

Because of the potential for boric-acid driven corrosion of the low-alloy steel head, it is desirable to avoid not only structural failure of the nozzles but also leakage. The MRP inspection program suggests that plants can be divided into regions of "low," "moderate," and "high" risk of leakage. The boundaries of these regions are determined by examining the risk of leakage for a plant with the average value of  $\theta$  (or median value since they are the same for a symmetric triangular distribution). A plant at a lower head temperature can operate for many more effective full power years (EFPY) than a plant with the same susceptibility to cracking operating at higher temperature. As shown in Fig. 1, however, when the expected variability in susceptibility is taken into consideration, there will be plants with a "high" risk of leakage at about the same operating time that a "median" plant has a "moderate" risk of leakage.

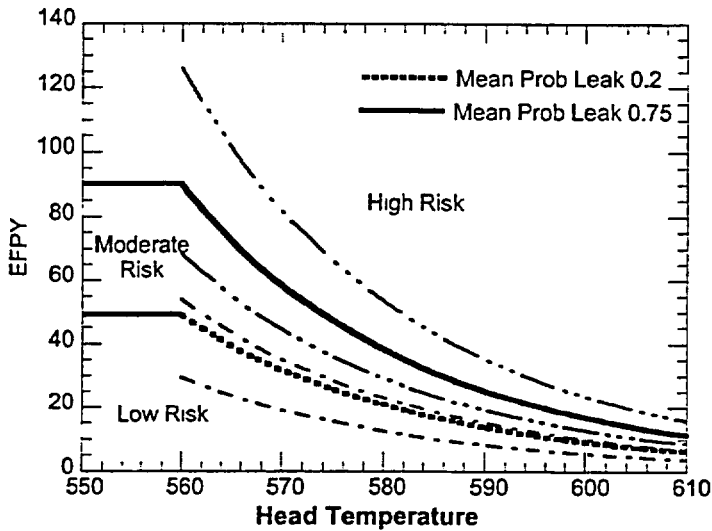


Figure 1. Number of EFPY of operation as a function of operating head temperature to reach probabilities of leakage of 0.2 and 0.75. The heavy curves are for median values. The chain-dot curves show the range of values expected for different degrees of susceptibility.

#### Crack Growth Rates in Alloy 600 Nozzles

As noted previously, it is assumed that although circumferential cracks form by the initiation, throughwall growth, and linking of cracks that initiate on the OD of the nozzle, the final failure of the nozzle is governed by the circumferential growth of the crack. Crack growth rates (CGRs) in Alloy 600 are strongly heat dependent. As in the case of crack initiation, this has been associated with different microstructures, but quantitative correlation is difficult and the relevant microstructural information is not available for heats in service.

Data on the CGR of Alloy 600 materials relevant to CRDM nozzles (i.e. not SG tubes) have been collected and analyzed in the report MRP-55.<sup>3</sup> The data were fit by heat to a correlation for the CGR  $\dot{a}$

$$\dot{a} = A(K - 9)^{1.16} \quad (2)$$

developed by Scott<sup>4</sup> where  $K$  the stress intensity is in  $\text{MPa}\cdot\text{m}^{1/2}$  and  $\dot{a}$  is in  $\text{m/s}$ . The correlation predicts a "threshold" at  $K = 9 \text{ MPa}\cdot\text{m}^{1/2}$ , which implies that until a crack is large enough that  $K$  is significantly larger than  $9 \text{ MPa}\cdot\text{m}^{1/2}$ , the circumferential growth of a crack may not dominate crack extension. A value of the parameter  $A$  in the Scott correlation has been obtained for each of the 23 heats of Alloy 600 nozzle material for which CGR data are available. The values of  $A$  in the population of heats in service are assumed to be represented by a log-normal distribution fit to the available sample of 23 heats. The values of  $A$  for the 23 heats and the log-normal fit are shown in Fig. 2. The CGR data have been normalized to a temperature of  $325^\circ\text{C}$  ( $617^\circ\text{F}$ ) using an activation energy for crack growth of  $130 \text{ kJ/mol}$  ( $31.0 \text{ kcal/mol}$ ). The log-mean of the log-normal distribution is  $-27.34$  and the log-standard deviation is  $1.02$  (with the CGR in units of  $\text{m/s}$  and  $K$  in  $\text{MPa}\cdot\text{m}^{1/2}$ ).

Because the infinite tails of the log-normal distribution are unrealistic, a log-triangular distribution has been used for the MRP integrated model and current studies. Except at the tails of the distributions, the log-normal and log-triangle distributions are almost indistinguishable, as shown in Fig. 2.

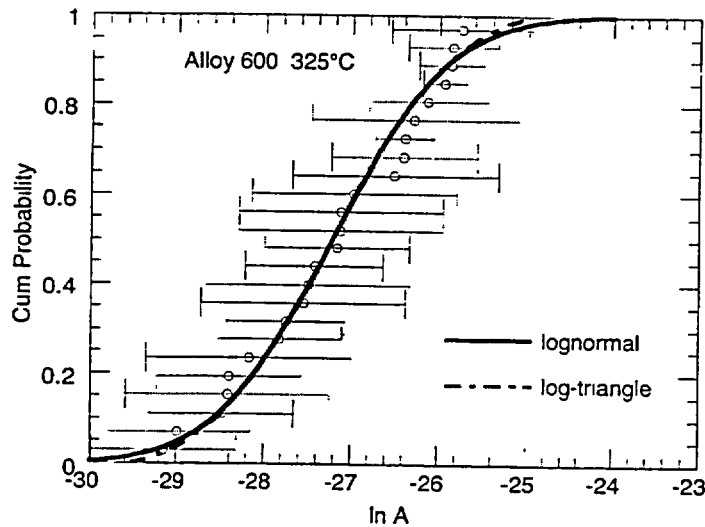


Figure 2.  
Distribution of the Scott parameter  $A$  for Alloy 600 CRDM nozzle materials. The data have been normalized to a temperature of  $325^\circ\text{C}$  ( $617^\circ\text{F}$ ) and the error bars shown the uncertainty in the values of  $A$  for each of the experimental heats.

The value of  $A$  varies by about a factor of 100 for different heats. At  $316^\circ\text{C}$  ( $600^\circ\text{F}$ ) for a typical  $K$  value of  $27.5 \text{ MPa}\cdot\text{m}^{1/2}$  ( $25 \text{ ksi}$ ),  $\dot{a} = 18 \text{ mm/y}$  ( $0.7 \text{ in./y}$ ) for the worst heat.

The fit to the data in MRP-55 does not consider the effect of uncertainties in  $A$  values on the resulting fits. However, Monte-Carlo analyses taking into account the effect of these uncertainties show that the best estimate of the distribution is close to that presented in MRP-55, and that fit has been employed for the analyses reported here.

## Stress intensity factor K distributions for circumferential growth of cracks

Calculations of the probability of failure of a CRDM nozzle require knowledge of the stress intensity factor associated with the nozzle. Until a crack becomes large ( $> 180^\circ$ ), K is dominated by the residual stresses due to welding, and the axial load on the nozzle due to the pressure load is relatively unimportant. For larger cracks the pressure loads become more important and dominate as the crack approaches failure ( $\approx 330^\circ$ ). Because the residual stresses due to welding vary with the yield stress of the material, K is also expected to vary with yield stress.

Values of K for CRDM nozzles for use in the integrated model developed by the MRP have been calculated by Structural Integrity Associates (SIA) using residual stresses calculated by Dominion Engineering.\* The USNRC has contracted with Engineering Mechanics Corporation of Columbus (EMC<sup>2</sup>), Ohio and the Oak Ridge National Laboratory to independently evaluate the residual stresses and the associated values of the stress intensity factor K in CRDM nozzles caused by welding. At this time, only values for the center nozzles are available from EMC<sup>2</sup>.\*\*

The results from EMC<sup>2</sup> for the center nozzles are compared with those computed by SIA in Fig. 3. The results depend on the value of yield stress. A base case and a high yield case are shown for the EMC<sup>2</sup> results. The SIA results are less sensitive to yield stress, and only the results for a 50 ksi (344 MPa) yield are shown. The EMC<sup>2</sup> curves are for throughwall cracks. The SIA curve is for a crack that starts as half throughwall and becomes fully throughwall at a crack angle of  $180^\circ$ .

The times to failure from initiation of  $30^\circ$  and  $60^\circ$  cracks (throughwall for EMC<sup>2</sup>, part throughwall for SIA) are shown in Table 1. The EMC<sup>2</sup> base solution gives a long life because at  $30^\circ$ , the K is just above threshold. This would suggest that in this case circumferential growth could be dominated by initiation, throughwall growth, and linkage of surface cracks rather than the circumferential growth of the primary crack.

Table 1 Time to Failure (years) at  $316^\circ\text{C}$  ( $600^\circ\text{F}$ ) for  $\dot{a}_{\text{max}}$

Initial Crack	SIA	EMC <sup>2</sup> base	EMC <sup>2</sup> high
$30^\circ$	7.8	14.5	5.4
$60^\circ$	6.8	8.1	4.5

\* Personal Communication, P. Riccardella, Structural Integrity Associates, to W. J. Shack, Argonne National Laboratory, October 2, 2002. See also

<http://www.nrc.gov/reactors/operating/ops-experience/vessel-head-degradation/vessel-head-degradation-files/5-pfm-inspection-plan.pdf>

\*\* Personal Communication, G. Wilkowski, Engineering Mechanics Corporation of Columbus, to W. J. Shack, Argonne National Laboratory, July 1, 20002. Also included in the proceedings of this conference in the paper "Summary of Ongoing NRC Efforts to Define Circumferential Crack-Driving Force Solutions for CRDM Nozzles," G. Wilkowski et al.

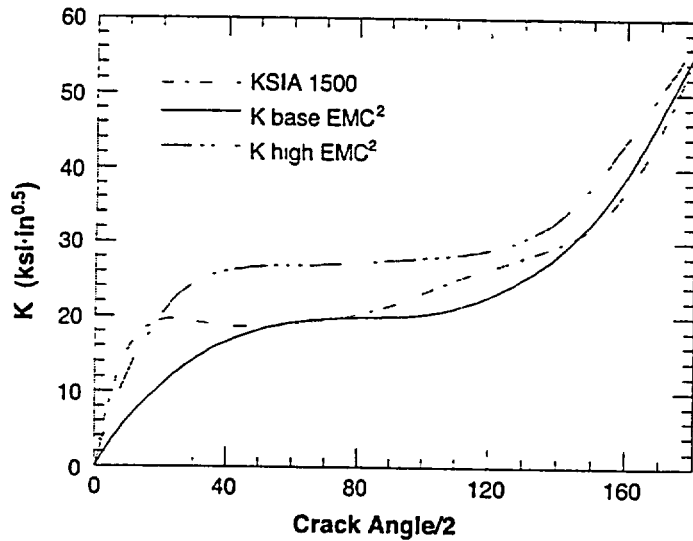


Figure 3. Variation of the stress intensity factor K for circumferential crack growth at center nozzles computed by SIA and EMC<sup>2</sup>.

Although both the Weibull initiation parameter  $\theta$  and the CGR  $A$  are statistically distributed, they are not independent variables. The metallurgical factors that make a heat of Alloy 600 susceptible to the initiation of cracking also appear to result in high CGRs once a crack has initiated. One way to visualize the correlation is in terms of a "window" that for a particular value of the initiation parameter  $\theta$  defines the distribution of the CGR parameter  $A$  that is associated with  $\theta$ . Low values of  $\theta$  (short times, high susceptibility to initiation) are correlated with high values of  $A$  (high CGRs). Some potential correlation "windows" for a value of  $\theta$  corresponding to the midpoint of a distribution for  $\theta$  are shown in Fig. 4. The most realistic "window" probably resembles the Gaussian-like distribution shown schematically on the left in Fig. 4b. Although it is clear that the values of  $\theta$  and  $A$  should be correlated, no data are available on which to quantitatively base the correlation, and it appears necessary to use engineering judgment to develop a correlation. For the present calculations, the two uniform distributions shown on the right in Fig. 4b have been used. The "window" on the far right appears to be clearly conservative. All the lower values are cut off, but all the high values are included with uniform likelihood. The other uniform distribution cuts off the "tail" of the distribution for  $A$  above 0.9 and is included for comparison.

#### Probability of Failure of CRDM Nozzles

The probability that a CRDM nozzle will fail at a time  $t_f$  less than  $T$ ,  $P(t_f < T)$ , can be calculated from

$$P(t_f < T) = \int_0^T p(t)P_c(t_f < T - t)dt \quad (3)$$

where  $p(t)$  is the probability that a crack will initiate at a time  $t$ , and  $P_c(t_f < T - t)$  is the conditional probability that a crack which initiates at  $t$  will fail at a time  $t_f$  less than  $T$ .  $P_c(t_f < T - t)$  is determined by fracture mechanics analysis. In the case where it is assumed that a circumferential crack forms immediately on the occurrence of a leak, the probability  $p(t)$  is

equal to the probability of leakage, the empirical Weibull probability based on field data, times the fraction of the leaks that are associated with circumferential cracks. This fraction has been taken as 0.2 in the current calculations, again based on field data.

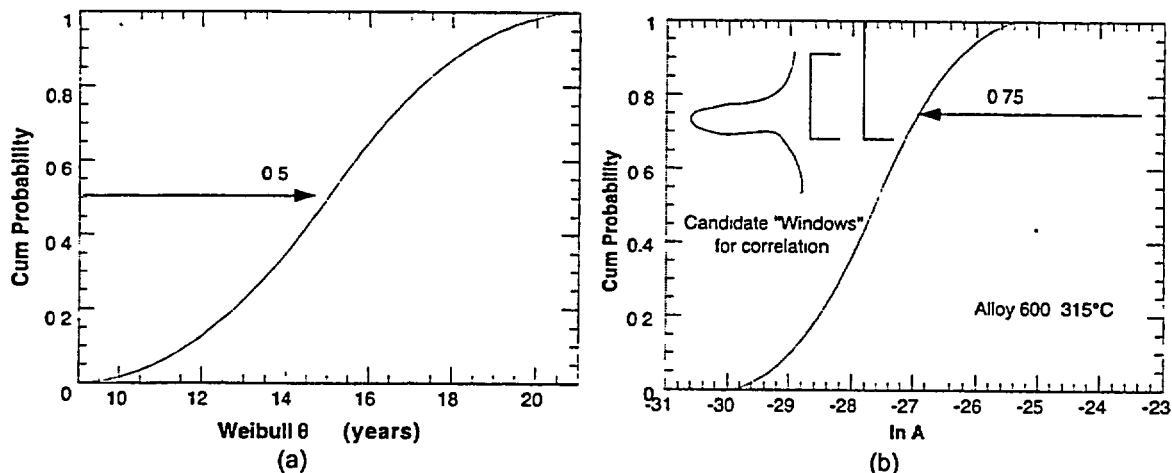


Figure 4. (a) Representative distribution for the Weibull parameter  $\theta$  describing initiation of leakage; (b) Candidate "windows" representing the values of  $A$  associated with a value of  $\theta$  corresponding to the midpoint of the distribution.

Equation (3) gives the probability of failure for a single nozzle. The probability that one of  $n$  penetrations will fail at a time  $t_f < T$  is then  $P_n = 1 - (1 - P)^n$ . For a given initial crack size and a given  $K$  distribution, the failure time needs to be calculation only for a single value  $A_1$  of the CGR parameter  $A$ . If the corresponding failure time is  $t_1$ , the failure time  $t_f$  for another value of  $A$  is determined from the simple scaling relation  $A * t_f = A_1 t_1$ . The probability  $P_c(t_f \leq T)$  that a nozzle will fail in a time  $t \leq T$  is the probability that  $A \geq A_1 t_1 / T$ . This is just

$$P_c(t_f \leq T) = 1 - F\left(\frac{A_1 t_1}{T}\right), \quad (4)$$

where  $F(A)$  is the appropriate cumulative distribution function for the crack growth rate, i.e., either the cumulative log-normal distribution from MRP-55 or the corresponding log-triangular distribution multiplied by an appropriate correlation "window" distribution.

The probability of failure, Eq. (3), corresponds to a given value of the initiation parameter  $\theta$ . The current MRP model uses a Monte Carlo analysis in which sampling is done over the whole distribution of Weibull  $\theta$  to get an "average" for all plants. This is equivalent to integrating Eq. (3) over  $\theta$ :

$$P(t_f < T) = \int_{\theta_{\min}}^{\theta_{\max}} f(\theta) \left[ \int_0^T p(t | \theta) P_c(t_f < T - t) dt \right] d\theta. \quad (5)$$

where  $f(\theta)$  is the probability density function for  $\theta$ .

The calculation of  $P(t_f < T)$  through Eq. (3) incorporates the main probabilistic variables—time to initiation and time to failure directly. The calculation can be built into a Monte Carlo loop to consider other parameters such as the range of values for  $\theta$ , yield stress effects on  $K$ , and other uncertainties. The Monte Carlo runs then would give distributions of probability of failure, and one could choose what percentile is appropriate for the decisions being considered. Since the variability due to variations in  $\theta$  appear to be much larger than that due to variations in the yield stress,  $\theta$  is considered as the primary variable of interest in the calculations presented here. Instead of a formal analysis using a distribution for  $\theta$ , point estimates are obtained for the range of  $\theta$  of interest, but they are not rigorously chosen 95th and 5th percentile values.

#### Parametric Studies on Center Nozzles

Because at present  $K$  solutions from EMC<sup>2</sup> are available only for center nozzles, the initial parametric studies focused on center nozzles. The particular case considered assumes that there are five nozzles from a particular heat, and only the probability of failure due to the failure of one of those nozzles is evaluated. Figure 5 illustrates the effect of the choice of the  $K$  solution. Because for the EMC<sup>2</sup> base case the circumferential growth of the primary crack is expected to be the dominant contributor to the circumferential expansion of the cracked region only for fairly large cracks, the initial crack size was taken to be 60°. The variation in  $K$  values gives rise to about a factor of 3 variability in the probability of failure.

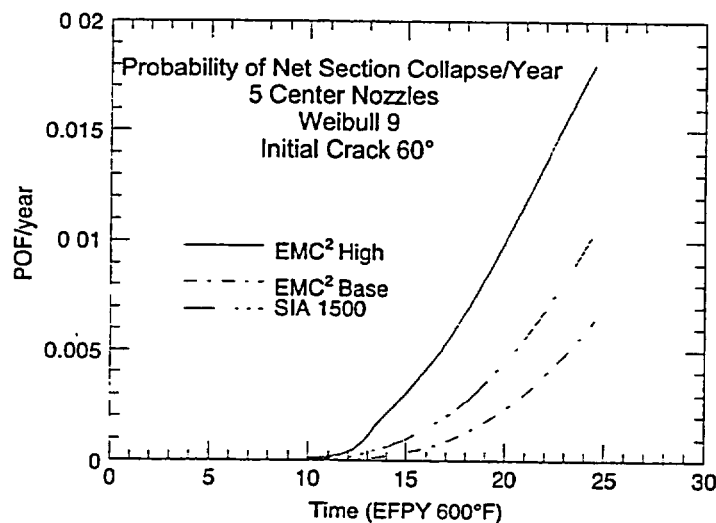


Figure 5. Effect of the choice of  $K$  solution on the probability of failure (POF) per year for 5 center nozzles with a Weibull  $\theta$  for initiation of leakage of 9 years.

Figure 6 shows the effect of initial crack size. Two initial crack sizes, 30° and 60° are considered. For the EMC<sup>2</sup> high and the SIA  $K$  solutions, the effect of the different crack sizes is small, less than a factor of two. It is much more significant for the EMC<sup>2</sup> base  $K$  solutions, as expected from the deterministic calculations in Table 1. However, this apparent decrease in the probability of failure may not be real, since it does not take into account the possibility of other modes of expansion for the circumferential crack.

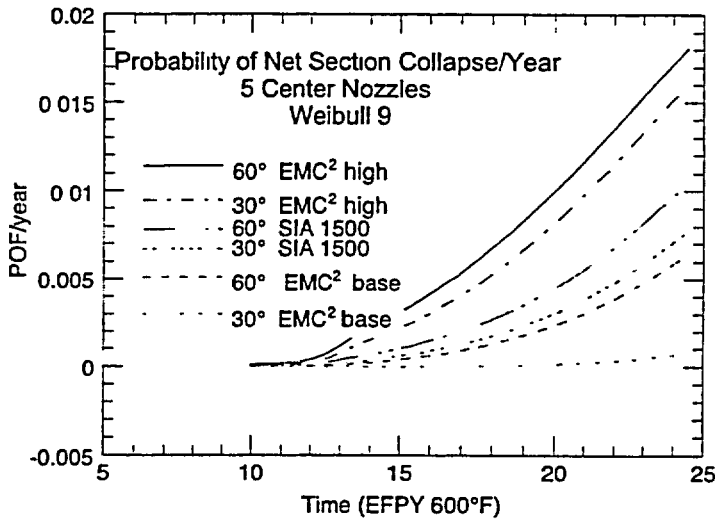


Figure 6.  
Effect of the initial crack size on the probability of failure per year.

Figure 7 shows the effect of the choice of the correlation "window". There is a very dramatic change depending on how effectively the "window" cuts off the high end of the CGR distribution curve. Assuming a high degree of correlation makes the "worst" plants worse, but leads to much lower estimates of the probability of failure for plants with lower susceptibility to crack initiation. The choice of the "window" has less effect on the worst plants, since any reasonable correlation "window" would include a significant contribution from the high end of the CGR distribution.

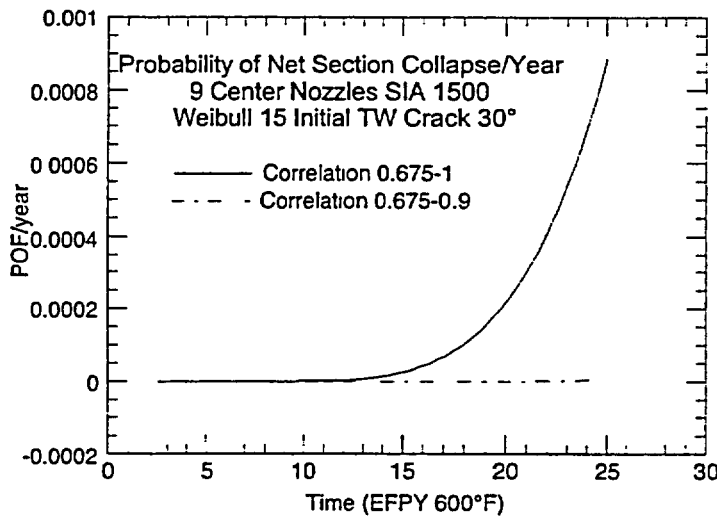


Figure 7.  
Effect of the choice of the correlation "window" on the probability of failure for plant with a "typical" Weibull initiation value.

Estimates of the probability of failure of a head

Because results for hillside nozzles are not yet available from EMC<sup>2</sup>, calculations for the probability of failure of an entire head use the SIA distributions for K. The current calculations take no credit for inspections. The calculations were done for Weibull parameter values of 15 years and 9 years, representing a "typical" case and a "bad" case. The correlation "window"

corresponds to the uniform distribution shown on the right in Fig. 4b, which includes the "tail" of the CGR distribution and is probably quite conservative for the "typical" case, but realistic for the "bad" case. The results for the Weibull parameter of 15 years, shown in Fig. 8, are about a factor of 2 higher than the MRP results, which represent an "average" plant. The difference between the calculations may reflect the differences in the choice of correlation "windows". The correlation "window" for the MRP approach has not been defined explicitly but probably resembles the Gaussian-like "window" on the left in Fig. 4b.

Calculations with a correlation "window" with a cutoff at 0.9 (the middle distribution in Fig. 4b) reduce the probabilities shown in Fig. 8 by a factor of >50.

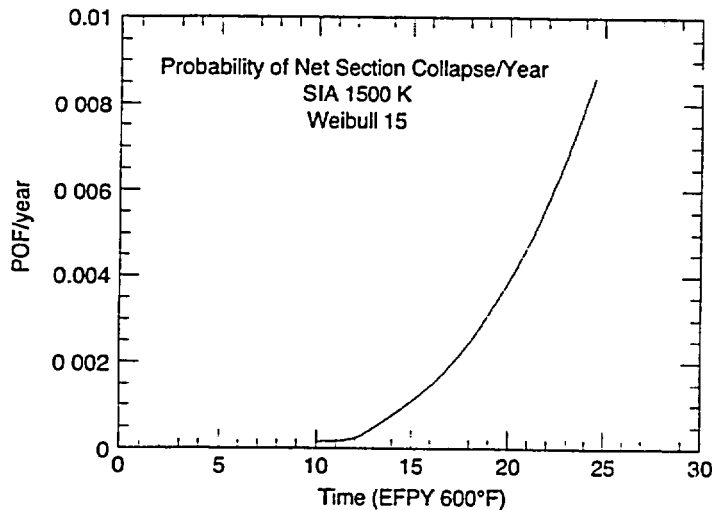


Figure 8. Probability of failure for a vessel head with a Weibull parameter for the initiation of leakage of 15 years.

The results for the Weibull parameter of 9 years are shown in Fig. 9. At 25 EFPY, the probability of failure is about a factor of 7 higher than the case for the more typical plant with a Weibull  $\theta$  of 15 years.

The integrated model can also be modified to consider the probability of occurrence of a large (> 160°) crack. The cumulative probabilities of a large crack are shown in Fig. 10 and also would be expected to vary widely among plants.

The MRP has suggested that inspection of reactor vessel heads should be risk informed. They suggest a three region approach based on probabilities of head failure of  $10^{-3}$  and  $10^{-4}$ /year. The MRP calculations of the probabilities of failure are based on the behavior of an "average" plant and are shown as the heavy solid and short dashed curves in Fig. 11. The ranges of times needed to reach  $10^{-3}$  or  $10^{-4}$ /y are also shown for plants with  $\theta$  values for initiation to leakage ranging from 9 to 21 years. Predictions based on "average" behavior may not be representative of all plants.

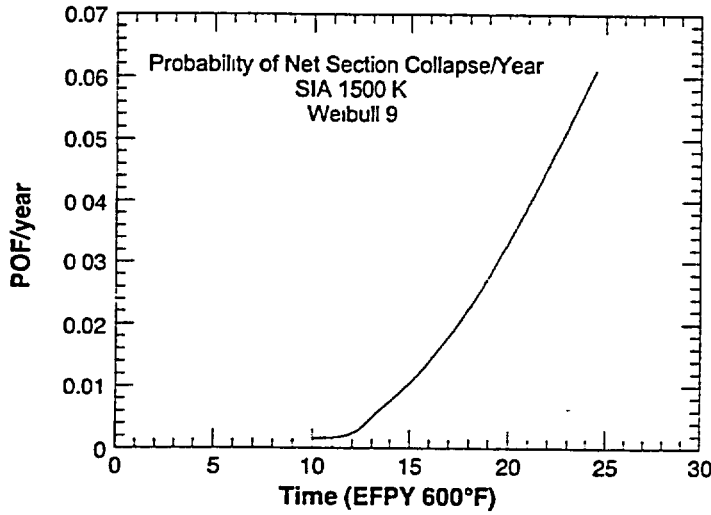


Figure 9.  
Probability of failure for a vessel head with a Weibull parameter for the initiation of leakage of 9 years.

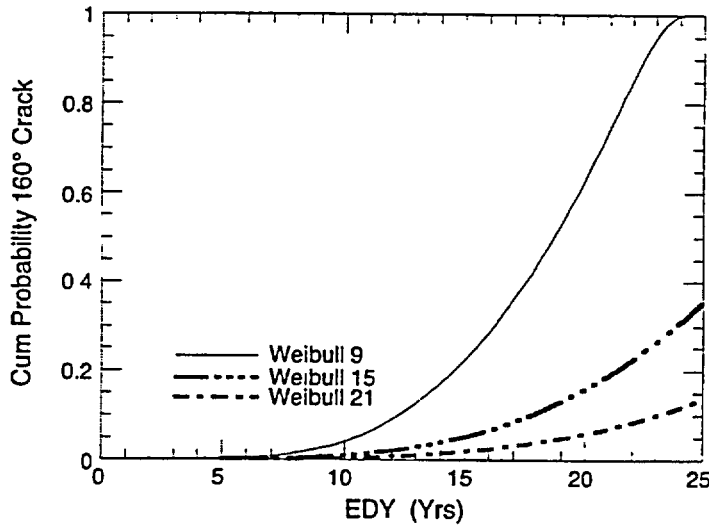


Figure 10.  
Cumulative probability of the occurrence of a large (> 160°) crack for Weibull  $\theta$  values of 9, 15, and 21 years. EDY are effective degradation years, i.e., years of operation at 600°F (316°C) equivalent to the actual operating time at the actual operating temperature.

As noted previously, the slope for Weibull distribution for the initiation of leakage has been taken as 3, based on data for the initiation of PWSCC in laboratory test specimens. This assumption would seem reasonable, but the initiation of PWSCC is only one step in a process that actually leads to leakage. The limited data available from repeated inspections suggest that values of  $b > 3$  may be possible, although the apparent higher rate of initiation may be an "inspection transient." Parametric calculations for  $b$  equal to 3 and 6 are shown in Fig. 12. Higher values of  $b$  would imply more margin in time for a first inspection, but a more rapidly increasing degradation rate as the head ages.

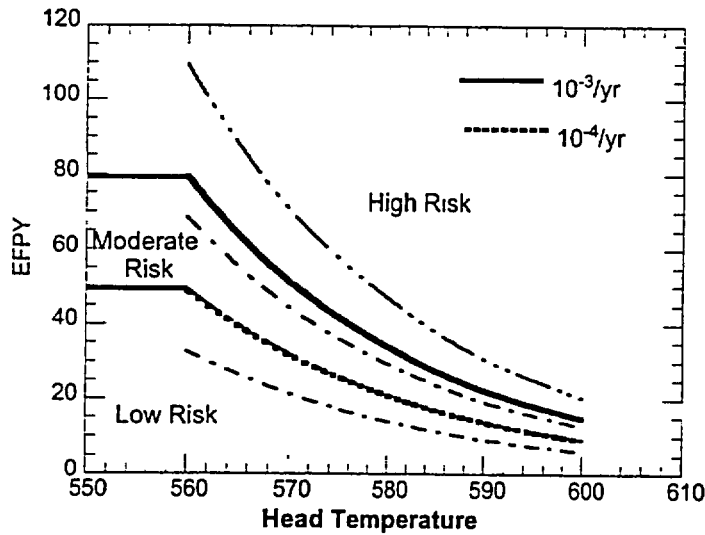


Figure 11. Probabilities of failure per year as a function of operating head temperature ( $^{\circ}\text{F}$ ) and effective full power years (EFPY) of operation. The triple dash curves show the expected range of operating times needed to reach  $10^{-3}/\text{yr}$  (the lower triple dash curve is nearly coincident with the  $10^{-4}/\text{y}$ ). The single dash curves show the range of times needed to reach  $10^{-4}/\text{y}$ .

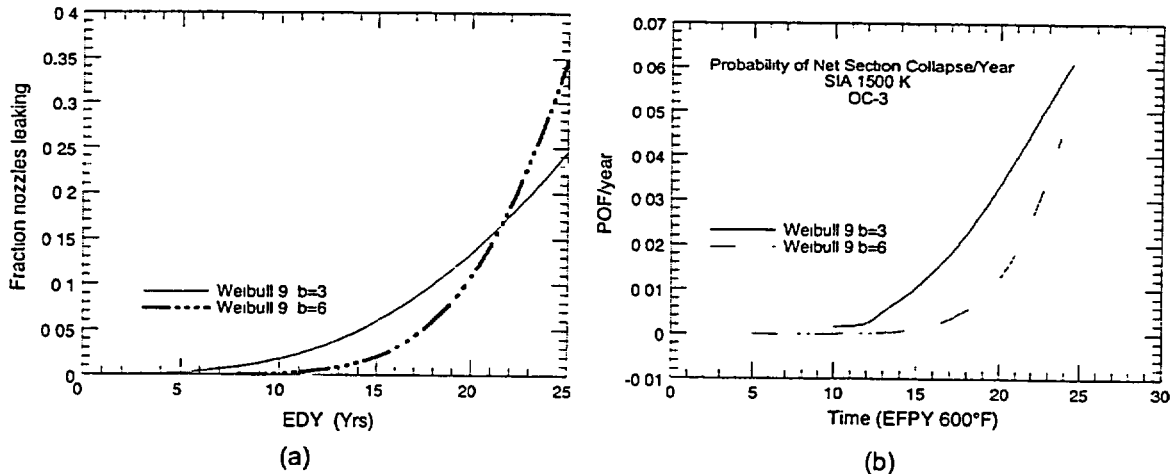


Figure 12. Effect of changing Weibull slope  $b$  on (a) the fraction of nozzles leaking for a head with a Weibull  $\theta$  of 9 and (b) the probability of failure for a head with a Weibull  $\theta$  of 9.

#### References

1. P. M. Scott, "Prediction of Alloy 600 Component Failures in PWR Systems," *Proceedings of the CORROSION/96 Research Topical Symposia 1996*, National Association of Corrosion Engineers (NACE), Houston, 1996.
2. J. Gorman, R. Staelhe, and K. D. Stavropoulos, *Statistical Analysis of Steam Generator Tube Degradation*, EPRI NP-7493, EPRI, Palo Alto:1991.
3. *Materials Reliability Program (MRP) Crack Growth Rates for Evaluating Primary Water Stress Corrosion Cracking (PWSCC) of Thick-Wall Alloy 600 Materials (MRP-55) Revision 1*, EPRI, Palo Alto, CA, TR-1006695, 2002.

4. P. M. Scott "An analysis of primary water stress corrosion cracking in PWR steam generators," *Proc. NEA/CSNI-UNPEDE Specialist Meeting on Operating Experience with Steam Generators*, Paper 5.6, Brussels, 16-20 September 1991.

EPRI Materials Reliability Program for Alloy 600  
Larry K. Mathews

Abstract

The Alloy 600 Issues Task Group of the EPRI managed Materials Reliability Program (MRP) initiated an industry program to address the generic aspects of the Alloy 182 weld cracking in the A hot leg nozzle weld at V. C. Summer and the cracks in the Alloy 600 Control Rod Drive Module (CRDM) and thermocouple (T/C) nozzles at Oconee 1. Further cracking in head penetrations at other pressurized water reactors and the corrosion of the vessel head at Davis-Besse have further emphasized this need for a concerted industry effort.

The MRP program was established to address these areas and has evolved significantly as more information has become available. It includes activities in assessment and management of the issue, inspection capability, and repair and mitigation. Because of the safety implications of these issues, the Nuclear Regulatory Commission has issued several NRC Bulletins and other generic communications. The MRP program also includes work to assist utilities in responding to these bulletins. Long term activities to provide utilities with appropriate tools for managing the PWSCC of reactor head penetrations are planned.

## INTRODUCTION

Inspections at Pressurized Water Reactors (PWR's) in the United States have yielded unexpected results in every outage season since the fall of 2000. That fall, at V. C. Summer Nuclear Station, a small leak in the Alloy 182 weld between the low alloy steel nozzle of the reactor vessel and the 29-inch stainless steel pipe of the hot leg was discovered. Also, a leaking Control Rod Drive Mechanism (CRDM) head penetration and leaking thermocouple nozzles were discovered at Oconee 1 during the November 2000 refueling outage. The Alloy 600 Issues Task Group of the EPRI managed Materials Reliability Program (MRP) initiated an industry program to address the weld cracking and the generic aspects of the head penetration cracking issue in December 2000. The Task Group originally organized into subcommittees addressing safety assessment, inspection, and repair and mitigation. The first activities of the Group were preparation of an interim safety assessment for both the weld cracks and the cracking in the head penetrations.

## EVOLUTION OF INDUSTRY PROGRAM

In the spring of 2001, circumferential flaws above the J-groove attachment weld of the head penetrations were discovered at two of the Oconee units, and a leaking penetration was found at Arkansas Nuclear One (ANO) Unit 1. See Figure 1 for a general description of the head penetrations. The main form of cracking discovered worldwide in the Alloy 600 nozzles between 1991 and these events had been axially oriented cracks. Because of this, there had been little concern from a safety standpoint. Axial cracks in the CRDM penetrations could eventually lead to leaks if they grew through wall, but would not directly result in an accident. The circumferential cracking discovered at the Oconee units presented the potential safety issue of penetration failure, leading to a small break Loss of Coolant Accident (LOCA) and possibly a control rod ejection event. Even though these are analyzed events in the Final Safety Analysis Reports of all PWR's, the safety significance of the new crack locations and orientations had to be addressed.

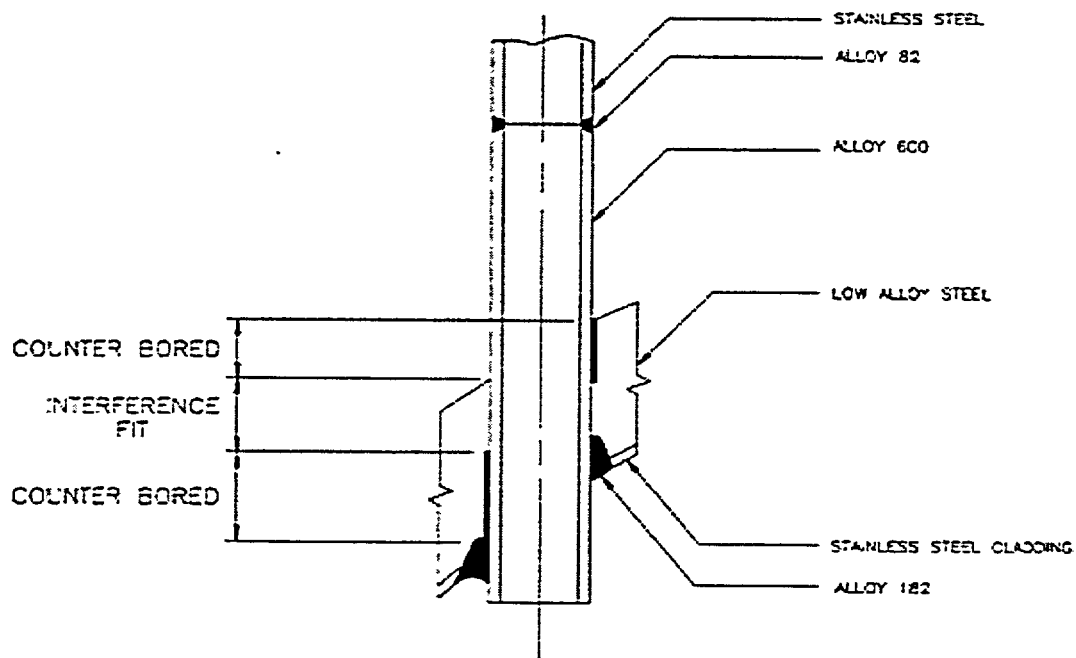


Figure 1. General Description of Reactor Vessel Head CRDM Penetration

During the spring 2001 outage season, the MRP was in the process of preparing an interim safety assessment of cracks in the head penetrations. A ranking of plants similar to that prepared in response to Generic Letter 97-01 [1] was desired, and an initial model for ranking was developed that used only the head temperature and the operating time for each unit. An effective operating time, measured in EFPY, was calculated for each unit. This was normalized to a head temperature of 600° F, using the Arrhenius equation with

an activation energy of 50 Kcal/mole. Oconee 3, the unit with the worst experience to date, was chosen as the benchmark, and the remaining EFPY for each unit to reach the equivalent time-at-temperature as Oconee 3 was calculated. The units were then sorted based on their remaining time, and a histogram was constructed. Figure 2 represents this ranking of the units at that time. The four units that had already found leaks were among the highest ranked units in this time-at-temperature ranking, lending credibility to the process.

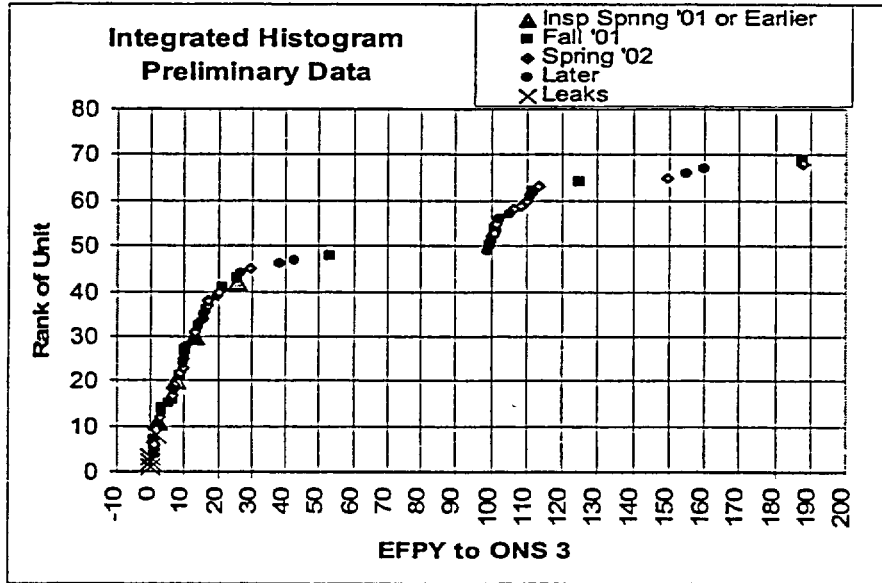


Figure 2. Initial Ranking of Units Relative to Oconee 3

In March, 2001, a recommendation [2] was made to all plants that particular attention be paid when performing boric acid walk-downs near Alloy 82/182 welds because of the V. C. Summer issue and also around the vessel head because of the experience at Oconee and ANO 1. In April 2001, the MRP recommended that a “best effort” visual inspection be made of the top of the vessel head for those plants with spring outages and less than 10 EFPY from Oconee 3. By the time the models had been developed, the plants ranked, and the recommendations issued, some of those units were either already back to power or were in or very near startup. Other units had insulation that severely restricted the ability to perform visual examinations. Very thorough visual exams were performed at several units, however, and limited visual exams were performed at some other units. No other units detected evidence of leakage in the spring of 2001.

In May 2001, the MRP submitted to the NRC MRP-44 Part 2 [3]. This report was an interim safety assessment for head penetrations. It presented the concept of a time-at-temperature ranking of the units to determine which units were most susceptible, and presented an assessment of the significant structural margin that remained at Oconee 3 at the time of the discovery of the circumferential cracks. A preliminary assessment of the interference fit designs in the industry concluded that a sufficient gap at operating

conditions would be present such that most nozzles would be expected to show evidence of leakage if a through wall flaw occurred. The report concluded there was no significant near-term impact on plant safety, but recommended visual examinations for those plants less than 10 EFPY from Oconee 3 with fall outages. Recommendations for future actions included an assessment of inspection technology, an assessment of crack growth rate data by an expert panel, and a workshop to advise the industry on the recent events. The workshop was conducted in June 2001 and the other activities have proceeded.

NRC Bulletin 2001-01 [4] was issued on August 3, 2001, as a one-time request for information from all PWR units relative to their inspection plans. The NRC requested a graduated examination effort that went beyond the initial recommendations of the MRP. Units that had detected cracks should perform a volumetric examination of all the head penetrations by the end of 2001; units less than 5 EFPY from Oconee 3 should perform "qualified" visual examinations of the top of the head by the end of 2001; and units between 5 and 30 EFPY from Oconee 3 should perform "effective" visual examinations at the next refueling outage. An "effective" visual examination should not be compromised by the presence of insulation, existing deposits on the head, or other factors that could interfere. A "qualified" visual examination further required a plant-specific demonstration that a through-wall crack would provide sufficient leakage to be identified by a visual inspection. To assist utilities in responding to the bulletin, the MRP prepared and submitted MRP-48 [5] on August 21, 2001. This report provided updated rankings and design information on head penetration configurations for utilities to reference in their individual submittals.

The examinations that were requested by the NRC in Bulletin 2001-01 presented various difficulties for several utilities. Some of the requested examinations would have required unscheduled shutdowns to perform, and others were particularly difficult to do in the proposed time frame because of the difficulty of insulation removal and the lack of time for planning. These individual utilities proposed various alternatives and presented justifications for their proposed actions to the NRC during the fall 2001 outage season.

Visual examinations were conducted at several units, with no evidence of leakage reported. However for other units, either leaking penetrations were found, or boric acid deposits on the head necessitated non-visual examinations to determine the source of leakage. The visual examination techniques included direct observation where possible and remote visual examinations under the reflective insulation panels using either video probes or remotely operated video cameras. Non-visual examinations consisted of eddy current or ultrasonic examinations from the inside surface of the penetration tubes. Examinations of welds and the outside of the penetration tubes below the head was performed by eddy current or liquid penetrant methods. Some of the non-visual examinations confirmed leaks, but one unit found shallow non-leaking inside surface cracks that were evaluated and found suitable for a limited period of continued operation. Circumferential cracks above the attachment weld were discovered at two units. All leaking penetrations were repaired and the units returned to service. Two units (Cook 2 and Davis-Besse), because of refueling outage schedules, eventually delayed the inspections requested by Bulletin 2001-01 into early 2002.

The most significant issues arising from the fall 2001 inspections included:

- 1) Discovery of several leaking penetrations during a re-inspection after only a few months of operation, including one with a circumferential flaw above the attachment weld
- 2) Significant circumferential flaws were discovered in the weld metal at two units.

The MRP had developed a Strategic Plan to manage Alloy 600/82/182 corrosion. It contained a strategy and approach for the following areas; Alloy 600/82/182 primary system butt welds, reactor pressure vessel (RPV) head penetrations, all other Alloy 600/82/182 locations (except steam generator tubes), and an Alloy 600 management guideline for all locations. As a part of this strategic approach, the MRP was also developing a detailed inspection plan for RPV head penetrations along with the technical bases to support the plan.

In the early 2002, Cook 2 performed a complete visual and non-visual inspection of the RPV head. Cook 2 had discovered a part through wall axial crack in one penetration in 1994 and had repaired that crack through excavation and weld repair in 1996. Based on accelerated laboratory testing that had been performed by the industry, in which cracks in tube base metal developed at the edge of a repaired area, indications associated with the repaired area could have been reasonably expected. The 2002 inspection showed no indications, even around the repair area.

An inspection at Davis-Besse in late February and early March of 2002 revealed the presence of a significant cavity in the low alloy steel pressure boundary material adjacent to a cracked and leaking penetration. This type of wastage had not been expected because the high temperature of the vessel head was expected to quickly drive away any moisture and the very low corrosion rates are associated with dry boric acid powder. It appears that a significant amount of accumulated deposits and the magnitude of the leak allowed concentrated liquid boric acid to remain in contact with the low alloy steel for a significant period of time. The cavity in the head extended all the way to the stainless steel cladding on the inside of the head and progressed most of the way toward an adjacent penetration.

As a result of the Davis-Besse findings, the NRC issued Bulletin 2002-01 [6] in March, 2002, requesting information relative to vessel head conditions and boric acid corrosion control programs. Also, the MRP responded to the incident by sending two people from EPRI and one of the MRP contractors to participate on the root cause analysis team. The MRP also performed an industry survey to categorize plants relative to their RPV head conditions, especially relative to any boric acid deposits. A checklist for plants to use in preparing their 60-day response to Bulletin 2002-01 was distributed and the MRP created a root cause review team to review reports generated by the Davis-Besse root cause team for generic implications for the PWR fleet. The MRP continues to monitor progress of

the various investigations that are underway and lessons that are being learned from the incident.

The survey that the MRP performed indicated that all units at less than 10 EPFY from Oconee 3 would have inspected their RPV heads by the end of spring in 2002. This included the twenty highest ranked units in the United States and would provide reasonable assurance of no significant corrosion of the head or CRDM leakage. Also, 34 out of the 45 plants at less than 30 EPFY from Oconee 3 would have performed inspections by the end of spring in 2002. Of the remaining eleven units, six were scheduled for fall 2002 outages and only five would remain to be inspected in Spring, 2003. The MRP concluded that the visual inspections would be capable of identifying leakage prior to significant head wastage and that any plants that identified through-wall flaws need to ensure that wastage has not occurred.

A slight modification to the ranking process was developed at this time based simply on years of operation, normalized to a head temperature of 600° F. This term was designated Effective Degradation Years (EDY) and may be a more appropriate ranking for wastage potential, since a leaking crack can be as important from a wastage standpoint as a large circumferential flaw in a penetration from a nozzle ejection standpoint. EDY is independent of the Oconee 3 unit, the original benchmark unit. Figure 3 presents the initial ranking based on EDY.

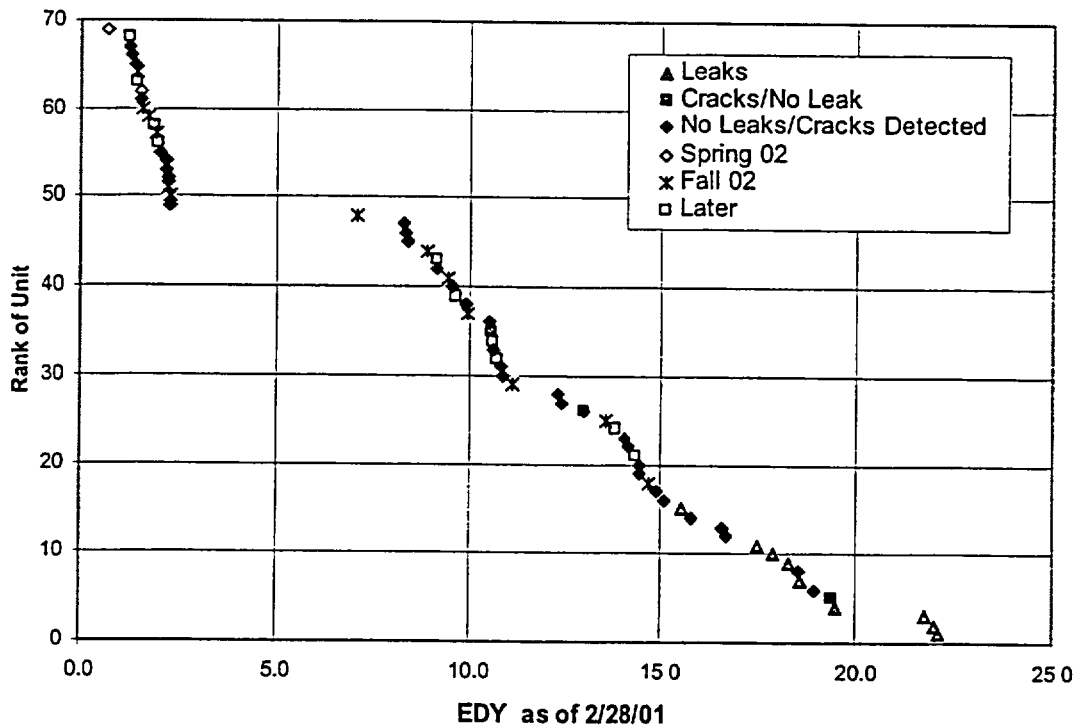


Figure 3. Ranking of Units Based on Effective Degradation Years

Throughout the spring and summer of 2002, the MRP continued to develop an inspection plan for head penetrations. After discussions with the NRC, it was agreed that the plan would address the corrosion of the vessel head material in addition to nozzle ejection from circumferential cracks. MRP-75 [7] was submitted to the NRC in September, 2002, documenting the proposed plan and the technical bases for it. This inspection plan provided guidance and the basis for a graduated degradation management program for RPV head penetrations. It requires inspections to allow early detection of leakage or degradation prior to challenging structural integrity. In the plan, the MRP defined low susceptibility plants as those with less than 10 EDY accumulated, moderate susceptibility plants as those between 10 EDY and 18 EDY, and high susceptibility plants as those with greater than 18 EDY or a leaking penetration. Inspection requirements and frequencies were defined, depending on the susceptibility of a given unit. Included in the document were three technical basis documents addressing the probabilistic fracture mechanics analysis that formed the main basis for protection against circumferential flaws in the nozzle tube, the probability of leak detection via bare metal visual examinations, and the adequacy of a proposed supplemental visual inspection schedule to ensure low risk of rapid corrosion of the low alloy steel head.

The MRP had mockups constructed of head penetration nozzles with embedded flaws for use by the NDE vendors in demonstrating their inspection capabilities. These demonstrations took place in August and September of 2002.

In the meantime, the NRC issued Bulletin 2002-02 [8] in August, 2002. This bulletin conservatively specified an acceptable inspection program which required more comprehensive and more frequent examinations than the plan laid out by the MRP in MRP-75, and which lowered the thresholds for susceptibility categorization from 10 EDY to 8 EDY and from 18 EDY to 12 EDY. In the near term, the bulletin requested visual, volumetric, and surface examinations at the next outage for all plants greater than 12 EDY, with similar exams within a few years for lower susceptibility units.

All fall 2002 outage units greater than 12 EDY have, or are, performing bare metal visual examinations and non-visual NDE of their heads. Other plants have responded to the Bulletin with varying commitments, but many committed to follow the MRP's recommended inspection program.

Inspection results from the fall outages again included results which were different than had been expected, based on previous inspections and analyses. North Anna 2 found cracks in almost all of the J-groove attachment welds, visual indications of leakage from a previously repaired nozzle, and circumferential flaw indications in nozzle tubes with no visual evidence of leakage on top of the head. Oconee 2 inspections revealed several new leaking penetrations, and ANO 1 found the nozzle they had previously repaired in 2001 to be leaking again.

These results bring into question some of the previous assumptions. The circumferential indications, some of which were very near the root of the J-groove weld, at least call into question the previous industry position that cracks would be detectable via top of the head visual inspections before circumferential flaws in the nozzle tubes would develop. The leaks from previously repaired nozzles require an explanation to justify continued use of the repair techniques.

Another interesting result was the fact that no indications were discovered at Farley 2 which had the same heat of material as the penetrations that had cracked extensively at Oconee 3 and Davis-Besse. While Farley 2 is ranked slightly behind Oconee and Davis-Besse in EDY, it has accumulated enough time that indications of early crack initiation could have been anticipated, yet none were found.

### CURRENT ACTIVITIES

Currently the MRP is reviewing data from the fall 2002 inspections for the overall implications to the safety assessments and proposed inspection plans. Specific questions relate to the continued reliance on bare metal visual exams for detection of cracks, the probability of leakage assumptions and implications for the risk assessments, and the recommended timing of non-visual NDE examinations. The MRP continues to evaluate the research needs, including possible removal of samples from replaced RPV heads, and to complete the final safety assessment. Additionally, the inspection demonstration program will continue, with improvements where possible, and the Alloy 690 data and archival needs will be assessed.

### REFERENCES

- [1] NRC Generic Letter 97-01: Degradation of Control Rod Drive Mechanism Nozzle and other Vessel Closure Head Penetrations, US Nuclear Regulatory Commission, Office of Nuclear Reactor Regulation, April 1, 1997.
- [2] Bailey, J., "MRP 82/182 Weld Integrity Inspection Committee, Short Term Inspection Guidance," MRP-2001-015, letter to MRP Senior Representatives, March 1, 2001.
- [3] PWR Materials Reliability Program, Interim Alloy 600 Safety Assessments for US PWR Plants (MRP-44): Part 2: Reactor Vessel Top Head Penetrations, EPRI, Palo Alto, CA: 2001. TP-1001491, Part 2.
- [4] NRC Bulletin 2001-01: Circumferential Cracking of Reactor Pressure Vessel Head Penetration Nozzles, US Nuclear Regulatory Commission, Office of Nuclear Reactor Regulation, August 3, 2001.
- [5] PWR Materials Reliability Program Response to NRC Bulletin 2001-01 (MRP-48), EPRI, Palo Alto, CA: 2001. 1006248.
- [6] NRC Bulletin 2002-01: Reactor Pressure Vessel Head Degradation and Reactor Coolant Pressure Boundary Integrity, US Nuclear Regulatory Commission, Office of Nuclear Reactor Regulation, March 18, 2002.
- [7] PWR Reactor Pressure Vessel (RPV) Upper Head Penetrations Inspection Plan (MRP-75): Revision 1, EPRI, Palo Alto, CA: 2002. 1007337.

[8] NRC Bulletin 2002-02: Reactor Pressure Vessel Head and Vessel Head Penetration Nozzle Inspection Programs, US Nuclear Regulatory Commission, Office of Nuclear Reactor Regulation, August 9, 2002.



**Inservice Inspection of PWSCC in Alloy 600\182\82 Material**  
**Steven R. Doctor**  
**Pacific Northwest National Laboratory**  
**Deborah A. Jackson**  
**U. S. Nuclear Regulatory Commission**

**Abstract**

In the past several years there have been a number of occurrences of primary water stress corrosion cracking (PWSCC) in pressurized water reactor (PWRs) containing Inconel alloy 600 and both 182 and 82 welds. The PWSCC degradation has been found in the main coolant nozzles (V. C. Summer) and in many control rod drive mechanism (CRDM) head penetrations (Ocone, North Anna, etc.). This paper provides background information on this degradation process, discusses the inspections being conducted to detect this degradation, provides results from related research and describes the USNRC research efforts being pursued to address this issue.

**Background**

In the past several years there have been a number of occurrences of primary water stress corrosion cracking (PWSCC) in pressurized water reactor (PWRs) containing Inconel alloy 600 and both 182 and 82 welds. This material degradation has been detected in the main coolant outlet nozzles of PWRs and in the control rod drive mechanism (CRDM) head penetrations. One of the most significant aspects of these recent failures is that they resulted in through wall cracking and in the case of Davis-Besse the aggressive attack of the surrounding ferritic steel vessel head. An USNRC Office of Nuclear Regulatory Research program (JCN Y6604) is being conducted at the Pacific Northwest National Laboratory (PNNL) and one task of this program is to address the reliability of inservice inspection (ISI) to reliably detect and accurately characterize PWSCC in these susceptible components. This includes the review and assessment of current industry practice, assessment of evolving nondestructive evaluation (NDE) techniques, the assessment of conducting reliable volumetric inspections of the CRDM j-groove weld, assessing the potential to detect and accurately characterize voids in the ferritic steel behind CRDM nozzles, and to assess the effectiveness of visual testing (VT) for boric acid deposits.

Cracking in CRDMs was first reported in the early 1990s at the French reactor Bugey. This cracking was located on the inner diameter (ID) of the CRDM nozzle. Special saber or blade probes were developed to allow the inspection of the CRDM nozzles by inserting these probes between the thermal sleeve and the CRDM nozzle. Because the PWSCC initiated from the ID of the CRDM, eddy current probes were found to be very effective in detecting cracks. Ultrasonic techniques were developed to provide the capability to depth size the detected cracks.

During 2000 there were two new cases of PWSCC that were detected that caused a whole new level of concern about degradation of Inconel. These two cases occurred at about the same time but at two different U. S. reactors. The first was detected when the V. C. Summer reactor shut down for a refueling outage and during the walk down discovered large deposits of boric acid. The source of the boric acid leakage was found to be PWSCC in the loop A hot leg nozzle to pipe dissimilar metal weld. There were a number of predominately axial cracks in this

weldment with one axial crack that spanned from the 508 forging to the austenitic pipe. The crack was arrested at both the forging and the austenitic pipe material. The PWSCC was located in the Inconel weld buttering and structural weld but only came through wall at the center of the weld crown. This weld was inspected on a 10-year basis during the reactor pressure vessel ISI and thus, the inspection was conducted from the ID. The ID geometry presented some challenges because there was a change in diameter between the nozzle and the pipe, the root of the weld varied from a concave to a convex shape, the counterbore transition started at about 25 mm on each side of the weld centerline. In addition a number of repairs had been made to this weld during construction with some of these going all the way to the ID. All of these factors made it a challenge to effectively inspect this weld. The only other reported incident of cracking in PWR primary circuit piping was at Sweden's Ringhals plant. In this case the cracking was detected while it was shallow and boat samples were removed to verify the cracking process. ISI is being used to continually track the flawed area to determine if the PWSCC has been arrested or if it will re-initiate.

The second case of PWSCC cracking was at Oconee 2 where boric acid was detected on the head of the vessel. Further testing resulted in the identification of a several cracked CRDMs. One unique feature of this cracking was that some of it occurred along the J-groove to CRDM nozzle fusion area of the penetration leading to circumferential outer diameter (OD) PWSCC initiating on the nozzle above the J-groove weld. A major concern about this cracking was its location above the J-groove weld, which raised the possibility of a CRDM ejection during operation. The PWSCC was located on the OD of the CRDM and it cracked along the fusion zone of the J-groove weld and the CRDM nozzle. Since that time a number of reactors have discovered PWSCC in their CRDMs. Some of the cracking has been discovered to occur in the J-groove weld while in other cases the cracking is associated with the buttering. In 2002 another problem associated with CRDM cracking was uncovered at Davis-Besse where the leakage lead to a very aggressive attack of the surrounding ferritic steel head producing a cavity approximately 125 mm by 125 mm by 175 mm. The only material containing the reactor operating pressure was the stainless steel cladding and it was dimpled upwards about 3 mm and there were some cracks in this cladding.

These incidents raised concerns about the integrity of components manufactured with Inconel. PWSCC is not understood including the factors that control crack initiation and growth rate. There seems to be some limited correlations with particular CRDM nozzles heats being more susceptible and that some fabrication techniques can lead to J-groove weld contaminates which accelerate cracking. This information provides some insights but it is not comprehensive and it does not explain what is happening. Some susceptible CRDM heats have cracked in one reactor but nozzles of the same heat in another reactor have not cracked. This problem has many similarities to the intergranular stress corrosion cracking (IGSCC) in boiling water reactors (BWRs) in the early 1980s. It was found in that case that there were many factors that influenced IGSCC initiation and growth with dominate factors being stress, the environment, and sensitized material. For PWSCC, these key factors are not known at this time and there is a need to conduct extensive laboratory testing and compilation of operating information in order to create a database from which definitive conclusions can be drawn. NDE is the first line of defense in detecting PWSCC and is used to manage it. Because most of the cracking occurrences have been associated with the CRDMs, this will be the focus of this paper. However, in out years on the program there are specific studies to more closely examine the reliability of inspecting dissimilar metal welds made with Inconel.

## Current ISI Practices

The strategy that industry has chosen to use relies on using a sequence of tests. The first test is to rely upon a visual test (VT) of the reactor pressure vessel head. If boric acid deposits are detected, then further NDE is required to determine the source of the leakage and this may involve a number of NDE techniques. When the reactor is shut down a robot with a TV camera is typically used to inspect the head around each CRDM looking for boric acid deposits. This is not always easy to conduct because of the limited clearance provided by some types of thermal insulation. There is also the problem of boric acid deposits related to leakage from CRDM mechanical seals located above the head, which can cause deposits that must be carefully evaluated to determine their source. There are also concerns related to whether a through wall leak around the J-groove weld will always lead to boric acid deposits on the head. The biggest concern about this strategy is that it waits until leakage of the primary circuit has occurred before it is pursued and resolved – unfortunately, this erodes one layer in the defense in depth of reactor operation.

The supplemental NDE that is employed consists of a number of different techniques which includes:

- UT from the inside of the CRDM nozzle
- ET from the inside of the CRDM nozzle
- PT of the entire nozzle wetted surface area including the J-groove weld
- ET of the J-groove weld crown

The industry through the Materials Reliability Program (MRP) has been developing mockups for ISI vendors to demonstrate that the NDE techniques chosen can be effective in detecting PWSCC and size it. Over the past several years the mockups have been changing because of the discovery of PWSCC in new CRDM locations. In addition the flaws that are being used for the demonstrations have evolved in order to provide a practical means to locate flaws at the failure sites found inservice and that have similar NDE response properties to real PWSCC in locations that are very difficult to access for implanting. These mockups have had a positive impact on the NDE techniques chosen and the means by which they are deployed. The MRP mockups are not intended to be like an ASME Section XI Code Appendix VIII performance demonstration test but are intended to challenge the procedures being used and provide confidence that if PWSCC were in a CRDM, the techniques would have a good likelihood of detecting it. In reviewing the mockups, the location of the flaws is certainly challenging but realistic based on service experience and the use of cold isostatic process (CIP) controls the NDE response of the flaws to much better simulate the NDE response from PWSCC detected in the field. The data supports the position that if the flaws are located in the CRDM nozzle, they stand a good chance of being detected. The only case where there is little evidence that PWSCC can be detected is if it is located entirely in the J-groove weld or the buttering. This is the classical far-side austenitic coarse grained inspection problem that has been and still is a challenge.

## Coarse Grained Material Inspection Studies

The term coarse grained materials refers to a number of austenitic stainless steel and Inconel weld configurations that are commonly found in many locations in light water reactor piping. PNNL has been conducting studies on these configurations for many years in order to assess the effectiveness of NDE to detect degradation in these components. One of these studies has dealt with the inspection of core shroud welds in boiling water reactors

(BWRs). These welds are either 304 stainless steel or Inconel alloy 600. This work is currently being prepared for formal publication in a NUREG/CR report this coming year. What will be included here is a brief summary of the work. The study consisted of 40 welded assemblies with 35 of them made from 304 stainless steel and 5 of inconel alloy 600. These specimens contained notches at various tilt angles, thermal fatigue cracks and weld solidification cracks. The specimens were all 50 mm thick and the weld profiles included single "V", double "V" and "K" designs. The study evaluated UT techniques for inspections from the ID and OD of the specimen for both near side and far side access.

Figure 1 shows the results for the most successful ultrasonic procedure used for the far side inspection of the specimens, which was based on utilization of phased array technology. This data shows that small cracks are very difficult to detect but as they approach 40% in through wall size the reliability improves dramatically.

PNNL has been conducting a special series of studies on the far side inspection of 304 austenitic stainless steel piping welds. In this study the techniques being evaluated include central ray transducers, phased arrays and low frequency synthetic aperture focusing technique for ultrasonic testing (SAFT-UT). The specimens being used in this study are 610 mm diameter by 36 mm wall thickness piping specimens. The results to date are very consistent with those reported in Figure 1 for the core shroud work. Further work is planned to study more cracks, remove the weld crowns to assess better inspection access, and evaluate the potential improvement and to evaluate further refinements of the phased array transducers (lower frequencies and shear wave mode), as well as refinements to the low frequency SAFT-UT transducers (using piezocomposites with the transducer size and bandwidth selected for optimal zone focused insonification).

The important conclusions from these studies are:

- Coarse grained materials are challenging to inspect
- Both shear and longitudinal wave modes are useful
- Imaging facilitates data interpretation
- Cracks on the far side can be reliably detected but not to ASME Section XI IWB-3500 sizes
- Crack depth sizing is very difficult

Figure 2 shows a specimen that is being used to study the inspection reliability of CRDM J-groove welds. This is a CRDM that was cut from the Midland reactor pressure vessel head by Framatome and provided to Oak Ridge National Laboratory and now has been provided to PNNL for inspection reliability assessment. The specimen was tested with fluorescent penetrant and found to be acceptable to ASME Section III Code requirements. As can be seen in this figure, the CRDM has been machined so that the ferritic steel and clad surrounding the CRDM nozzle is concentric with the nozzle. The further studies that are planned for this specimen will include conducting ultrasonic and eddy current inspections to characterize the J-groove weld, which will involve inspections from the ID of the nozzle, from the OD of the ferritic steel cylinder and from the crown of the j-groove weld. After the weld microstructure is characterized, further studies will be conducted to assess the capability to detect and to characterize reflectors at various locations in the J-groove weld and the buttering.

In addition alloy 600 sheet and tube material will be used along with ferritic reactor pressure vessel steel from canceled plants to conduct other studies on detecting and characterizing

flaws and cavities in the ferritic steel. This will include the assessment of eddy current and ultrasonic techniques and any other techniques that are found to be of potential value in detecting and characterizing degradation in these complex welds.

ISI work, industry studies and demonstrations will be followed and evaluated as part of this work. Efforts are being made by the NRC to set up an international cooperative to address these issues and leverage resources from many different countries on this very difficult inspection problem.

### Conclusions

Although the inspection of coarse grained materials is very difficult, there are improvements being made in NDE technology that need to be evaluated and advances in modeling are providing a better understanding of the wave propagation through coarse grained materials. The work described here provides the direction of the work that the NRC is funding to address this important inspection issue. At a minimum this work will provide quantitative guidance on the reliability with which degradation can be detected and the accuracy with which it can be sized with special emphasis on the J-groove weld

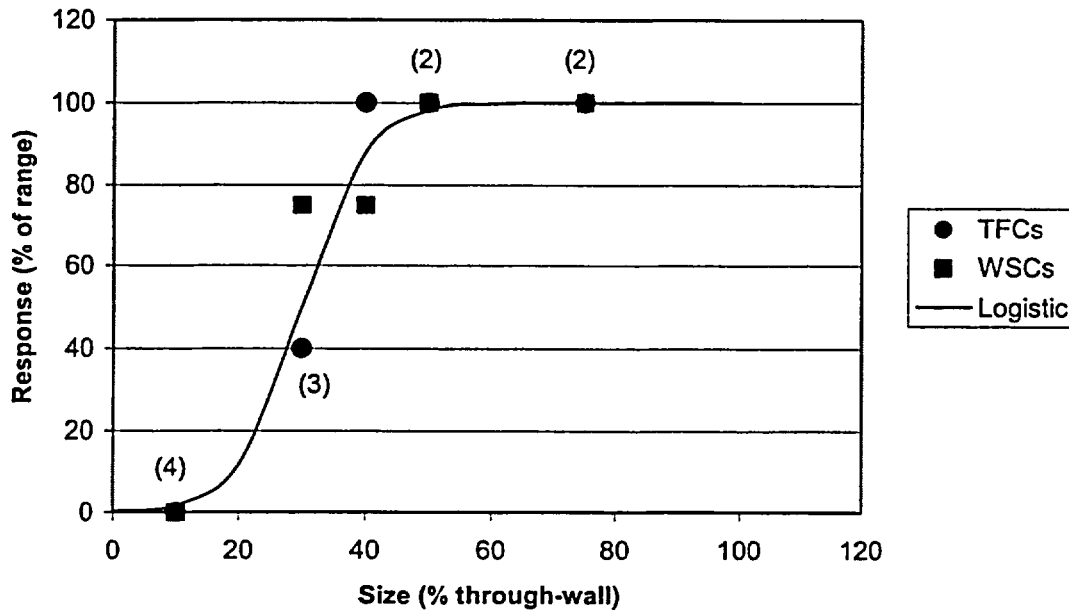


Figure 1. Core shroud study showing the performance of a phased array inspection.



Figure 2. Showing the Midland CRDM after machining in preparation for NDE studies.

# **Thermal-Hydraulic Research Issues Relevant to Advanced Light Water Reactors**

**Stephen M. Bajorek  
Senior Technical Advisor  
Division of Systems Analysis and Regulatory Effectiveness  
Office of Nuclear Regulatory Research**

**Nuclear Safety Research Conference  
October 28–30, 2002  
Washington, DC**

Currently, the staff is anticipating or is actively reviewing several advanced light water reactor designs; AP1000, ESBWR, SWR-1000, ACR-700, and International Reactor Innovative and Secure (IRIS). These designs offer significant improvements in safety by taking advantage of prior testing, analysis, and operational experience gained from existing plants. Advanced light water reactor designs generally rely on natural processes to insure that the core remains adequately cooled and containment integrity is maintained in the event of an accident. In some designs, the large break loss of coolant accident (LOCA) is eliminated and the limiting accident scenario becomes a small LOCA or transient.

While these new designs promise significant safety benefits, their unique features create new challenges to thermal-hydraulic analysis. Physical processes such as natural circulation with low driving heads, condensation in the presence of a non-condensable gas, and entrainment and de-entrainment play an important role in advanced plant accident scenarios. This paper discusses several thermal hydraulic issues that are important to advanced light water reactors and are being addressed as part of the staff's code development and review effort.

## Introduction

In 2002, there has been a re-emergence in licensing review activity for advanced light water reactors. Currently, the staff is anticipating or is actively reviewing several new designs; AP1000, ESBWR, SWR-1000, ACR-700, and IRIS. Table 1 summarizes the general design of each. These designs offer significant improvements in safety by taking advantage of prior testing, analysis, and operational experience gained from existing plants. Advanced light water reactor designs generally rely on natural processes to insure that the core remains adequately cooled and containment integrity is maintained in the event of an accident. In some of these designs, the large break loss of coolant accident (LOCA) is eliminated and the limiting accident scenario becomes a small LOCA or transient.

While these new designs promise significant safety benefits, their unique features create new challenges to thermal-hydraulic analysis. Physical processes such as natural circulation with low driving heads, condensation in the presence of a non-condensable gas, and entrainment and de-entrainment play an important role in advanced plant accident scenarios. The following sections discuss several thermal-hydraulic issues that are important to advanced light water reactors and are being addressed as part of the staff's code development and review effort.

Design	Applicant	Type
AP1000	Westinghouse	Passive PWR
ESBWR	General Electric	Passive BWR
SWR-1000	Framatome-ANP	Passive BWR
ACR-700	AECL	Light-Water Cooled, Heavy-Water Moderated PWR
IRIS	Westinghouse	Passive PWR

Table 1: Advanced Light Water Reactors

First, it is informative to ask the question, "Why are there thermal-hydraulic issues?" The nuclear industry has invested considerable resources in experimental test programs and in the development of advanced computational methods. One's initial expectation is that previous work should be sufficient to resolve any thermal-hydraulic problem. With advanced reactors, however, there are several reasons why new research may be necessary:

- (1) Most of these advanced reactors utilize novel design features. While engineering judgement leads to the conclusion that these new features are beneficial, they must be considered over a broad range of conditions. Because of a lack of operational experience, it is not clearly evident that the performance of new devices and passive safety systems is well understood.
- (2) Some accident scenarios are eliminated by design. In some cases for example, the traditional large break LOCA is not a possibility. As a result, the focus of attention shifts to a new critical accident scenario. For designs in which the large break LOCA analysis previously limited the core power, some other accident scenario must be identified and evaluated in detail.
- (3) Passive safety features generally result in a dependence on natural circulation and small driving heads. While this is a major objective of these new safety systems, thermal-hydraulic codes generally have difficulty in simulating transients that progress slowly and without large driving potentials. Small uncertainties in thermal-hydraulic models when propagated over long periods of time can result in large differences in predicted system performance. Thus, thermal-hydraulic code assessment needs may change for these new plant designs.
- (4) The state of the art in boiling, condensation and two-phase flow remains weak for some important physical processes. In spite of extensive research and development, it is difficult to assess with certainty processes such as subcooled nucleate boiling, flow pattern transition in rod

bundles, condensation in the presence of a non-condensable gas, and two-phase separation. Many correlations developed for boiling and two-phase flow are known to be geometry dependent, and the geometry and surface conditions change, existing models, and correlations may become very inaccurate.

### Thermal-Hydraulic Considerations

With the exception of the AP1000, the staff has not received extensive documentation on the new advanced designs. The AP1000 has been under review for some time, and the staff expects to begin writing a Safety Evaluation Report in 2003. The other designs (ESBWR, SWR-1000, ACR-700, and IRIS) are entering the pre-design certification stage. Discussions have been held with the applicants, and the designs have been described in several workshops. While these initial discussion and workshops have been useful and informative, a full assessment of research needs can not be made until formal documentation is submitted. Thus, in what follows, only a preliminary estimation of research needs is presented.

**AP1000:** The AP1000 is an advanced pressurized water reactor (PWR) that relies on passive systems for emergency core cooling. The basis for AP1000 performance was established in the review of the previously accepted AP600 design. Most of the test and analysis programs that supported AP600 also apply to the AP1000, which incorporates several modifications to accommodate the increase in core power. One of the key features of the AP1000 design is the Automatic Depressurization System (ADS), which acts to reduce primary pressure and increase the delivery of coolant to the vessel in case of an accident. Thermal-hydraulic processes that affect performance of the ADS and are of significant research interest include the hot leg flow patterns, entrainment from horizontal-stratified flows to the ADS, and entrainment and de-entrainment of water in the upper plenum. Each of these phenomena affect the two-phase pressure resistance in the ADS and the rate of mass loss from the primary system.

**ESBWR:** The ESBWR is an advanced boiling water reactor (BWR) that also relies on passive systems to maintain adequate core cooling. The design is similar to the SBWR design that received considerable attention from the staff in the early 90's. While that review was not completed, it serves an important role in defining the major thermal-hydraulic phenomena for an advanced BWR. Potential research issues include performance of the Passive Containment Cooling (PCC) heat exchangers, which must condense steam in the presence of non-condensable gas. Long term containment pressure is also affected by the distribution of non-condensables and phenomena that affect the wetwell vapor pressure. The close relationship between vessel and containment thermal-hydraulics may necessitate a coupling between codes now used to independently evaluate vessel and containment performance.

**SWR-1000:** The SWR-1000 is also an advanced, passive BWR. It has numerous similarities with the ESBWR, and as such, thermal-hydraulic phenomena with large uncertainties in ESBWR have high importance in the SWR-1000. Thus, condensation in the presence of a non-condensable gas and its impact on passive containment cooling is a likely candidate for additional research in SWR-1000. Also important in the SWR-1000 are the performance of several novel design features such as the Passive Pressure Pulse Transmitter, which is a novel device for actuation of various safety signals.

ACR-700: The ACR-700 is an advanced CANDU reactor, with the important distinction that the fuel is light-water cooled. Moderation is performed by heavy water in the calandria, the volume of which is significantly reduced compared to previous CANDU reactors. The ACR-700 has a negative void coefficient, and a negative power coefficient over its operating range. Of particular challenge to the staff in evaluating the ACR-700 thermal-hydraulics are post critical heat flux and quench in horizontal fuel channels and modeling the two-phase distribution in the inlet and outlet headers to the fuel channels. Each of these may require testing and model development. Because both light water and heavy water are used in the same system, there may be unique challenges in modeling kinetic and thermal-hydraulic feedback.

IRIS: The IRIS is an advanced pressurized water reactor. Unlike other PWRs however, the reactor coolant pumps, the pressurizer, and steam generators are internal to the reactor vessel. As a result, typical Class IV accidents are either eliminated or reduced in consequence. Several thermal-hydraulic issues may merit new research, including two-phase performance of the integral helical coil steam generators and interaction between the primary and a containment that is designed to withstand relatively high pressures.

### Conclusions

The new light-water reactor designs represent significant advancements in nuclear power technology. The designs offer improved economics, and at the same time, may provide enhanced safety margins. Verification of improved safety may require new research to investigate the performance of some of the novel design features and to improve the understanding of complex thermal-hydraulic processes. Research needs are expected to evolve and become better defined as these designs are reviewed by the staff.

## **Modeling Issues for High Temperature Gas-Cooled Reactor Designs**

Donald Carlson, Richard Lee, and Frank Odar  
Office of Nuclear Regulatory Research  
U.S. Nuclear Regulatory Commission

Because high temperature gas-cooled reactor (HTGR) designs are substantially different from current light-water reactors (LWRs), revised computer codes and new models will be needed to give NRC staff the necessary capabilities to realistically predict reactor system response. The development of a suite of validated reactor system analysis (nuclear analysis, thermal hydraulic analysis, and severe accidents and source terms) tools and data will permit the NRC staff to (a) conduct confirmatory analyses in the review of applicants' reactor safety analyses, (b) support development of the regulatory framework by assisting in the identification of safety-significant licensing basis events and associated success criteria, and (c) conduct exploratory analyses to better understand the technical issues, uncertainties, and safety margins associated with new designs.

### **1. Introduction**

The existing NRC research and regulatory infrastructure for the reactor safety arena primarily supports licensing and regulation of the current generation of LWRs. Although there are several areas in which the research infrastructure needs to be improved to address advanced LWRs, many of the largest research infrastructure gaps for advanced reactors are those that relate to HTGRs. The NRC has developed an Advanced Reactor Infrastructure Assessment to identify the new information and revised technical capabilities that would be needed to support the future licensing of HTGRs and other types of advanced reactors. The assessment addresses the full spectrum of regulatory and technical areas, including the modeling issues for HTGR reactor systems analysis as summarized in this paper. Representative of the HTGR designs considered herein are the pebble bed modular reactor (PMBR) under development in South Africa and the low-enriched uranium (LEU) fueled version of the gas turbine modular helium reactor (GT-MHR) that is being developed by General Atomics.

The primary goal of the advanced reactor research program is to establish an appropriate database and develop the analysis tools to help the staff make sound decisions on key technical and regulatory issues concerning the safety of advanced reactors. To address these infrastructure needs for staff capabilities in reactor and plant analyses, RES will acquire or develop data, tools, and methods that will allow the staff to independently assess advanced reactor safety margins and to evaluate reactor safety analyses submitted by applicants in support of future advanced reactor license applications. This research effort is also designed to provide analytical support for the development of a regulatory framework for advanced reactor licensing and establish the technical basis for related policy decisions.

This paper will discuss research activities needed in the area of reactor systems analysis, which includes nuclear analysis, thermal hydraulic analysis, and severe accident and source term analysis. Nuclear analysis research for reactor systems analysis will include the development and testing of: (1) reactor physics codes and methods for modeling reactor control and feedback and for predicting the in-reactor heat sources from fission chain reactions and fission-product decay and (2) neutron transport and shielding models as needed in analyzing

reactor material activation and damage fluence. Nuclear analysis research activities will start with the development of modern, general-purpose nuclear data libraries that will support all nuclear analysis activities throughout the arenas of reactor safety, materials safety, waste safety, and safeguards. For the thermal hydraulic analysis of HTGRs, the discussion will describe data and modeling tools needed for predicting HTGR-specific heat transfer and fluid flow phenomena, including "multi-phase (helium with air and/or water ingress)" fluid flow with convective, conductive, and radiative heat transfer in irregular and complex geometries. In the area of severe accident and source term analysis, the discussion will address the data and analysis tools needed for: (1) evaluating the progression of accident scenarios up to and including fuel melting or high-temperature chemical attack and (2) modeling any resulting releases and transport of radioactive fission products within and outside the reactor system boundaries.

## 2. HTGR Reactor Systems Analysis Overview

In advanced HTGR designs, the integrity of the coated particle fuel in its function as primary fission product barrier depends strongly on the maximum fuel temperatures reached during irradiation and in accidents. These fuel temperatures are predicted by reactor system calculations using a combination of codes and models for core neutronics, decay heat power, system thermal hydraulics, and severe accident phenomena such as graphite oxidation caused by air ingress. So-called melt-wire experiments performed in Germany's (AVR) pebble-bed reactor showed the unexpected presence of in-core hot spots, where maximum local operating temperatures were much higher than predicted with codes like those now being used by the PBMR developers. Moreover, the AVR's true maximum local operating temperatures remain unknown due to measurement inadequacies in those experiments. For all advanced HTGR designs, significant uncertainties also exist in predicting the maximum fuel temperatures and vessel temperatures during heatup accidents. Such uncertainties relate to basic data like irradiation- and temperature-dependent thermal conductivities as well as the integral effects of variable local power densities with conductive, radiative, and convective heat transfer through the core and surrounding structures. Appropriate data measurements and system analysis tools will therefore be needed to support the staff's understanding and assessment of factors that govern fuel temperatures and uncertainties in relation to fuel integrity and HTGR safety margins.

Related analyses with codes and data will also be needed for assessing the safety-related technical and policy issues associated with severe accidents and fission product release phenomena that differ dramatically from those in current and advanced LWRs. To meet needs on all aspects of advanced reactor system analysis (i.e., nuclear analysis, thermal hydraulics, severe accidents, and mechanistic release of fission products), the staff will seek to minimize costs and maximize benefits to the agency through active engagement in the planning and performance of domestic and international cooperative research efforts.

This paper outlines the specific information that should be incorporated into a suite of reactor system analysis tools (i.e., computer codes and methods) to give NRC staff the necessary capabilities to reliably predict system responses. The reactor systems analysis capabilities will also provide needed information to many other parts of the research program. This will include providing fluences and temperatures, pressures, and mechanical loads for use in work described in the sections on Materials Analysis and Fuel Analysis as well as information on damage sequences for PRAs.

### 3. HTGR Nuclear Analysis

The term “nuclear analysis” describes all analyses that address the interactions of nuclear radiation with matter. Nuclear analysis thus encompasses the analysis of: (1) fission reactor neutronics, both static and dynamic; (2) nuclide generation and depletion as applied to reactor neutronics and to the prediction of decay heat generation, fixed radiation sources, and radionuclide inventories potentially available for release; (3) radiation transport and attenuation as applied to the evaluation of material damage fluence, material dosimetry, material activation, and radiation protection; (4) nuclear criticality safety, (i.e., the prevention and mitigation of critical fission chain reactions ( $k_{\text{eff}} \geq 1$ ) outside reactors). This section addresses nuclear analysis issues encountered in the evaluation of reactor safety for HTGRs.

All areas of nuclear analysis make use of nuclear data libraries derived from files of evaluated nuclear physics data, such as an Evaluated Nuclear Data File, Volume B (ENDF/B) in the U.S., Joint European File (JEFF) in Europe, or Japanese Evaluated Nuclear Data Library (JENDL) in Japan. The nuclear data files include, for example, fundamental data on radionuclide decay as well as neutron reaction cross sections, emitted secondary neutrons and gamma rays, and fission product nuclide yields, all evaluated as complex functions of incident neutron energy. The neutron reaction evaluations also provide cross-section uncertainty information in the form of covariance data that can now be processed and used with advanced sensitivity and uncertainty analysis techniques, as developed in recent years under RES sponsorship, to assist in the identification and application of appropriate experimental benchmarks for problem-specific code validation.

Many of the processed nuclear data libraries in use today were developed in the 1980s or earlier. For example, the PBMR design team in South Africa now relies on the German VSOP reactor physics code with multi-group nuclear cross section libraries derived in the early 1980s from the evaluated physics data in ENDF/B-IV. Pre-1990s cross section libraries are similarly being used for preparing the LWR nodal physics data used by the NRC’s reactor spatial kinetics code, Purdue Advanced Reactor Core Simulator (PARCS), and for the criticality, depletion, and shielding analysis sequences in the NRC’s Shielding and Criticality Analysis for Licensing Evaluation code system. While these legacy cross section libraries have proven largely adequate in a variety of applications, their known limitations and shortcomings in relation to modern nuclear data evaluations and processing techniques would call for reevaluation in the context of advanced reactors and their fuel cycles and would continue to limit the implementation of modern nuclear analysis methods.

NRC has sponsored Oak Ridge National Laboratory (ORNL) to upgrade the AMPX, a Modular System for Processing Nuclear Data Evaluations code suite, to enable its eventual use in creating new cross section libraries that would take full advantage of the expanded resolved resonance ranges and the improved/corrected nuclear data and covariance evaluations now available in the latest releases of ENDF/B-VI and its foreign counterparts JEFF-2 and JENDL-3. With the recently completed AMPX upgrades and continued improvements to the Nuclear Data Processing System from Los Alamos National Laboratory (NJOY) nuclear data processing codes, opportunity and motivation now exist to produce and test state-of-the-art nuclear data libraries for use in the analysis of reactor safety, nuclear material safety, waste safety, and safeguards issues associated with conventional and advanced reactor technologies.

### 3.1 Identification of HTGR Nuclear Analysis Modeling Issues

The defining features of HTGRs include their use of fission-product retaining coated fuel particles, graphite as the moderator and structural material, and neutronically inert helium as the coolant. Both the PBMR and GT-MHR are modular HTGR designs that are fueled with low-enrichment uranium (LEU, <20%  $^{235}\text{U}$ ) instead of the high-enrichment uranium (HEU, >90%  $^{235}\text{U}$ ) and thorium used in earlier HTGRs. Both also have long annular core geometries, locate control and shutdown absorbers in the graphite reflector regions, and lack traditional in-core instrumentation. In many respects, the PBMR and GT-MHR designs therefore have similar code modeling and validation issues for the prediction of reactor neutronics phenomena and decay heat generation.

Reactor neutronics and decay heat analysis issues unique to the PBMR relate mainly to its use of multiple-pass on-line fueling, its pebble-bed annular core with statistical packings of fuel pebbles of varying burnups, the intermixing of graphite pebbles and fuel pebbles near the boundaries between the fueled core region and the central graphite region, and the potential for seismic compaction events, misloading events, anomalous local packing and clustering of pebbles, and anomalous flow patterns of pebbles through the core such as might be caused by localized pebble bridging, jamming of chipped or fractured pebbles, unanticipated funneling effects near the core exit, or unanticipated radial gradients of pebble flow velocity resulting from the strong temperature dependence of pebble-to-pebble friction (i.e., as seen in the Thorium Hochtemperaturreaktor (THTR)-300 pebble bed reactor). Related research activities include the mechanics of pebble beds with pebble flow and intermixing, statistical packing, bridging, and seismic pebble-bed compaction.

Physics analysis issues unique to the GT-MHR relate mainly to the effects of burnable poisons, the presence of both 19.9% enriched "fissile" coated particles and unenriched "fertile" coated particles in the fuel compacts, reactivity control for cycle burnup effects, and the power shaping effects of zoned fuel and poison loadings.

Nuclear analysis issues anticipated in evaluations of PBMR and GT-MHR reactor safety, and related aspects of tri-isotropic (TRISO) fuel performance, include the following:

- **Temperature coefficients of reactivity:** The reactivity feedback effects from temperature changes in the fuel, moderator graphite, central graphite region, and outer reflector graphite play an important role in HTGR analysis. Based on sensitivity studies and validation against representative experiments and tests, the analysis of reactivity feedback coefficients should account for computational uncertainties in the competing physical phenomena, including for example the positive contributions to the fuel and moderator temperature coefficients associated with  $^{135}\text{Xe}$  and bred fissile plutonium.
- **Reactivity control and shutdown absorbers:** Depending on design details, the reactivity worths of in-reflector control and shutdown absorbers may be sensitive to tolerances in the radial positioning of the absorbers within the reflector-block holes. The tests and analytical evaluations for reactivity control and hot and cold shutdown should also account for absorber worth variations through burnup cycles (GT-MHR) and the transition from initial core to equilibrium core loadings as well as absorber worth validation and modeling uncertainties and absorber worth variations caused by temperature changes in the core and reflector regions, xenon effects, variations or aberrations of pebble flow, and accidental moisture ingress.

- **Moisture ingress reactivity:** Although the absence of high-pressure, high-inventory water circuits in closed Brayton cycle systems makes this issue less of a problem than in earlier steam cycle HTGRs, the effects of limited moisture ingress will nevertheless have to be evaluated for depressurized or underpressurized accident conditions in the PBMR and GT-MHR. Effects to be evaluated include the moisture reactivity (i.e., from adding hydrogenous moderator to the undermoderated core), the effects of moisture on temperature coefficients (e.g., from spectral softening), shortened prompt-neutron lifetimes (i.e., faster thermalization), and reduced worths of in-reflector absorbers (i.e., fewer neutrons migrating to the reflector).
- **Reactivity transients:** T/H-coupled spatial reactor kinetics analyses will be needed for assessing axial xenon stability as well as reactivity transients caused by credible events such as overcooling, control rod ejection, rod bank withdrawal, shutdown system withdrawal or ejection, seismic pebble-bed compaction, and moisture ingress. Of particular importance in the safety evaluations for PBMR and GT-MHR is the need to identify, through safety analysis and risk assessment efforts, any credible events that could produce a prompt supercritical reactivity pulse. Should any such prompt-pulse events be identified as credible, their estimated probabilities and maximum pulse intensities should be considered in establishing any related plans or requirements for pulsed accident testing and analysis of HTGR fuels (see Section on Fuels). For loss-of-cooling passive-shutdown events with failure of the active shutdown systems (i.e., anticipated transient without scram [ATWS]), the delayed recriticality that occurs after many hours of xenon decay may also require spatial kinetics analysis models to account for the unique spatial power profiles and feedback effects caused by the higher local reactivity near the axial ends and periphery of the core where temperatures and xenon concentrations are lower.
- **Pebble burnup measurements and discharge criteria:** The PBMR designer states that selected fission-product gamma rays will be measured to determine the burnup of each fuel pebble and that this measured burnup will serve as the criterion for discharging the pebble or passing it back through the reactor. The particular burnup value used as the discharge/recycle burnup criterion will be chosen to limit the maximum pebble burnup, which is stated as nominally 80 GWd/t. Therefore, determining a suitable value for discharge/recycle burnup criterion (<80 GWd/t) will require consideration of in-core pebble residence time spectra, together with supporting neutronics calculations, in order to statistically characterize the maximum burnup increment that might accrue during a pebble's final pass through the core. Burnup measurement uncertainties will also have to be considered. Furthermore, since pebble burnup measurements (unlike the pebble reactivity measurements used in THTR-300) cannot distinguish pebbles with different initial fuel enrichments, the same discharge burnup criterion will need to be applied to the initial charge of 4%-enrichment fuel pebbles as to the 8%-enrichment pebbles that are added in transitioning to an equilibrium core. Neutronics calculations will be needed to bound the higher neutron fluence experienced by the 4%-enrichment pebbles in reaching the maximum burnup levels allowed in the transitional cores.
- **Pebble-bed hot spots:** The results of melt-wire experiments conducted in the German AVR test reactor demonstrated the existence of unpredicted local hot spots under normal operating conditions in pebble bed cores and that such hot spots determine the maximum normal operating temperatures of the fuel. These hot spots may arise from a combination of higher local power density (e.g., due to moderation effects near the

reflector wall or from chance clustering of lower burnup pebbles), lower local bed porosity due to locally tight pebble packings, and reduced local helium flow due to the increase of helium viscosity with temperature. Whereas the slow evolution of loss-of-cooling heatup transients in the PBMR will tend to wash out any effects of pre-accident local flow starvation on subsequent peak fuel temperatures, the effects of higher local fission power densities will be retained throughout the heatup transient in the form of higher local decay heat powers. Therefore, the effect of decay-power hot spots, in particular, may need to be considered in evaluating the maximum fuel temperatures arising in pressurized or depressurized loss-of-cooling accidents.

- **Pebble fission power densities and temperatures:** The computational models may need to account for pebble-to-pebble burnup and power variations within nodes or meshes. Computational studies with higher-order methods, such as exact geometry, continuous-energy Monte Carlo (MCNP), may be used to investigate the distribution of power among assumed clusterings of pebbles with various burnups located in the core interior, in the inner-reflector mixing region, and near the outer reflector wall. Note that in calculating operating temperatures inside a pebble, the reduction of pebble power with pebble burnup may tend to be offset by the reduction of pebble thermal conductivity with neutron fluence.
- **Pebble bed decay heat power densities:** Much as with fission power densities (see previous item), each node in the core calculational model will contain pebbles with a broad range of decay heat power densities. Further computational studies may, therefore, be needed to establish technical insights on acceptable modeling approximations (e.g., mesh averaging methods) and assumptions (e.g., local hot spots, power histories) for calculating decay heat sources in pebble bed reactors while accounting for validation uncertainties associated with the shortage of applicable experimental data.
- **Graphite annealing heat sources:** Although continuous annealing effectively prevents any significant buildup of Wigner energy at the high operating temperatures of HTGR graphite, there is a significant accumulation of higher-energy graphite lattice distortions that anneal out only at the elevated graphite temperatures encountered in loss-of-cooling accidents (e.g., conduction cooldown events). This high-temperature annealing heat source should be evaluated and, where significant, added to the nuclear decay heat sources used in the analysis of loss-of-cooling heatup events. Note that the recovered thermal conductivity caused by high-energy lattice annealing during slow graphite heatup accidents can substantially reduce the peak fuel temperatures reached during the accident, an effect that may need to be considered in the heat removal models used for HTGR accident analyses.
- **Radionuclide decay before accident testing of TRISO fuel:** In understanding how out-of-reactor heatup and power-transient tests can be used to demonstrate the performance of TRISO fuels in reactor accidents, one should consider the potential effects from physical changes that can occur in the fuel during the time intervals between fuel irradiation and testing. Such physical changes would include those arising from the decay of short-lived fission products and actinides and from other time- and/or temperature-dependent processes (e.g., chemical reactions, material cooling, creep, annealing, precipitation, condensation, diffusion, permeation, migration) that could affect the mechanical loading and effective strength of particle coatings under the respective

simulated or actual accident conditions. Specific analyses of nuclide generation, depletion, and decay will therefore be needed for evaluating how radioactive decay changes the fuel's inventory of important actinides and fission products (e.g., those that potentially affect gas pressure and layer strength in the coated particles) during the time intervals between fuel irradiation and out-of-reactor accident testing.

- **Physics of TRISO fuel irradiation in test reactors versus HTGRs:** The extensive use of various test reactors for the irradiation testing of HTGR TRISO fuels raises questions about the nonprototypicality of the neutron energy spectra, accelerated fuel burnup rates, and fuel temperature histories in the test reactors. It may be beneficial to perform reactor-specific calculations of neutron fluxes and nuclide generation, depletion, and decay to validate and assess the sensitivity of computed fluences and fuel nuclide inventories between the test reactors and HTGRs.

#### 4. HTGR Thermal-Hydraulic Analysis

T/H analyses are used to assess plant performance under accident and transient conditions to ensure that the safety limits are not exceeded and that there is sufficient margin to account for uncertainties. Understanding the effects of these features on local and system-wide T/Hs is necessary in order to confirm and quantify the expected safety margins of the proposed plants and to audit the applicant's calculations.

##### 4.1 Identification of HTGR Thermal Hydraulic Modeling Issues

NRC staff has completed a preliminary survey of the analysis capabilities needed to model HTGR fluid flow and heat transfer in support of the staff's review of an HTGR safety analysis. Given the nature of HTGR transients, the preliminary findings indicate that a code will need to reliably and efficiently predict transients that evolve over time scales of days, not hours as we have become accustomed to in LWR analyses. Some design basis transients are driven by radiative and conductive heat transfer through porous and solid structures not convection, and this capability, although it currently exists in all codes, may have to be extended to three dimensions, and a spherical fuel element model will have to be added for analyzing transients in pebble bed reactors. The NRC analysis tools should be able to model all the turbo-machinery and passive decay heat removal systems, and accurately model gases (helium and air) in natural circulation. These systems are important for long-term heat removal and recovery as well as determining initial steady state operating parameters and conditions. Turbo-machinery will likely be simulated using existing pump models, but this capability will have to be assessed and modified as needed. For pebble bed designs, the staff needs the capability to model flow and heat transfer in a packed bed configuration. The code will need to model two different working fluids at once to model component cooling water systems. Finally, the capability to model graphite as a solid structure will have to be added.

Two types of codes may be used to fulfill this need for HTGRs. These are the traditional reactor systems analysis codes, analogous to TRAC-M or MELCOR, and general-purpose computational fluid dynamics codes, such as FLUENT. FLUENT will be used because it gives us the ability to more reliably predict parts of the fluid system when we need to assess the capability of our reactor system code against some assumed known reference standard or when we need to assess a particular phenomenon in more detail.

Where appropriate, the acquisition or development of new HTGR thermal hydraulic analysis capabilities will use or build upon corresponding features in the two earlier HTGR accident analysis codes, Graphite Reactor Severe Accident Code (GRSAC) and Thermal Analysis for Temperatures in the Core of an HTGR (THATCH). The forerunners of GRSAC, called ORECA and MORECA, were developed in the 1975 to 1993 time frame at ORNL, largely under NRC sponsorship, to support the staff's licensing safety evaluation for Fort Saint Vrain and the pre-application review for the DOE MHTGR. After 1994, MORECA became GRSAC and, through non-NRC funding sources (mainly the Defense Nuclear Agency), was further developed to model past accidents and postulated events in various non-HTGRs, such as Windscale, Magnox, and AGRs. ORNL is now adding pebble-bed and Brayton cycle code models to GRSAC for their near-term use in support of an NRC interagency agreement with DOE on assessment of generic HTGR safety analysis code requirements and the staff's pre-application review activities for the PBMR. The THATCH code was developed at Brookhaven National Laboratory, likewise through NRC sponsorship in the 1975 to 1993 time frame, and was likewise used to support the staff's review activities for Fort Saint Vrain and the MHTGR. Unlike GRSAC, the THATCH code was not maintained after the NRC's MHTGR review activities were terminated in 1994, although THATCH code documentation is still available.

## 5. HTGR Severe Accident and Source Term Analysis

Reactor risk studies performed by NRC and industry have shown that public risk from reactor operation is dominated by accidents involving severe core damage coupled with containment bypass or containment failure. These accidents result from sustained loss of core cooling and can release substantial quantities of radioactive fission products (FPs) into the environment. The ability to model progression of severe accidents and estimate releases of FPs into the environment is required to quantify risk and to address severe accident issues. NRC has developed several codes to model severe accidents.

NRC's severe accident codes for LWRs are based on a large number of experiments performed in the 1980's following the Three Mile Island 2 accident, which have been incorporated in the MELCOR code. MELCOR is chosen as the NRC consolidated severe accident code which can model most aspects of a severe accident including thermal hydraulics, core melt progression, FP transport in the reactor system and containment. For LWRs, many experiments (U.S. and international) have also been carried out in support of development of a fundamental understanding of the phenomena of severe accident and FP transport.

### 5.1 Identifying HTGR Severe Accident and Source Term Modeling Issues

As part of the NRC's review of advanced reactors development of FP transport and source terms will play an important part in several policy issues, such as the need for leak tight containments and the choice of design basis accidents. There is a need for data and modeling methods for the new materials and configurations that will be used in the advance reactors (particularly in HTGRs). Research will be needed to perform confirmatory analysis and to identify and resolve many of the source term driven policy issues discussed above.

HTGR accidents that can potentially lead to FP release need to be identified and, if credible, modeled. For today's LWRs, such accidents include a loss of coolant coupled with the failure of safety systems, reactor coolant system boundary failure, and containment failure or bypass. Accordingly, severe accident codes have been developed and used to estimate the probability

and timing of the failure of the reactor coolant system boundary and the failure or bypass of the containment. Severe accident analysis methods using codes such as MELCOR have been developed to estimate the magnitude and timing of FP release to the containment and subsequently to the environment.

For HTGRs the types of sequences and the process by which FPs may be released from HTGR fuel will differ dramatically from those in LWRs. Incremental releases of FPs may occur as the result of diffusion during normal operation, rupture of coated fuel particles as a result of accidents, and vaporization during high-temperature degradation of the fuel.

The risk from HTGR operation is the risk from releases during normal operation, from accidents involving rupture of coated fuel particles, and from accidents involving high temperature fuel degradation. Technical expertise and technical capability in the area of FP transport and behavior during high temperature fuel degradation is needed in order to assess the risk from HTGR operation. Because FPs released from the fuel are transported through the primary system and containment predominantly as aerosols, the offsite releases and offsite radiological consequences may be significantly reduced by FP deposition in the primary system and containment. Aerosol deposition occurs through a variety of mechanisms such as gravitational settling, thermophoresis, and diffusiophoresis. Therefore, research activities will focus on FP transport and behavior in the primary system and containment.

MELCOR has most of the capabilities needed to analyze beyond design-basis accident issues for HTGRs. However, modifications to MELCOR would be needed to model these reactors, because of the different fuel design and the different reactor internal structure design. Proposed modifications are described below, together with an activity to assess MELCOR, in combination with GRSAC where appropriate, against available experimental data and other codes.

This page left intentionally blank

## **IRRADIATION AND ACCIDENT CONDITION TESTING OF HIGH-TEMPERATURE GAS-COOLED REACTOR FUEL**

**Stuart D. Rubin**

Senior Technical Advisor for Advanced Reactors  
Office of Nuclear Regulatory Research  
U. S. Nuclear Regulatory Commission

Modular high-temperature gas-cooled reactors, such as the Pebble Bed Modular Reactor and the Gas Turbine-Modular Helium Reactor have unique safety features and design characteristics. Foremost among these is the all-ceramic fuel element containing tri-isotropic (TRISO) coated fuel particles. The fuel safety concept and intended design characteristic is to contain and retain essentially all radiologically important fission products within the billions of coated fuel particles contained within the fuel elements (e.g., fuel pebbles, fuel compacts) within the core. Effective fission product retention within the coated fuel particles is critical to the high-temperature gas-cooled reactor safety case for all licensing basis conditions. The paper describes the irradiation testing and accident condition testing that is needed to obtain fuel performance data to better establish operating and accident condition fuel safety performance and safety margins; to assess the acceptability of an applicant's fuel irradiation and accident simulation testing programs, to verify an applicant's claims of fuel performance and fission product release during operations and accidents and; to provide data to develop and validate analytical fuel performance tools. These test data are also considered important to support a policy decision on mechanistic source term and modular HTGR application technical reviews.

### Background

Advanced high-temperature gas cooled reactors (HTGRs), such as the Pebble Bed Modular Reactor (PBMR) and the Gas Turbine Modular Helium Reactor (GT-MHR), are being designed to assure the containment of radiological fission products in a much different manner than the current generation of light-water reactors (LWRs). LWRs are licensed with a robust pressure-retaining containment building that is designed for very low leakage in the event of an accident. An LWR containment building is designed to provide a diverse and effective second barrier against the release of fission products to the environment should significant fuel failures and fission product transport (FPT) occur due to a postulated accident, such as a loss-of-coolant core heatup accident. The approach to fission product containment being taken by the designers of advanced HTGRs is to primarily retain fission products where they are produced—within the fuel—in the event of an accident. The PBMR and the GT-MHR designs and safety cases both rely on the ability of the billions of tiny ceramic-coated fuel particles (CFPs) to stay intact and to effectively retain and contain fission products during normal operation as well as during postulated accidents. The approximate 5 billion CFPs in the pebble fuel elements in a PBMR core and the approximate 10 billion CFPs in the prismatic fuel elements in a GT-MHR core individually and collectively provide the principal barrier against fission product release. The containment designs being proposed for advanced HTGRs, although as structurally robust as those of LWRs, are not designed to contain fission products at high pressure and low leakage under accident conditions. Due to the limited operating experience and current state-of-the-art for CFP performance analysis, production fuel testing is

expected to provide the single most important basis for assessing CFP failure behavior and determining CFP integrity probabilities over the range of applicable HTGR plant operating conditions, transient conditions, and postulated accident conditions. HTGR fuel performance testing is therefore expected to be an essential aspect of advanced HTGR licensing.

It is also understood that applicants for a GT-MHR or a PBMR license will propose a mechanistic<sup>1</sup> basis for the accident source term. The fission product release from the fuel is the sum of initial CFP defects and heavy metal contamination from manufacture; CFP failures that occur during normal plant operations, including anticipated operational transients; and CFP failures that occur during design basis accidents or accidents beyond the design basis (i.e., "severe" accidents). The source term would be based on a mechanistic calculation of: (1) fuel failure (probability) due to the combination of manufacturing defects, failures in operations and accident induced failures; (2) release of fission products from intact, defective and failed fuel particles, and initial heavy metal contamination, (3) transport/holdup of fission products through the fuel element, (4) transport/holdup of fission products within the primary pressure boundary, and (5) transport/holdup of fission products within the reactor building confinement system. (See Figure 1, "HTGR Fission Product Source Term Factors (GT-MHR)," for GT-MHR source term factors.) This is different from the traditional licensing approach used for LWRs, which involves a deterministic bounding approach to the accident source term. Although only limited information has been provided by potential HTGR applicants, it is expected that the mechanistic source term will be based on a core-wide spacial census of CFP failure probabilities. It is expected that applicants will propose that this spacial census be event-specific and determined on the basis of a conservative calculation of the spacial distribution of the core conditions that drive CFP failure (e.g., fuel maximum temperature). Due to the limited operating experience and database for FPT, HTGR production fuel and related production fuel materials testing is expected to provide an essential basis for qualifying the fission product release and transport models used in the mechanistic source term calculations over the range of applicable HTGR plant operating and transient conditions and postulated accident conditions.

Extensive international irradiation (operational) testing has been conducted in Germany, United Kingdom, United States, Japan, Russia, Netherlands, and China to understand and characterize the behavior and safety performance of TRISO coated fuel particles during normal operation and operational transients. The fuel development and qualification irradiation testing philosophy of the international programs has generally focused on demonstrating acceptable and predictable fuel performance within the specified design, manufacturing, operating, and accident condition envelope applicable to a particular HTGR fuel design. Far less testing has been conducted to explore conditions beyond the specified envelope to understand the conditions wherein large and unacceptable increases in particle failure rates will begin to occur for otherwise qualified production fuel. The limited available irradiation test data involving operating temperature, burnup, fast fluence, and power levels well beyond the design-specific

---

<sup>1</sup>SECY-02-0139, "Plan for Resolving Policy Issues Related to Licensing Non-Light Water Reactor Designs," identified seven policy issues on HTGR designs. One issue involved whether, and under what conditions, scenario specific accident source terms might be acceptable for HTGR licensing decisions. The staff committed to provide a policy decision paper to the Commission in December 2002. The paper will contain options and recommendations for Commission policy guidance to resolve these issues. The acceptability of a mechanistic source term for HTGR licensing has therefor not yet been decided by the NRC.

envelopes results in significant uncertainties regarding the operational safety margins to elevated TRISO CFP failure rates. Additional production fuel testing to explore and map the operational and accident safety margins is considered essential to more fully understand and quantify these safety margins. Such testing is considered necessary to reduce uncertainty and to enhance both regulatory confidence and public confidence that advanced HTGR fuels can effectively retain and contain fission products where they are produced—within the fuel—for all credible conditions.

### TRISO Coated Fuel Particle Design, Manufacture, and Fission Product Retention Basis

There are two advanced HTGR designs involving NRC reviews: the PBMR and the GT-MHR. The PBMR, representative of pebble bed concepts, uses thousands of TRISO coated fuel particles randomly distributed within a graphite matrix in a sphere the size of a billiard ball. (See Figure 2, “Pebble Fuel Element Design.”) The fuel spheres (i.e., pebbles) are recycled slowly through the reactor core in a continuous online refueling process until the design burnup is achieved. The GT-MHR, representative of prismatic block core concepts, uses TRISO coated fuel particles agglomerated into cylindrical compact matrix. Compacts are stacked and inserted into an array of bored fuel holes within a hexagon-shaped graphite fuel element. Fuel elements are stacked in an array that makes up the annular reactor core. The prismatic block fuel elements are periodically relocated or replaced in a batch reload process. (See Figure 3, “Prismatic Fuel Element Design.”)

The performance of the fuel, particularly the fission product retention capability of the TRISO coated particles during normal operation and accidents, is the primary factor in determining the radiological safety performance of advanced HTGRs. Each layer of the particle is engineered to protect against degradation or failure that can lead to fission product release. The fuel kernel is designed to provide a transport holdup for fission products and plays a role in reducing the release of fission gases from broken particles. The transport holdup provides for a significant delay in the release of iodine-131 from failed particles. The buffer layer provides a porous void volume. The buffer layer accommodates fission gas release (to avoid excess pressure buildup in the particle), attenuates fission product recoils and accommodate irradiation-induced swelling of the fuel kernel. The buffer layer thereby protects the high-density layers from damage. The inner high density carbon layer also provides a barrier against fission product release. However, its main function is to provide an impervious barrier to protect the kernel from attack by corrosive chemicals associated with the fabrication process of the (next) silicon carbide (SiC) layer. The layer also strengthens the SiC layer, which has limited tensile strength. The SiC layer provides the primary containment barrier against the release of solid and gaseous fission products. It serves as the coated particle's primary pressure vessel and contributes the most to the overall strength, dimensional stability, and structural support of the particle. However, silver in the form of silver-110m readily diffuses through the SiC and the other layers of the particle. The outer carbon layer protects the SiC against chemical attack during the particle-coating processes and adds strength to the SiC layer by keeping it under compression. It also provides an additional barrier to fission product release. Neither the graphite matrix for pebble fuel, nor the compacts and nuclear graphite prismatic fuel blocks for GT-MHR fuel are expected to retard iodine-131 gas release from failed particles. Metallic cladding is not a part of the HTGR CFP fuel design. Thus the all-ceramic CFP design has the potential to retain fission products at temperatures that are well above the normal fuel operating temperatures.

Figure 4, "Relative Fission Product Concentration Within an Irradiated TRISO Fuel Particle," depicts the relative fission product concentration in the various layers for an intact irradiated TRISO CFP at normal operating temperature. The figure is based on isotopic composition measurements. Almost all of the fission products are retained in the kernel itself. The buffer is designed to retain most of the fission products that escape from the kernel, especially the gaseous fission products in intact CFPs. The concentration drops off from the inner to the outer surface of the buffer layer. A small amount of solid fission products is retained by the inner high-density carbon layer. The concentration drops off to essentially zero at the SiC layer. Fission products do not penetrate an intact SiC layer to get to the outer high-density carbon layer. Fission products that enter the coolant are due either to defective CFPs from manufacture, from trace uranium outside the silicon carbide layer, from the chemical vapor deposition coating process, or to the fraction of particles that fail during operational irradiation.

#### HTGR Fuel Particle Irradiation Testing Experience and Fuel Failure Mechanisms

Figure 5, "Comparison of U.S. and German TRISO Fuel Irradiation Performance (Source- INEEL)," provides a graphic illustration of the mixed results in the irradiation performance of TRISO CFPs over the past several decades. The figure provides a comparison of the irradiation performance of TRISO CFPs made in Germany (utilizing the so-called German fuel fabrication processes) with the irradiation performance of TRISO CFPs made in the United States (utilizing a U.S.-developed fuel fabrication process). A comparison of the irradiation data for German-made TRISO coated particle fuel with U.S.-made TRISO coated particle fuel shows that the krypton-85 gas release rate (i.e., particle failure rates) during irradiation for U.S. fuel is three orders of magnitude higher than for the German fuel.

A recent INEEL critical study of the causes for these differences confirmed the long-held view that differences in the process parameters used for applying the individual coating layers of the TRISO coated particle were a key factor in the differences in irradiation performance. Although the U.S. fuel met the established specifications for the measurable fuel particle layer physical, material, and chemical characteristics (e.g., thickness, density, strength, impurities), which were consistent with the design and safety requirements, the differences in processes were found to result in critical differences in layer micro-structures, differences in bonding between layers, differences in layer anisotropy, etc. These were critical differences which resulted in significant differences in in-reactor (irradiation) fuel performance and behavior. The importance of manufacturing process was recognized in Germany and was included in the fuel manufacturing specification along with the product specifications.

The GT-MHR and PBMR vendors have stated that the manufacture of the TRISO fuel particles for their fuel will be equivalent to the German fuel manufacture. To achieve this goal, both vendors are currently implementing a major fuel manufacturing development program with the assistance of available German fuel fabrication technology specialists. The Department of Energy has also established an HTGR fuel development and qualification program which is intended to duplicate the success of the German fuel fabrication technology and to determine the relationship between CFP manufacturing process, CFP product characteristics and CFP irradiation performance. A major goal of these efforts is to develop a raw materials supply and equipment, procedures, process specifications, and product specifications which will re-establish the German production fuel quality and characteristics and duplicate the German fuel irradiation performance. For this reason it is important that fuel performance, qualification and margin testing be conducted with test fuel that has been fabricated with the same

materials, equipment, procedures, process specifications and product specifications that are intended to be used (i.e., proven) for the production fuel that would be loaded into the power reactor core. Extensive fuel irradiation testing, accident condition testing, and safety margin testing will need to be carried out to determine the extent to which these efforts are successful and to qualify the fuel as meeting the fuel performance requirements needed to meet the proposed licensing basis for radiological consequences for these plants.

In addition to fuel fabrication as an important determinant of fuel performance (i.e., CFP failure probability), the actual test conditions associated with fuel irradiation testing, accident condition testing, and safety margin testing are a similarly important determinant.

### TRISO Coated Fuel Particle Failure Mechanisms

TRISO CFP failure mechanisms and their underlying causes are key considerations in the development of an HTGR fuel safety performance test matrix (i.e., test conditions). Failure mechanisms can be attributed to design, manufacture, operating conditions, and accident conditions. Manufacturing-related causes and the controls against TRISO CFP failures that occur in the manufacture of the CFPs and the fuel elements (i.e., initial particle defects) are generally known, can be quantified, and typically occur at a fractional rate of about  $10^{-5}$ . Initial manufacturing defects, such as broken CFPs due to fuel compacting (GT-MHR) or fuel pebble (PBMR) pressing are also readily and immediately observed in fuel irradiation tests and are not the focus for the design of a fuel performance test matrix.

Active and latent particle failure mechanisms are revealed as actual failures some time later in fuel irradiation tests (operations) and/or during accident conditions. The causes and the specific mechanisms can be attributed to design and manufacturing factors, as well as to the operational environment and the accident condition environment. The design of an HTGR fuel safety performance test matrix does need to consider active and latent failure mechanisms.

Potential active operational (in-service) failure mechanisms include damaging direct interaction between the fuel kernel and the particle coatings. This can occur when, over time, the fuel kernel migrates away from "center" of the CFP due to an elevated radial temperature gradient (environmental factor) and attendant carbon transport within the CFP. This can become a possible failure mechanism if the particle power level is sufficiently high to cause a large radial temperature gradient. (See Figure 6, "TRISO Coated Fuel Particle Kernel Migration Failure.")

Active failure of the CFP can also occur if the pressure within the CFP becomes sufficiently high to cause the stress in the SiC layer to exceed its ultimate tensile stress (i.e., "pressure vessel failure"). For a given CFP design, pressure inside the particles is time-dependent and a function of burnup and temperature. The higher the burnup the larger the fission gas release from the kernel, and the higher the CFP temperature the higher the pressure. (See Figure 7, "TRISO Coated Fuel Particle Pressure Vessel Failure.")

In addition to irradiation temperature and burnup, stress in the SiC layer is also a time-dependent function of such factors as: neutron fluence, particle geometry, and particle layer densities. Maintaining the SiC layer in a state of compression for as long as possible (i.e., for the highest possible burnup) is an important goal in the design of CFPs. For example, fast fluence will cause the pyrolytic carbon (PyC) to shrink over time, causing the adjacent bonded SiC layer to be in a state of compressive stress. However, further increases in fast

fluence will cause the PyC layer to grow from the shrunken state and in time will allow the SiC layer to be in tension. Shrinkage can also cause PyC local cracking and debonding of the PyC layer from the SiC layer, which can result in a high local stress on the adjacent SiC layer, leading to its premature failure. Lower CFP temperature can theoretically increase stresses and failure of the PyC due to the lower rate of PyC creep. Higher creep rates allow the PyC stresses to be reduced, which lowers the potential for PyC cracking and debonding, which lowers the potential for SiC cracking failure. (See Figure 8, "TRISO Coated Fuel Particle Outer Pyrolytic Carbon Layer Cracking/Debonding Failure.")

Another potential failure mechanism is fission product corrosion of the SiC layer. This can occur due to chemical attack by lanthanides and palladium due to fission in the fuel kernel and can be an important factor at irradiation temperatures below 1600°C.

Potential active failures that can occur during accident conditions include pressure vessel failure, thermal decomposition of the SiC, effects of steam or water on CFPs, and the rapid deposition of energy in the fuel particles, among others. The pressure vessel failure mechanism is the same as for operational failures. Thermal decomposition involves a shift in the chemical equilibrium away from SiC and toward the elemental silicon (Si) and carbon (C) and occurs when SiC is subjected to very high temperatures. To the extent that steam or water ingress can reach CFPs, it has the potential to cause oxidation-induced degradation of the PyC and SiC layers, and hydrolysis-induced degradation and failure of the SiC layer. Finally, a rapid deposition of energy in advanced HTGR coated fuel particles can be associated with a large global or local reactivity insertion event such as a postulated control rod ejection accident. Potential reactivity events are generally less of a concern in a PBMR since online refueling limits the amount of excess reactivity available to cause a reactivity addition event. A power pulse, if large enough, has the potential to fail CFPs. At very high power pulses, fuel compact or pebble element fracture might occur.

Fuel fabrication product specifications (e.g., layer thickness, density, and anisotropy), fuel fabrication process specifications (e.g., layer coating temperature, pressure, gas flow rates), and fuel fabrication manufacturing equipment (e.g., continuous coaters vs. batch coaters) are of central importance to HTGR fuel irradiation and accident condition test programs (i.e., the rate of CFP latent failures). Different fuel fabrication processes result in significant differences in CFP performance during normal operation (see Figure 5) and accidents. Assessing the effects of fabrication is vital and is accounted for in the CFP sampling schemes and the CFP and fuel element sample size used for establishing the fuel used in the test. The design of an HTGR fuel safety performance test matrix implicitly rather than explicitly considers active and latent failures mechanisms due to fuel manufacture.

#### Design, Manufacture, Operations, and Accident Condition Factors Effecting TRISO Coated Fuel Particle Performance

Many design and fabrication factors and operating and accident condition factors have an important effect on the performance and failure of TRISO CFPs. A recent NRC-sponsored effort to identify important performance-shaping phenomena developed at least 19 different design factors and 32 separate manufacturing factors. Design factors included such aspects as fuel kernel sphericity and buffer layer thickness and density. Manufacturing factors included PyC coating gas pressure, temperature, flow rate and anisotropy, SiC layer grain size and microstructure, and fuel element heat treatment, to name a few. As mentioned earlier, the

design of an HTGR fuel safety performance test matrix implicitly rather than explicitly considers active and latent failure mechanisms due to fuel design and manufacture. These factors are addressed in the sampling schemes and sample size of the fuel which is to be included in the test matrix.

Of importance to the design of the test matrix are the factors of the operating environment (operating conditions) and the factors of the accident environment (accident conditions) that affect CFP performance and failure. Additionally, irradiation conditions that "precondition" the fuel (short of actual CFP failure) can affect performance and failure potential in the accident environment. These preconditioning factors must also be considered in the design of the test matrix.

The recent NRC-sponsored effort to identify important operational performance-shaping factors included the identification of the following environmental factors: fuel element operating temperature, fuel burnup (percent fission of initial heavy metal atoms), fast fluence, power density, and operating temperature vs. time history. The effort also identified conditions that were viewed as important influences on fuel performance for each of three different types of accidents: core heatup accidents without chemical attack, core heatup accidents with chemical attack (e.g., air, water ingress), and reactivity accidents. Important environmental factors for core heatup accidents without chemical attack included maximum fuel temperature during core heatup, time at the maximum temperature, and time versus temperature transient conditions. Important environmental factors for core heatup accidents with chemical attack included oxidation kinetics, which depends on fuel temperature, velocity of air flow past the fuel element, oxygen partial pressure, and graphite impurities. Important environmental factors for a rapid reactivity insertion accident included the maximum temperature attained by the fuel kernel during the accident, the time at maximum temperature, the amount of energy deposited in the kernel, and the rate at which energy is deposited in the kernel.

#### Safety Performance Testing Expectations for Reactor Licensing

As noted earlier, it is expected that GT-MHR or PBMR license applicants will propose a mechanistic accident source term. Additionally, GT-MHR and PBMR license applicants have proposed that a license be based on meeting selected dose limits for the spectrum of events considered in the licensing basis. Therefore, the fuel performance requirements are established so as to show that the dose limits are not exceeded for the spectrum of events. Again, the source term is predominantly based on the sum of core-wide fuel fission product releases due to (1) initial CFP defects (failures) from fabrication, (2) initial heavy metal contamination in the fuel elements and outside intact CFPs (e.g., "tramp" uranium), (3) CFP failures which occur during normal operation and operational transients, and (4) CFP failures which occur during accidents. Additionally, a very low level of fission product releases can be attributed to the migration of fission products through intact particles and the fuel matrix. Quality control statistical analysis of destructive tests performed on manufactured fuel pebbles and compacts has been developed to assess the (equivalent) number of broken CFPs. Furthermore, to the extent that broken CFPs and initial heavy metal atoms may be within the particular production fuel pebbles or compacts that are used in the fuel test program, fission product gas release effects will be evident and quantified during fuel irradiation performance testing.

## Irradiation Performance Testing

As mentioned earlier, a major focus of irradiation performance testing for fuel qualification is to quantify the CFP failure rates and fission product releases of production fuel due to actual failures associated with normal plant operation and operational transients. Operational CFP failures arise from latent factors associated with (less than optimum) fuel design and fuel fabrication, as well as factors associated with the irradiation environment (i.e., test conditions). The vision for the irradiation environment for HTGR fuel irradiation performance testing would involve environments which would subject the fuel to (1) conditions out to the limits of the key plant parameters that establish the plant-specific licensing basis for normal and abnormal plant operations, (2) conditions that are significantly beyond these limits, and (3) conditions which are even further beyond these conditions to establish the threshold where large and unacceptable CFP failure fractions will begin to occur. The testing associated with Types 1 and 2 is generally included in historical HTGR fuel qualification test programs, and Type 2 conditions can be substituted as a conservative basis for Type 1 conditions. Testing associated with Type 3 is referred to here as "safety margin" operating condition testing to assess the available safety margins to significant fuel failures during normal operations. The environmental factors envisioned for the irradiation performance test matrix for these three types of testing are determined based on the previously discussed failure modes and operational performance-shaping factors. It would be expected that the fuel irradiation performance test matrix would include, as a minimum, appropriate combinations of the following key performance-shaping environmental parameters:

1. Irradiation temperature (maximum local conditions)
2. Fuel burnup (maximum discharge design value)
3. Fast fluence (maximum calculated value)
4. Power (maximum local value for fuel pebble or compact)
5. Time dependency of key plant parameters associated with normal operations (e.g., pebble flow) and transients (i.e., anticipated operational events)

With respect to parameter 4 above, it should be noted that HTGR fuel irradiation safety testing is generally "accelerated." Accelerated testing is conducted to obtain results (i.e., fuel performance information) in a shorter time. Accordingly the fuel target burnup is attained in much less (e.g., 1/3) time than would be attained in the specific reactor application. Acceleration results in fuel element and CFP particle powers that are significantly higher than the maximum local power for the specific reactor design. German and United States HTGR fuel irradiation data suggests that accelerated irradiations are conservative, especially with respect to CFP failure mechanisms such as kernel migration. However, this may not be so clear for mechanisms such as SiC layer corrosion. SiC chemical attack by lanthanides and palladium is a time-dependent phenomenon and accelerated (i.e., shorter) irradiations may not be conservative. This issue is discussed further in the section on irradiation testing for the validation of test methods.

The following are illustrative examples of potential test matrixes to assess TRISO CFP performance in connection with Type 1 and Type 2 testing for fuel qualification and Type 3

safety margin testing (boxes shown with a grey background) for several of the above parameters. However, the parameter values for Type 1 and Type 2 tests depend on the design-specific conditions. These design-specific values have not yet been finalized or reported in many cases for the PBMR or the GT-MHR designs. However, since somewhat more information is available for the PBMR, illustrative examples are provided for the PBMR preliminary design. Accordingly, the lower end of the parameter values is provided for illustrative purposes only.

#### Irradiation Temperature

The following illustrative test matrix is intended to map the performance of TRISO CFPs over the range of steady-state irradiation temperatures between the maximum design value (at the low end) and temperatures for which an elevated fuel failure fraction might be expected occur (at the high end).

Irradiation Temp (°C)	Burnup	Fast Fluence
Max Design	≥ Max Design	≥ Max Design
Max Design + 200	≥ Max Design	≥ Max Design
Max Design + 300	> Max Design	> Max Design
Max Design + 400	> Max Design	> Max Design

#### Fuel Burnup

The following illustrative test matrix is intended to map the performance of TRISO CFPs over the range of fuel burnup conditions between the maximum design value (at the low end) and burnups for which an elevated fuel failure fraction could be expected (at the high end).

Burn-up	@ Irradiation Temperature	@ Fast Fluence
0 to Max Design	≥ Max Design	> Max Design
Max Design to > Max Design	≥ Max Design	> Max Design
> Max Design to >> Max Design	> Max Design	> Max Design

#### Time Dependency of Conditions

Figure 9, "PBMR Fuel Temperature Cycling During Irradiation (Irradiation Test Approximation of Actual Temperature vs Time Profile)," illustrates the kind of irradiation temperature history needed to assess CFP performance over time for thermal cycling of CFPs due to cyclic downward pebble motion through a PBMR core (due to continuous online refueling) and due to core-wide temperature heatup transients (due to periodic loss of normal power conversion system heat removal). The thermal cycling during irradiation would address both high-temperature and low-temperature failure mechanisms and the dynamic effects of thermal cycling of the fuel. This irradiation testing is considered part of fuel qualification rather than margin testing.

For the PBMR core design, CFP irradiation temperature cycling occurs in parallel with CFP power cycling due to the effects of the fuel pebble flowing downward through the core many times to achieve the design burnup. The superposition of these two effects is not generally possible in test reactor facilities unless the reactor irradiation activities are dedicated to the HTGR fuel testing.

Plant parameters considered to be of relatively minor importance to CFP performance include environmental factors such as helium coolant pressure, helium coolant flow, and fuel element in-core mechanical loadings. However, it would be expected that coolant impurities (e.g., oxygen, water at the specified operating limits) which could lead to slow chemical attack of fuel elements (and possibly the CFPs) over long periods would be considered in the test program. Measurements (or calculations) of in-reactor fuel irradiation conditions would be expected to include parameters such as fuel element effective full-power days, percent fissions of initial metal atoms (FIMA), fuel element surface temperature, and fuel element power.

In-reactor CFP performance measures during irradiation (i.e., indicators of fission product release and CFP failures) would include release-to-birth (R/B) values for gaseous fission products such as krypton-85m, krypton-88, krypton-87, xenon-133 and xenon-35. For reasons of costs and efficiency, the number of fuel pebbles or compacts generally tested in HTGR fuel irradiation tests is typically small and results in a CFP sample size (e.g.,  $10^5 - 10^6$ ) which is a very small fraction of the number of CFPs in an actual HTGR core (e.g.,  $\sim 10^{10}$ ). Accordingly, the CFP failures rates during irradiation must be statistically analyzed. It would be expected that a 95% confidence level would be applied to the statistical analysis for determining the failure rate in the large population of CFPs in an HTGR core. Thus even if zero CFP failures were to occur in the test, following a statistical analysis, a non-zero failure rate would be calculated indicative of a theoretical irradiation test where the number of CFPs tested approached the number in an HTGR core.

It would be expected that out-of-reactor measures of fuel performance would include post-irradiation examination techniques such as metallography on intact particles and metallography and scanning electron microscope examinations on failed CFPs to determine the failure mechanism(s), if any. It is also expected that Type 1 and Type 2 testing would involve a level of quality assurance (QA) that is consistent with the applicable criteria in 10 CFR Part 50, Appendix B, "Quality Assurance Requirements for Nuclear Power Plants and Fuel Reprocessing Plants." However, since Type 3 testing addresses fuel behavior for conditions that are substantially beyond the licensing basis, the level of QA, although expected to be considerable, would not be expected to reach that of Appendix B.

#### Accident Condition Testing

A major focus of accident condition performance testing for fuel qualification is to quantify the CFP failure rates and fission product releases associated with production fuel during potential accidents. In this regard, HTGR accidents generally fall into one of three types: heat-up accidents, chemical attack accidents (e.g., oxidation), and reactivity accidents. Based on the historical testing and analysis of HTGR fuel with TRISO CFPs, the prior irradiation history (e.g., irradiation temperature, fuel burnup) "preconditions" the fuel and is an important influence on CFP performance during heatup accidents. Preconditioning may also contribute to fuel performance during chemical attack accidents and reactivity accidents.

Similar to failures that occur during irradiation, CFP failures that occur during accidents can result from latent factors associated with (less than optimum) fuel designs and (less than optimum) fuel manufacturing specifications, as well as factors associated with the environment (i.e., accident conditions). Additionally, CFP failures can result from CFPs which are fabricated outside the manufacturing specification or for which needed specifications were lacking (i.e., so called "weak fuel").

The vision for HTGR fuel accident condition testing would involve production fuel with CFPs that were (a) initially preconditioned due to the operating environments defined by the envelope of Type 1 and/or Type 2 irradiation tests and then (b) subjected to: (i) the limiting accident conditions that define the plant-specific licensing basis for each of the three types of accidents, (ii) accident conditions that are significantly beyond these limits for each type of accident, and (iii) accident conditions which are even further beyond these accident conditions to establish the threshold where large and unacceptable CFP failure fractions, and/or unacceptable fuel behavior (e.g., dispersion) will begin to occur. The accident condition testing associated with Types i and ii heatup tests is generally included in historical HTGR fuel qualification test programs, and Type ii conditions can be substituted as a conservative basis for Type i accident conditions. Accident condition testing associated with Type iii tests is referred to here as "safety margin" accident condition testing to assess the available safety margins to significant CFP failure rates during postulated accidents.

The accident conditions envisioned for the fuel performance test matrix for Type i, Type ii, and Type iii tests would be determined based on the previously discussed failure modes and the design-specific events that are part of the PBMR and GT-MHR licensing bases. It would be expected that the accident condition test matrix would utilize fuel that had been previously irradiated (i.e., preconditioned) with Type 1 or Type 2 testing in appropriate conservative combinations (e.g., irradiation temperature, burnup, time dependency of conditions). These combinations are discussed further for heatup events, chemical attack events, and reactivity events.

The following are illustrative examples of potential test matrixes to assess TRISO CFP performance in connection with Type i and Type ii testing for fuel qualification and Type iii safety margin testing (shown with a grey background) for several of the above parameters.

The parameter values for Type i and Type ii tests depend on the design-specific conditions. Again, the design-specific accident condition values have not yet been finalized or reported for either the PBMR or the GT-MHR. However, since somewhat more information is available for the PBMR, illustrative examples are provided for the PBMR preliminary design. Accordingly, the lower end of the parameter values is provided for illustrative purposes only.

### Heatup Testing

The following illustrative test matrix is intended to assess the accident condition performance of TRISO CFP for a range of prior irradiation preconditioning. The accident condition maximum heatup temperature (degrees centigrade) involves both the maximum design value (at the low end) and significantly higher temperature at which an elevated fuel failure fraction might be expected to occur.

Prior Irradiation Conditions <sup>2</sup>			Max Accident Temp (°C) <sup>3</sup>		
Condition	Value	Type	Max Design	Safety Margin	Type
Irradiation Temperature	Max Design	1 or 2	1600	1800	i & iii
Irradiation Temperature	Safety Margin	3	1600	-	i
Fuel Burnup	Max Design	1 or 2	1600	1800	i & iii
Fuel Burnup	Safety Margin	3	1600	-	i
Time Dependency of Conditions	Max Design	1 or 2	1600	1800	i & iii

### Chemical Attack Testing

Among the most limiting events that could challenge HTGR CFP integrity are those involving large-scale chemical attack such as air intrusion following a large pipe break in the reactor coolant pressure boundary (RCPB) and moisture intrusion for a postulated heat exchanger tube failure with the reactor helium pressure falling below the heat exchanger tube pressure. While there have been experiments on oxidation of unirradiated HTGR fuel in air and water at HTGR accident temperatures and measurements of HTGR fuel oxidation due to air or moisture impurities in helium during fuel experimental irradiations, relatively few experiments have been conducted on fully irradiated HTGR fuels to simulate the effects of large air or water ingress events. Additional post-irradiation accident simulation tests that closely simulate air or water intrusion events and take the fuel to the onset of CFP failures would be needed to fully assess the adverse effects of air and water corrosion on HTGR fuels and the margins to failure for such events.

The following illustrative test matrix is intended to assess the accident condition performance of fuel elements with TRISO CFPs for chemical attack testing. The accident condition chemical attack involves air ingress and would simulate the maximum oxidation for both the licensing basis worst case air ingress event and a significantly higher level of oxidation for which an elevated CFP failure fraction might be expected to occur. Based on currently available information the worst case licensing basis temperature might be as high as 1200° to 1400°C with an upper bound of 1600°C for safety margin testing. The velocity of air flow past the fuel would be representative of the rate of air flow through the core during the accident. The PBMR fuel design involves a thinner layer of unfueled "sacrificial" graphite between the fuel element surface and the CFPs compared to the GT-MHR design. Accordingly, potential air-induced chemical attack of the CFPs may be less over a given time for a GT-MHR than for a PBMR.

---

<sup>2</sup> With Fast fluence > Max design

<sup>3</sup>Over Several hundred hours

Prior Irradiation Conditions			Accident Chemical Attack Temp (Degrees C)		
Condition	Value	Type	Max Design	Safety Margin	Type
Temperature, Burnup and Fluence	Max Design	1 or 2	TBD	CFP Failures	i & iii

In addition to fuel element (e.g., pebble) testing, it is expected that testing of loose CFPs will be conducted. The loose CFPs would also be preconditioned first. Loose CFP accident testing would assess the performance capability of CFPs that are exposed directly to an oxidizing accident environment as a result of the prior oxidation loss of the surrounding fuel element matrix material.

### Reactivity Testing

Very limited testing has been conducted on fuels with TRISO CFPs to assess the capabilities and the margins to CFP failure for reactivity events involving a large energy deposition in the fuel over a very short time interval (< 1 second). Some limited testing was conducted in Japan for a postulated control rod ejection accident in support of the High Temperature Test Reactor (HTTR) licensing and was one of the limiting licensing basis events. The staff has been told that the PBMR design does not have a potential for such large and rapid reactivity events. Further, the GT-MHR control rods, which are located in the central core (fueled) region, are expected to incorporate engineered safety features to prevent a failed drive housing from rapidly and fully ejecting a control rod from the core. In order to fully understand the margins to failure for reactivity events, fuel irradiation experiments involving such reactivity insertion events would need to be conducted.

The reactivity addition testing is to simulate the worst case reactivity event and a significantly higher energy deposition and deposition rate at which an elevated CFP failure fraction will occur. GT-MHR core design involves higher excess reactivity than a PBMR core due to the need for extended cycle lengths between refueling. The continuous online refueling of a PBMR core results in relatively low excess reactivity. Hence energy depositions and deposition rates are expected to be low. Nevertheless, reactivity addition testing should be conducted and should consider the competing effects of burnup. At lower burnups the higher reactivity additions and energy depositions are possible. However, at low burnup the CFPs would be expected to better withstand the effects of a reactivity accident since limited adverse fuel preconditioning would have yet to occur. At higher burnup less reactivity is available for energy deposition but the fuel conditioning may make the CFPs more susceptible to failure. Accident condition testing of reactivity additions appropriate for a range of burnups should be considered to identify the worst case situation. The following illustrative test matrix is intended to assess the accident condition performance of fuel elements with TRISO CFPs for reactivity addition accidents.

Prior Irradiation Conditions			Reactivity Addition		
Burnup (GWd/t)	Irradiation Temp	Type	Max Design	Safety Margin	Type
0	Fresh Fuel	Fresh Fuel	TBD	CFP Failures	i & iii
60	Max Design	1 or 2	TBD	CFP Failures	i & iii
125	Max Design	1 or 2	TBD	CFP Failures	i & iii

Accident condition CFP performance measures (i.e., indicators of fission product release and CFP failures during heatup) would include release-to-birth (R/B) values for gaseous fission products such as krypton-85m, and solid fission products such as iodine-131 and iodine-132, cesium-137 and cesium-134 and strontium-90. It would also be expected that out-of-reactor measures of fuel performance would include post-irradiation examination techniques such as metallography on intact particles and metallography and scanning electron microscope examinations on failed particles to determine the CFP failure mechanism(s), if any.

#### FPT Testing

The CFP failure fraction due to manufacture, normal operation, and accident conditions is meant to be very, very small (i.e.,  $10^{-5}$  to  $10^{-4}$ ). If successful, the planned approach, to primarily retain fission products where they are produced—within the fuel—would be nearly fully achieved. However, HTGRs such as the GT-MHR may not meet the specified offsite radiological dose limits unless credit is also taken for the FPT delays provided by the fuel kernel, CFP coatings, fuel matrix material, nuclear graphite structure, and fission product plateouts provided by the primary coolant pressure boundary metallic surfaces and the reactor building concrete surfaces. Accordingly, if credit is to be taken for the FPT transport delays in the source term analysis, testing will be needed to develop and validate the applicable FPT models. The following are some of the HTGR fuel-related FPT modeling issues and test data needs.

1. Fission gas release from failed production particles. This would involve the measurement of fission gases from either loose kernels or kernels in fuel matrix material during both irradiation and heatup accidents as a function of fuel temperature.
2. Transport (i.e., diffusion) of irradiated kernels from failed production CFPs. This would involve the measurement of metallic fission product release from either loose kernels or kernels in fuel matrix material during irradiation.
3. Transport of fission products through intact production CFPs.
4. Transport (i.e., diffusion and holdup) of metallic fission products through irradiated production matrix material and the irradiated nuclear grade graphite selected for the fuel elements (GT-MHR only) as a function of temperature and fast fluence.

Validation of Test Methods

The following is a discussion of issues related to the applicability of methods that are traditionally used for HTGR fuel irradiation and accident condition performance testing. Tests to assess and resolve these issues are also provided.

Irradiation Test Methods

Virtually all of the past and ongoing worldwide irradiation testing research of HTGR fuel designs with TRISO CFPs has involved accelerated irradiations in materials testing reactors. Although there subsequently was significant large-scale, real-time, integrated irradiation operating experience with these fuels in plants such as the AVR in Germany, accident simulation tests (i.e., fuel heatup tests following irradiation) to qualify the fuel involved accelerated irradiations in test reactors. German and U.S. HTGR fuel irradiation data suggests that accelerated irradiations are conservative, especially with respect to CFP failure mechanisms such as kernel migration. However, as noted previously, this may not be the case for mechanisms involving SiC chemical attack by lanthanides and palladium, which are time-dependent phenomena. Thus accelerated (i.e., shorter) irradiations may not be conservative. Additionally, there is not a well-established and thorough understanding of the mechanics and properties (e.g., outer pyrolytic carbon shrinkage and creep) of CFP behavior, or test data, to conclude with certainty that fuel accident simulation tests following accelerated irradiations are conservative as compared to the rate of fuel irradiation in a power reactor. Irradiations in real time followed by accident simulation heatup tests either after real-time fuel irradiation tests (or after fuel irradiations in a power reactor) would be needed to resolve this issue.

The following illustrative test matrix is intended to compare the irradiation performance and accident condition heatup performance of fuel elements with TRISO CFPs for irradiation testing conducted using both the traditional accelerated irradiation testing method and the real-time irradiation testing method.

Prior Irradiation Conditions			Max Accident Temperature (°C)
Condition	Value	Type	
Irradiation Temperature	Max Design	1 or 2	1600
Fuel Burnup	≥Max Design		
Fast Fluence	≥Max Design		
Irradiation Rate	Accelerated		
Irradiation Temperature	Max Design	1 or 2	1600
Fuel Burnup	≥Max Design		
Fast Fluence	≥Max Design		
Irradiation Rate	Real time		

### Accident Condition Test Methods

Virtually all of the accident simulation tests for TRISO CFPs involved so called "ramp and hold" temperature increases. As shown in the Figure 10, "Comparison of Ramp and Hold versus Transient Accident Simulation Temperature Profiles," these typically consist of increasing fuel temperature at about 50°C/hr up to a set temperature (e.g., 1600°C, 1700°C or 1800°C) and then holding the fuel at the set temperature for several hundred hours while fission product release measurements are taken. The results of ramp-and-hold tests up to 1600°C, for German qualified fuel, show that no additional CFP failures occur. However, there were a few tests conducted in Germany in which the temperature was controlled to closely simulate the predicted accident heatup curve to about 1600°C for a design basis heatup accident. For this test, a small number CFP failures were observed to occur within the irradiated fuel.

To address the issue of whether ramp-and-hold testing is appropriate, additional post-irradiation accident simulation tests that closely simulate the predicted temperature curve for a design basis reactor coolant pressure boundary failure would be required to determine if the traditional ramp-and-hold test accident simulation approach is conservative with respect to establishing CFP failure rates for postulated accidents.

The following illustrative test matrix is intended to assess the accident condition performance of fuel elements with TRISO CFPs for heatup testing conducted using both the ramp and hold test method and the simulated time versus temperature test method.

Prior Irradiation Conditions			Accident Simulation Method	
Condition	Value	Type	Max Temp 1600°C	Max Temp 1600°C
Irradiation Temperature Fuel Burnup Fast Fluence Irradiation Rate	$\geq$ Max Design $\geq$ Max Design $\geq$ Max Design Accelerated	1 or 2	Ramp and Hold	Simulated Accident time versus temperature

### Summary

The intended safety characteristic of the TRISO coated fuel particles within fuel elements is to provide the principal barrier and the primary containment function against the release of fission products to the environment during both normal operation and postulated accident conditions. Given the significance of the fuel barrier for the HTGR designs, the fuels research program will be used to provide insights on fission product source term for normal operation and accident conditions. The advanced reactor research infrastructure assessment identified the need for fuel irradiation and accident condition testing to obtain data to establish operating and accident fuel safety margins; to assess the acceptability of an applicant's fuel irradiation and accident simulation testing programs; to verify an applicant's claims of fuel performance and fission product release during operations and accidents; and to provide data to develop and validate analytical fuel performance tools. These data are needed to support a policy decision on the use of an HTGR mechanistic source term and HTGR licence application reviews.

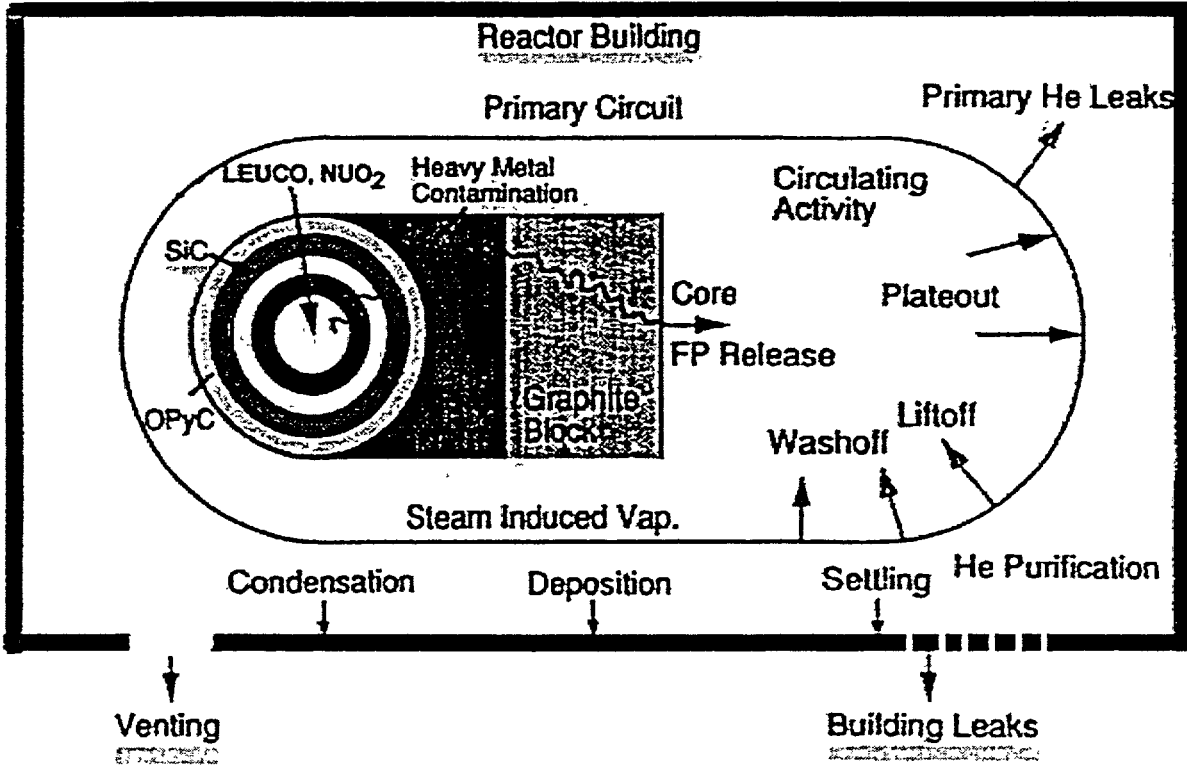


Figure 1: HTGR Fission Product Source Term Factors (GT-MHR)

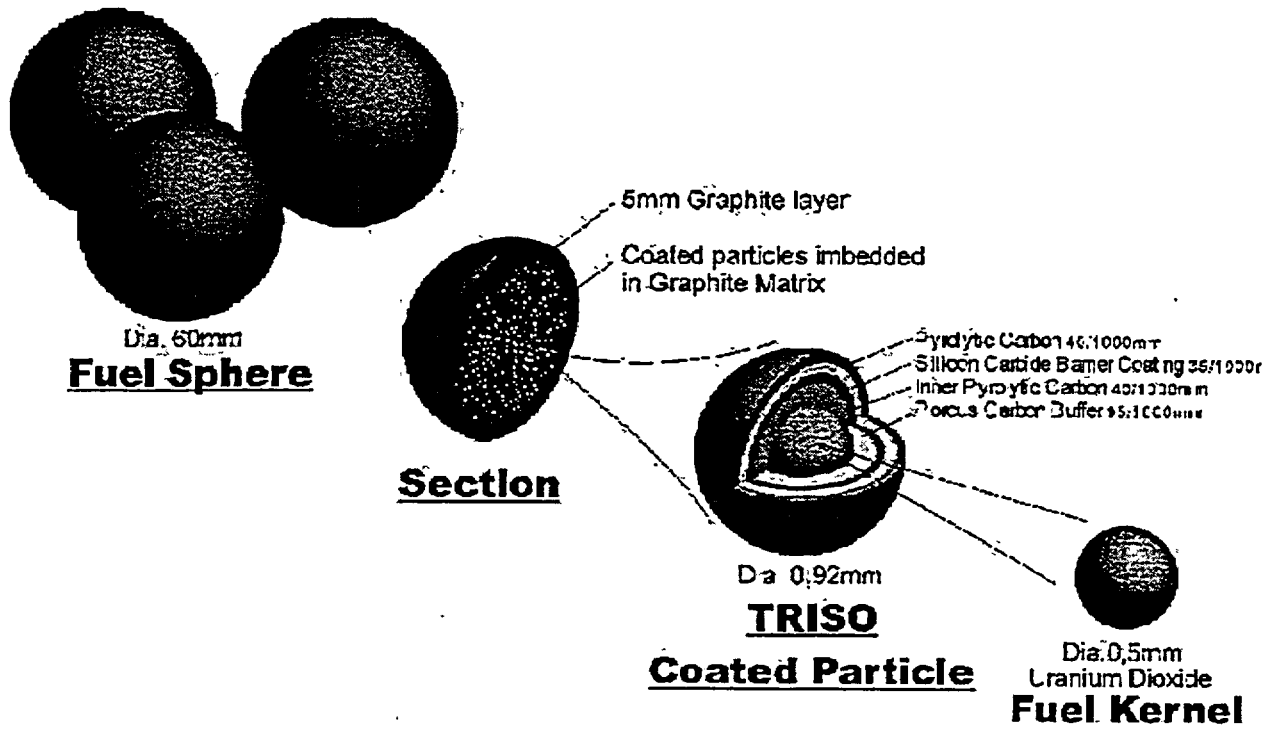


Figure 2: Pebble Fuel Element Design

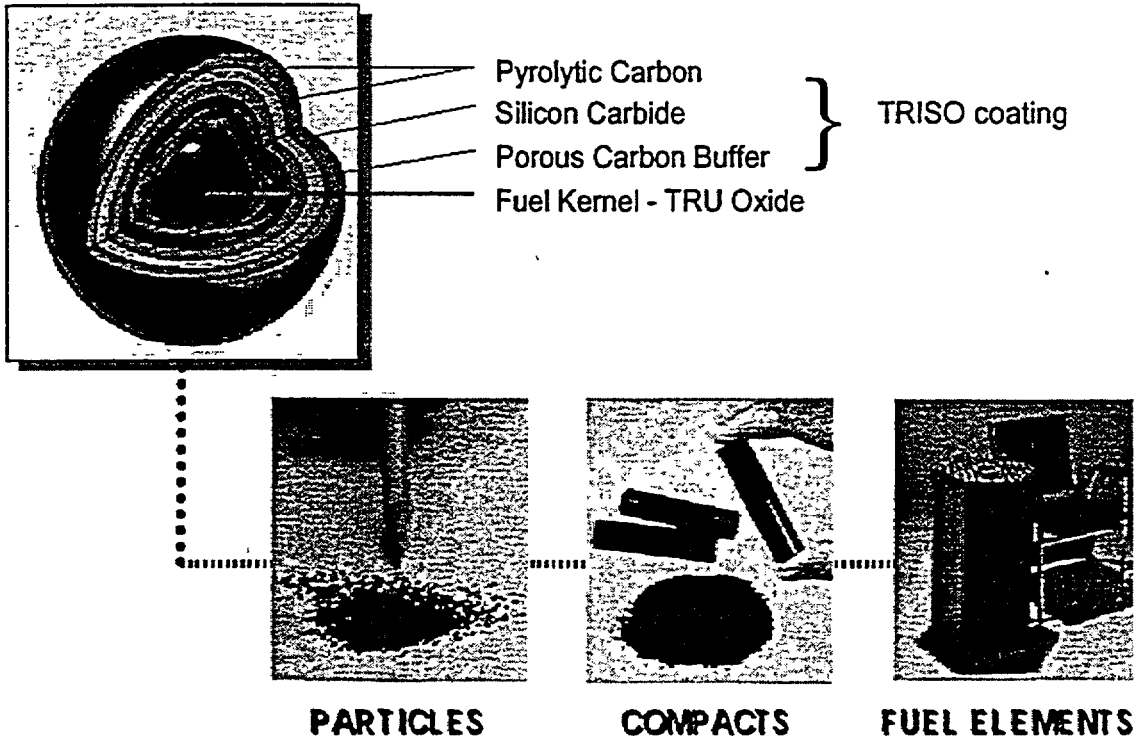


Figure 3: Prismatic Fuel Element Design

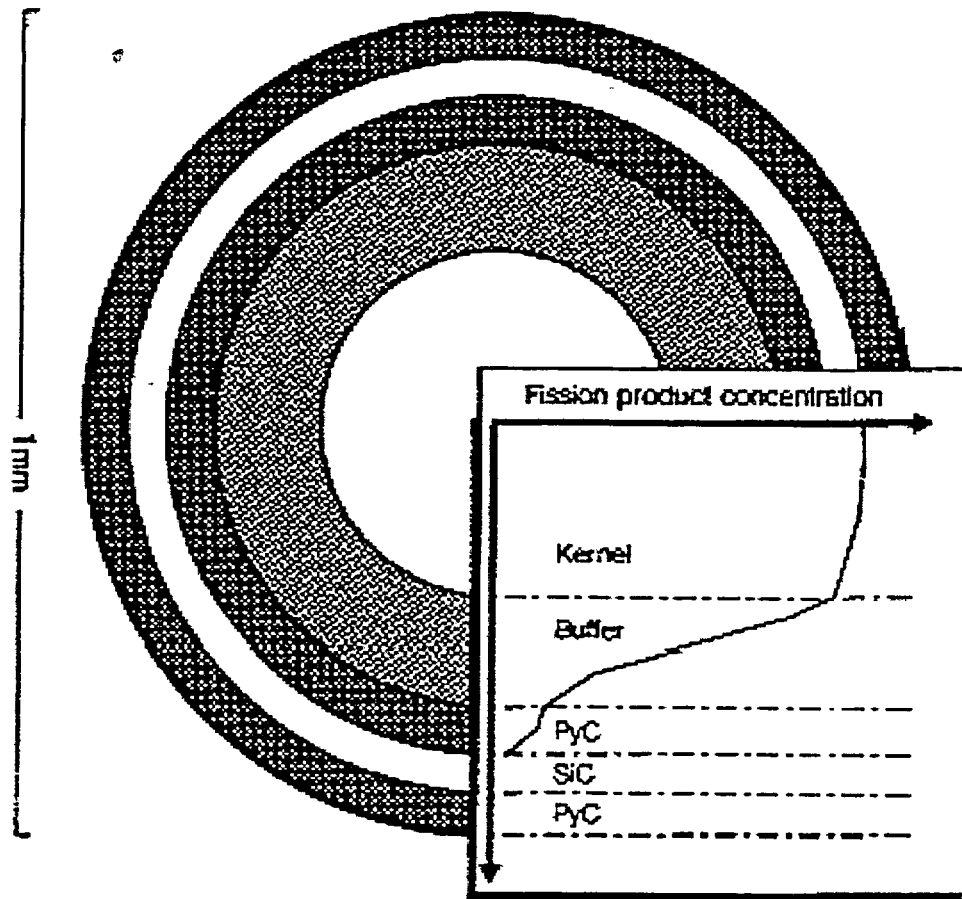


Figure 4: Relative Fission Product Concentration Within an Irradiated TRISO Fuel Particle

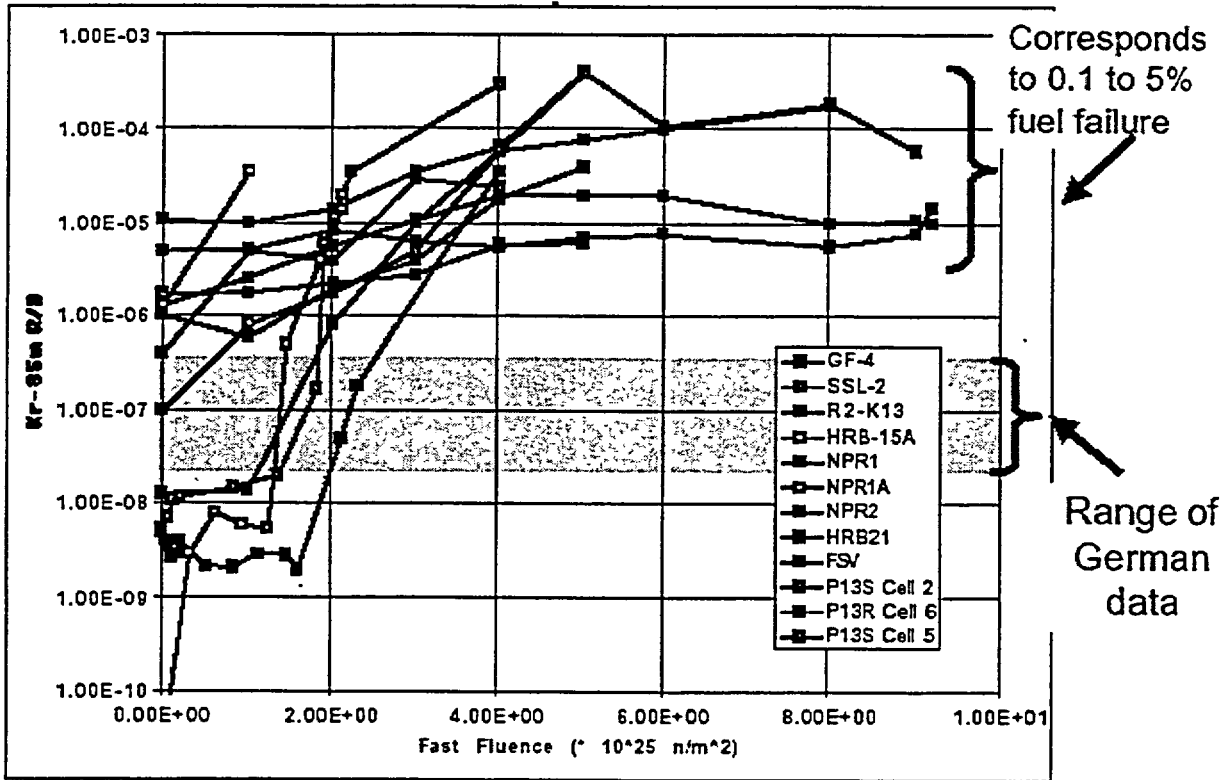


Figure 5: Comparison of U.S. and German TRISO Fuel Irradiation Performance (Source INEEL)

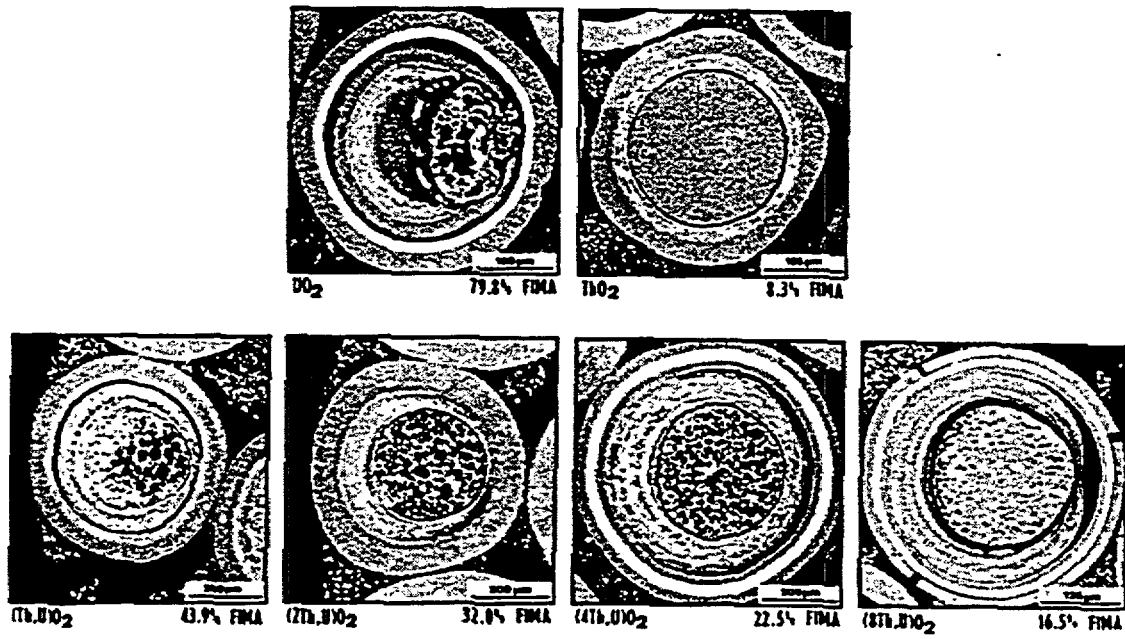


Figure 6: TRISO Coated Fuel Particle Kernel Migration Failure

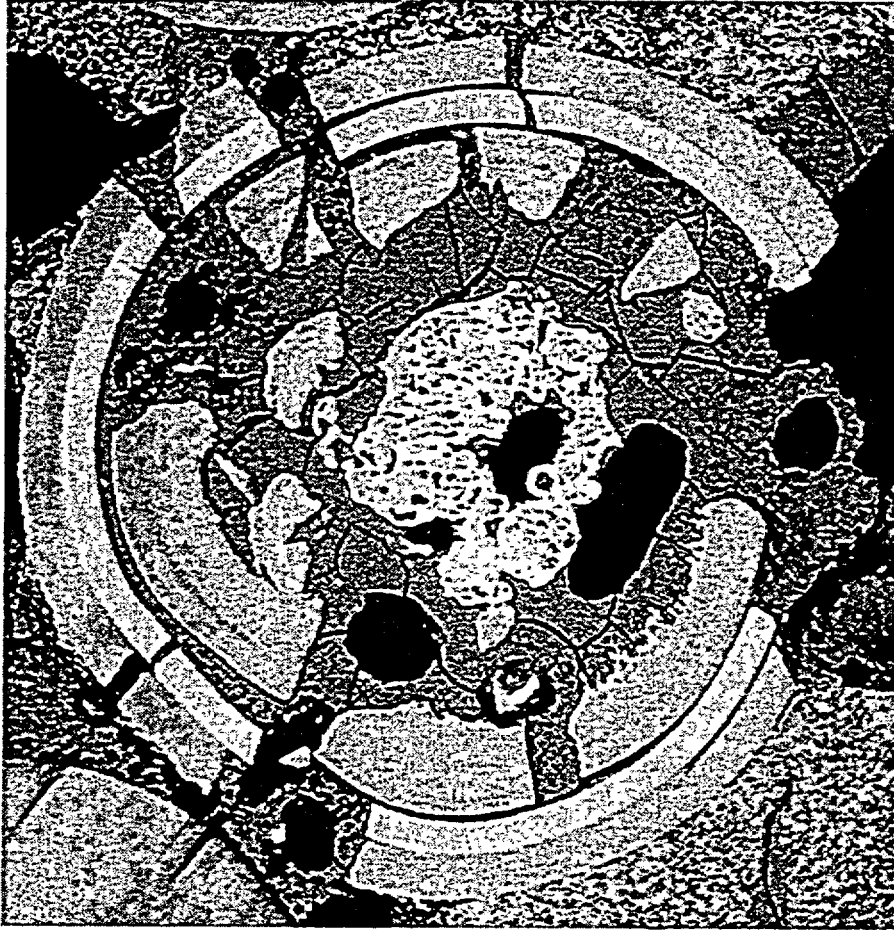


Figure 7: TRISO Coated Fuel Particle Pressure Vessel Failure

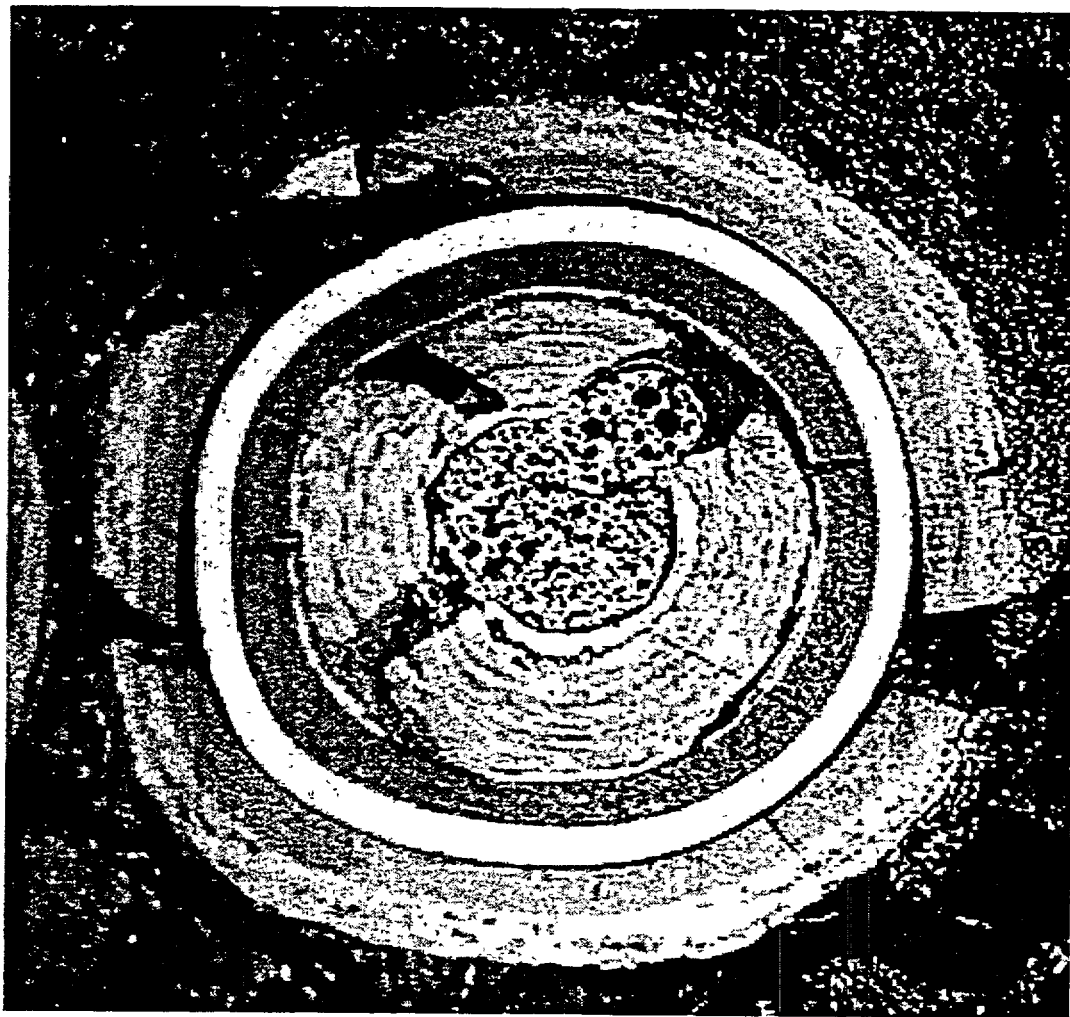


Figure 8: TRISO Coated Fuel Particle Outer Pyrolytic Carbon Layer Cracking/Debonding Failure

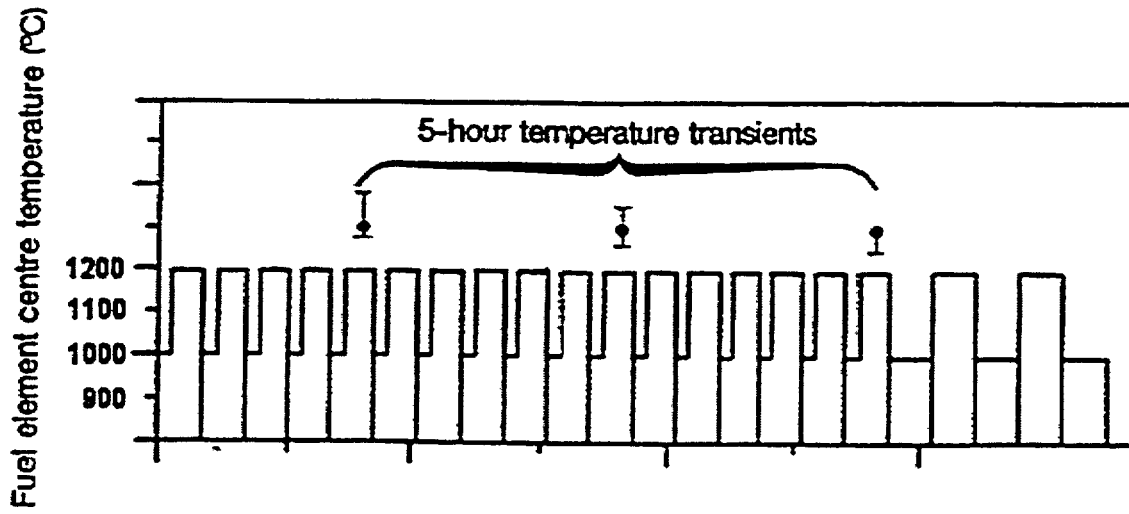


Figure 9: PBMR Fuel Temperature Cycling During Irradiation  
(Irradiation Test Approximation of Actual Temperature vs Time Profile)

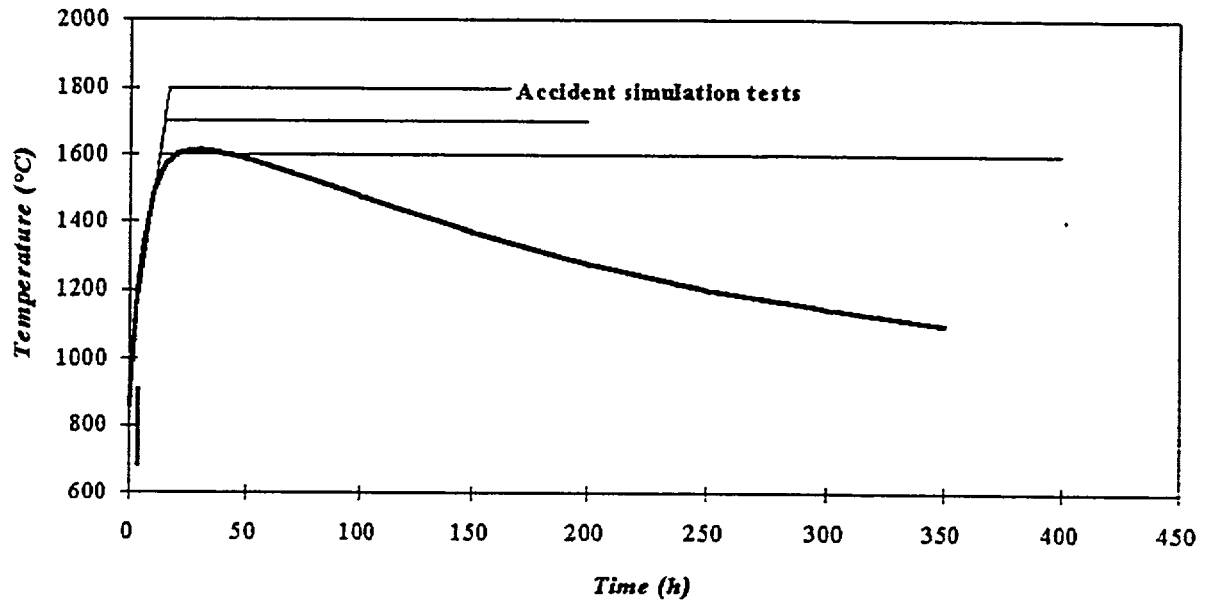


Figure 10: Comparison of Ramp and Hold versus Transient Accident Simulation Temperature Profiles

## **MATERIALS RESEARCH NEEDS FOR ADVANCED REACTORS**

**Charles A. Greene, Joseph Muscara, Makuteswara Srinivasan  
Office of Nuclear Regulatory Research  
U.S. Nuclear Regulatory Commission**

Metallic and graphite components in advanced high-temperature gas-cooled reactors (HTGRs) may experience creep, fatigue, oxidation, aging, corrosion cracking, irradiation damage, and dimensional changes. The safety design of these reactors, such as the pebble bed modular reactor (PBMR) and the gas turbine modular helium reactor (GT-MHR), depends heavily on the long term integrity of metallic and graphite components needed to maintain pressure boundary integrity, core geometry, adequate cooling of the core, and reactivity control and shutdown systems. Failure of these components could result in air, water and/or steam ingress, and accompanying adverse consequences. In most Advanced Light Water Reactors (ALWRs), the operating conditions, materials, and coolant environments are similar to those of conventional LWRs. Nevertheless, there may be a need for new research in the materials area specifically for ALWRs. This paper discusses the information gaps that exist in terms of analytical tools and data shortcomings and describes research needed to establish an acceptable technical understanding of the behavior of metallic and graphite components in advanced reactor environments.

### **BACKGROUND**

A key research area important to the safety of advanced reactors is the behavior of metallic and graphite components. These components are relied on for structural, barrier, and retention functions during normal and off-normal reactor conditions. Therefore, a sound technical basis must be available for evaluating expected lifetime and failure modes of reactor pressure vessel materials and components whose failure would result in loss of core geometry and/or ingress of air, water, or steam to the pressure boundary. In the HTGR design, high-temperature materials are required to maintain core geometry, adequate cooling of the core, access for reactivity control and shutdown systems and, in the case of the Pebble Bed Modular Reactor (PBMR), a defueling route. This paper emphasizes the need for research to establish a technical understanding of the metallic and graphite components under high-temperature operating and accident conditions.

The licensing approach for HTGRs used by the U.S. Nuclear Regulatory Commission (NRC) to independently confirm design and support safety evaluations relies heavily on the use of probabilistic risk assessment (PRA). Information from the materials research area is needed for conducting PRAs. Since failure probability data for components of advanced reactors are not available from experience, the information can be developed from materials research on potential degradation processes and quantification of their progression. Evaluation of component service life, safety margins, and behavior under accident conditions is dependent on environmental factors such as temperature, pressure, coolant composition, and fluence.

The operating conditions, materials, and coolant environments used in ALWRs are similar to those of conventional LWRs. Therefore, lessons learned from the design, materials choices, and environments of LWRs should be taken into account for ALWR applications. Despite this similarity, the perception should be avoided that there is not a need for new research in the materials area specifically for ALWRs. A large body of research data, from both the U.S. and Japan, has shown a detrimental effect of the coolant environment in reducing the fatigue life of LWR components. Methods have been developed and are widely available in the literature (NRC NUREG reports and Pressure Vessel Research Council (PVRC) report) for taking into account the effects of the operating environment in the fatigue design of components. Although the American Society of Mechanical Engineers (ASME), through its on-going code activities, is addressing the issue of the effects of the environment, it has not yet incorporated changes in its design rules and correlations. Therefore, during design and review of ALWRs, caution must be exercised to ensure that the effects of the environment are appropriately accounted for in the fatigue design and evaluation of components. The ASME should continue to update its rules for fatigue design of components. In addition, design rules for advanced reactor designs may need to incorporate different materials and correspondingly different deformation mechanisms.

Several aspects of the HTGR and ALWR designs raise the potential for the need for improved inservice inspection (ISI) programs and for continuous monitoring. More components are enclosed in pressure vessels making access for inspection difficult, and there are longer operating cycles between scheduled, short-duration, refueling outages when inspections can take place. This suggests a need for evaluating effectiveness of the less frequent ISIs for timely detection of cracking and degradation of components and the potential for excessive growth of cracks before the next ISI. If periodic ISI is found to be ineffective for maintaining safety, the use of continuous online monitoring techniques for structural integrity and leakage detection may be required.

## **RESEARCH PURPOSE**

The advanced reactor designs exhibit a departure from traditional LWRs in terms of the materials used, such as high-temperature metals and graphite; higher coolant temperatures; a coolant that does not change phase; different degradation mechanisms such as creep; and expected behavior of the components in this environment. This departure thrusts the materials – environment combination into a regime where more information is needed to define long term behavior and safety margins.

In HTGRs, graphite acts as a moderator, reflector, major structural component that will provide channels for the fuel, coolant gas, control and shutdown rods, and a thermal and neutron shield. Additionally, graphite components are employed as supports. Graphite also acts as a heat sink during reactor trip and transients. During reactor operation, many physical properties of graphite are significantly modified as a result of temperature, environment, and irradiation. Significant internal shrinkage, bowing, and stresses can develop which may cause component failure, and/or loss of core geometry. When graphite is irradiated to a very high radiation dose, ensuing swelling causes rapid reduction in strength, making the component lose its structural integrity. In the event of an accident allowing air ingress, subsequent graphite oxidation causes further changes in its physical and mechanical properties.

Research had progressed through the 1980s on the high-temperature design (creep, fatigue) of metal components for the Liquid Metal Fast Breeder Reactor. This research formed the basis for some ASME code cases and requirements for the design of high-temperature components. The NRC staff has initiated a program to review and evaluate this research and that which has progressed since the 1980s/1990s, in particular with respect to the temperatures, coolant environment, and materials to determine applicability to current HTGR designs and develop its own capability.

Development of a research capability in the materials area beyond the licensing basis is needed to understand safety margins, failure points, and reduce uncertainties. To conduct independent PRAs of advanced reactors, information is needed on the probability of failure of various reactor components. Because of the lack of operating experience, this information will have to be developed analytically using probabilistic fracture mechanics. Thus, potential degradation mechanisms of metallic and graphite components need to be identified and progression of degradation quantified under the operating reactor conditions. Potential technical issues that need to be addressed are: (1) national codes and standards for design and fabrication of metallic and graphite components for service in HTGR helium environments; (2) appropriate data bases for calculating fatigue, creep, and creep-fatigue interaction lifetimes of components in high-temperature applications; (3) the effects of impurities, including oxygen, in the high-temperature helium on degradation of components; (4) sensitization and aging behavior of alloys during elevated temperature exposures; (5) treatment of pipe as a vessel in a HTGR; (7) degradation by carburization, decarburization, and oxidation of metals in HTGRs; (8) issues related to inspection of HTGR and ALWR reactor components; (9) long term performance and degradation of graphite and new reactor pressure vessel materials under high levels of irradiation; (10) modeling and methodology that predict irradiated graphite properties from non-irradiated properties; and (11) comprehensive understanding of the governing rates and mechanisms for the oxidation of reflector grade graphite, fuel pebble matrix graphite, and graphite dust. Each of these potential technical issues is addressed in the following paragraphs. As mentioned, information is needed to develop research capability for the high-temperature behavior of materials in HTGRs and the materials – environment combination of ALWRs beyond the licensing basis to reduce uncertainty and to gain confidence and understanding of defense-in-depth.

## **CONSIDERATIONS FOR METALLIC COMPONENTS**

Research is needed to evaluate the integrity of important components in advanced reactors under operating and accident conditions. Research on metallic components will need to be conducted to evaluate and quantify degradation processes, metallurgical aging and embrittlement, carburization, decarburization, nondestructive examination, and ISI. In addition, currently available (international) procedures for design against fatigue, creep, and creep-fatigue will be reviewed and evaluated. The objective of this review is to evaluate current code design rules and procedures and to provide input for improvements as necessary. The best procedures will be updated to incorporate correlations developed from more recent research.

The availability and acceptability of national codes and standards for the design and fabrication of metallic components for service in HTGRs and ALWRs is a key issue. For high temperatures, background studies and activities for eventual development of codes and standards were conducted in the 1980s for application to the liquid metal breeder reactor. Of particular note is the work conducted by the PVRC in their preparation of several technical reports that provided the basis for development of high-temperature design codes by the ASME. These reports give

background and procedures for design of components to resist fatigue, creep and creep-fatigue failures. However, the effects of the helium environment, including the presence of impurities such as oxygen, were not addressed. In addition, improved correlations for creep and creep-fatigue have been developed from research of the 1990s. These improvements are not included in the PVRC reports and the procedures need to be updated before they are included in National Codes and Standards.

Another area of codes development has been taking place internationally for the Advanced Candu Reactor (ACR). The pressure tube material for this ALWR is not covered by the ASME codes and standards. The Canadian Standards Association (CSA) has published rules to complement those of ASME. The CSA codes have followed the ASME code where applicable, but augmented the code as necessary to include zirconium alloys for pressure tube in a reactor with on-power refueling capability. Activity should be undertaken to review and evaluate incorporation of the new materials and environments covered by the CSA codes into the ASME code.

Although methodologies could be assembled from existing knowledge for calculating fatigue, creep, and creep-fatigue lives of components in high-temperature applications, appropriate data bases are needed for these calculations. Based on past experience and research, we have found that environmental effects play an important role in reducing fatigue lives and in enhancing degradation of materials. For example, small levels of impurities, such as less than 1 part per million of oxygen in the high purity water coolant of LWRs, can greatly decrease fatigue life and resistance to stress corrosion cracking of metallic components. These effects were not originally addressed in the ASME Code. For example, the design data for fatigue was obtained from materials tests in air. Because helium is inert, there has been a tendency to obtain design data in pure helium; in impure helium, but not all impurities included; or in air. The effects of all important impurities, such as oxygen, in helium need to be taken into account with respect to reductions in fatigue and creep life and such data and understanding need to be developed. Environmental effects on fatigue under ALWR operating conditions need to be addressed as well.

Research will be conducted on the effects of an impure helium environment, especially the effects of oxygen, temperature, and strain rate, on the fatigue life of HTGR metallic components. Similarly, the effects of impure helium environments on the creep and creep-fatigue life of HTGR components will be investigated. The objective of this research is to ensure that the design rules and procedures available address reductions in life due to the operating environment. If the codes and procedures do not consider these phenomena, then the data base developed can be used to update the codes and procedures to provide design procedures and rules that avoid failure of HTGR components during service. In addition, research will need to be conducted to quantify the effects of carburization and decarburization on the reduction of fatigue and creep life to ensure that these reductions are accounted for in the design procedures and analyses.

To address degradation and aging of metals in HTGRs, the effects of high-temperature helium with impurities including oxygen at levels present in HTGRs need to be evaluated with respect to stress corrosion crack initiation and growth rate, crevice corrosion crack initiation and growth rate, and cyclic crack growth rate. Low levels of impurities in high-temperature, high purity aqueous environments are known to cause these types of degradation and to accelerate the crack growth rates. The potential exists for these phenomena to occur in a high-temperature helium environment with low levels of impurities.

Research will be conducted on the effects of the high-temperature helium environment containing impurities, including oxygen, at levels typical of HTGRs on stress corrosion crack initiation and growth rates, crevice corrosion crack initiation and growth rate, and cyclic crack growth rate. The tests will be conducted on materials in the as-received condition and in carburized and decarburized conditions. The objective of this research is either to confirm that these degradation mechanisms do not occur and crack growth rates are not enhanced in the environments of interest or to quantify the crack initiation times, quantify increases in growth rates, and define the environmental conditions under which these occur.

Many alloys undergo solid state transformation and precipitation during elevated temperature exposures. These transformation reactions are known as aging and can lead to embrittlement of the alloy. Aging and embrittlement occurs, for example, in cast stainless steel components under temperatures and time conditions experienced in operating LWRs. At the operating temperatures of HTGRs, the reaction rates can be much higher, (i.e., the aging and embrittlement would occur sooner). The different alloys and higher temperatures of HTGRs would indicate potentially different aging reactions and mechanisms, some of which could occur relatively rapidly and render the material embrittled and susceptible to cracking. The aging reactions, as a function of time and temperature, in the different alloys used in important components of HTGRs need to be studied to establish the potential for material property degradation and embrittlement during the lifetime of operating HTGRs.

Another solid state reaction that occurs in stainless steels (and austenitic alloys) is called sensitization. Sensitization is caused by the precipitation of chromium carbides at the grain boundaries of the stainless steel. This precipitation normally occurs during slow cooling of the metal through high temperatures such as when cooling from the high temperatures following welding. Formation of the carbides depletes the chromium from the grain boundary areas rendering the stainless steel susceptible to intergranular stress corrosion cracking (cracking along the grain boundaries) in oxidizing and impurity environments. A less well known method for producing sensitization is through low-temperature sensitization. This occurs over long periods of exposures to relatively low temperatures. Low-temperature sensitization in stainless steel has been studied under temperature conditions relevant to LWRs. Under these conditions, low-temperature sensitization would not occur in times less than 40 years. However, the sensitization rate is exponential with temperature, and at the higher operating temperatures of HTGRs, there is a potential for sensitization during the lifetime of these plants thus rendering the stainless steel components susceptible to stress corrosion cracking.

Thermal aging and sensitization research will need to be conducted on high-temperature alloys used in HTGRs on samples in the as-received and the welded conditions. Samples will be exposed for different times to temperatures at and above the operating temperatures of the HTGR components. Exposure to higher temperatures will provide acceleration in the aging and sensitization reactions. As long as the aging mechanisms at the higher temperatures are the same as at the operating temperatures, correlations can be developed for quantifying the times required to reach different levels of aging and sensitization at the operating temperature. Mechanical property testing will be conducted on the aged samples to quantify the degree of embrittlement and other property changes as a function of aging time and temperature. Metallographic and microscopy studies will be conducted to identify the aging and precipitation reactions if they occur, to ensure that the reactions are the same at the operating and higher temperatures, and to evaluate the potential for and degree of low temperature sensitization. The objective of the research is to identify the potential and the degree to which thermal aging,

embrittlement, and sensitization can occur during operation of HTGRs and to evaluate the impact of these changes on the structural integrity of reactor components.

In HTGR designs, the connecting pipe which carries hot helium from the core to the power conversion system is treated as a vessel because this pipe is designed, fabricated, and inspected to the same rules as a reactor pressure vessel. The consequence of this assumption is that a design basis double ended break is not considered for the connecting pipe, and therefore, no mitigating systems are incorporated in the design. Considering this pipe as a vessel will require further investigation, because the pipe is of much smaller diameter and therefore, much thinner wall than a reactor pressure vessel designed to the same working pressure. If an unexpected degradation mechanism should initiate in the pipe because of the thin wall, it can propagate through the wall in a relatively short time and possibly not be detected by ISI. Conversely, if an unexpected degradation mechanism were to initiate in a pressure vessel, it would require long times to propagate through the greater wall thickness, allowing enough time to be detected by ISI.

Carburization, decarburization, and oxidation of metals in HTGRs are other phenomena that can lead to degradation caused by the operating gaseous and particulate environment. Carburization is a phenomenon where carbon, either as a particulate or from carbon containing gases, diffuses into steel to form a surface layer with high carbon content. This surface layer may be hard, brittle, and have higher strength than the substrate. Differences in strength and other physical properties between the surface layer and substrate may lead to high stresses in the surface layer when the component is under load. In addition, carbides may form in the high carbon surface layer of stainless steel leaving the matrix depleted of chromium and susceptible to stress corrosion cracking and oxidation. Cracking, stress corrosion cracking, and oxidation can more easily develop in the surface layer which could then propagate into the component.

Decarburization is a process whereby carbon is depleted from the steel depending on the composition of the gaseous environment. Depletion of carbon results in a softer steel and in reduced fatigue and creep lives. The presence of oxygen results in the formation of scale and general corrosion of metallic components, and more importantly, it can oxidize the graphite and render metallic components susceptible to stress corrosion cracking. To control the phenomena of carburization, decarburization, and oxidation, a very careful control of the level of different impurities in the coolant is required. Conditions that lead to avoidance of one of the above phenomena can lead to development of another. For example, to avoid carburization, some HTGRs might use slightly oxidizing conditions by addition of oxygen to the gas stream. However, this can lead to oxidation of graphite, general corrosion of metals and an increased susceptibility to stress corrosion cracking. Some research has been conducted to study the phenomena described above; however, additional confirmatory research is needed to better define the conditions under which the phenomena occur for important metallic components of HTGRs. In addition, much of the available research did not include oxygen in the gaseous environment. Since oxygen will be present in HTGRs at high enough levels to affect the progression of the above phenomena and to reduce fatigue life, creep life, and resistance to stress corrosion cracking, oxygen needs to be included in new experimental studies.

Carburization, decarburization, and oxidation of HTGR high-temperature metals will need to be studied as a function of time and temperature in helium gas with impurities, including oxygen. Different levels and ratios of impurities will be studied. Metallographic studies and mechanical testing will be conducted on the exposed samples to determine the degree of deterioration and loss of strength. The objective is to define the environmental conditions under which the phenomena can occur, to what degree they occur under the different conditions, the potential for

occurrence under the operating conditions of HTGRs, and the significance on structural integrity of components.

A number of potential degradation and aging mechanisms in the operating environment of HTGRs have been discussed. There is an opportunity to evaluate and validate these potential degradations by conducting research on components removed from operating reactors. The AVR HTGR operated for over twenty years in Germany. An international research program will need to be conducted on components removed from the AVR, including microstructural studies and mechanical tests. Microstructural studies will be conducted to determine if solid state changes and precipitation have occurred during operation to produce thermal aging, sensitization, carburization, and decarburization. In addition, metallographic studies will establish if stress corrosion cracking, crevice corrosion, general corrosion, and oxidation have occurred. Mechanical tests on materials removed from the AVR will be conducted to determine if any degradation in materials properties has occurred. Fatigue and creep tests will determine if fatigue and/or creep damage have occurred, if the design codes and methods correctly predict the damage, and if the coolant environment had an effect in reducing fatigue and creep lives. The results will help determine if and how the design codes/procedures need to be changed to take into account the potential degradation mechanisms.

With respect to international agreements, there is considerable research that has been performed or is ongoing in the European Community (EC) and Japan on high-temperature metals for HTGRs. Through interactions with technical staff in the EC and Japan, the NRC staff identified several areas that address NRC research objectives. Work of interest in the EC is (a) review of RPV materials, focusing on previous HTRs, in order to set up a materials property database on design properties, (b) compilation of existing data on materials for reactor internals and selection of the most promising alloys for further development and testing, and (c) compilation of existing data on turbine disk and blade materials and selection of the most promising alloys for further development and testing. Experimental work in these areas includes a) research on a pressure vessel steel containing 9% Cr (irradiation testing, fatigue, creep-fatigue, tensile, fracture toughness); both heavy-section base metal and weldments are included in the studies; b) mechanical and creep tests of candidate alloys for reactor internals at temperatures up to 1100° C with focus on the control rod cladding; and c) tensile, fatigue, and creep tests from 850° C up to 1300° C for two different turbine blade materials, one forming an aluminum oxide protective layer, the other a chromium oxide layer.

Work of interest that has been conducted by Japan Atomic Energy Research Institute (JAERI) includes development of a high-temperature metallic component design guide, research on high-temperature metal corrosion, and irradiation effects on a 2 1/4 Cr-1Mo reactor pressure vessel steel.

Other international efforts may include determining the long term degradation mode of glass fiber encased insulation components. This phenomenon has been identified in the UK gas-cooled reactors as discussed at the workshop on HTGR safety and research issues (October 2001, US NRC, Rockville). The objective would be to conduct studies of the effects of vibrations and service conditions to determine the reliability of this insulation since it protects the metallic components and pressure boundaries in the HTGR designs from unacceptably high temperatures. With regard to new materials and environments in the ALWRs, international efforts to augment the ASME codes and standards with the CSA codes and standards should be explored.

As mentioned above, considerable research on high-temperature materials for HTGRs of interest to NRC has been conducted, is ongoing, or planned in the EC and Japan. To leverage NRC resources and obtain data in a timely manner, the staff has visited facilities and met with members of the international community to initiate a dialogue on cooperation. Descriptions of research on high-temperature materials described in this paper and the NRC technology assessment for planning advanced research have been shared with the international community, in particular with Japan and the EC. NRC staff has met with technical staff and officials of the EC and JAERI to discuss potential cooperation. The EC has agreed with the importance and need for the research outlined in our infrastructure assessment and welcomes the NRC to participate in their high-temperature materials research (HTR-M) program. Similarly, JAERI has agreed in principle to cooperate with the NRC. Participation is through the exchange of research results, and not funds, from the parties' research programs. Some of the work described in the advanced reactor research infrastructure assessment will be addressed in the EC current program and their future program to initiate in 2003. Some of the key work possibly not fully addressed in the EC programs is in the areas of a) effects of the helium environment with impurities on degradation of materials and b) aging and sensitization. Exchange of NRC research results in these areas could be used for cooperation with the EC HTR-M programs.

## **DESCRIPTION OF ISSUES AND RESEARCH FOR INSERVICE INSPECTION AND MONITORING**

There are a number of potential issues related to the inspection of some HTGR and ALWR reactor components. Because some of these reactors are designed to operate for long periods of time between scheduled short-duration shut-downs for maintenance or refueling, ISI intervals may be long and the amount of inspection limited. Therefore, there is a need to evaluate the effectiveness of various ISI programs as a function of the frequency of inspections and the number and types of components inspected. Additionally, many internal components are not easily accessible for ISI, and the impact of not inspecting these components needs to be assessed. An alternative to conducting periodic ISIs during reactor shut-downs is to conduct continuous online, nondestructive monitoring for structural integrity and leakage detection of the entire reactor or reactor components during operation. Techniques for continuous monitoring have been developed, validated, and codified for use in LWRs. If ISIs of HTGRs and ALWRs cannot be conducted on a frequent enough basis and certain components cannot be inspected, then continuous monitoring may become necessary. The continuous monitoring techniques need to be evaluated and validated for the materials, environments, and degradation mechanisms of the HTGRs and ALWRs.

In the nondestructive examination area, research will be conducted to evaluate the impact of different ISI plans on structural integrity and risk. The key variables in the study will be the length of time between inspections, the reliability of the inspection methods, and the number of components and locations tested for HTGRs and ALWRs. Different degradation mechanisms appropriate to the reactor design and operating environment, along with the inspection variables, will be considered in probabilistic fracture mechanics analyses to evaluate the impact of potential failures on risk. Results of this work will be used to support the evaluation of proposed ISIs of HTGRs and ALWRs and to determine the technical basis for improved, more frequent, or more extensive ISIs. The results will also provide guidance on the need for continuous online monitoring of structural integrity.

Because some components are inaccessible and because the interval between ISIs may be too long, research will need to be conducted to evaluate continuous monitoring of reactor components

for crack initiation and crack growth and for leak detection. Acoustic emission techniques will be used for laboratory testing of specimens under simulated HTGR and ALWR conditions (respective temperature, noise sources, coolant flow, etc.) to evaluate fatigue, creep, and stress corrosion cracking. Correlations will be developed for crack initiation and crack growth rates with the acoustic emission signals for the materials and environments of the HTGRs and ALWRs. Similar research was conducted by the NRC in the 1980s and 1990s where acoustic emission techniques were developed, validated, and codified for application to LWRs. The research, methods, and techniques for HTGRs and ALWRs will take advantage of the knowledge gained in earlier work. Similar acoustic emission techniques will be evaluated for detection, location, and quantification of coolant leakage from the pressure boundary and internal components under the operating conditions of HTGRs and ALWRs. Again, similar work was conducted for LWR applications and the research for HTGRs and ALWRs will benefit from this. Once the laboratory research is completed and correlations of acoustic emissions to crack initiation and growth developed, an operating or test HTGR will be instrumented with acoustic emission sensors and monitored during its operation to validate the methods and correlations developed in laboratory testing. The results from this work will provide an alternative to periodic ISIs and the advantages of continuous online monitoring of reactor structural integrity and leakage. The results will also provide technical data bases for incorporating the techniques into codes and standards.

The ACR design incorporates a gas annulus surrounding each zirconium-niobium alloy pressure tube. The dry annulus gas is continuously monitored for water content. Significant increases in the rate of water increase in the gas are an indication of pressure boundary leakage. The unique Candu reactor design allows this continuous on-line monitoring of the pressure boundary to augment periodic ISI. Experience with detecting water leakage through a tight crack in the pressure tubes prior to unstable crack growth and pressure boundary failure using this on-line monitoring technique may be adaptable to other ALWR designs.

Areas of international cooperation and exchange would involve work planned by the EC on evaluation of ISI methods, and work on risk-informed inspection program evaluation by NRC. Of additional interest would be potential international cooperation on evaluations of online continuous monitoring techniques for structural integrity and leak detection using HTGR test reactors.

## **CONSIDERATIONS FOR GRAPHITE COMPONENTS**

To be able to effectively review the new HTGR designs, there is a need to conduct confirmatory research to establish an information base related to the long-term performance and behavior of nuclear-grade graphite under the temperatures, radiation, and environments expected during normal operating and accident conditions. Potential loss of strength and of resistance to fatigue and creep, shrinkage, swelling, cracking, and corrosion during operation could impact the performance and function of the graphite core structural elements, reflectors (side and bottom), and moderator balls. Various graphite variables, including coke source, size, impurity, and structure; manufacturing processes; density; grain size; crystallite size and uniformity, determine the as-received and irradiated properties of the graphite component.

Research will need to be conducted to evaluate graphite for HTGR application. This will involve studies of the performance and degradation of graphite under high levels of irradiation and temperature. A review will be conducted of available high dose irradiation data for nuclear grade graphite. High dose irradiation data on "old graphites" will be evaluated to determine its applicability to "new graphites." The data will be utilized to determine the behavior of current

graphites planned for HTGRs under operating conditions. In general, there is a lack of data in the high dose, high-temperature regime of HTGR operating environment; additional research will be conducted on current graphites planned for HTGRs to determine high dose material behavior, properties, and degradation. Experiments will be conducted at different temperatures at high dose irradiation in a high flux test reactor. Microstructural evaluations, spectroscopy, dimensional measurements, mechanical testing, and physical property testing of the irradiated specimens will determine the effects of high dose and high temperature on new graphites.

Some irradiation studies have been conducted on older graphites that are no longer available due to loss of raw materials supply and/or manufacturers. In addition, limited results are available at high levels of irradiation exposure. Thus, two key issues are the lack of data on irradiated properties of current graphites, and the lack of data at higher doses of irradiation. As discussed earlier, the irradiated material properties are heavily dependent on the particular make-up of the graphite and the manufacturing process; therefore, at issue is whether the irradiated materials properties of the "old graphites" can be assumed to be the same as the "new graphites." Irradiation affects, and in many cases degrades, physical and mechanical properties of the graphite. Important properties that change with irradiation are density, thermal conductivity, strength, and dimensions. These changes have safety implications since they could degrade structural integrity, core geometry and cooling properties. Some of these changes are not linear with irradiation dose. Strength of graphite initially increases with irradiation dose, then, at higher levels, it begins to decrease. With respect to dimensional changes, graphite initially begins to shrink with increasing dose then, beyond turn-around, graphite begins to swell with increasing dose. During operation, thermal gradients and irradiation induced dimensional and strength changes result in significant component stresses, distortion, and bowing of components. These can lead to loss of structural integrity, loss of core geometry, and potential problems with insertion of control rods. At still higher doses, beyond turn-around, where the swelling makes the volume considerably greater than the original volume, graphite structures and fuel balls will start to disintegrate and experience total loss of integrity.

To evaluate the suitability of a particular graphite for HTGR application, property change data due to irradiation is needed in addition to the as-received properties. Development of irradiation data on graphite is difficult, expensive, and time consuming. Therefore, reactor designers/vendors have proposed to use radiation data from studies conducted on older graphites and attempt to use graphites produced in a similar manner. However, the as-received and irradiated graphite properties depend strongly on the raw materials and manufacturing processes. Small variations in these may have strong effects on the graphite properties. Since the exact raw materials and processes have changed and may continue to change in the future, the NRC may need to independently confirm whether a particular graphite will behave the same as the old graphites under operating irradiation conditions. To accomplish this without irradiation testing every time a change occurs in the graphite raw materials or processing, correlations are needed for predicting irradiated graphite properties and changes from the as-received graphite raw materials characteristics, composition, processing, and properties.

Research will need to be performed to determine irradiated graphite properties from as-received graphite properties. As-received graphite properties are determined by the raw materials and manufacturing process. Important parameters will be identified such as coke and pitch characteristics, and graphitization temperature. A number of different graphites will be selected with carefully varied parameters. Studies will be conducted to establish the as-received properties of the graphites. Selected properties to be measured are: x-ray crystallinity, density, open and closed porosity, pore size distribution, grain size and size distribution, grain orientation and

orientation distribution, thermal expansion, thermal contraction, thermal conductivity, absorption cross-section, sonic Young's modulus, stress-strain behavior, strength and strength distribution (Weibull modulus), and fracture toughness. In addition, chemistry, including impurities, of the graphites will be established. Due to the anisotropy of manufactured graphite, the materials properties will be determined for two orthogonal directions since graphite exhibits transverse isotropy. The graphites will then be irradiated at systematically varied irradiation doses and temperatures significant to HTGRs. Following irradiation, the materials properties will be reevaluated to determine the effect of irradiation and to establish correlations between the initial as-received properties and the post-irradiation properties that could apply to any particular graphite that may be used in HTGRs.

Graphite corrosion and oxidation can occur in HTGRs from oxidizing impurities in (or added to) the helium coolant, from in-leakage during normal operation, or from air or water ingress during accidents. The oxidation of graphite is an exothermic reaction, and it is important to know the rate of heat generation particularly during accidents. Oxidation also will remove the surface layers of graphite components resulting in loss of structural integrity. Further, oxidation will change the thermal conductivity and reduce the fracture toughness and strength of graphite components. The loss in strength may be due to attack of the binder. The oxidation rates vary for different graphites, and can be greatly affected by the impurities in the original graphite. Therefore, oxidation rate data is needed for the graphites proposed for new reactors.

Investigations will need to be undertaken to understand oxidation effects on the physical, thermal, and mechanical characteristics of nuclear graphite. There is a lack of data on oxidation kinetics of reflector grade graphite, fuel pebble matrix graphite, and graphite dust. Experiments will be conducted to determine weight loss and loss of mechanical integrity due to oxidation of graphite samples. The heat generated from oxidation of graphite dust and the potential detrimental effect on surrounding components due to this elevated temperature will be studied. Research will be performed to determine if oxidation occurs along binder paths through the bulk graphite which could lead to diminished fracture, fatigue, and creep resistance of components.

The PBMR will use advanced gas-cooled reactor type fuel sleeve graphite for the replaceable and permanent structures in the core. The proposed graphite properties used for design, operating, and accident analyses of these structures will have the same values as those for the sleeves. The sleeves are relatively thin structures manufactured differently from the large structural blocks of the PBMR, and the mechanical and other properties will be different. Furthermore, the properties of the large block graphite will vary through the thickness of the block. The difference in properties between the sleeves and large blocks and through-thickness variations need to be established. The potential for different irradiated properties of sleeve graphite and large block graphite also needs to be evaluated.

Research on large blocks of graphite will need to be conducted to characterize the through-thickness variability of key properties in full size blocks and to establish the variability between batches of graphite. Large graphite blocks to be used for reflector material will be sectioned, tested, and evaluated to determine if properties measured on thin graphite components can be extrapolated to large blocks. Graphite materials properties are typically anisotropic and vary with the forming method and size of the final fabricated component. The sectioned large block specimens will be tested to measure important parameters such as strength, fracture

toughness, density, thermal conductivity, coefficient of thermal expansion, level of chemical impurities, isotropy, and absorption cross-section. Based on the results obtained, an assessment will then be conducted to determine if the large block bulk properties would vary under high-temperature and high dose irradiation in a manner similar to thin sleeve graphite material.

There is a lack of standards for nuclear grade graphite. Designers of HTGRs intend to use measured properties of the particular graphite in their design calculations. However, nuclear graphites should meet certain minimum requirements with respect to important properties, such as strength, density, and thermal conductivity as is the case for materials used in other reactor systems. If a particular graphite has excessively low strength and the designer uses that value in designing various components, that may not result in a suitable component for the intended service. There are underlying reasons why the strength may be excessively low. For example, the graphite might contain excessive cracking and porosity resulting in low strength. Although the component might have been designed using the low strength (resulting in possibly a thicker component), the excessive cracks in the component may grow during service and cause failure. Specific impurities in the graphite might be detrimental to irradiation properties of the component, and they should be limited in nuclear graphites. Other elements, such as halides, which can be released during operation and cause degradation of other components in the reactor, should also be limited in nuclear grade graphite. Thus, there is a need to develop standards to establish the acceptable physical, thermal, and mechanical properties; composition; and manufacturing variables for nuclear grade graphite.

Staff efforts will be directed toward development of consensus standards for nuclear-grade graphite. Design and fabrication codes are also needed. The NRC staff will work with the international community, industry organizations, and professional societies to develop a nuclear-grade graphite material specification consensus standard. The standard will specify requirements on density, strength, fracture toughness, thermal conductivity, coefficient of thermal expansion, absorption cross-section, impurities, and any other appropriate parameter. The staff will also work with the codes and standards organizations to develop the design and fabrication requirements for graphite components to address processes such as strength, fracture, fatigue, creep, irradiation damage, dimensional stability, oxidation, and any other appropriate design and fabrication considerations for HTGR service.

An effort will be conducted to review and evaluate experimental data, analyses, and appropriate models for predicting pebble flow through and across a PBMR reactor core. Evaluations will be conducted on how the predictive models were validated and how well they predict field experience. Pebble flow, temperature effects, friction, mixing of fuel and graphite pebbles in the central reflector core, compaction, hang-up, and bridging will be considered in the above evaluations. Conclusions will be reached regarding the application of currently available methods and codes, and recommendations will be developed for any necessary follow-on studies.

The EC research effort is currently reviewing the state of the art on graphite properties in order to set up a suitable database. The EC is planning to perform oxidation tests at high temperatures on fuel matrix graphite and on advanced carbon-based materials to obtain oxidation resistance in steam and in air. Recently, the EC began extensive characterization and irradiation testing of five different graphites that are currently produced and could be used in future HTGRs. The properties of these graphites as a function of temperature and irradiation exposure will be studied.

As mentioned above for the high-temperature metallic components, the EC plans to address a considerable amount of work, however a key area possibly not fully addressed in the EC programs is the correlations of as-received graphite properties and manufacturing parameters to irradiated graphite properties. Exchange of NRC research results in this area could be used for cooperation with the EC HTR-M programs.

The UK is conducting ongoing research on graphite properties and has had experience with operating gas-cooled reactors that may be useful for NRC cooperation. As part of international cooperation with the UK, the NRC has assigned a staff member from RES to the Nuclear Installations Inspectorate (NII) for three months to develop expertise on graphite behavior under high-temperature and irradiation conditions and develop knowledge of the inspection and monitoring programs of graphite in HTGRs. The NRC staff member will have discussions with experts on the reasons for a lack of available correlations of as-received graphite properties with irradiated graphite properties. NRC staff work while on this assignment would include discussing, reviewing, and obtaining input from experts on the important manufacturing parameters, physical and mechanical properties, composition, etc. of the as-received graphite that could have an effect on irradiated graphite properties. With input from the UK (and other) experts, the staff would devise a matrix of tests/research plan for developing correlations between irradiated graphite properties and initial as-received properties.

Additional work for the NRC staff member during this international effort with the UK includes gaining a better understanding of ongoing and past research results at the University of Manchester and exploring potential cooperation in their program. In this effort, the staff would obtain information on the scope and objectives of NII's center of excellence for graphite research at the University of Manchester. The staff can obtain details from University of Manchester researchers on the graphite research being conducted for NII and other cooperating partners. The staff will then be able to evaluate potential benefits to the NRC of the research conducted at the University of Manchester and to explore different methods for NRC participation as appropriate.

The staff member will develop recommendations for requirements of a nuclear grade graphite material specifications standard, and for a graphite component design code. This effort would be performed in collaboration with NII and other experts to outline one or more potential standards for the manufacture, composition, and required properties for nuclear grade graphite. The NRC staff member will also obtain, review and discuss with NII and other experts different codes and procedures available for structural, fatigue, and creep analyses for the design of high-temperature graphite components. The staff will evaluate these codes and develop recommendations on the need to update them based on service experience and more recent research results produced after the codes were developed.

Finally, the NRC staff member will have the opportunity, with the help of NII staff, to gather data and information from the DRAGON test reactor experiments performed on graphite and fuels in the UK and to evaluate this information for applicability to currently proposed HTGRs.

## **APPLICATION OF RESEARCH RESULTS**

Results from the research described will provide the necessary information to estimate component probability of failure as input to NRC PRAs to independently confirm and support safety evaluations. Since failure probability data for components of advanced reactors is not available from operating experience, very large uncertainties are inherent in the values selected and in the

results of the PRAs. To reduce the uncertainties, information on failure probabilities would be derived from research results of potential degradation mechanisms (fatigue, creep, creep-fatigue, oxidation, thermal aging, stress corrosion cracking, crevice corrosion cracking, irradiation damage, and dimensional changes) of components in the operating environment of advanced reactors and with quantitative information of the initiation times and growth rates.

Due to the high temperatures and environments with which the industry has relatively little experience, careful analysis of the proposed materials needs to be carried out to indicate whether these materials are prone to degradation and provide the technical basis or criteria for materials acceptability. Aging effects and degradation due to the high-temperature helium environment and radiation need to be considered. Evaluation of potential degradation mechanisms and rate of degradation progression for materials used for connecting piping between the reactor pressure vessel and the power conversion systems will provide the NRC an independent basis to determine the validity of the contention that pipe break analysis does not need to be evaluated.

The research on nondestructive examination (NDE) and evaluations of ISI programs for HTGRs and ALWRs is applicable to independently confirm if an applicant's inspection plans are technically sound, or if additional requirements are needed. Currently accepted NDE and ISI programs may not detect materials degradation due to inaccessibility of components and long time periods between inspections. Research in this area may lead to regulatory requirements to modify NDE techniques and/or to use continuous online monitoring of structural integrity for structures and components of advanced reactors.

## LOCA DUCTILITY TESTS

Ralph O. Meyer\*

U.S. Nuclear Regulatory Commission  
Washington, DC 20555

### ABSTRACT

Safety analyses for loss-of-coolant accidents (LOCAs) address several phenomena related to the behavior of fuel rod cladding: (a) ballooning deformation, (b) conditions for bursting, (c) oxidation kinetics, and (d) embrittlement. The first three are described by correlations in a safety analysis, and cladding embrittlement is addressed by criteria in 10 CFR 50.46. These embrittlement criteria currently consist of a 17% limit on cladding oxidation and a 2200°F (1204°C) limit on cladding temperature. A program of LOCA testing is being performed at Argonne National Laboratory for the NRC in cooperation with the Electric Power Research Institute, Framatome ANP, and the Department of Energy. Ring-compression tests are being investigated as the means for determining embrittlement criteria for 10 CFR 50.46, provided that those tests can be confirmed to be adequate. Four-point bend tests on segments containing a ballooned and burst region will also be performed in the program. Schematic diagrams of the test procedures and the test matrix have been developed and are described in the paper.

### INTRODUCTION

Safety analyses for loss-of-coolant accidents (LOCAs) address several phenomena related to the behavior of fuel rod cladding: (a) ballooning deformation, (b) conditions for bursting, (c) oxidation kinetics, and (d) embrittlement. The first three are described by correlations in a safety analysis, and cladding embrittlement is addressed by criteria in 10 CFR 50.46. These embrittlement criteria currently consist of a 17% limit on cladding oxidation and a 2200°F (1204°C) limit on cladding temperature.

The original motivation for the LOCA testing at Argonne National Laboratory (ANL) was to look for burnup effects on the embrittlement criteria, with burnup effects on ballooning, bursting, and oxidation as secondary interests. Interest was intensified in 1998 and 1999 when NRC first issued an Information Notice and then established the position that the 17% oxidation limit should encompass accident and pre-accident oxidation thus approximately accounting for the significant corrosion that accumulates with burnup [1,2].

---

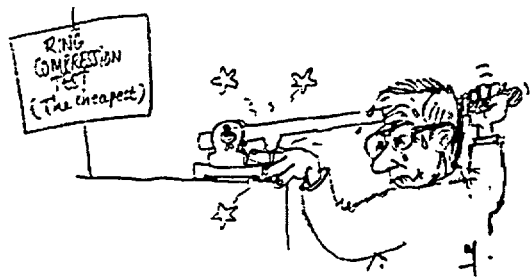
\*with illustrations by Nicolas Waeckel, Electricité de France

Later, when Framatome's M5 cladding was introduced in the U.S., there was a desire to confirm that this new alloy, and the earlier Westinghouse ZIRLO alloy, both behaved adequately under LOCA conditions. While it was known that their ballooning deformation might be altered because of changes in the phase diagram for these niobium-bearing alloys in comparison with the tin-bearing Zircaloy alloys, data showed that oxidation and embrittlement were about the same as for the Zircaloys [3,4]. Data on another niobium-bearing cladding alloy, however, showed very different behavior [5,6,7,8]. It therefore became important to examine alloy effects more carefully and to understand the factors that could cause different LOCA behavior in some zirconium-based cladding alloys.

More recently, proposals have been made to replace the Zircaloy-based 17% and 2200°F limits with a performance-based requirement in 10 CFR 50.46 to avoid the need for regulatory exemptions when new alloys are introduced and to accommodate any burnup effects. These current numerical limits were derived from ductility tests, so the proposal included the substitution of some suitable ductility test [9,10]. In addition to defining a suitable ductility test, additional research would be needed to confirm the similarity of oxidation kinetics for all zirconium-based alloys in order to substantiate other assumptions needed relative to peak cladding temperature [10].

After considering several possibilities, it has been decided to continue investigating the ring-compression test as the potential performance-based ductility test for 10 CFR 50.46, provided that it can be confirmed to be adequate. Ring-compression tests are less expensive to perform than the alternatives, and because such tests were used to develop the original embrittlement criteria, their continued use should contribute to regulatory stability. Two basic questions of adequacy will be addressed in the current research program. One is about our ability to interpret the results of ring-compression tests unambiguously, and the other is about the efficacy of a test on a small ring specimen to represent the behavior of a fuel rod in a ballooned and ruptured region. These are discussed in the following paragraphs.

## RING-COMPRESSION TESTS



The schematic arrangement for a ring-compression test, as performed by Hobson and others, is shown below in Fig. 1 [see 11]. Segments of tubes were oxidized on the inside and the outside at various high temperatures in the range of 920-1320°C. After cooling, they were mechanically tested in compression over a range of relatively low temperatures and evaluated at 135°C. This temperature was selected as the lowest water temperature that would be present in a reactor after a LOCA. Based on Hobson's data, it was found that specimens would

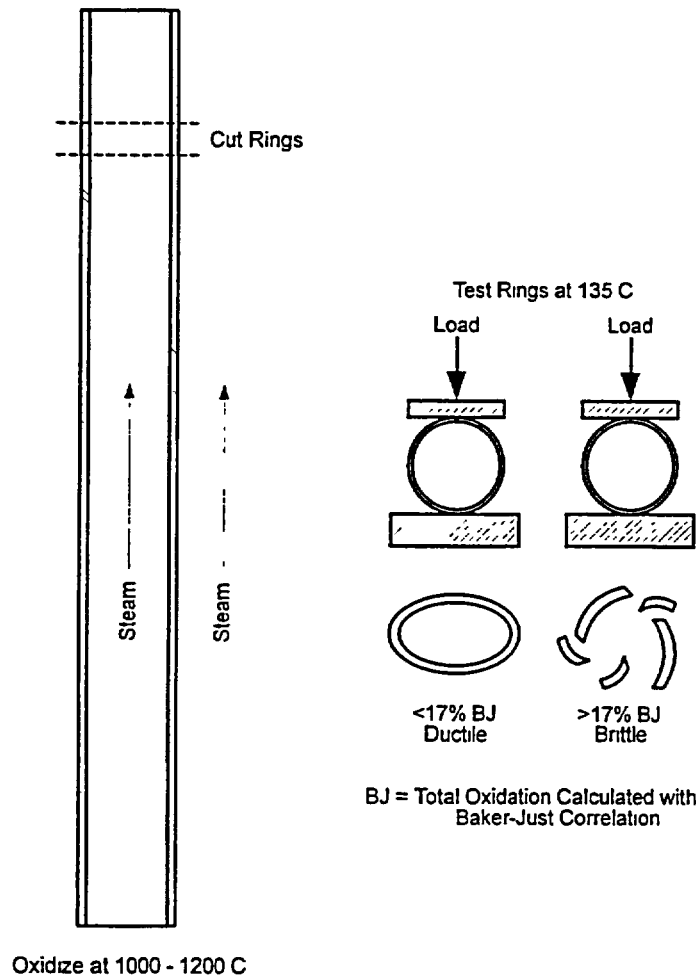


Fig. 1. Diagram of Hobson-type ring-compression tests that were used to obtain current LOCA embrittlement criteria

exhibit ductile behavior if the calculated oxidation (using the Baker-Just correlation) was less than 17% equivalent cladding reacted (ECR) as long as the oxidation temperature was not much above 1200°C. Hobson did not measure actual oxidation in the specimens, and we believe the critical ECR (boundary between ductile and brittle behavior) is really around 13% rather than 17% because of the over prediction of the Baker-Just correlation. We will measure the amount of oxidation in all of our tests and will therefore work with true values.

The principal stresses in the ring specimen are tensile stresses that result from bending, and these stresses are shown qualitatively in Fig. 2 by double-ended arrows. This stress pattern usually results in four cracks through the cladding wall: two starting from the outside at the 3 and 9 o'clock locations, and two starting from the inside at the 6 and 12 o'clock locations. None of these cracks completely unloads the test apparatus, so instead of getting a load that drops to

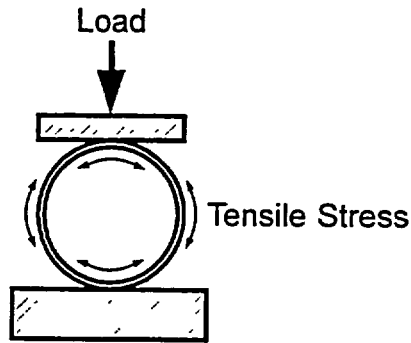


Fig. 2. Large OD and ID tensile stresses in ring between flat plates

zero when a crack occurs, one gets a saw-tooth load-vs-deflection curve such as seen in Fig. 3. This figure is from recent work at the Russian Research Center, Kurchatov Institute [8]. Figure 3 shows how Kurchatov analyzed the data to eliminate deformation in the load train and get a measure of plastic deformation in the specimen.

For a combination of reasons, it seems desirable to oxidize the specimens from the outside only. One advantage of this is that it will make the ring specimen more ductile on the inside diameter and, therefore, less susceptible to fracture at the 6 and 12 o'clock locations as just discussed. If, in addition, the top and bottom loading plates have curved surfaces, the bending stress at the top and bottom will be reduced thus further diminishing the potential for cracking at the 6 and 12 o'clock locations such that cracking should always occur at the 3 and 9 o'clock locations. This situation is sketched in Fig. 4 and should result in fewer saw teeth in the

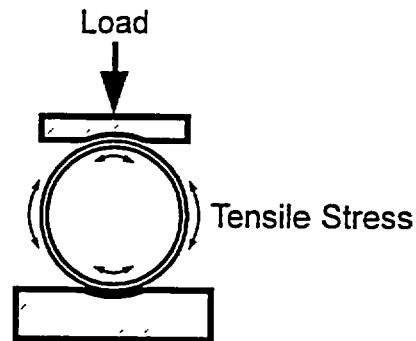


Fig. 4. Smaller ID tensile stresses in ring between curved plates

load-vs-deflection curves. This arrangement and the Kurchatov analysis procedure have been selected for the ring-compression tests. A transducer may be placed inside the rings to directly measure deformation if that is found to be practical. Some microscopy of fracture surfaces will also be performed to confirm the brittle or ductile failure mode. Tests will be conducted primarily at 135°C with some at 23°C to bound the range of interest and to facilitate comparison with earlier data bases.

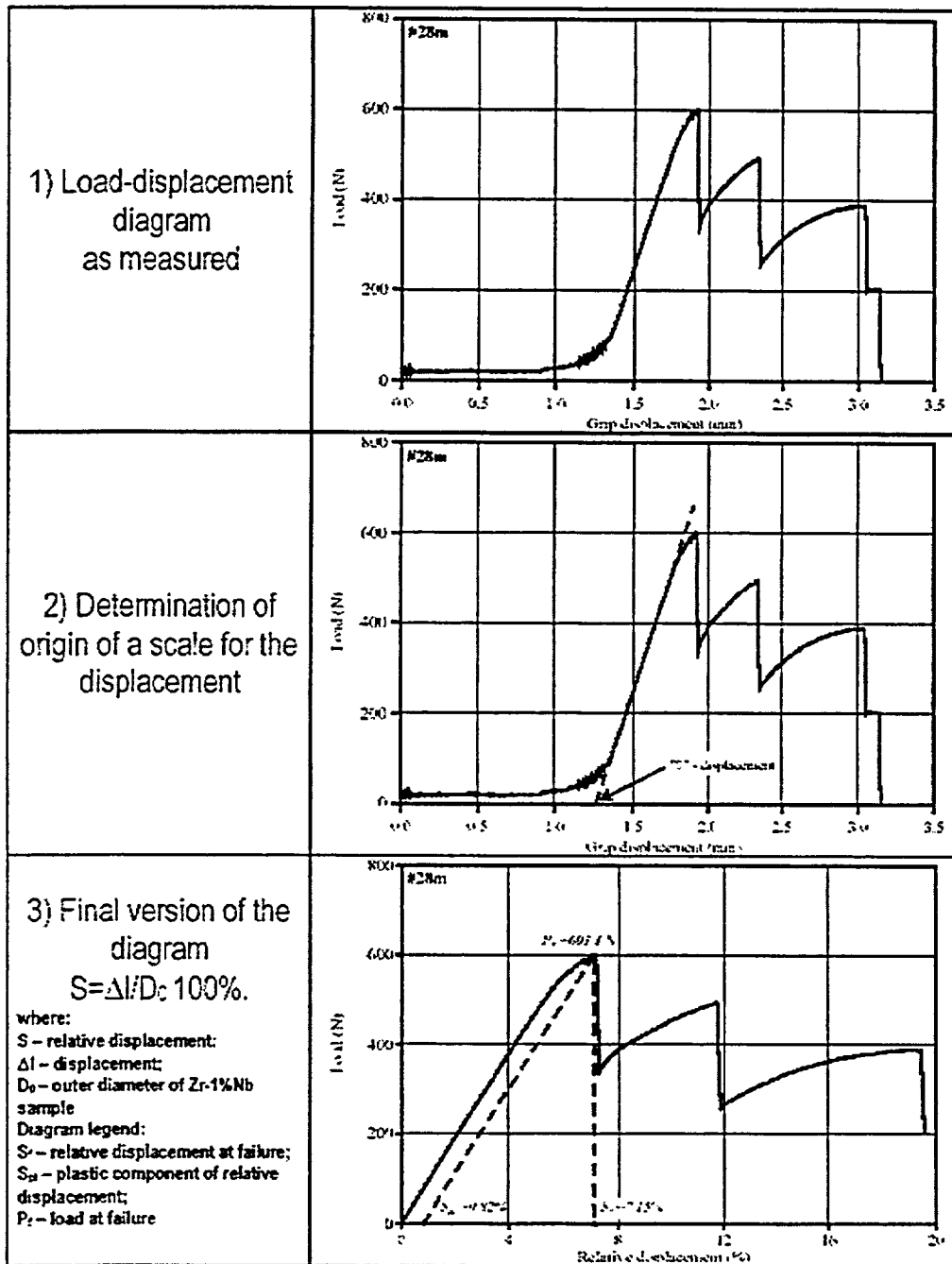


Fig. 3. Load-vs-displacement curve for ring-compression tests showing Kurchatov method of analyzing results

## THREE-POINT BEND TESTS



Although more costly, a three-point bend test is probably better in several respects than a ring-compression test. Such a bend test is sketched in Fig. 5 along with a double arrow to indicate

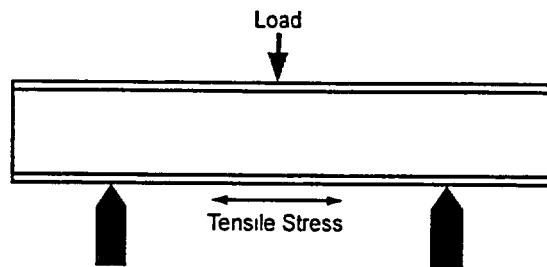


Fig. 5. Three-point bend test with tensile stress on lower OD surface

the location of maximum stress. The first advantage of this test is that the tensile loads are applied in the axial direction rather than in the circumferential direction. This is probably more representative of stresses that might arise from horizontal accelerations (earth quakes), plant vibrations, and spacer grid interactions. Furthermore, the load-vs-deflection curve for this test is simple and easy to interpret. As soon as a crack propagates through the tube, the load falls to zero without any ambiguity as seen in Fig. 6 from Framatome's recent work [3].

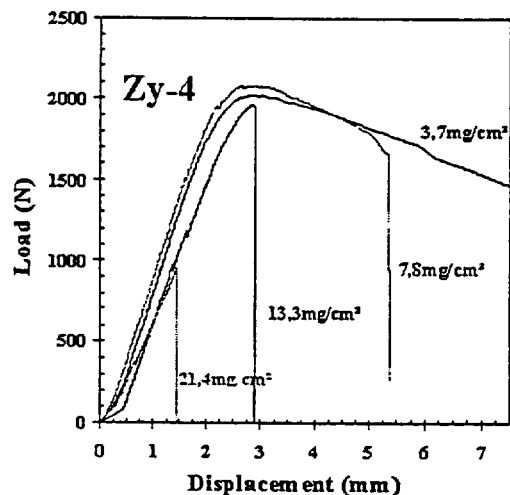
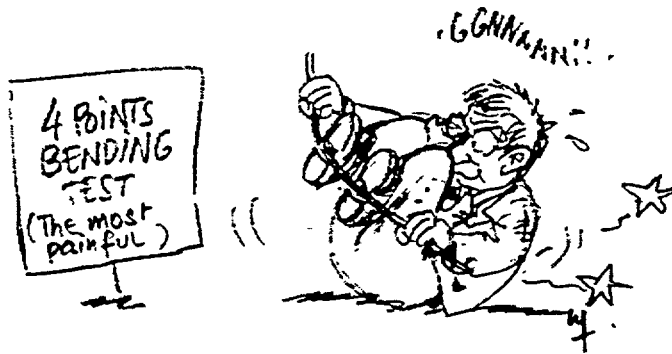


Fig. 6. Load-vs-displacement curve for four Framatome three-point bend tests

If the ring-compression test and the three-point bend test both show the same critical ECR for the same material, then we can use the less expensive ring-compression test. Framatome has performed ring-compression tests and three-point bend tests on M5 tubing. If those data become openly available, an assessment will be made to see if the two tests produce the same result. Otherwise, some three-point bend tests will be performed at ANL to generate data for this assessment.

#### FOUR-POINT BEND TESTS



The four-point bend test that we plan to use is shown schematically in Fig. 7. This test, with

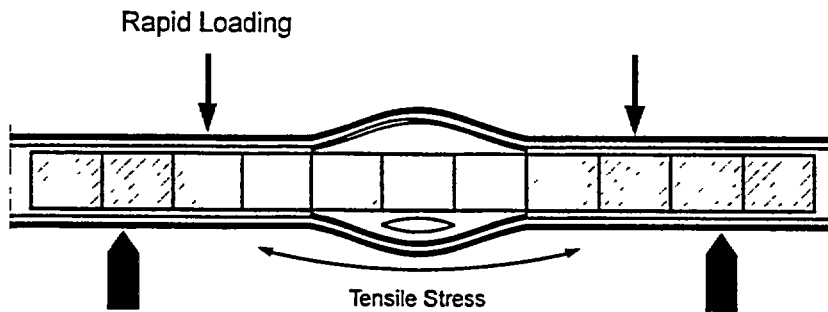


Fig. 7. Four-point bend test on ballooned and ruptured segment of rod containing fuel; tensile stress on lower OD surface

fuel pellets inside, is most prototypical for investigating the behavior of the ballooned region of a fuel rod. Double-sided oxidation will take place as appropriate, with steam entering through the burst opening. Any enhanced hydride absorption due to inside oxidation will be present. Loading points are away from the deformed region, and the specimen will break naturally at its weakest location. While this is clearly the most expensive test, it only needs to be used in a confirmatory way. If results from the ring-compression tests can be applied in the ballooned region, and if that adequately predicts ductile or brittle behavior, then the ring-compression tests will have been confirmed. In a way, Chung & Kassner's 0.3 Joule impact tests of 1980 provided this confirmation for the 17% and 2200°F values for unirradiated Zircaloy [11].

## TEST MATRIX

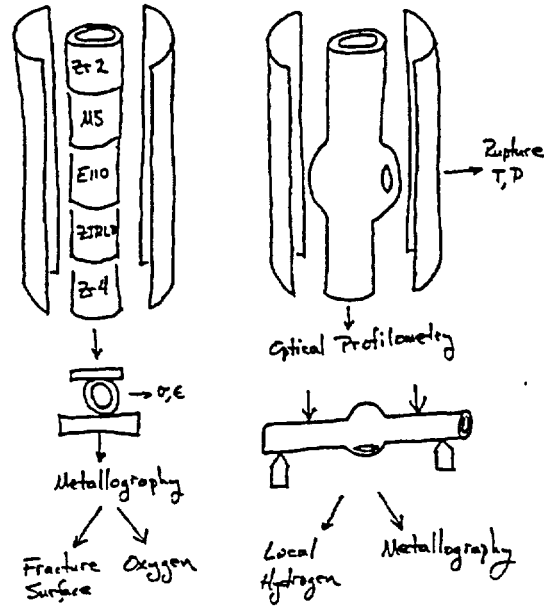


Fig. 8. Schematic diagram of testing sequence

Figure 8 shows a schematic diagram of the testing sequence. The ring-compression tests and the four-point bend tests will be integrated into the overall LOCA test program. Unirradiated tubing, as received, will be tested first. Irradiated cladding, as it becomes available, and hydrogen-charged tubing will be tested later to investigate burnup effects. Two or more alloys will be oxidized together in the same furnace to reduce the number of furnace runs needed to produce ring specimens (and three-point bend specimens, if necessary). Oxidation kinetics can also be obtained from these furnace runs, and examination of ring fragments after compression will give fracture morphology and oxygen content. Specimens for the four-point bend tests will consist of those specimens that survive thermal shock in the integral tests. After optical profilometry, those specimens will be tested in the four-point bend apparatus and will likely break. Metallography and hydrogen measurements can be made on fragments after the bend tests.

The number of integral tests will be small. Approximately three tests per alloy type will be performed for irradiated material along with a somewhat larger number of tests on unirradiated tubing. The number of these tests will govern the number of four-point bend tests that are performed.

The number of ring-compression tests will be large, however, and attention is needed to control the test matrix to a manageable size. First we noticed that Kurchatov has performed tests under a variety of conditions including heating rate, cooling rate, test temperature, and inside-vs-outside oxidation [8]. Differences in the test results were small. Figure 9, for example, shows various combinations of heating and cooling rates (e.g., F/S means fast heating and slow cooling). These rates had very little effect on the critical ECR of around 8% for E110 cladding. These plots also show that multiple ECR values need to be tested to determine a critical ECR value.

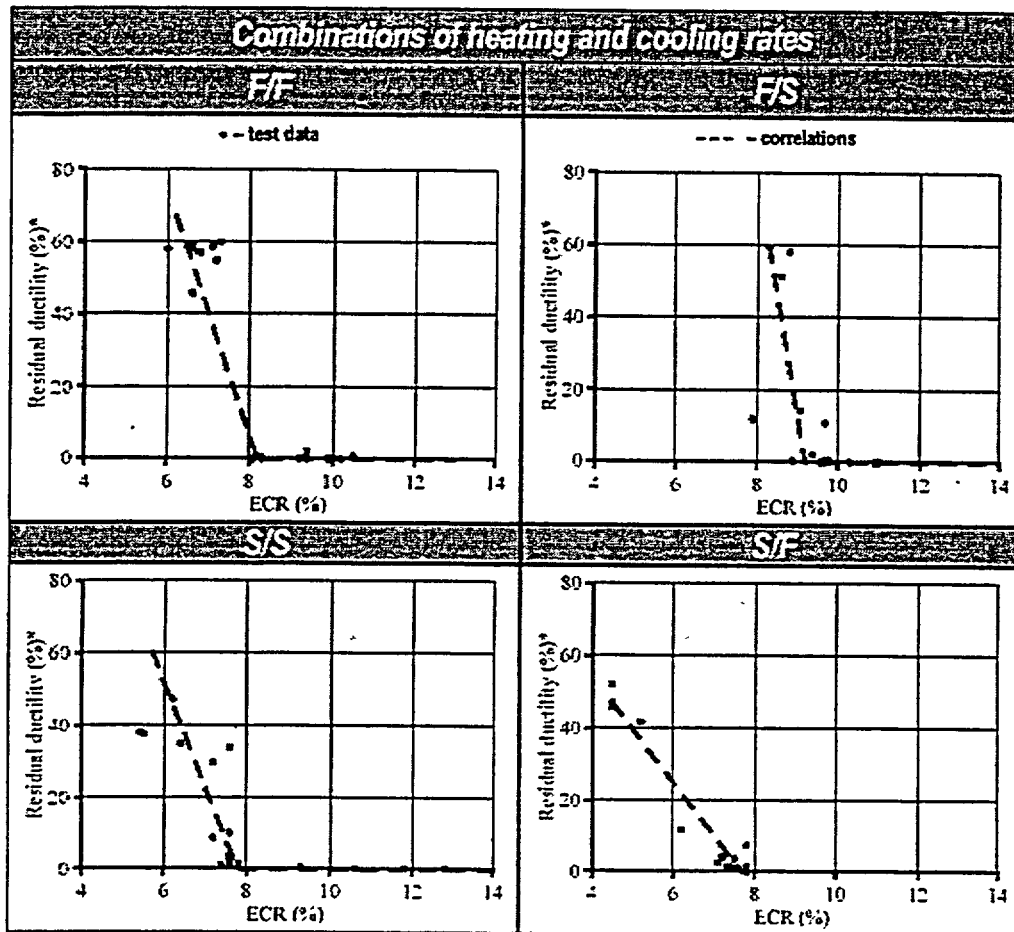


Fig. 9. Residual ductility versus oxidation for four Kurchatov combinations of heating rates

Five nominal ECR values will be tested for each of the five materials (Zircaloy-2, Zircaloy-4, ZIRLO, M5, and E110) with the one-sided oxidation produced at three different temperatures spanning the range of interest (approx. 1000-1265°C). The first tests will be done with specimens oxidized at 1200°C to 5% ECR as this will provide one point with significant residual ductility for all alloys and permit the measurement techniques to be worked out. The next tests will be done with specimens oxidized at 1200°C to 10% ECR. One alloy (E110) should be brittle at this level, but the rest should still be ductile. This test will let us evaluate the ability of the test to discriminate between alloy types. The third tests will be done with specimens oxidized at 1200°C to 20% ECR to ensure that all specimens are brittle. The fourth and fifth tests will be done with intermediate ECR values to home in on the critical ECR values as well as possible. Decisions will be made later about oxidation temperatures above and below 1200°C that need to be tested. In light of the above, it is clear that some scheme of oxidizing multiple specimens in a furnace run is needed to prevent the number of furnace runs from becoming impractically large. This capability exists at ANL with the use of alumina spacers and zirconia washers between tubing pieces in the furnace. Testing of unirradiated tubing is now underway.

## REFERENCES

1. NRC Information Notice, "Predicted Increase in Fuel Rod Cladding Oxidation," IN-98-29, August 3, 1998.
2. Gary M. Holahan (NRC) letter to David J. Modeen (NEI), November 8, 1999.
3. A. Le Bourhis, "Justification of the M5 Behavior in LOCA," *Proceedings of the Topical Meeting on LOCA Fuel Safety Criteria* (Aix-en-Provence, 22-23 March 2001), OECD Report NEA/CSNI/R(2001)18, p. 105-133.
4. W. J. Leech, "Ductility Testing of Zircaloy-4 and ZIRLO Cladding after High Temperature Oxidation in Steam," *Proceedings of the Topical Meeting on LOCA Fuel Safety Criteria* (Aix-en-Provence, 22-23 March 2001), OECD Report NEA/CSNI/R(2001)18, p. 135-143.
5. J Böhmer, "Embrittlement of ZrNb1 at room temperature after high-temperature oxidation in steam atmosphere," *Kerntechnik* 57 (1992) p. 55-58.
6. A. Griger, L. Maroti, L. Matus, P. Windberg, "Ambient and High Temperature Mechanical Properties of ZrNb1 Cladding with Different Oxygen and Hydrogen Content," *Proceedings of Enlarged Halden Program Group Meeting* (Loen 1999), HPR-351/35.
7. "Conclusions and Recommendation of the LOCA Topical Meeting," *Proceedings of the Topical Meeting on LOCA Fuel Safety Criteria* (Aix-en-Provence, 22-23 March 2001), OECD Report NEA/CSNI/R(2001)18, p. 11-13.
8. V. Asmolov et al., "Understanding LOCA-Related Ductility in E110 Cladding," *Proceedings of the Nuclear Safety Research Conference* (this issue).
9. SECY-01-0133, "Status Report on Study of Risk-Informed Changes to the Technical Requirements of 10CFR Part 50 (Option 3) and Recommendations on Risk-Informed Changes to 10 CFR 50.46 ECCS Acceptance Criteria, July 23, 2001.
10. Ashok C. Thadani, "Research Information Letter 0202, Revision of 10 CFR 50.46 and Appendix K," NRC memorandum to Samuel J. Collins (ADAMS #ML021720744), June 20, 2002.
11. H. M. Chung, T. F. Kassner, "Embrittlement Criteria for Zircaloy Fuel Cladding Applicable to Accident Situations in Light-Water Reactors: Summary Report," NUREG/CR-1344, January 1980.

## UNDERSTANDING LOCA-RELATED DUCTILITY IN E110 CLADDING

*V.Asmolov, L.Yegorova, K.Lioutov*

*Nuclear Safety Institute of Russian Research Center "Kurchatov Institute", Moscow, Russian Federation*

*V.Smirnov, A.Goryachev, V.Chesanov, V.Prokhorov*

*State Research Center "Research Institute of Atomic Reactors", Dimitrovgrad, Russian Federation*

### Abstract

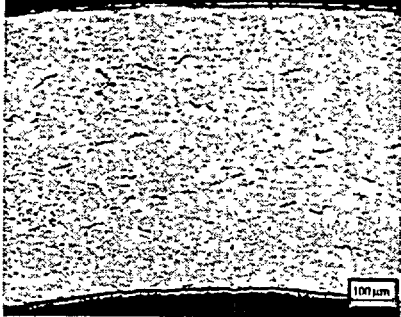
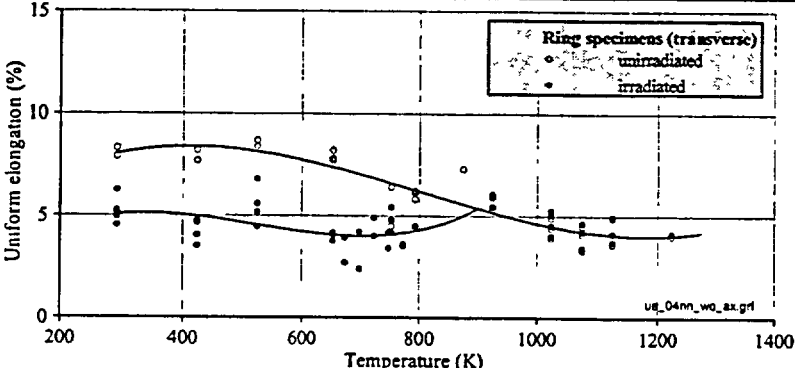
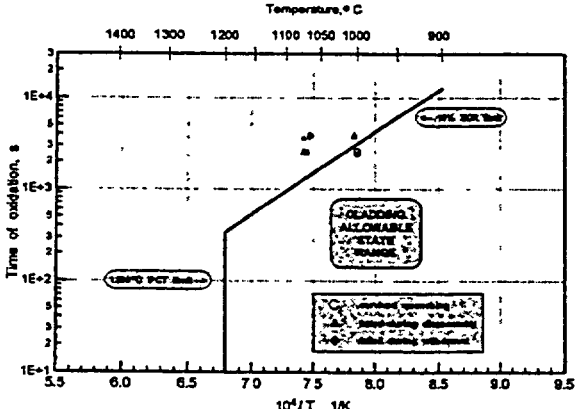
Recent results of a research program to study the mechanical behavior of E110 (Zr-1%Nb) oxidized claddings are presented in this paper. The major focus of the investigations was on the determination of the zero ductility threshold of E110 cladding as a function of such LOCA-related parameters as oxidation level, oxidation scenario, oxidation type, and temperature of mechanical tests. In addition, reference tests were performed to compare the mechanical behavior of different cladding materials after high temperature oxidation.

### 1. Introduction

One of the major economic needs of the nuclear industry around the world is to extend the fuel cycle length and to increase fuel burnup (60 MW d/kg U and higher). Numerous investigations performed during the last ten years showed that the mechanical properties of irradiated cladding are the key factor of this problem. Moreover, the analysis of associated test data showed that zirconium-niobium alloys are the best candidates for the cladding material of high burnup fuel. This conclusion correlates with results of more than thirty year Russian experience in operation of VVER (Russian type of pressurized water reactors) nuclear power plants with Zr-1%Nb (E110) clad fuel rods. Besides, this statement is confirmed by special tests performed to justify the behavior of the high burnup fuel with E110 cladding under design basis accident conditions. Some results of these tests are presented in Table 1. Analysis of the data indicates the following:

- Zr-1%Nb (E110) irradiated commercial cladding is characterized by very low oxidation and hydriding up to 60 MW d/kg U of burnup;
- Zr-1%Nb (E110) irradiated commercial cladding keeps a sufficient margin of residual ductility at the temperature of normal operation; the increase of the temperature (to the design basis area) leads to the disappearance of difference between mechanical properties of irradiated and unirradiated cladding;
- the existing ductility margin of Zr-1%Nb irradiated claddings proved to be sufficient to retain a high failure threshold with no fragmentation under reactivity-initiated-accident (RIA) conditions; the threshold of fragmentation of oxidized irradiated E110 cladding under the loss-of-coolant accident (LOCA) conditions corresponds to the license safety criteria currently in force (1200°C, 18%) with a reasonable margin (in accordance with results of thermal shock type of tests).

**Table 1. Major findings of special test programs with E110 irradiated commercial claddings.**

Purpose of program	Results of investigations	
Cladding characterization at the end of operation	Corrosion behavior [1]	 <p data-bbox="1149 478 1430 575">← Typical view of the E110 irradiated cladding (~60 MW d/kg U)</p>
Behavior under RIA conditions [4, 5]	Mechanical properties [2, 3]	 <p data-bbox="1149 709 1377 785">Ring specimens (transverse) ○ unirradiated ● irradiated</p> <p data-bbox="1256 982 1377 1003">us_04nn_wd_ax.grf</p>
Behavior under LOCA conditions [6]	<p data-bbox="477 1255 1357 1289">Thermal shock tests with E110 oxidized irradiated fuel rods (50 MWd/kg U)</p>  <p data-bbox="894 1297 997 1318">Temperature, °C</p> <p data-bbox="634 1436 656 1562">Time of oxidation, s</p> <p data-bbox="894 1688 980 1709">10<sup>4</sup>/T, 1/K</p> <p data-bbox="721 1325 1078 1339">1400 1300 1200 1100 1050 1000 900</p> <p data-bbox="721 1352 753 1373">3</p> <p data-bbox="721 1373 753 1394">2</p> <p data-bbox="721 1394 753 1415">1E-4</p> <p data-bbox="721 1415 753 1436">5</p> <p data-bbox="721 1436 753 1457">3</p> <p data-bbox="721 1457 753 1478">2</p> <p data-bbox="721 1478 753 1499">1E-3</p> <p data-bbox="721 1499 753 1520">5</p> <p data-bbox="721 1520 753 1541">3</p> <p data-bbox="721 1541 753 1562">2</p> <p data-bbox="721 1562 753 1583">1E-2</p> <p data-bbox="721 1583 753 1604">5</p> <p data-bbox="721 1604 753 1625">3</p> <p data-bbox="721 1625 753 1646">2</p> <p data-bbox="721 1646 753 1667">1E-1</p> <p data-bbox="894 1667 932 1688">5.5</p> <p data-bbox="894 1688 932 1709">6.0</p> <p data-bbox="894 1709 932 1730">6.5</p> <p data-bbox="894 1730 932 1751">7.0</p> <p data-bbox="894 1751 932 1772">7.5</p> <p data-bbox="894 1772 932 1793">8.0</p> <p data-bbox="894 1793 932 1814">8.5</p> <p data-bbox="894 1814 932 1835">9.0</p> <p data-bbox="894 1835 932 1856">9.5</p> <p data-bbox="721 1394 753 1415">← GRAPE SRT tests</p> <p data-bbox="721 1499 753 1520">← GRAPE PCT tests</p> <p data-bbox="721 1499 753 1520">READABLE ALLOWABLE STATE RANGE</p> <p data-bbox="721 1604 753 1625">GRAPE SRT tests</p> <p data-bbox="721 1604 753 1625">GRAPE PCT tests</p>	

But in spite of these and other results of tests with Zr-Nb alloys, a broad international discussion was

launched on the analysis of the cladding fragmentation under LOCA conditions. The major issues of this discussion could be formulated as follows:

- are the current safety criteria developed approximately thirty years ago for the unirradiated Zircaloy cladding representative now (especially for irradiated Zircaloy cladding and new cladding materials)?
- what types of tests should be used to validate the mechanical behavior (fragmentation threshold) of different oxidized claddings?

Besides, a special question was formulated within the context of the discussion: can we consider that the mechanical behavior (margin of ductility) of oxidized unirradiated zirconium-niobium cladding as a function of equivalent-cladding-reacted (ECR) is similar to that of the unirradiated Zircaloy cladding?

The preliminary analysis of the comparative data shows that different answers on this question were obtained:

- German mechanical tests (J.Böhmert) [7] and Hungarian mechanical tests (AEKI) [8] with oxidized Zr-1%Nb (E110) claddings have demonstrated significant differences in the behavior of zirconium-niobium and Zircaloy alloys.
- French mechanical tests (CEA-Saclay, EDF, FRAMATOME) with oxidized Zr-1%Nb (M5) cladding [9] and American mechanical tests (Westinghouse) with oxidized Zr-1%Nb (Zirlo) cladding [10] have demonstrated that there were no general differences in the mechanical behavior of both types of oxidized claddings (Zr-1%Nb and Zry-4).

The consideration in detail of results of investigations performed previously with Zr-1%Nb alloys showed that more thorough mechanical tests should be carried out to understand LOCA-related ductility of zirconium-niobium claddings. An appropriate program was developed by Russian Research Center "Kurchatov Institute" in cooperation with Russian State Research Center "Research Institute of Atomic Reactors" under the support of Joint Stock Company "TVEL" (Russian Federation), U.S. Nuclear Regulatory Commission (USA), and Institute for Radiological Protection and Nuclear Safety (France).

It should be emphasized that the following issues were beyond this research:

- analysis of the representativity of current safety criteria;
- selection of the best test procedures to validate the mechanical behavior of oxidized claddings under LOCA conditions;
- analysis of LOCA scenarios.

Ring compression tests have been selected as the program basis because this approach has a good historical tradition (such type of tests was used to develop the first NRC fuel safety criteria for Zircaloy cladding (1204°C, 17%) and this approach offers the prospect of direct comparison of results obtained by different researchers for E110 cladding material and other cladding alloys. The goal of the work was formulated as: *to obtain the multifactor test data base characterizing the sensitivity of the zero ductility threshold of the E110 oxidized cladding to specially selected parameters (oxidation conditions, alloying elements, the temperature of mechanical tests)*. The results of this program are reviewed in this paper .

---

\* The experimental part of the program is not quite completed and the analysis and adjustment of results of the work are in a progress now. Therefore, authors of this paper reserve the right to correct some test data and appropriate conclusions in the future final report

## 2. Test Program

The program of oxidation and ring compression tests included two subprograms:

1. Determination of the zero ductility threshold of the cladding as a function of such oxidation parameters as heating and cooling rates under the following fixed conditions:
  - cladding material (E110 unirradiated as-received tubes);
  - double-sided oxidation with steam at 1100°C;
  - ring compression tests at 20°C.
2. Determination of the sensitivity of the zero ductility threshold for a fixed combination of heating and cooling rates to the following parameters:
  - cladding material (E110, Zry-4, E110K, E635);
  - type of oxidation;
  - temperature of oxidation;
  - temperature of mechanical tests;
  - irradiation of cladding (unirradiated E110 claddings and irradiated E110 claddings from commercial fuel rods with burnup ~50 MW d/kg U).

A special oxidation facility was designed for this program. The major characteristics of the cladding specimens and experimental procedures were as follows:

- indirect heating of specimen;
- oxidation by a steam flow of the initial specimen 100 mm long;
- high temperature uniformity along the specimen length;
- two types of oxidation: single-sided, double-sided.

Each of the 100 mm oxidized specimens was cut into approximately 10 rings. These rings were used for mechanical compression tests and for such special investigations as: the ECR measurement, hydrogen content measurement, metallography, fractography, Zr, Nb, O distributions measurement and so on. As for the ECR measurement, a special procedure was developed and certified. Besides, the method of analyzing ring compression tests (see Fig. 1) was studied.

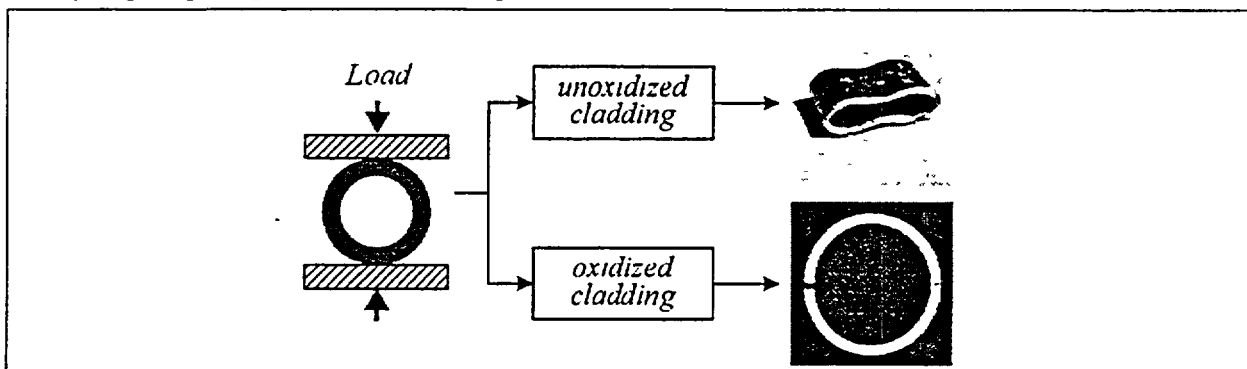


Fig. 1. Scheme of ring compression tests.

Some findings of these studies are as follows:

- relative displacement at failure is not a function of the ring height;
- the first through crack in the specimen is clearly fixed on the load-displacement diagrams.

But the major focus of this stage of the program was concentrated on the development of a reasonable procedure for the interpretation of ring compression test results (see Fig. 2).

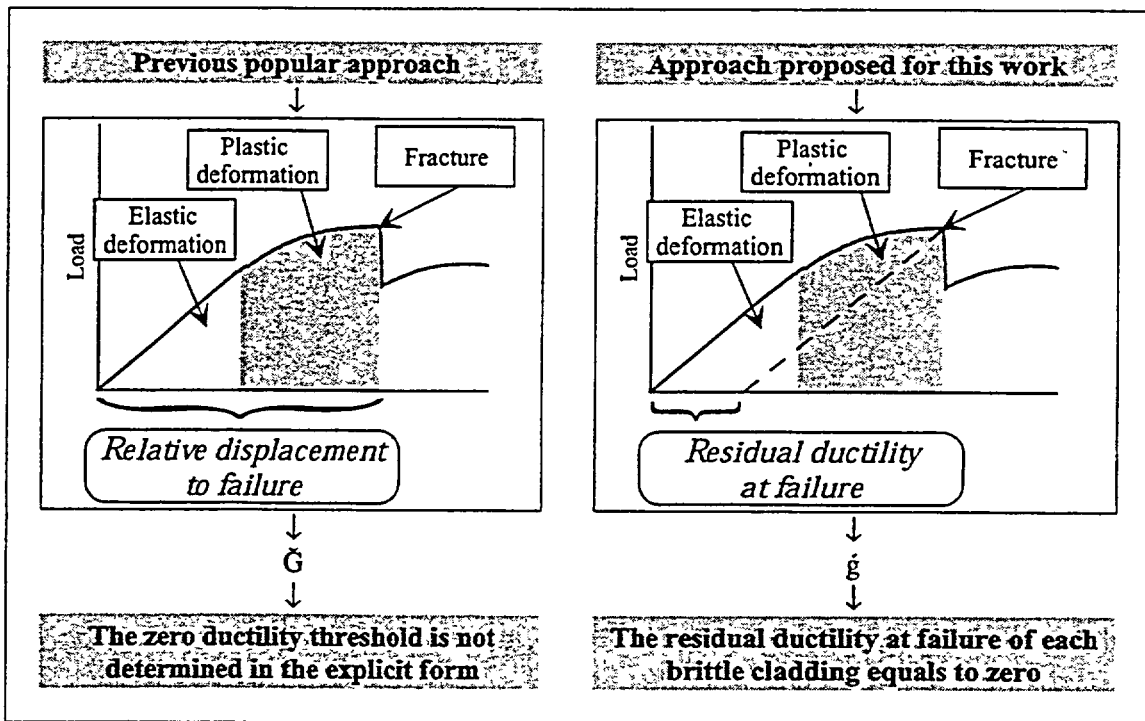


Fig. 2. Methods for the processing of the load-displacement diagram.

A review of the previously published data with results of ring compression tests showed that the "Relative displacement to failure" was used as a rule for the interpretation of results of compression mechanical tests. But this parameter is the sum of elastic and plastic deformation of the specimen. Taking into account that completely embrittled specimens have some elastic deformation, the final data base obtained with this approach did not allow one to estimate the zero ductility threshold in the explicit physical form. Therefore, a new approach to determine the zero ductility threshold was developed for this work (see the right side of Fig. 2). This approach is based on the following principles:

- ductility margin (residual ductility) of the oxidized specimen is characterized only by the plastic portion of deformation;
- the residual ductility at failure of each brittle specimen equals to zero;
- processing of ring compression test results obtained for specimens oxidized at the different ECR allows us to determine the zero ductility threshold in an explicit form.

### 3. Analysis of Experimental Results

The schematic description of the major results and preliminary analysis of key phenomena are presented in this chapter.

#### 3.1. Sensitivity of the zero ductility threshold of E110 cladding to the heating and cooling rates for high temperature oxidation

To determine the dependence of the zero ductility threshold on the dynamic parameters of the oxidation scenario, a variety of special tests was performed at the program beginning. Fixed parameters of tests were as follows:

- E110 as-received unirradiated cladding;
- double-sided oxidation at 1100°C;
- ring compression tests at 20°C (ring height 8 mm).

The parameters varied in these tests were heating and cooling rates (see Fig. 3).

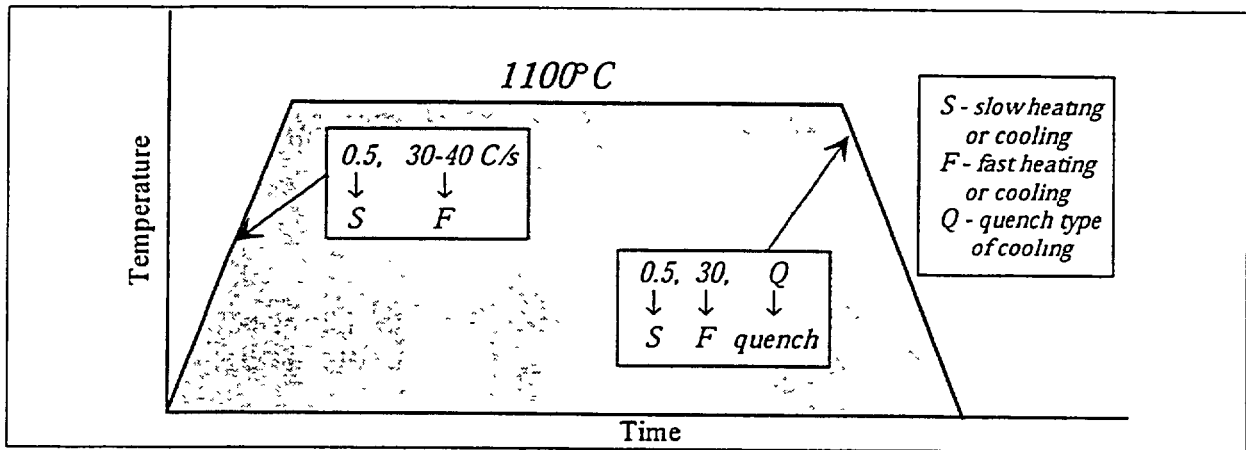


Fig. 3. Variation of heating and cooling rates under high temperature oxidation conditions.

The cycle of these tests shows the following (see Fig. 4):

- transition of the E110 oxidized cladding from a highly ductile state to the brittle one happens suddenly in the narrow range of the ECR;
- critical values of the ECR (7.6 – 9.2%) corresponding to the zero ductility threshold are relatively independent of the combination of heating and cooling rates;
- E110 embrittlement threshold is about 8.3% ECR for the major combination of heating and cooling rates (F/F).

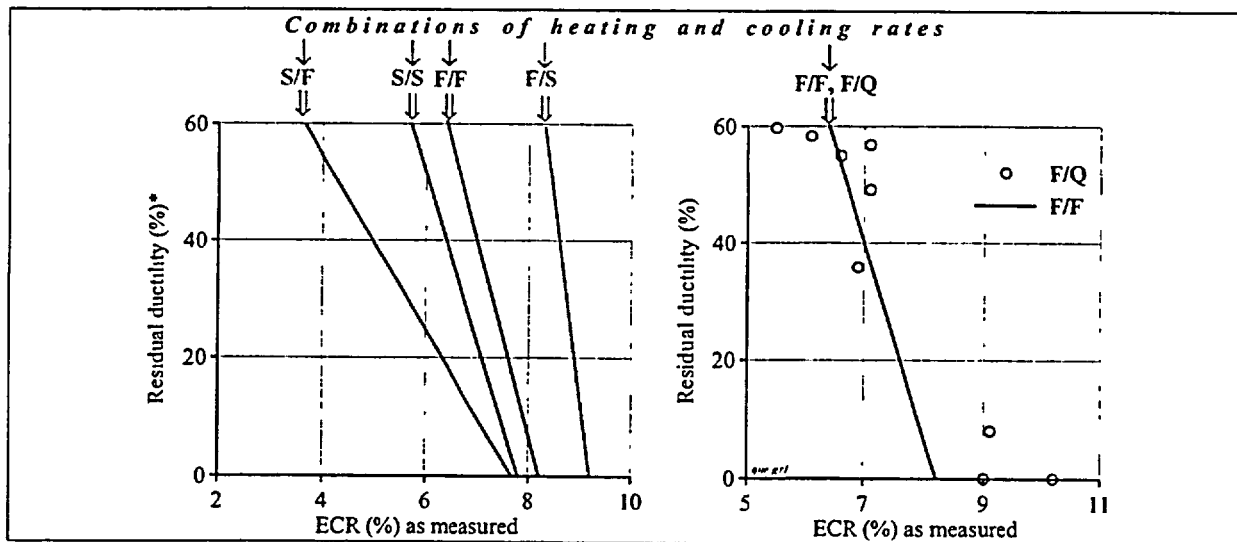


Fig. 4. Sensitivity of E110 zero ductility threshold to heating and cooling rates.

3.2. Comparison of the mechanical behavior of E110 and Zry-4 oxidized claddings

To obtain the comparative data base for these two alloys, several reference tests with Zry-4 cladding were performed with the following fixed parameters:

- double-sided oxidation at 1100°C;
- F/F combination of heating and cooling rates;
- ring compression tests at 20°C.

The results of tests are presented in Fig. 5.

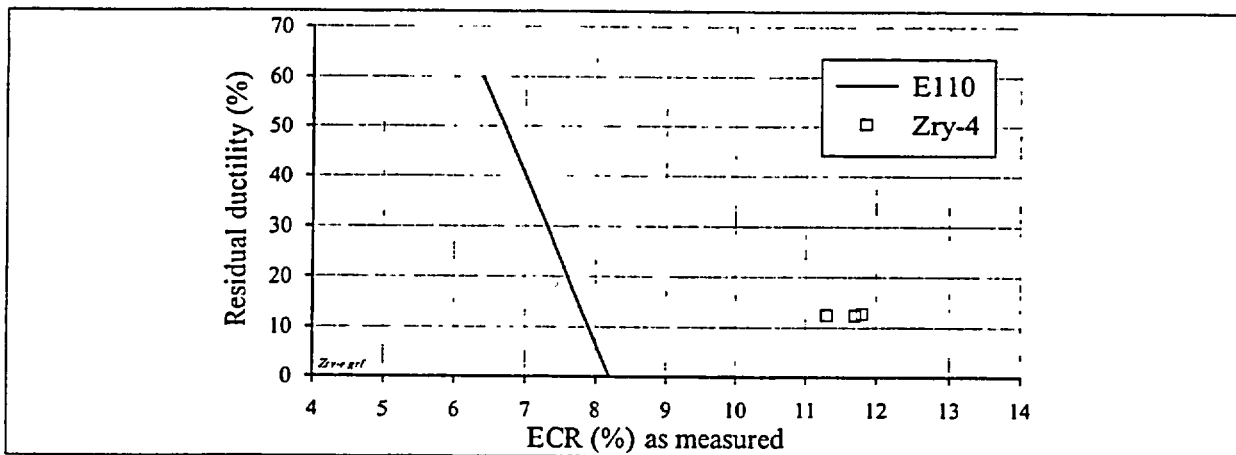


Fig. 5. E110/Zry-4 comparative data on the residual ductility vs. the ECR.

\* Residual ductility is the plastic component of displacement at failure (see Fig. 2) normalized on the cladding initial outer diameter

The analysis of obtained results confirms that the zero ductility threshold of E110 unirradiated cladding is lower than that of Zry-4 unirradiated cladding under ring compression test conditions. To clarify revealed differences in the mechanical behavior of these two alloys, the following additional investigations with oxidized claddings were performed:

- visual identification of  $ZrO_2$  oxide type;
- measurements of  $H_2$  concentration in the E110 oxidized cladding vs. the ECR;
- determination of the sensitivity of the cladding residual ductility to the  $H_2$  concentration;
- microstructure measurements and analysis.

The determination of the oxide type for E110 and Zry-4 cladding as a function of the ECR could be made using the data presented in Fig. 6.

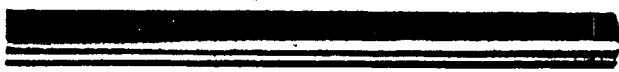
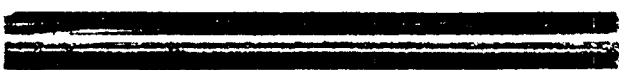
<u>E110</u> ECR=6.5%		Double-sided oxidation at 1100 C and F/F combination of heating and cooling rates
<u>E110</u> ECR=10.5%		
<u>Zry-4</u> ECR=11.3%		

Fig. 6. View of E110 and Zry-4 claddings after high temperature oxidation tests.

Major observations are summarized in Table 2.

Table 2. Types of  $ZrO_2$  oxide vs. the cladding type and the ECR.

Type of cladding	Type of $ZrO_2$ oxide
E110 (ECR=6.5%)	Nonstoichiometric black protective oxide
E110 (ECR=10.5%)	Spalled light stoichiometric oxide
Zry-4 (ECR=11.3%)	Nonstoichiometric black bright oxide

These observations allow us to make two conclusions:

1. Breakaway oxidation occurs in E110 cladding within this range of the ECR (6.5 – 10.5%);
2. Different physical mechanisms are responsible for the embrittlement threshold of E110 and Zry-4 claddings.

As for physical mechanisms of E110 embrittlement, previous investigations demonstrated that high hydrogen uptake corresponded to the zero ductility threshold of E110 alloy [7, 8]. Taking into account these data, special measurements of  $H_2$  concentration in E110 oxidized cladding were performed. Obtained data are presented in Fig. 7.

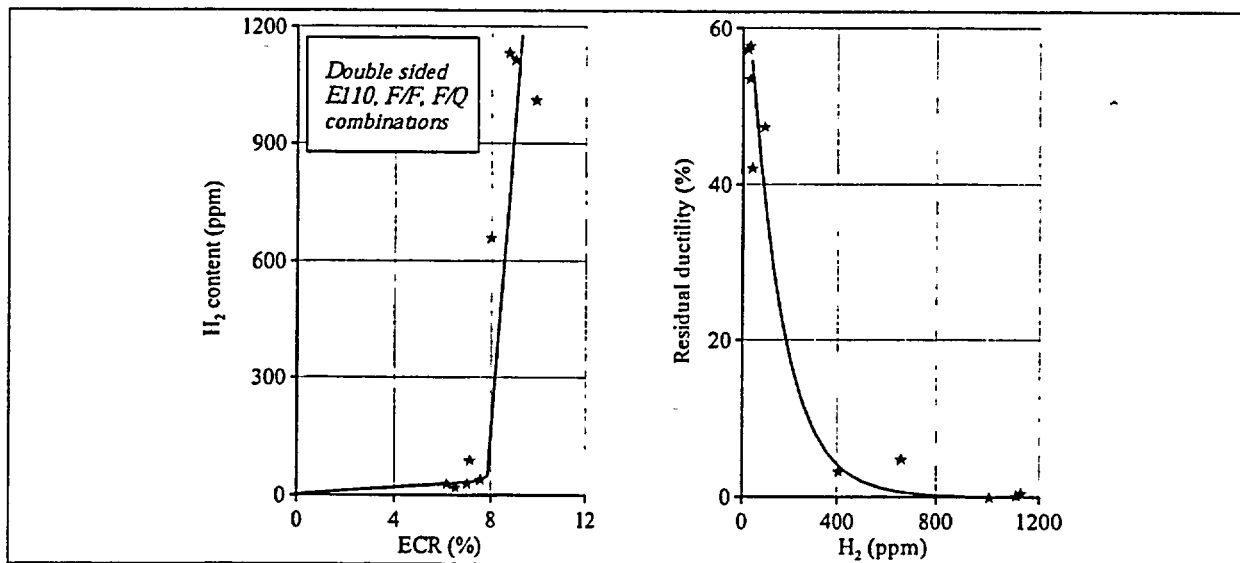


Fig. 7. H<sub>2</sub> content vs. the ECR and the sensitivity of residual ductility of E110 oxidized cladding to the hydrogen concentration.

The analysis of appropriate test results leads to the following observations:

- slow increase in hydrogen concentration vs. the ECR characterizes the oxidation behavior of E110 cladding for ECR < 7%;
- fast increase in hydrogen uptake occurs for ECR > 7%;
- cladding zero ductility threshold corresponds to 800 ppm of hydrogen content (ECR ≈ 8.3%).

Thus, these data confirm that hydrogen absorption is one of key factors determining the E110 cladding embrittlement for high temperature oxidation. The oxygen specific behavior (the next key factor of the embrittlement) in E110 oxidized cladding could be illustrated with the data presented in Fig. 8, Fig. 9.

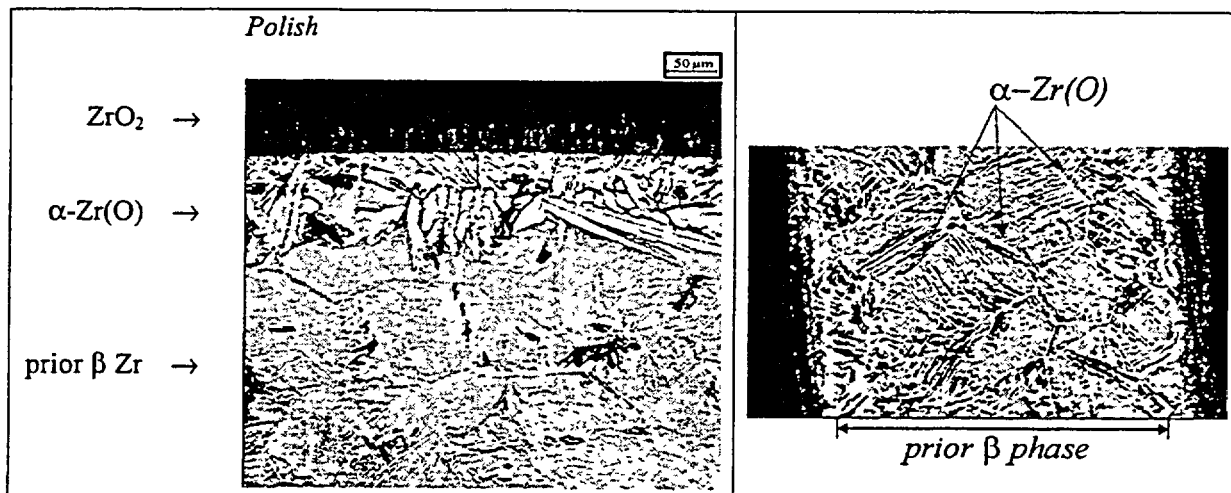


Fig. 8. The microstructure of E110 oxidized cladding.

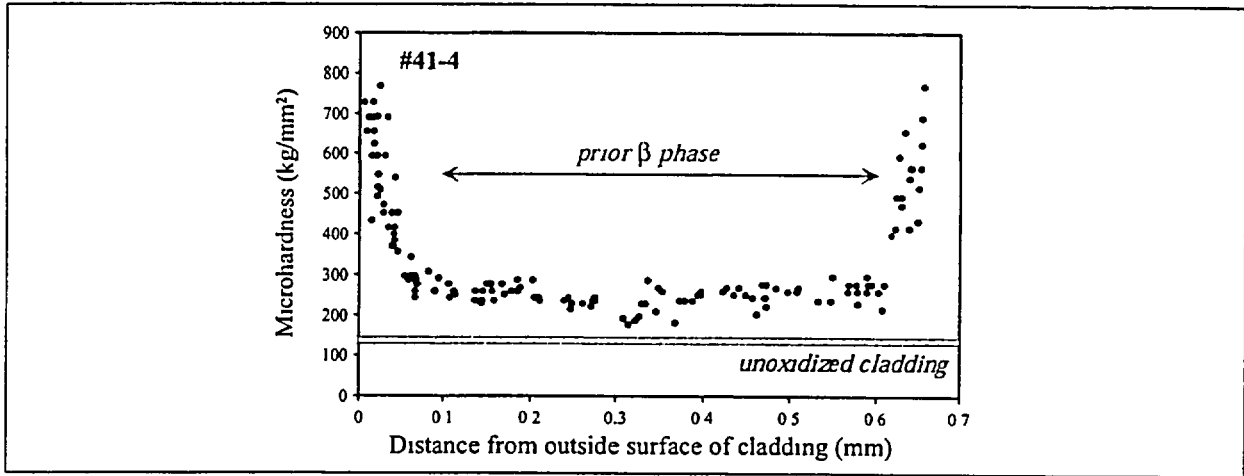


Fig. 9. Microhardness of E110 oxidized cladding near the zero ductility threshold (specimen #41-4, double-sided oxidation at 1100°C, ECR=8.6%).

These data suggest the following:

- there is a nonuniform boundary between  $\alpha$ -Zr(O) layer and prior  $\beta$  phase layer;
- $\alpha$ -Zr(O) layers are observed on the boundaries of grains in the prior  $\beta$  phase of E110 cladding oxidized to the zero ductility threshold;
- relatively uniform increase of the microhardness (oxygen concentration) along prior  $\beta$  phase thickness is observed.

The whole set of presented data demonstrates the differences in the behavior of zirconium-niobium and Zircaloy claddings. Additional demonstration of some general differences in the mechanical behavior of both alloys is presented in Fig. 10.

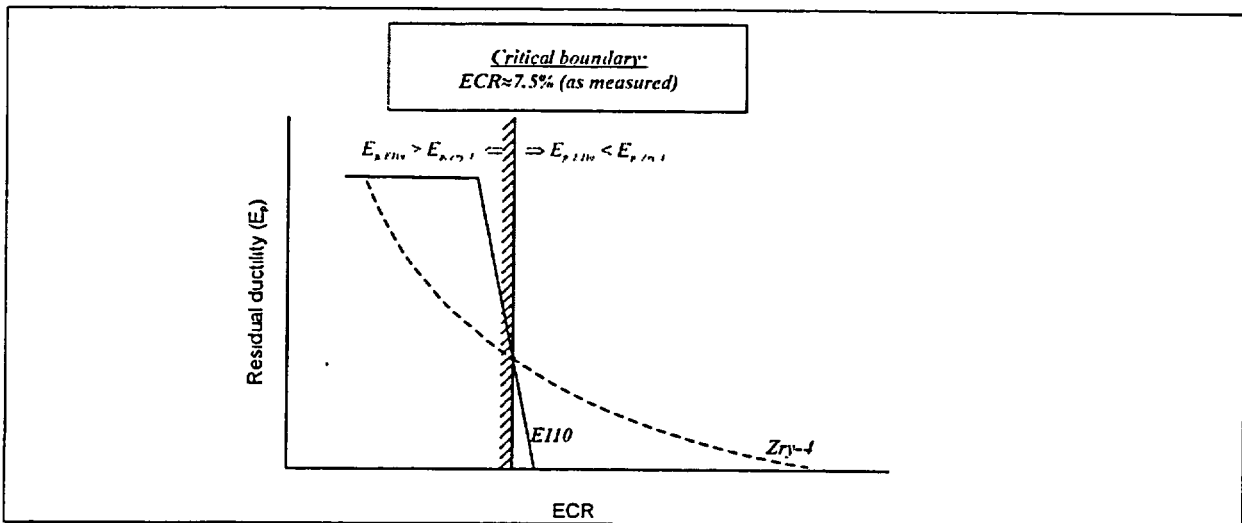


Fig. 10. Comparative schematic diagram shows the ductility of E110 and Zry-4 alloys versus the ECR (E110 data: this work; Zry-4 data are based on Böhmer's results [7]).

The analysis of these data is presented in Table 3.

**Table 3. General observations and possible explanations of differences in the mechanical behavior of E110 and Zry-4 oxidized cladding.**

Observations	Possible explanations
Unlike Zry-4, the residual ductility of the E110 cladding is practically insensitive to the oxidation up to the ECR=6.5%. Therefore, the margin of the E110 cladding residual ductility is higher than that of Zry-4 cladding up to the ECR=7.5%	All absorbed oxygen is concentrated in surface layers of the E110 cladding
Unlike Zry-4, a sharp decrease of E110 ductility down to zero is noted at the ECR higher than 7.5%	The change of the mechanism of the E110 cladding oxidation results in substantial hydrogen (and oxygen?) uptake

*3.3. Determination of the E110 oxidized cladding residual ductility as a function of the oxidation type (single-sided, double-sided)*

The motivation to perform a special cycle of single-sided oxidation of E110 specimens was based on the following background:

- single-sided oxidation of fuel rod claddings characterized the LOCA scenarios up to cladding burst;
- double-sided oxidation of Zr-1%Nb (E110) and Zry-4 claddings performed in the frame of this work and previous investigations [7, 8] showed significant differences in the residual ductility of these alloys;
- but ring compression tests performed with Zr-1%Nb (M5) single-sided oxidized claddings did not reveal significant differences in the residual ductility of M5 and low-tin Zry-4 alloys.

The studies of mechanical behavior of single-sided oxidized E110 cladding were performed under following fixed conditions:

- combination of heating and cooling rates: F/F;
- temperature of oxidation: 1100°C;
- temperature of the ring compression tests: 20°C.

The results of these tests are presented in Fig. 11. Analysis of the results allows us to make the following general conclusions:

- the residual ductility of Zr-1%Nb (E110) oxidized cladding is quite sensitive to the oxidation type;
- changing of the oxidation type from double-sided to single-sided leads to an increase of the zero ductility threshold from 8.3% up to 11% (as measured).

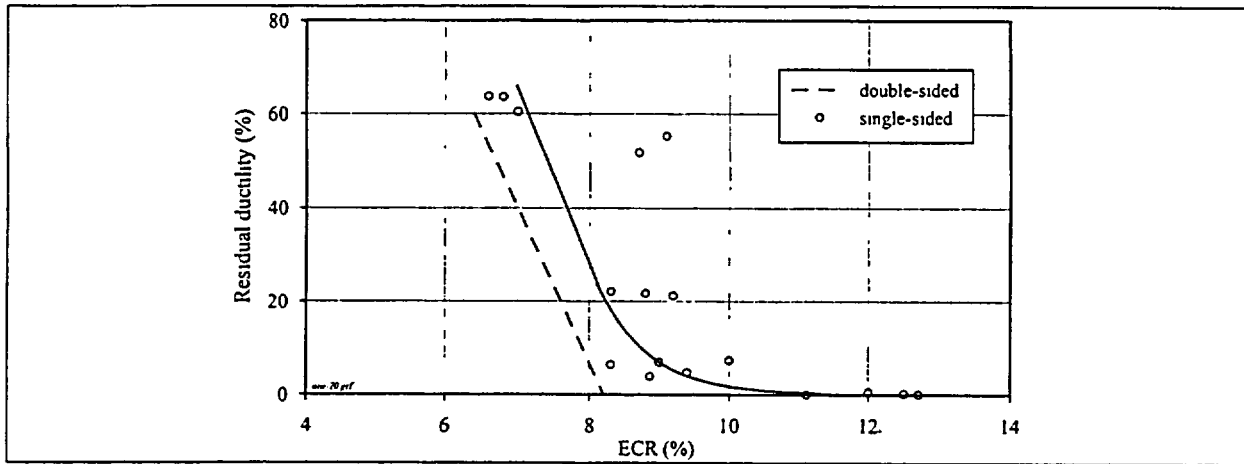


Fig. 11. The E110 cladding residual ductility vs. the oxidation type.

### 3.4. Sensitivity of the E110 oxidized cladding residual ductility to the temperature of mechanical tests

This stage of the program was motivated by several important issues:

- correlations between the loads on the oxidized cladding and the cladding temperature vs. major events under late LOCA conditions are not well known; therefore, the assessment of sensitivity of the mechanical behavior of oxidized cladding to the temperature could be very useful;
- the approach used for the development of current LOCA safety criteria was validated for Zry-4 unirradiated oxidized cladding tested at 135°C under ring compression tests conditions (Hobson's tests);
- recent mechanical tests of oxidized zirconium-niobium claddings of the Zirlo type performed at 135°C did not reveal significant differences in the residual ductility of zirconium-niobium alloy (Zirlo) and Zry-4 [10].

The appropriate results obtained with E110 oxidized claddings tested at 135°C are shown in Fig. 12.

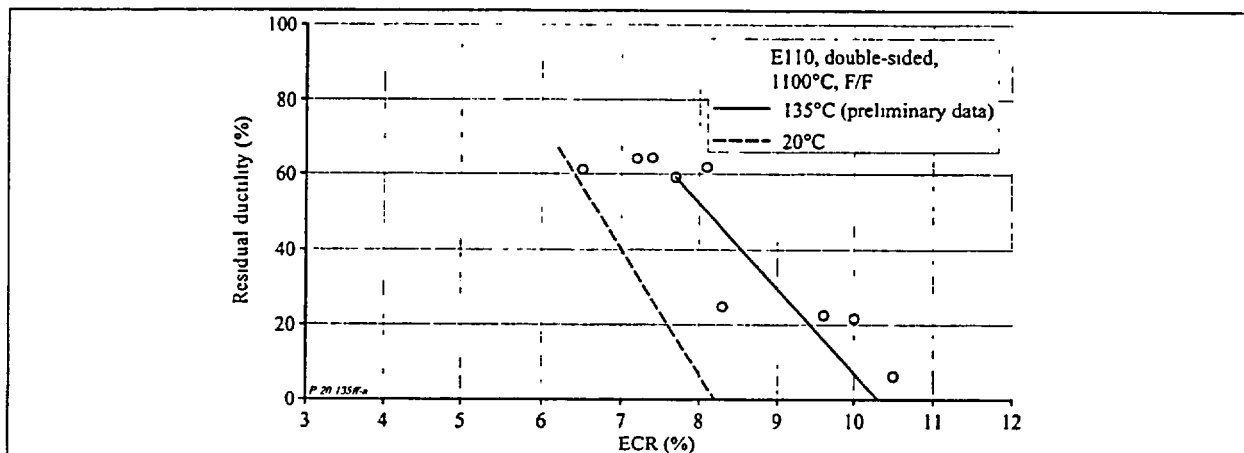


Fig. 12. Comparative results of ring compression tests with E110 oxidized cladding at 20°C and 135°C.

In accordance with these data, the temperature increase of mechanical tests from 20°C up to 135°C leads to an increase of the E110 zero ductility threshold from the ECR=8.3% up to the ECR=10.3% (at the minimum). This effect suggests that the precipitation of solid hydrides during the cooling phase is one of the major reasons for cladding embrittlement at room temperature. A possible explanation for the increase of the cladding ductility with the increase of temperature is based on the analysis of behavior of hydrides as a function of temperature (the increase of the ductility of hydrides). Additional mechanical tests (ring compression and ring tensile tests) performed with E110 cladding, which was brittle at RT, have shown that a sharp increase of cladding ductility is observed at temperature higher than 150 – 200°C.

### 3.5. Determination of the sensitivity of the mechanical behavior of oxidized zirconium-niobium claddings to the alloying components

The analysis of test results performed at the intermediate stage of the program has shown that it is very important to answer the following question: *does the observed difference between the mechanical behavior of E110 and Zry-4 oxidized claddings characterize these two particular alloys or do these data reflect a general differences in the behavior of zirconium-niobium alloys in comparison with zirconium-tin?*

To obtain the appropriate answer to the formulated question, special tests were carried out with the variation of alloying components in the zirconium-niobium cladding. The program approach to this research is presented in Table 4.

**Table 4. Characteristic of some most important types of zirconium-niobium alloys.**

1. Zr+1%Nb+low initial concentration of oxygen (~0.03–0.05%)	⇒	E110 alloy
2. Zr+1%Nb+high initial concentration of oxygen (>0.11%)	⇒	E110K, M5
3. Zr+Nb+Sn+Fe	⇒	E635, Zirlo

Thus, it could be assumed that tests with such types of alloys as E110K and E635 allow to obtain the needed preliminary comparative data base to assess the sensitivity of the mechanical behavior of oxidized zirconium-niobium claddings to the alloying components. The results of appropriate tests are presented in Fig. 13.

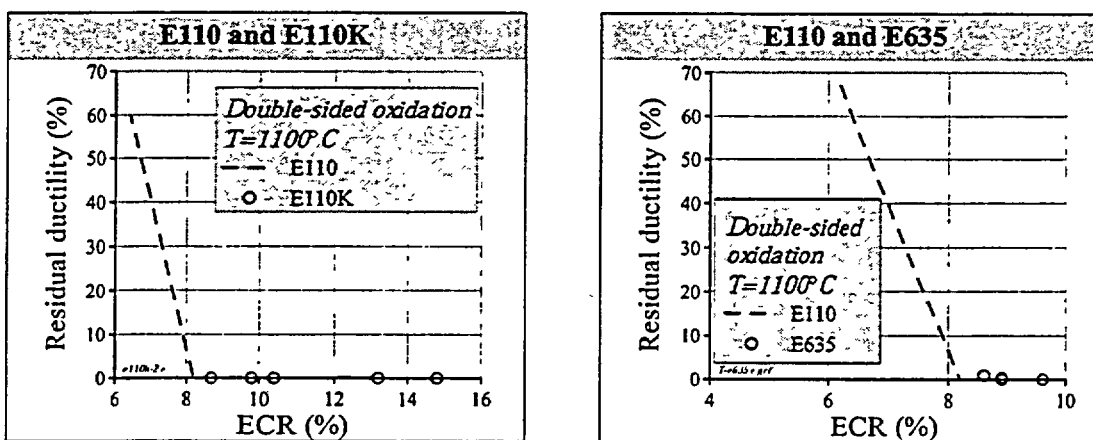


**Fig. 13. Results of comparative tests with the variation of alloying components in zirconium-niobium alloys.**

Analysis of these results shows the following:

- in the context of this test procedure, a qualitative influence of alloying components in Zr-1%Nb alloys on the zero ductility threshold has not been revealed;
- it is possible that general differences in the mechanical behavior of E110 and Zry-4 oxidized claddings are determined by specific features of the tin and niobium behavior during oxidation (appropriate research is now in progress).

### 3.6. Sensitivity of the E110 cladding zero ductility threshold to cladding irradiation

Taking into account that this stage of the program has not been completed yet, the preliminary results of tests with irradiated claddings are presented in Fig. 14. Analysis of these first data indicates that the zero ductility threshold of irradiated E110 cladding is higher than 6% ECR when the temperature of mechanical tests is 20°C.

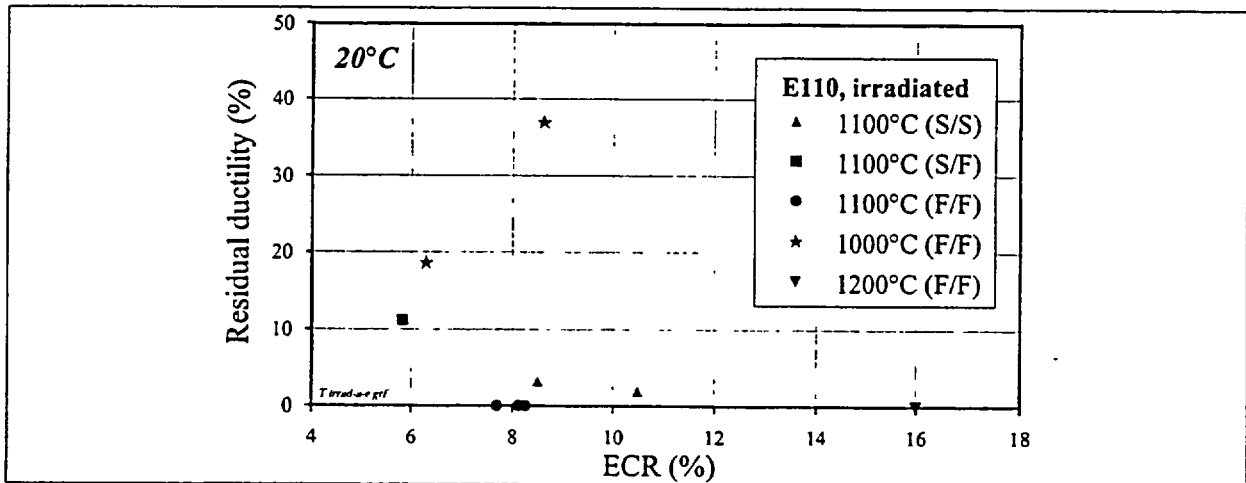


Fig. 14. Results of ring compression tests with E110 irradiated claddings.

### 3.7. Determination of relationship between the values of measured and calculated ECR

For a correct interpretation of the experimental data presented in this paper it is very important to take into account the following:

- test data characterizing zero ductility thresholds of oxidized claddings are presented as a function of measured ECR;
- current LOCA safety criteria (17% in USA and France, 15% in Japan, 18% in Russia) are based on calculated ECR using a conservative oxidation kinetics correlation.

These approaches can be illustrated using the appropriate data for the Zry-4 cladding (see Fig. 15). Presented data allow to note that:

- for any alloy the measured ECR must not be compared with the safety criteria (as calculated) directly;
- the comparison of E110 and Zry-4 safety criterion (18% and 17% (or 15%) as calculated) does not have a physical meaning because the degree of the conservatism for both can be different.

To clarify this issues for the E110 cladding, additional research is being carried out now. The results of these investigations will be published later.

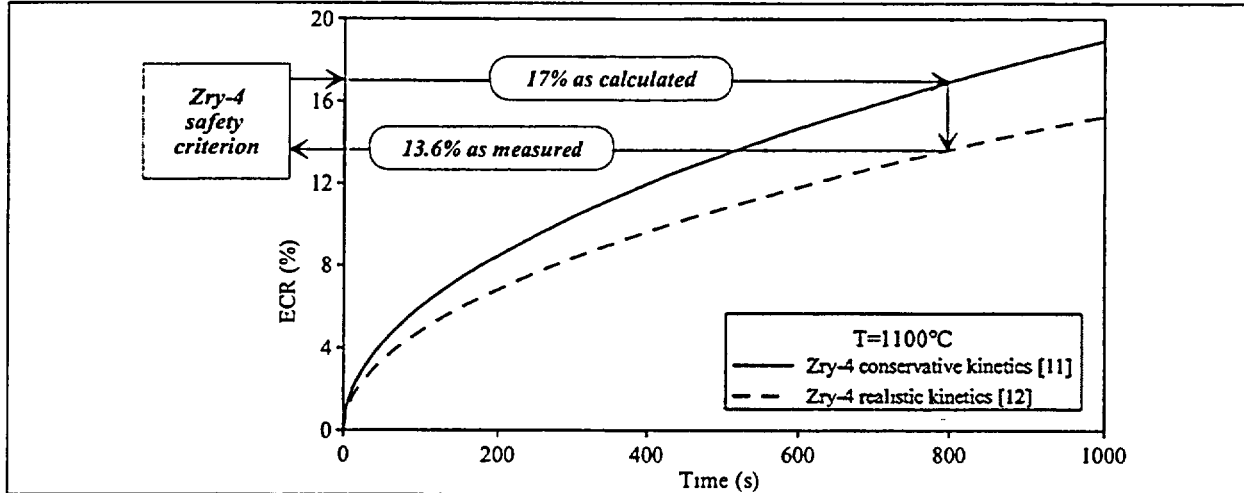


Fig. 15. Comparison of measured and calculated criteria values of the ECR for the Zry-4 cladding.

#### 4. Major conclusions

Experimental studies of the LOCA-related ductility in E110 cladding were performed on the basis of ring compression mechanical tests. Results of several parts of this research program show that:

- the E110 unirradiated oxidized cladding (after double sided oxidation at 1100°C) retains a very high level of ductility (>50%) up to:
  - ECR=8.5% for the best combination of heating and cooling rates;
  - ECR=4.5% for the worst combination of heating and cooling rates.
- After that, a sharp decrease of residual ductility is observed due to a breakaway oxidation effect.
- A sharp increase in hydrogen content in the prior  $\beta$ -phase of the E110 cladding (>800 ppm) is responsible for the differences in mechanical behavior between E110 and Zry-4 claddings.
- The reference value for the zero ductility threshold (at 20°C) of E110 double side oxidized cladding is 8.3% (the ECR as measured).
- Comparative tests with Zry-4 cladding confirm that the Zry-4 oxidized cladding has a residual ductility margin and a low content of hydrogen at the ECR=11.5% (as measured).
- The zero ductility threshold of E110 one side oxidized claddings is increased up to the ECR=11%

(these data and the French ones with the M5 alloy may be compared directly only after reconciling test and data processing procedures).

- The E110 cladding zero ductility threshold is sensitive to the mechanical test temperature. An increase of this temperature up to 135°C (the so-called ZDT used on developing the Zry-4 safety criterion) leads to an increase of the embrittlement threshold up to ECR=10.3% (as measured).
- Special tests performed to reveal the ductility threshold sensitivity to the composition of Russian zirconium-niobium alloys (the increase of oxygen concentration (E110K alloy), the presence of such alloying components as Sn, Fe (E635 alloy)) show that there are no principle differences in the mechanical behavior of oxidized claddings of all tested alloys.
- The zero ductility threshold of the E110 irradiated oxidized cladding is higher than ECR=6% (as measured).

## References

- 1 V.P.Smirnov, A.V.Smirnov, V.A.Tsykanov, Ye.G.Bek, A.K.Panioushkin, A.A. Enin, V.Rozhkov, "Characteristics of VVER fuel after operation at steady-state and transient conditions. Forecasting of ultra-high burnup". *Proceedings of Scientific&Technical Conference "Nuclear Power on the Threshold of XXI Century"*, 8-10 June 2000, Electrostal, Russia.
- 2 E.Kaplar, L.Yegorova, K.Lioutov, A.Konobeyev, N.Jouravkova, V.Smirnov, A.Goryachev, V.Prokhorov, O.Makarov, S.Yeremin, A.Svyatkin, *Mechanical properties of unirradiated and irradiated Zr-1%Nb cladding*, NSI RRC 2241, NUREG/IA-0199, IPSN 01-16, April 2001.
- 3 L.Yegorova, K.Lioutov, E.Kaplar, "Overview of test results on mechanical properties of unirradiated and irradiated Zr-1%Nb (E-110 alloy) cladding". *Proceedings of Nuclear Safety Research Conference*, NUREG/CP-0176, May 2002, p.34-35.
- 4 Yu.K.Bibilashvili, L.A.Yegorova, O.A.Nechaeva, I.G. Smirnov, V.P.Smirnov et.al. "Experimental Study of VVER High Burnup Fuel Rods at the BIGR Reactor under Narrow Pulse Conditions", *2000 International Topical Meeting on Light Water Reactor Fuel Performance*, Park City, Utah, April 10-13, 2000, p.306-314.
- 5 Yu.Bibilashvili, O.Nechaeva, A.Salatov, A.Goryachev, V.Sazhnov, I.Smirnov, N.Sokolov, Yu.Trutnev, V.Ustinenko, L.Yegorova. "Study of High Burnup VVER Fuel Rods Behaviour at the BIGR Reactor under RIA Conditions: Experimental Results", *OECD RIA Topical Meeting, CABRI Seminar (open part)*, Aix-en-Provence, France, May 13, 2002.
- 6 Bibilashvili Yu.K., Sokolov N.B., Andreeva-Andrievskaya L.N., Tonkov V.Yu., Salatov A.V., Morozov A.M., Smirnov V.P. "Thermomechanical Properties of Zirconium-Based Alloys Oxidized Claddings in LOCA Simulating Conditions", *Proc. of IAEA Technical Committee Meet. on "Fuel Behavior under Transient and LOCA conditions"*, Halden, Norway, September 10-14, 2001.
- 7 Böhmert J., Dietrich M., Linek J. "Comparative Studies on High-Temperature Corrosion of Zr-1%Nb and Zircaloy-4", *Nuclear Engineering and Design*, 147 No1, 1993, p.53-62.
- 8 Hozer Z., Maroti L., Matus L., Windberg P. "Experiments with VVER Fuels to Confirm Safety Criteria", *Proc. of Top Fuel-2001 Meet.*, Stockholm, May 27-30, 2001, paper P2-14.

- 9 Brachet J., Pelchat J., Hamon D., Maury R., Jaques P., Mardon J. "Mechanical Behavior at Room Temperature and Metallurgical Study of Low-Tin Zry-4 and M5™ (Zr-NbO) Alloys after Oxidation at 1100°C and Quenching", *Proc. of IAEA Technical Committee Meeting on "Fuel Behavior under Transient and LOCA Conditions"*, Halden, Norway, September 10-14, 2001.
- 10 W.J.Leech "Ductility Testing of Zircaloy-4 and ZIRLO™ Cladding after High Temperature Oxidation in Steam", *Proc. of the Topical Meeting on LOCA Fuel Safety Criteria*, Aix-en-Provence, France, March 22-23, 2001, OECD NEAR/CSNI/R(2001)18, p.135-143.
- 11 L. Baker and L.C. Just, *Studies of Metal-Water Reactions at High Temperatures*, ANL-6548 (1962).
- 12 J.V. Cathcart, et al., *Zirconium Metal-Water Oxidation Kinetics IV. Reaction Rate Studies*, ORNL/NUREG-17, 1977.

This page left intentionally blank

## LOCA RESEARCH RESULTS FOR HIGH-BURNUP BWR FUEL

Y. Yan, R. V. Strain, and M. C. Billone

Argonne National Laboratory (ANL)  
Argonne, Illinois, USA

### Abstract

LOCA-relevant steam oxidation kinetics and LOCA Integral Test results are reported for high-burnup BWR cladding. Zircaloy-2 samples heated to 1000-1200°C in saturated steam exhibit weight gain values consistent with Cathcart-Pawel model predictions, as well as with data for other cladding alloys. The 10- $\mu$ m coolant-side oxide layer on this cladding appears to be non-protective during high-temperature steam oxidation. LOCA Integral Test fueled samples (300-mm-long) are stabilized in Ar at 300°C, heated (5°C/s) in saturated steam to 1204°C, held at 1204°C for 1-10 minutes, slow-cooled (3°C/s) to 800°C and water quenched. Results for irradiated and unirradiated test specimens are similar: burst at  $\approx$ 750°C and  $\approx$ 8 MPa,  $\approx$ 40% burst strain, and  $\approx$ 13 $\times$ 2.5-mm burst opening. These results indicate excellent permeability for high-burnup BWR fuel. High-burnup results differ from those of unirradiated specimens in: axial extent of ballooning (shorter), burst shape (oval vs. dog bone), ejection of volatile fission products and/or fuel fines during burst, and fallout of fuel particles during post-burst testing and post-test handling.

### Introduction

Argonne National Laboratory (ANL) is conducting research on high-burnup BWR and PWR fuel to provide data for assessing the licensing criteria for Loss of Coolant Accident (LOCA) events. LOCA-relevant research includes fuel and cladding characterization, cladding high-temperature steam oxidation kinetics studies, LOCA Integral Testing of fueled segments, post-quench ductility testing of LOCA Integral specimens and post-quench ductility testing of unirradiated zirconium-based cladding alloys (Zircaloy-2, Zircaloy-4, ZIRLO, and Zr-1Nb alloys). The work completed on samples from Limerick BWR fuel rods ( $\approx$ 56 GWd/MTU) is reported.

The LOCA licensing criteria (10 CFR 50.46) limit peak cladding temperature to 2200°F (1204°C) and maximum Equivalent Cladding Reacted (ECR) to 17% to ensure adequate ductility during the Emergency Core Cooling System quench and during possible post-LOCA events (e.g., seismic). High burnup phenomena that may affect cladding response during ballooning and burst, steam oxidation, water quench and post-quench events are: loss of cladding base metal thickness due to oxidation, hydrogen pickup, inner-surface oxide-layer formation, decreased fuel permeability and tight fuel-cladding bonding, and the effective thickness, oxygen content, hydrogen content and hydride morphology of the prior-beta-phase layer following steam oxidation. The LOCA Integral Tests are being conducted with high burnup fueled cladding segments in order to include all of these high-burnup characteristics.

Limerick cladding is Zr-lined Zircaloy-2 (Zry-2) from the GE-11 9×9 assembly design. The in-reactor-formed outer-surface oxide layer is ≈10 μm. Axial variation of layer thickness is minimal compared to circumferential variation (3-18 μm) for rod locations from which samples have been taken. The tenacious crud layer thickness is ≈5-10 μm and varies inversely with the oxide thickness. The inner-surface oxide layer is ≈10 μm. Oxygen and hydrogen contents are ≈0.7 wt.% and ≈70 wppm, respectively.

The outer surface of defueled cladding samples has been exposed to saturated steam at high-temperature to determine weight gain, ECR, and layer thicknesses as functions of time at temperature. As reported in Ref. 1, 21 tests have been conducted (1000-1200°C) using unirradiated Zry-2 (9 tests) and irradiated high-burnup Zry-2 (12 tests). Weight gains deduced from detailed metallographic analysis of the 1200°C samples are consistent (within ≈5%) with the Cathcart-Pawel (CP) model predictions. Based on an assessment of the databases for Zry-2, Zry-4, ZIRLO and Zr-1%Nb alloys, these cladding materials exhibit about the same weight gain kinetics in steam at 1100-1500°C, consistent with the ANL data and the CP model predictions. Detailed metallographic analyses are in progress to determine the weight gain kinetics and layer thicknesses of the ANL Zry-2 samples tested at 1000°C and 1100°C.

The CP model has been used to plan the LOCA Integral Test times-at-temperature to achieve desired ECR values. The tests have the following sequential steps: stabilization at 300°C and ≈8.3 MPa internal pressure in Ar purge followed by saturated steam flow, temperature ramp (5°C/s) through ballooning and burst to 1204°C, hold at 1204°C for 1-10 minutes, slow-cooling (3°C/s) to 800°C, and initiation of water quench at 800°C. Four-point bend tests will be used to determine overall specimen integrity. Ring compression tests will be used for local ductility determination. The fueled LOCA specimens are ≈300-mm long with a 270-mm fuel column and a 13-mm top plenum connected to a He gas line (≈10 cm<sup>3</sup>). Temperature variations in the middle 100 mm of the specimen are ±15°C at 1204°C.

The LOCA Integral Test Apparatus was built and tested out-of-cell using archival Zry-2 samples filled with loose-fitting (0.1-mm radial gap) zirconia pellets. For the reference conditions, unirradiated Zry-2 bursts in the alpha phase at ≈750°C for a peak internal gauge pressure (i.e., pressure difference across the cladding wall) of ≈8.8 MPa with a peak burst strain of ≈50±10%. A second apparatus of the same design was built and installed into an Alpha-Gamma Hot Cell Facility (AGHCF) workstation. The in-cell and out-of-cell units share the same instrumentation and control system and can perform oxidation-kinetics and LOCA Integral tests. A schematic of the LOCA Integral Test Apparatus is shown in Fig. 1.

Because of the interest in high-burnup fuel permeability, ballooning, burst and possible fuel relocation, the first series of LOCA Integral Tests are being conducted in the following sequential steps: A) room temperature and 300°C pressurization to quantify fuel permeability, followed by ramping to burst; B) full LOCA sequence up to the cool-down to 800°C, followed by slow furnace cooling; and C) full LOCA sequence including water-quench initiation at 800°C. Tests A and B have been completed.

### Oxidation Kinetics and LOCA Integral Test Apparatus

The oxidation kinetics tests require a test train holder for the cladding sample, a quartz tube test chamber, an argon gas line to purge the test chamber, a steam supply system, and an argon line to purge the inner volume of the sample to inhibit possible inner-surface steam oxidation and hydrogen pickup. This inner purge line is at a higher pressure than the saturated steam. Test samples are 25-mm-long unirradiated and defueled-irradiated cladding. One-sided, outer-surface oxidation tests have been performed. Details of the oxidation test train are given in Ref. 1.

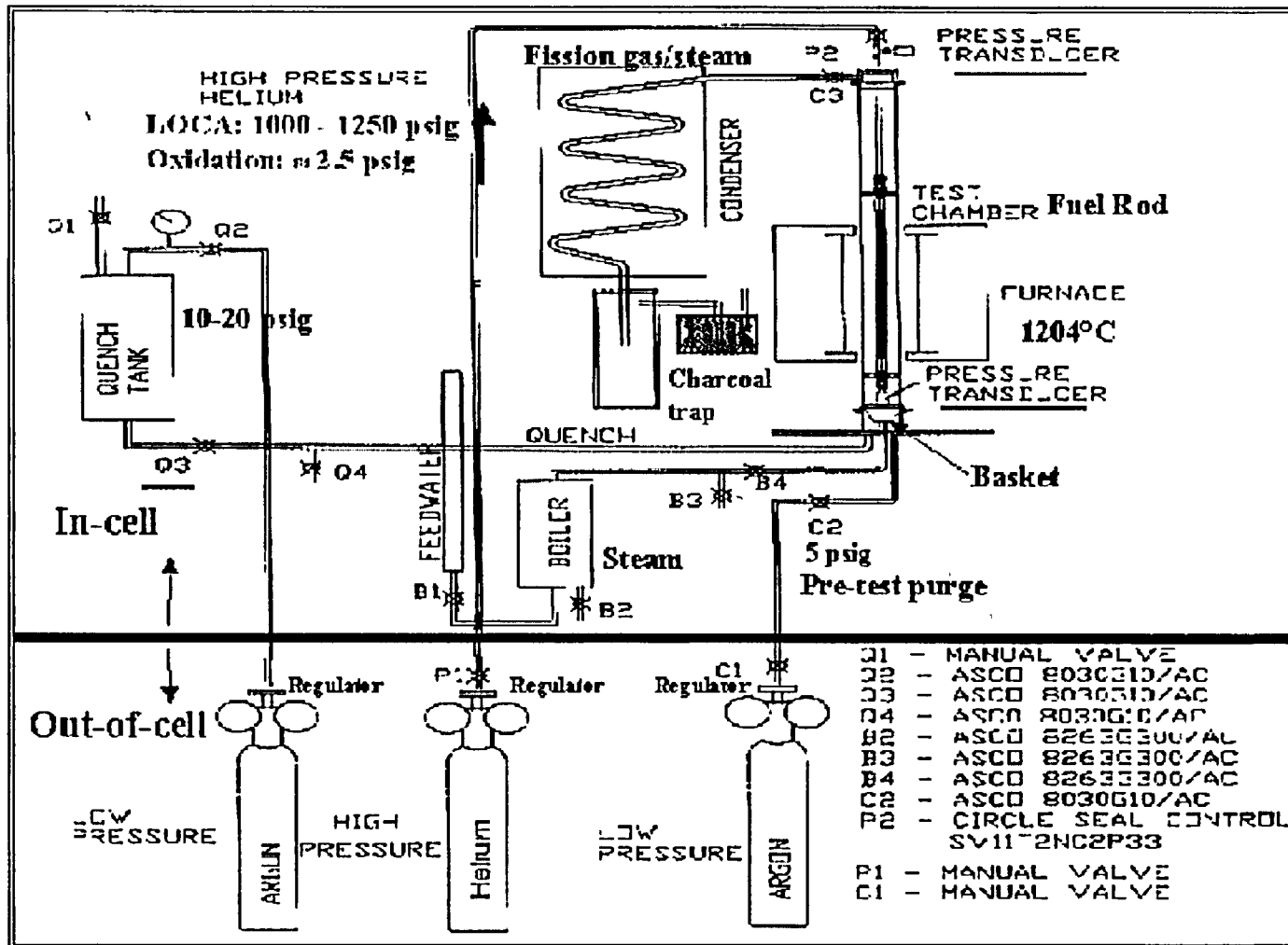


Fig. 1. Schematic of Oxidation Kinetics and LOCA Integral Test Apparatus; test train is for LOCA Integral Test.

The LOCA Integral Tests require features beyond those needed to conduct oxidation tests: a high-pressure internal He gas line, a condenser/filter unit, and a quench system. Because of the similarities of the oxidation and LOCA systems, they have been combined into one unit. Currently, a full Oxidation/LOCA-Integral Test Apparatus is positioned out-of-cell. The in-cell Oxidation Test Apparatus has been expanded to include most of the features required to run the full LOCA Integral Test sequence. Once the quench system has been installed in the AGHCF workstation, the out-of-cell and in-cell test apparatuses will be the same, both sharing the same out-of-cell control unit. Figure 2 shows an overview of the out-of-cell LOCA Integral Test Apparatus. In the background (upper right of center) is the shield window of Workstation 6, behind which is the in-cell apparatus.

The LOCA test train is shown in Fig. 3. This test train is supported at the top to minimize specimen bowing. The quartz tube encasing the test train provides an enclosed volume for steam flow and water quench, both of which are introduced through the bottom of the unit. The test train is centered within the quartz tube by means of two perforated spacer disks. Centering is very important as four vertical infrared lamps are focused within the furnace to heat the specimen. Swagelok fittings are used above the specimen to connect to the high-pressure gas line and top pressure gauge and below the specimen to connect to the lower pressure-gauge line. The total gas volume above the fuel column is 10 cm<sup>3</sup>, most of which is outside the heated zone. Four Type S thermocouple lead wires are fed in through the top. Two of the thermocouples are spot-welded at the specimen midplane, 180° apart. The other two are spot welded 50-mm above and 50-mm below the midplane at the same angular orientation as one of the midplane thermocouples. These thermocouples are accurate to ±3°C at 1200°C. The signal from the top thermocouple is used to control the furnace power to achieve the desired temperature ramp and hold temperature. The system is designed to allow switching of the control thermocouple in case the top one fails. For the out-of-cell tests, hands-on assembly is straightforward and bare-wire thermocouple beads are directly welded to unirradiated tubing. For remote in-cell assembly, outer-surface oxide is removed at the thermocouple locations and an iridium pad is welded to the thermocouple bead to provide the stiffness needed to position the thermocouples for welding to the specimen. The Ir pad also inhibits the Pt-Zr eutectic from forming.

Remote in-cell specimen preparation and test train assembly are more challenging than conducting the LOCA Integral Test. A drill with both rotary and cyclic horizontal motion is used to remove ≈13 mm of fuel from the bottom of the specimen (space for end-cap welding) and ≈20 mm of fuel from the top of the specimen (≈7 mm for end-cap welding and 13 mm for clearance). Following end-cap welding, the specimen is inserted into the Test Train Assembly Apparatus for attaching the Swagelok fittings, for outer-surface oxide removal, for positioning the thermocouples and for spot-welding the thermocouples. A simplified assembly device currently in-cell has been designed for making the Swagelok attachments and for strapping two thermocouples to the specimen ≈50-mm above the midplane. This device was used for the first two LOCA Integral Tests. The Test Train Assembly Apparatus has been tested in a cold-cell with remote handling capability. Also, thermocouple (TC) readings from the TCs welded to the sample through iridium pads have been compared to readings from TCs directly welded to the Zry-2 tubing in order to optimize the process and benchmark the results. The Apparatus is ready for transport into, and operation within, the hot cell.

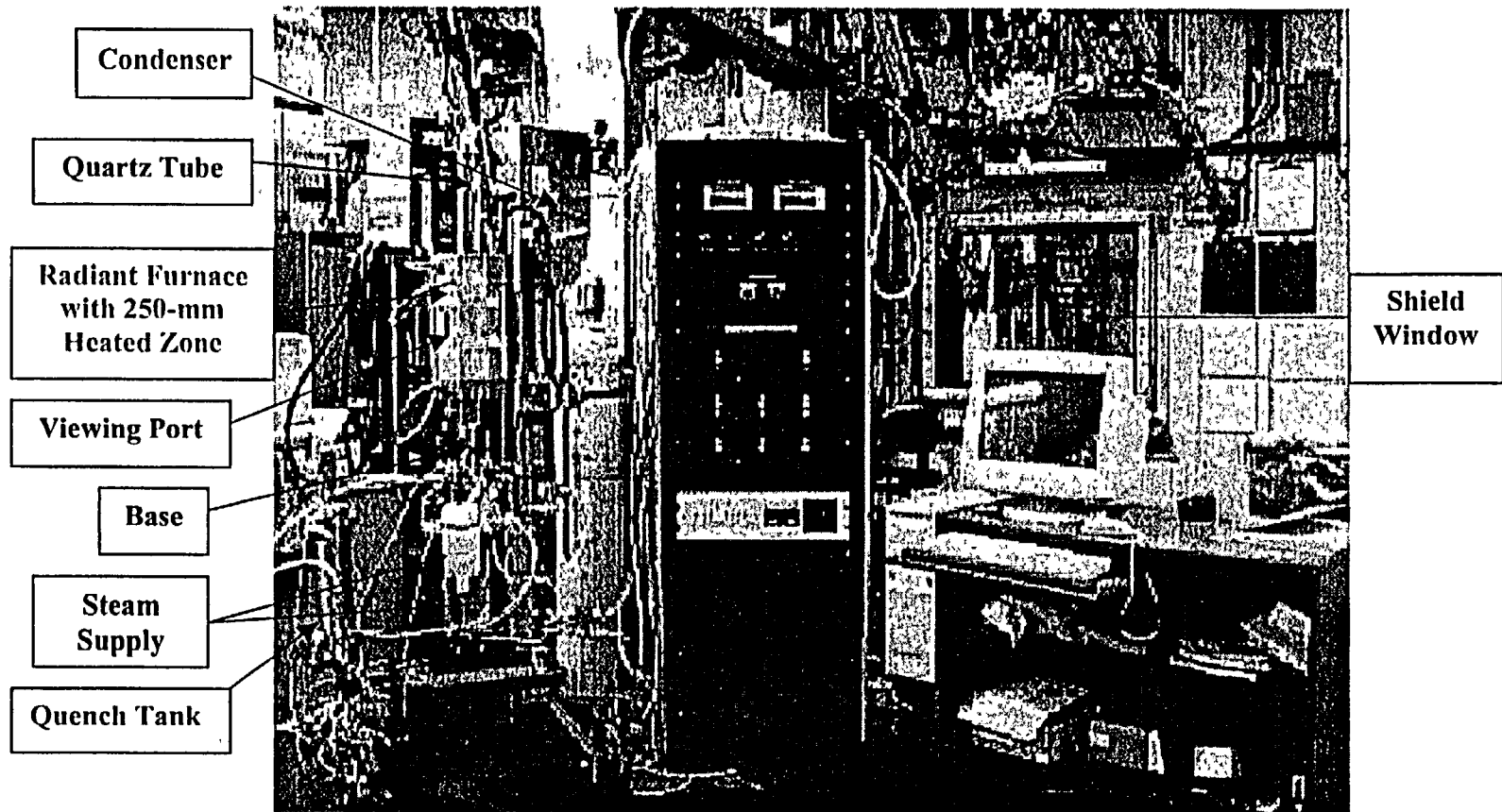


Fig. 2. Overview of the out-of-cell LOCA Integral Test Apparatus. The in-cell unit is located at Workstation 6 behind the hot-cell shield window.

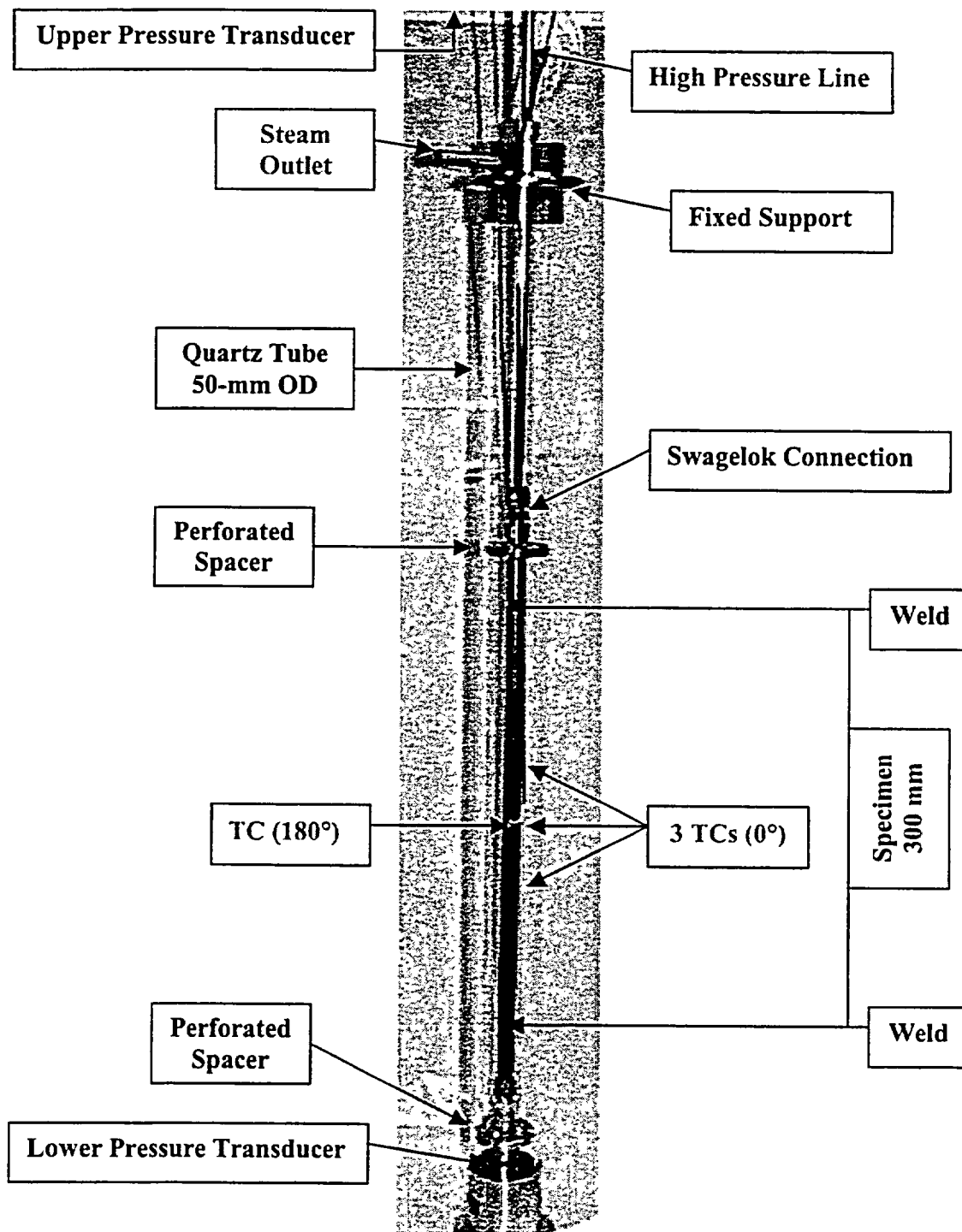


Fig. 3. LOCA Integral Test Train Assembly and Quartz Tube.

## Summary of Oxidation Kinetics Results

Test conditions, along with predicted and measured sample weight gain, have been reported in Ref. 1. For the one-sided, ANL tests conducted at sample temperatures of  $\approx 1200^{\circ}\text{C}$ , the normalized weight gains for unirradiated Zry-2 and high-burnup Limerick BWR Zry-2 are in excellent agreement. At this temperature, the in-reactor-formed oxide layer of  $\approx 10\ \mu\text{m}$  appears to be transparent to steam oxidation. The primary difference observed between the behavior of high-burnup Zry-2 and unirradiated Zry-2 is the non-uniformity of the alpha-beta interface for the steam-oxidized irradiated Zry-2 samples.

The  $1200^{\circ}\text{C}$  sample weight gains determined from the oxygen content of the measured oxide, alpha and beta layer thicknesses agree quite well with the predictions of the Cathcart-Pawel (CP) model [2]. Figure 4 summarizes the direct comparison of ANL Zry-2 weight gain data to the CP-model predictions. Cathcart and Pawel also did one-sided oxidation tests and used metallographic analysis to determine sample weight gain normalized to the outer surface area. The points labeled "Loi 6-8 Zry-2 (in cell)" are from oxidation tests (5, 10 and 20 minutes) of high-burnup Zry-2 tested in hot-cell Workstation #6. The points labeled "Lou 11-13 Zry-2 (in-cell)" are from oxidation tests of unirradiated Zry-2 conducted in the same in-cell apparatus for the same oxidation times. The other points in Fig. 4 were determined from the results of tests conducted out-of-cell. For the Zry-2 sample thickness of 0.715 mm, nominal test times at  $1204^{\circ}\text{C}$  resulted in "measured" ECR values of 8.5%, 11%, and 15% for the 5-, 10-, and 20-minute tests, respectively. As will be shown in the next section, a LOCA Integral Test with a 10-minute hold time at  $1204^{\circ}\text{C}$  results in a peak ECR of  $\approx 30\%$  due to wall thinning and double-sided oxidation in the ballooned and burst region.

Although the weight gains determined from the ANL tests are in very good agreement with the CP model prediction, the measured alpha layer thickness is considerably higher ( $\approx 40\%$ ) than predicted. Figure 5 shows that the combined oxide-plus-alpha layers measured for the in-cell Loi 6-8 and Lou 11-13 tests are  $\approx 25\%$  higher than predicted by the CP-model. It is assumed that the transport of oxygen from the beta layer to the alpha layer during the LOCA-relevant cool-down in the ANL tests results in a thickening of the oxygen-stabilized alpha layer. The cool-down rate from  $1200^{\circ}\text{C}$  to  $800^{\circ}\text{C}$  was  $\approx 5^{\circ}\text{C/s}$  in the ANL tests, whereas the CP cool-down rate was much faster. In a few tests conducted with slower cool-down rates, Cathcart and Pawel also observed alpha layers thicker than predicted by their model.

Based on a review of the extensive database for high-temperature steam oxidation of cladding alloys, it is evident that, in the temperature range of  $1100\text{-}1500^{\circ}\text{C}$ , differences in databases are more the result of differences in experimental and analytical methods than the result of different materials (Zry-2, Zry-4, ZIRLO [3], M5 and E110). Major differences in techniques are: one-sided vs. two-sided tests, internal vs. external heating, fast vs. slow heating/cooling rates, direct vs. indirect temperature measurements, and weight gain determined from sample weight change vs. weight gain determined from oxygen pickup deduced from metallographic analysis. In Fig. 6, the Baker-Just correlation [4] for Zr, the Leistikow correlation [5] for Zry-4, the Urbanic correlation [6] for Zry-4, ANL and EdF [7] data for Zry-2 (same heat), M5 data [8] and E110 data [9] are normalized to the CP-model predictions for the purpose of comparison. With the exception of the Baker-Just correlation, which clearly represents an upperbound correlation, data and correlations for the cladding alloys of interest are reasonably consistent in the temperature range of  $1100\text{-}1500^{\circ}\text{C}$ . Below  $1100^{\circ}\text{C}$ , differences in alloy composition and phase-change temperatures, as well as steam-pressure effects, become more significant with regard to steam oxidation.

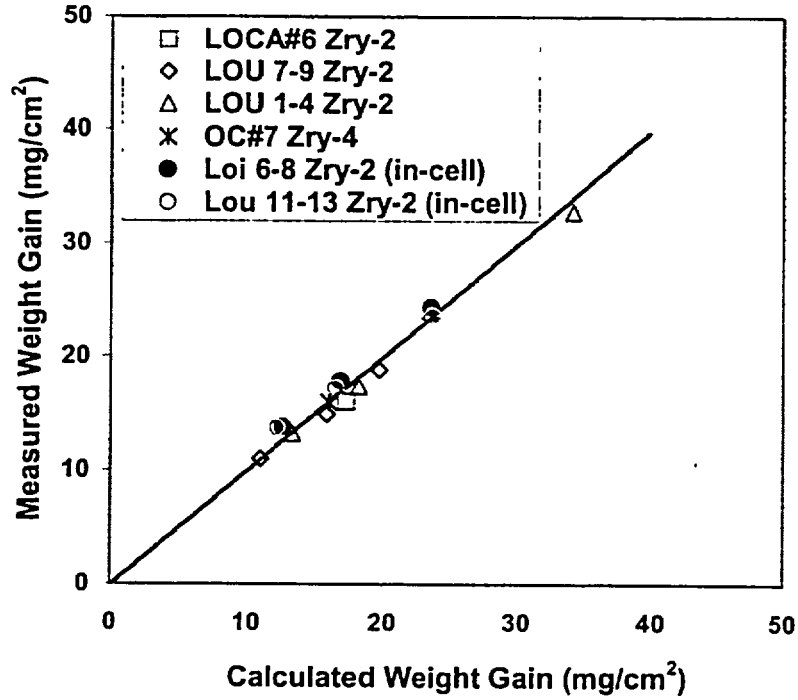


Fig. 4. Comparison between CP-model weight-gain predictions (calculated) and steam-oxidation data for Zry-2 and Zry-4 at  $\approx 1200^{\circ}\text{C}$ . Measured weight gains were determined from metallographic analysis. Loi 6-8 (irradiated) and Lou 11-13 (unirradiated) were tested in the same apparatus.

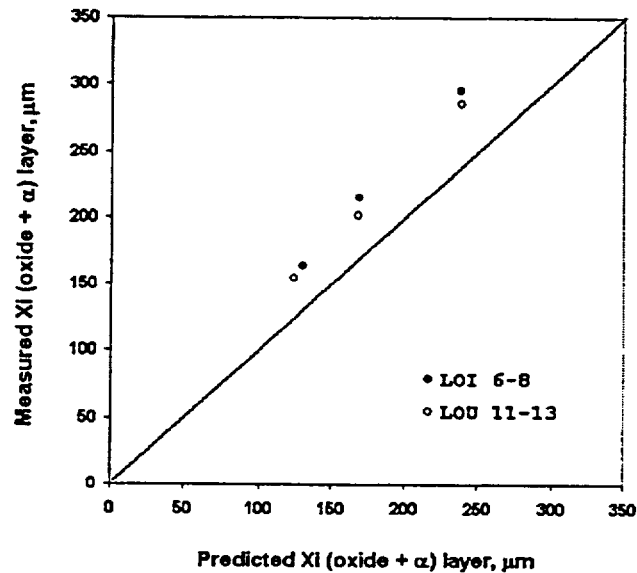


Fig. 5. Measured vs. CP-model-predicted Xi (oxide + alpha) layers after steam-oxidation tests (5, 10 and 20 minutes at  $\approx 1200^{\circ}\text{C}$ ) of irradiated (LOI 6-8) and unirradiated (LOU 11-13) Zry-2.

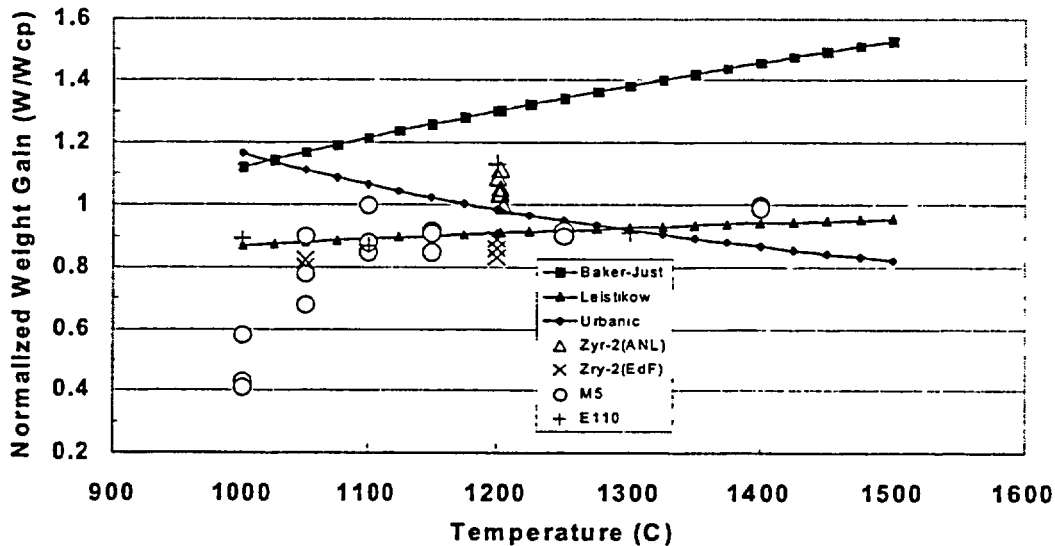


Fig. 6. Weight-gain (W) correlations for Zr (Baker-Just) and Zry-4 and data for Zry-2 (irradiated and unirradiated), M5 and E110 normalized to the Cathcart-Pawel model predictions (Wcp).

### LOCA Integral Tests: Out-of-Cell Results

During the development of the out-of-cell LOCA Integral Test Apparatus, numerous thermal benchmark tests were run to aid in the optimization of the apparatus and the test train for remote operation in the hot cell. These tests were conducted with specimens made from archival Limerick Zry-2 tubing (300-mm long, 11.2-mm OD and 0.715-mm wall) filled with dense zirconia pellets leaving a cold radial gap of  $\approx 0.1$  mm. Early designs used a bottom supported test train that resulted in specimen bowing due to compressive loads. For the quad-elliptic radiant-furnace, specimen bowing induces significant axial ( $\Delta T_z$ ) and circumferential ( $\Delta T_\theta$ ) variations in temperature. This problem was solved by supporting the test train at the top (see Fig. 3 for "hanging" test train). With the top-supported test train, the midplane  $\Delta T_\theta = \pm 15^\circ\text{C}$  (based on the readings from 4 TCs,  $90^\circ$  apart) and the axial  $\Delta T_z = \pm 15^\circ\text{C}$  within  $\pm 100$  mm of the midplane. In addition to thermal benchmarking, metallographic analysis was used to verify that the oxide layers formed in steam at  $\approx 1200^\circ\text{C}$  were consistent with oxidation kinetics test results.

Additional modifications were made based on the test results for specimens with 5-15 cm<sup>3</sup> of gas volume (7-9 MPa) above the pellet column, as well as the limitations imposed by remote in-cell operations. The last set of tests prior to in-cell testing of irradiated fuel segments was used to generate baseline data for ballooning and burst conditions and characteristics, oxygen and hydrogen pickup axial profiles and ECR axial profiles. These out-of-cell (OCL) tests were characterized by conditions relevant to the planned in-cell (ICL) LOCA Integral Tests: 300 mm cladding length, 15-mm clearance between top end-cap and pellet stack, 10 cm<sup>3</sup> of gas volume above the pellet stack (mostly in the high pressure line outside the heated zone), room-temperature gauge pressure = 8.62 MPa, stabilization at  $300^\circ\text{C}$  in Ar purge,

restabilization at 300°C in flowing steam, 5°C/s temperature ramp in saturated steam to 1204°C, 5-to-10 minute hold time at 1204°C, 3°C/s cool-down to 800°C, and ≈5 mm/s water quench initiated at 800°C. The gas volume is the minimum that can be achieved in-cell and less than the room-temperature void volume (30 cm<sup>3</sup>) measured for a full Limerick BWR rod. The pressure differential ( $P_g$ ) across the cladding wall is an upperbound for these Limerick BWR rods during a large-break BWR LOCA if the rods had achieved the full 62 GWd/MTU, as opposed to the 56 GWd/MTU for the F9 rod used to prepare the LOCA Integral Test specimens. However, the primary reason for choosing this pressure was to induce large ballooning and burst in the alpha phase ( $T < 800^\circ\text{C}$ ), so that fuel relocation – if it did occur – could be characterized. The 1204°C peak temperature was chosen to test the adequacy of the LOCA Acceptance Criteria in 10 CFR50.46.

The results of the 10-minute OCL#3 and OCL#4 tests are summarized in Table 1. OCL tests run as companion tests to the ICL tests are discussed in the next section. The only difference in test apparatus for the OCL#3 and OCL#4 was the improvement in the valve connecting the LOCA Apparatus pressure line to the line leading to the gas cylinder control valve. This tighter valve inhibited gas back flow from the LOCA line to the cylinder line in OCL#4 during heating. The OCL#3 gauge pressure ( $P_g$ ) peaked at 9.24 MPa; burst occurred at ≈760°C and ≤8.4 MPa. With OCL#4 having a more tightly sealed gas line,  $P_g$  rose from 8.62 MPa at RT to 9.66 MPa after stabilization at 300°C to a peak value of 10.27 MPa during the temperature ramp. Burst occurred at a lower temperature (≈730°C) and a higher  $P_g$  value (≤9.4 MPa). The burst location and the axial extent of ballooning were comparable for the two samples.

Although the OCL#3 sample survived quench and remained intact throughout disassembly and post-test nondestructive testing, the measured peak ECR at the center of the burst location is 29%, as compared to 33% calculated with the CP-model and 43% calculated with the Baker-Just correlation. These values are based on the circumferentially averaged wall thickness prior to oxidation and the circumferentially averaged oxygen pickup determined from metallography. Low and high magnification photographs of the cross-section at the burst location are shown in Fig. 7. Axial profiles of ECR, oxygen pickup and hydrogen pickup are shown in Fig. 8 for the OCL#3 sample. At this high ECR level, it is not surprising that OCL#4 experienced post-quench failure (see Fig. 9) in the furnace at ≈100°C under dead-weight loading (265 g).

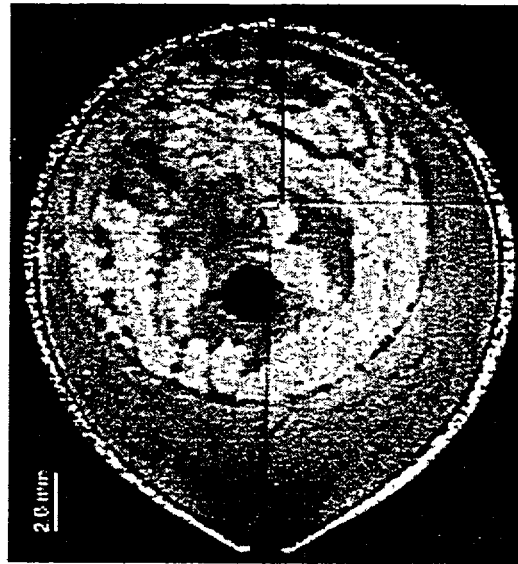
Based on the experience gained from these two tests, the hold time for the in-cell test was reduced from 10 to 5 minutes, and the procedure was changed such that the specimen would be repressurized to  $P_g \approx 8.3$  MPa at 300°C. This repressurization gives a peak  $P_g$  of ≈8.6 MPa during the temperature ramp.

Table 1 Out-of-Cell (OCL) LOCA Integral Test Results for Archival, Unirradiated Zry-2 Cladding Filled with Undersized (10-mm radial Gap at RT) Zirconia Pellets

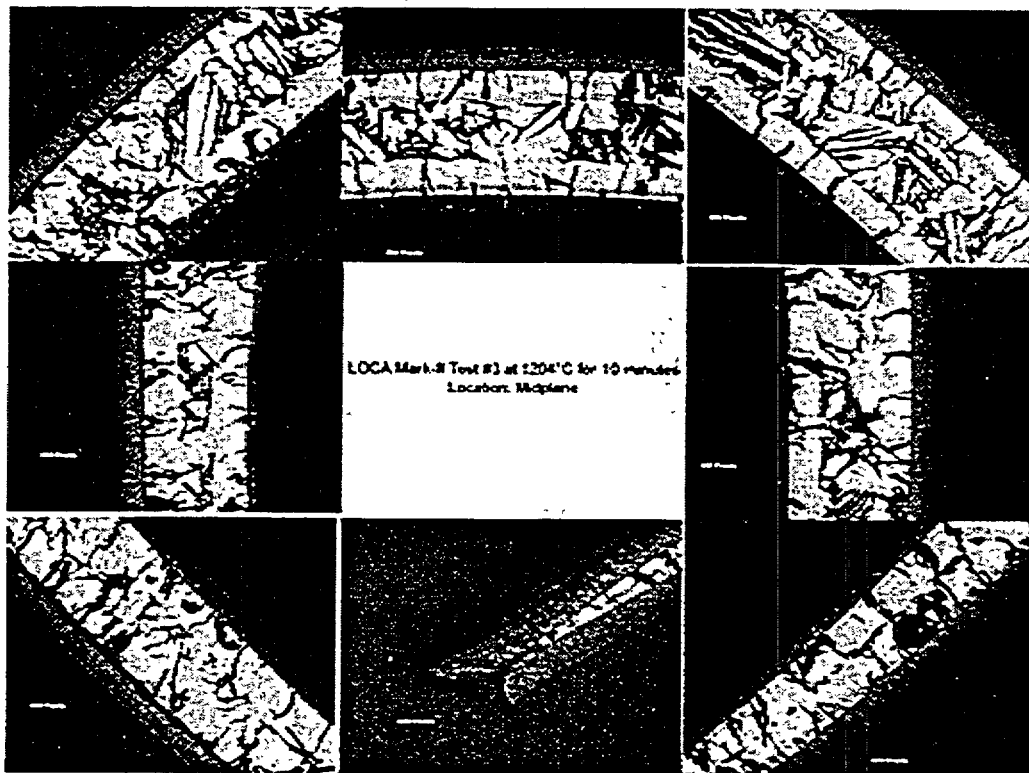
Parameter	OCL#3	OCL#4
Internal $P_g$ at RT, MPa	8.62	8.62
Internal $P_g$ at 300°C, MPa	8.97	9.66
Temperature Ramp from 300°C, °C/s	5	5
Peak Internal $P_g$ , MPa	9.24	10.28
Internal $P_g$ Just Prior to Burst, MPa	≤8.4	≤9.4
T at Burst, °C	760±10	730±10
Hold Temperature, °C	1204	1204
Hold Time, minutes	10	10
Cool-Down Rate to 800°C, °C/s	3	3
Quench Initiation Temperature, °C	800	800
Specimen Condition following Quench	Intact	Failed (see Fig. 9)
Burst Center Relative to Midplane, mm	-13	-10
Burst Shape	Dog Bone	Dog Bone
Burst Length, mm	13	---
Max. Burst Width, mm	2	---
Length of Balloon, mm	150	≈150
$(\Delta D/D_o)_{max}^a$ , %	58±5	---
$(\Delta C/C_m)_{max}^b$ , %	61	---
Reference Minimum Wall Thickness for ECR Calculation, mm	0.45	---
Maximum ECR, %		
Calculated (CP-Model)	33	---
Measured	29	---

<sup>a</sup>From profilometry at 0° and 90° relative to burst; includes outer-surface oxide

<sup>b</sup>Midwall circumferential strain determined from low-magnification photographs (see Fig. 7a)



(a)



(b)

Fig. 7. Low (a) and high (b) magnifications of OCL#3 sample cross-section at the burst location after 10 minutes in steam at  $\approx 1200^{\circ}\text{C}$ . The oxide layer in the top section of (b) is  $80\ \mu\text{m}$ .



Fig. 8a. OCL#3 test specimen after 10 minutes in steam at 1204°C, 3°C/s cool-down to 800°C and water quench initiated at 800°C.

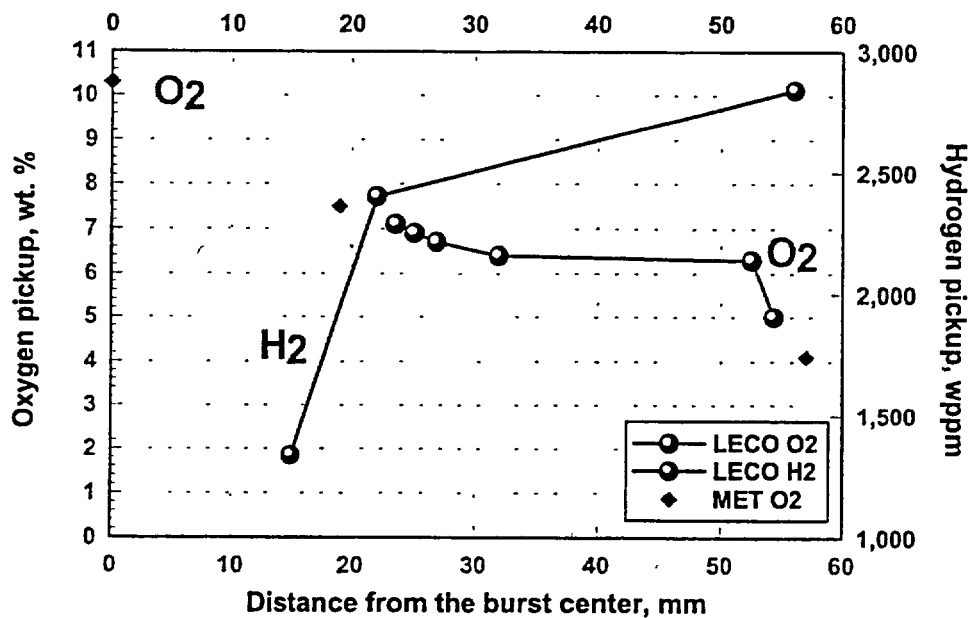


Fig. 8b. Distribution of hydrogen and oxygen pickup from the OCL#3-specimen burst center to 57 mm above the burst center. Oxygen pickup was determined from both LECO measurements and metallographic (MET) analysis of oxygen content in the oxide, alpha and beta layers.

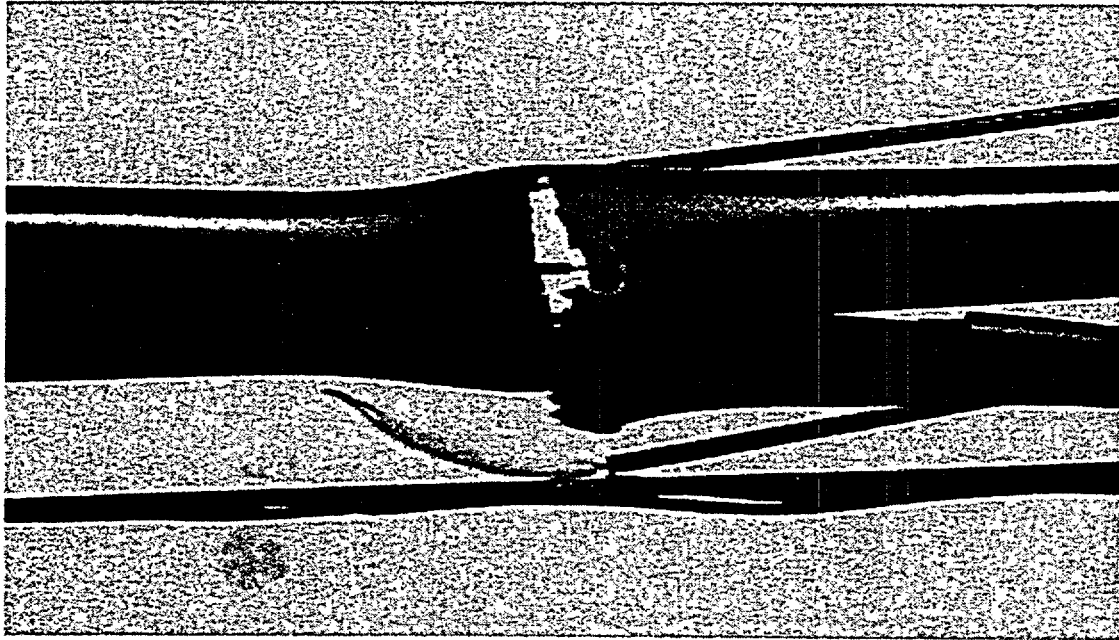


Fig. 9. OCL#4 test specimen after 10 minutes in saturated steam at 1204°C, slow-cooling to 800°C and quench water flow initiated at 800°C. Specimen failed at  $\approx$ 100°C under dead-weight loading (265 g).

### LOCA Integral Tests: In-Cell Results

#### Test Sequence

The testing sequence for the first set of in-cell LOCA Integral Tests was determined by four factors: goal of generating results that would allow direct comparisons between the responses of high-burnup fueled cladding and unirradiated specimens, LOCA Integral Apparatus components operable in-cell, auxiliary devices operable in-cell for specimen preparation and test-train assembly, and windows of opportunity for performing tests in the hot cell. Because of unresolved issues regarding the behavior of high-burnup fuel during LOCA transients, the Phase A test (ICL#1A) was designed to explore: fuel permeability at room temperature (RT) and 300°C; ballooning and burst behavior during the 5°C/s temperature ramp in slow flowing argon; and the degree of fuel relocation during ballooning and burst. The test results would also yield an unambiguous axial profile of cladding thickness prior to high-temperature steam oxidation (as defined in 10 CFR50.46 Appendix K) for calculating the maximum ECR vs. hold time at temperature for future tests. The test was performed on August 15, 2002.

The plan for the Phase B test (ICL#1B) called for ramping at 5°C/s in steam through burst to a control temperature of 1204°C, holding at 1204°C for 5 minutes, slow-cooling at 3°C/s to 800°C followed by slow furnace cooling. The test was run on September 23, 2002. During the month prior to running the test, the condenser unit was added to the In-Cell LOCA Integral Test Apparatus, as well as filters and traps to minimize the release of fuel particles and fission products to the hot-cell environment. This test

was designed to yield results on the axial profile of oxygen and hydrogen pickup. Based on the axial profile of oxide layer thickness, the cladding thickness prior to steam oxidation can be determined vs. axial location by using the Pilling-Bedworth ratio (assumed to be 1.56). The oxygen pickup determined from metallographic analysis and LECO results and the reference wall thickness determine the maximum ECR, as well as the ECR axial profile. As ballooning and burst location and characteristics are highly dependent on cladding temperature and  $\Delta T_0$ , it is important to determine the reference ECR for each test based on post-test examination. The thermal-hydraulics associated with flowing steam vs. slow flowing argon can impact the axial temperature profile and the ballooning and burst location and characteristics.

The plan for the Phase C test (ICL#1C) is identical to the Phase B test up through the slow cooling to 800°C. For the Phase C test, the quench water flow will be initiated at 800°C to determine the quench-resistance of high-burnup BWR fuel. It is expected that the oxide, alpha and prior-beta layers and oxygen contents will be essentially the same for the Phase B and Phase C specimens, but that the hydride precipitates may be different following quench. The distribution and morphology of these hydrides are important factors in determining the post-quench ductility of the high-burnup cladding. The Phase C test will be conducted after the quench system and the Test Train Assembly Apparatus are operable in-cell.

#### Specimen Preparation and Test Train Assembly

As the behavior of high-burnup fuel during a LOCA sequence may have a significant effect on ballooning, burst, fuel and/or fission product emission during burst, and fuel relocation, it is important that the fuel column not be disturbed during specimen preparation, test train assembly, transport, and loading into the LOCA Test Apparatus. Two 150-mm-long samples were cut from the upper end of Grid Span 6 and the lower end of Grid Span 7 of Limerick Rod F9 to demonstrate the remote in-cell fuel removal and end-cap welding, as well as to verify that the fuel column would not be disturbed by these processes. Cross-sections were examined by optical metallography at axial locations of  $\approx 20$  mm and  $\approx 60$  mm from the end of a drilled fuel column. Macro- and micro-cracking patterns, as well as the nature of the fuel-cladding bond, are consistent with results presented by Tsai and Billone [10] for cross-sections of Limerick F9 fuel that had not been subjected to fuel removal and end-cap welding. Thus, the integrity of the fuel column in the LOCA specimens is not compromised by the preparation techniques.

The axial locations from which the ICL#1A and ICL#1B samples were cut correspond to the middle of Rod F9 Grid Spans 6 and 5, respectively. Detailed fuel characterization at an axial location between the specimens is given by Tsai and Billone [10]. The fuel appears to be tightly bonded to the cladding. However, there also appears to be sufficient void space in the macro- and micro-cracks, as well as the separations at pellet-pellet interfaces near the cladding wall, to enhance gas flow through the fuel column. The results of the LOCA Integral Tests will resolve whether or not the resistance to gas flow is low enough to allow rapid flow of gas from the plenum region of a fuel rod to the potential ballooning and burst location.

### Results of 1<sup>st</sup> In-Cell LOCA Integral Test: Phase A (ICL#1A)

The ICL#1A test train was assembled in-cell in the simplified test train assembly. Two Type S thermocouples (TCs), 180° apart, were strapped to the specimen with the TC tips ≈50 mm above the specimen midplane. After assembly, the test train with the quartz tube was positioned in the In-Cell LOCA Integral Test Apparatus furnace and final connections, including the electrical connection for the lower pressure transducer, were made. During this stage, the lower pressure transducer failed. However, it was decided to proceed with the test because enough fuel-permeability information could be obtained from the upper pressure transducer reading, the ballooning and burst characteristics, the depressurization rate following burst, and the comparison of results with out-of-cell companion tests OCL#5 and OCL#8, which were run under the same experimental conditions.

As part of the operating procedure for the OCL#1A test, the system was pressurized at room temperature (RT) with He in stages to 10 MPa. The upper pressure transducer was calibrated to a mechanical pressure gauge during this increase. The pressure remained steady during the hold times at the intermediate pressures. The system was depressurized, heated to 300°C and stabilized before repressurizing to  $P_g = 8.28$  MPa. During the 15-minute stabilization phase,  $P_g$  increased to 8.56 MPa due to heating of a small portion of the gas within the specimen and the 15-mm-long plenum at the top of the specimen. The cladding control temperature (T) was then ramped at 5°C/s until burst was achieved, followed by slow furnace cooling. Based on the thermocouple readings (741°C and 768°C) ≈40 mm above the burst center, the circumferentially averaged burst temperature ( $T_B$ ) is estimated to be  $\geq 755^\circ\text{C}$ . The "≥" sign implies that  $T_B$  at 10 mm above the specimen midplane may be greater than the T measured 50 mm above midplane. Histories for  $P_g$  and T during the ramp are shown in Fig. 10.  $P_g$  increased to a maximum of 8.96 MPa during heating and decreased to 8.61 MPa just before burst. The change in  $P_g$  prior to burst is determined by the competing effects of the heating of gas that flows to the ballooned region and the increase in volume due to ballooning.  $P_g$  dropped from 8.61 MPa to 4 MPa in 0.2 s. As the data frequency was only 5 Hz, no intermediate  $P_g$  value was recorded. Thus, the burst pressure ( $P_B$ ) is assumed to be  $\leq 8.61$  MPa. The  $P_g$  history for ICL#1A is compared to that for companion test OCL#5 in Fig. 10. The results are very similar down to 4 MPa. The  $P_g$  decrease from 4 MPa to 0 is very fast for the OCL#5 specimen, whereas the presence of the fuel in the ICL#1A specimen slows down the gas release in this regime. In general, the results indicate that high-burnup BWR fuel has high enough permeability for gas flow to sustain the growth of the balloon through the burst phase.

Nondestructive results are shown in Figs. 11-12 for the ICL#1A and OCL#5 test specimens. Results for these tests, as well as companion test OCL#8, are summarized in Table 2. All three tests were ramped to burst in slow-flowing argon. With the exception of the oval burst shape and the shorter axial extent of ballooning for the ICL#1A specimen, the high-burnup test specimen behavior is remarkably similar to that of the OCL#5 unirradiated test specimen. With regard to ballooning strain, the difference between the two out-of-cell specimens (OCL#5 vs. OCL#8) is greater than the difference between the ICL#1A and OCL#5 specimens. The maximum burst width for the ICL#1A specimen is ≈3 mm. Fuel particles larger and smaller than 3-mm × 3-mm cross-section are evident in the burst region (Fig. 11). The particle sizes are consistent with the size of reported macro-crack sizes [10]. Although some fine particles may have been emitted during burst, no attempt was made to collect these particles. However, during post-test transport and handling, the specimen was rotated from the vertical to the horizontal position, as well as rotated about its axis. The fuel particles that fell onto the quartz tube were collected and weighed. The measured 5.2 g of fuel particles (≈25% of a pellet) represents a lower bound on the sum of the fuel emitted during the test and the fuel fallout during post-test transport and handling.

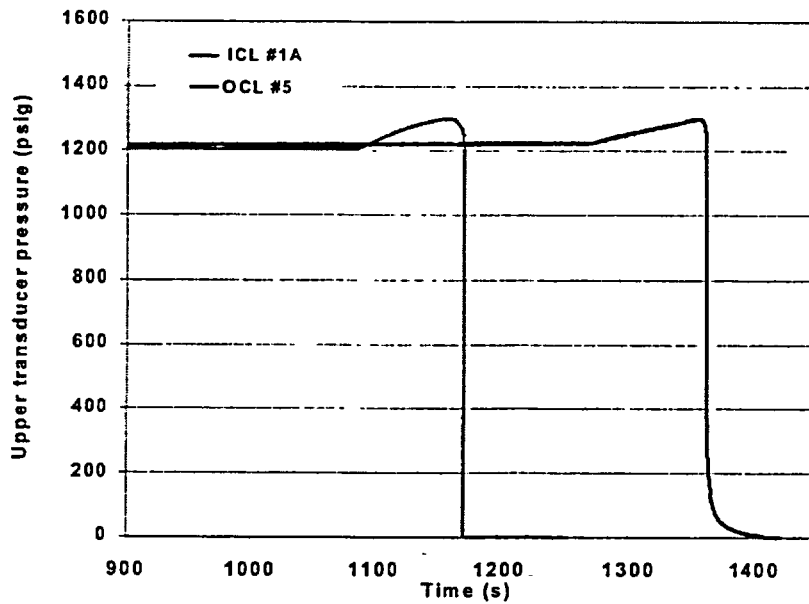
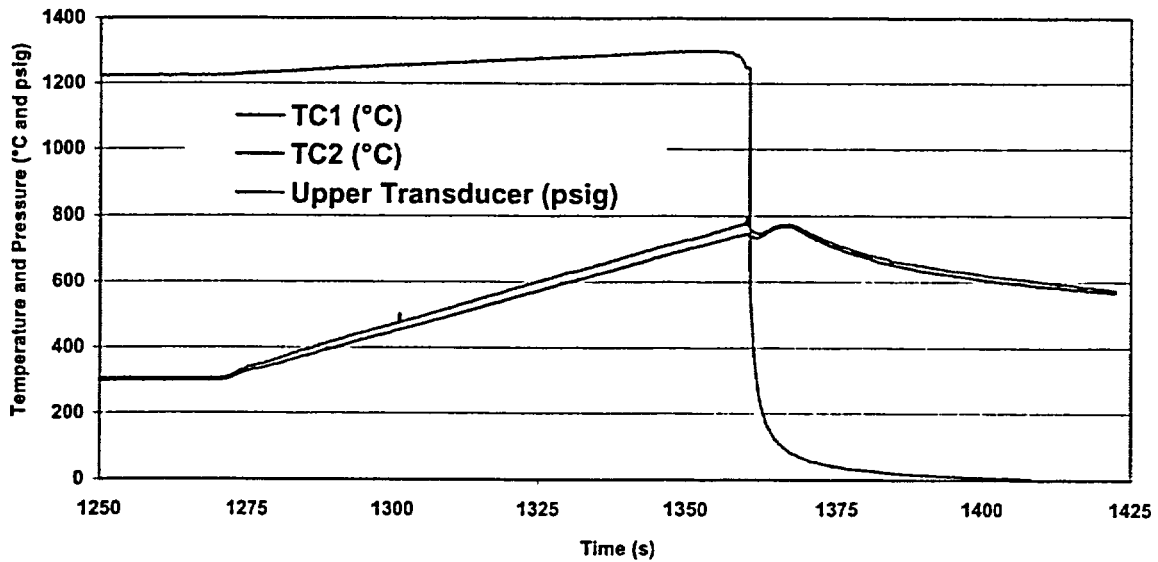


Fig. 10. Pressure and temperature histories for the Phase A 1<sup>st</sup> LOCA Integral Test (ICL #1A) compared to pressure history for companion out-of-cell test OCL #5. The OCL#5 specimen had a room-temperature radial gap of  $\approx 0.1$  mm.

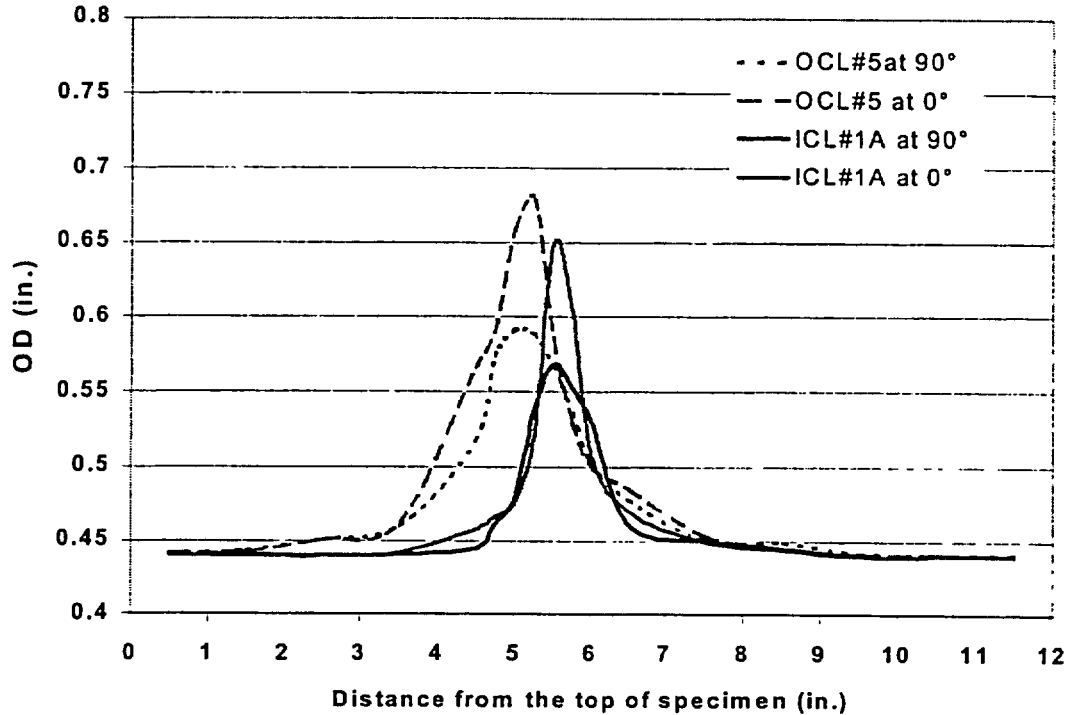
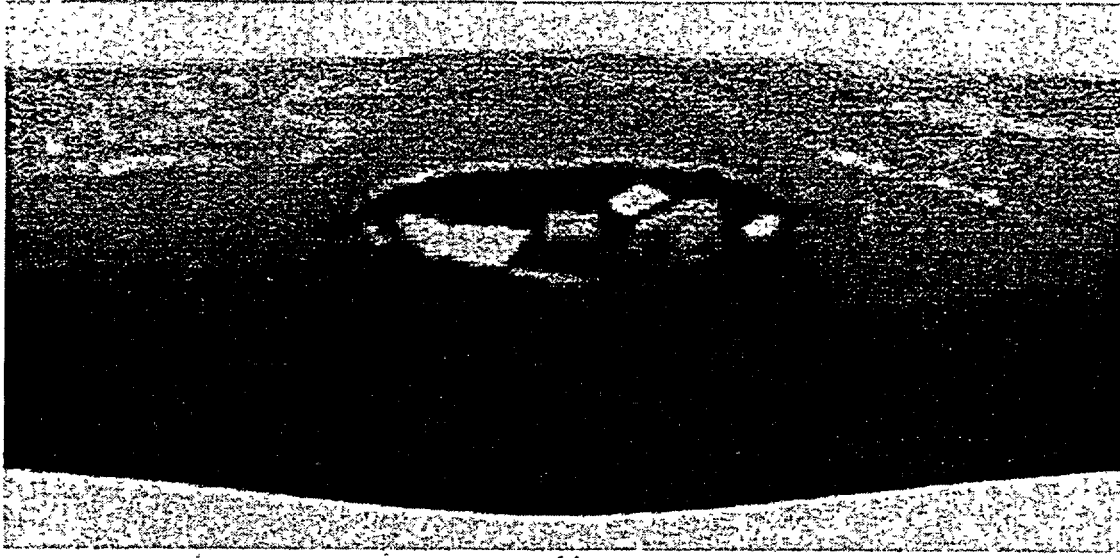


Fig. 11. Profilometry traces for specimen outer diameter (OD) after the In-Cell LOCA Integral Test ICL#1A and companion out-of-cell LOCA Integral Test OCL#5. Angular orientation is relative to the circumferential location of the burst opening.

Although the fuel rods are in a vertical position during LOCA, thermal-hydraulic phenomena induce significant vibration of these rods. Depending on the size of the balloon and burst opening, the potential exists for fuel to fall out of the burst opening. The amount of fuel that might be emitted would have an insignificant effect on coolability. However, the effect of fuel fallout might have a significant effect on decay heat and cladding temperature reduction in the ballooned region.

In addition to the fuel particle behavior, the high-burnup test resulted in a dark film-like deposit on the quartz tube opposite the burst opening and covering an area of  $>90^\circ$  circumferentially and  $\approx 50$  mm axially. It is likely that this deposit contains volatile fission products (e.g., Cs) and perhaps some fine fuel particles. The deposit became lighter over time and has all but disappeared since August 15<sup>th</sup>. Figure 13 shows the dark deposit a week after the test was run and some of the fuel particles that fell out of the burst area and settled on the quartz tube while the test train was rotated in the horizontal position. Additional handling since that time has resulted in more fuel fallout.



(a)



(b)

Fig. 12. Comparison of burst openings for (a) In-Cell LOCA Integral Test ICL#1A specimen from high-burnup Limerick BWR Rod F9 and (b) out-of-cell companion test OCL#5 specimen from archival Zry-2 cladding. Burst lengths are both  $\approx 13$ -mm long.

Table 2 Comparison of Results from In-Cell Phase A (ICL#1A) and Phase B (ICL#1B) LOCA Integral Tests with High-Burnup Limerick BWR Fueled Specimens and of Results from Companion Out-of-Cell Tests OCL#5, OCL#8 and OCL#11 with Archival Unirradiated Zry-2 Specimens Filled with Zirconia Pellets. ICL#1A, OCL#5 and OCL#8 are ramp-to-burst tests in slow-flowing argon. ICL#1B and OCL#11 are ramped to 1204°C in steam, held for 5 minutes at 1204°C, cooled at 3°C/s to 800°C and slow-furnace-cooled to room temperature.

Parameter	ICL#1A	OCL#5	OCL#8	ICL#1B	OCL#11
Environment	Argon	Argon	Argon	Steam	Steam
Hold Temperature, °C	---	---	---	1204	1204
Hold Time, minutes	---	---	---	5	5
$(P_g)_{max}$ , MPa	8.96	8.96	8.62	8.87	8.61
T at $(P_g)_{max}$ , °C	733	660	687	728	680
Burst Pressure ( $P_B$ ), °C	≤8.61	≤8.26	≤7.67	≤8.01	≤7.93
Burst Temperature ( $T_B$ ), °C	≥755	733±5	766±17	≥750	753±22
Burst Center Relative to Specimen Midplane, mm	+10	+20	-10	+25	+35
Burst Shape	Oval	Dog Bone	Dog Bone	Oval	Dog Bone
Burst Length, mm	13	13	17	14	11
Max. Burst Width, mm	3	2.5	2.5	3.5	1
Length of Balloon, mm	70	100	140	90	140
$(\Delta D/D_o)_{max}^a$ , %	38±9	44±10	60±10	39±10	43±10
$(\Delta C/C_m)_{max}^b$ , %	TBD	TBD	60	TBD	TBD
Reference Minimum Wall Thickness for ECR, mm	≈0.518 (TBD)	≈0.497 (TBD)	0.434	≈0.514 (TBD)	≈0.500 (TBD)
Maximum ECR, %					
Calculated	0	0	0	≈20	≈21
Measured	0	0	0	TBD	TBD

<sup>a</sup>From profilometry at 0° and 90° relative to burst

<sup>b</sup>Midwall circumferential strain determined from low-magnification photomicrographs



Fig. 13. Dark deposit (left) on quartz tube and fuel particles (right) that fell out of the burst opening during post-test transport and handling for the ICL#1A sample. Quartz tube diameter is 50 mm.

Results of 1<sup>st</sup> In-Cell LOCA Integral Test: Phase B (ICL#1B)

For the Phase B LOCA Integral Test, both the upper and lower pressure transducers were operable. They were calibrated to a manual pressure gauge during the staged pressurization process at RT. Because of the flow resistance of the 270-mm-long fuel column, the lower pressure transducer lagged the upper transducer by  $\leq 0.5$  MPa from 0-4 s up to  $P_g \approx 1$  MPa. From 1.0 to 8.6 MPa, the lower and upper pressure readings tracked very well. The system was depressurized by opening the valve between the gas cylinder control valve and the LOCA pressure line. During depressurization (Fig. 14), both pressure transducer values decreased rapidly down to  $\approx 2$  MPa. For upper transducer readings of 2 MPa to 0 MPa, the lower pressure transducer values decreased more slowly, with a maximum differential of 0.6 MPa.

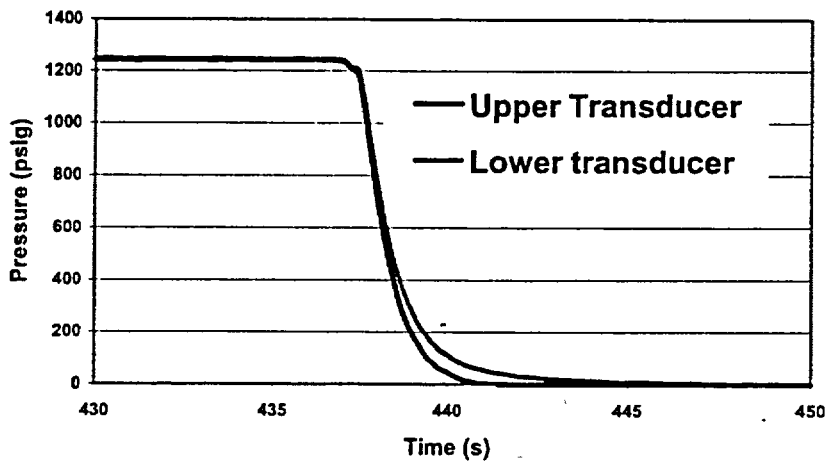


Fig. 14. Upper and lower pressure transducer histories for ICL#1B sample during RT depressurization.

The ICL#1B specimen was stabilized at 300°C in slow flowing argon before repressurization to ≈8.0 MPa. During the early stages of the pressurization (0-2 MPa), the lower transducer lagged the upper transducer by <1 MPa during the initial 0-4 s. There was excellent gas communication during the staged rise from 2 to 8 MPa. During the hold time at 300°C, the pressure rose to 8.4 MPa. Steam flow was initiated and stabilized. The response of the lower pressure transducer during pressurization is marginally slower at 300°C than at RT, but sufficiently rapid that fuel resistance to gas flow is not likely to affect ballooning and burst during the temperature ramp. Also, during the ramp, the cladding plastically deforms away from the fuel, thereby providing more flow area and even less resistance. The responses of the pressure transducers at 300°C are compared in Fig. 15.

Relative to the fuel column, the high-pressure line (890-mm-long with 7.3-mm<sup>2</sup> cross-sectional area) provides negligible resistance to gas flow. The resistance is proportional to the ratio of length (L) to flow area (A). For the gas line  $L/A = 122 \text{ m}^{-1}$ . Thus, for the 270-mm high-burnup fuel column,  $A < 2 \text{ mm}^2$ .

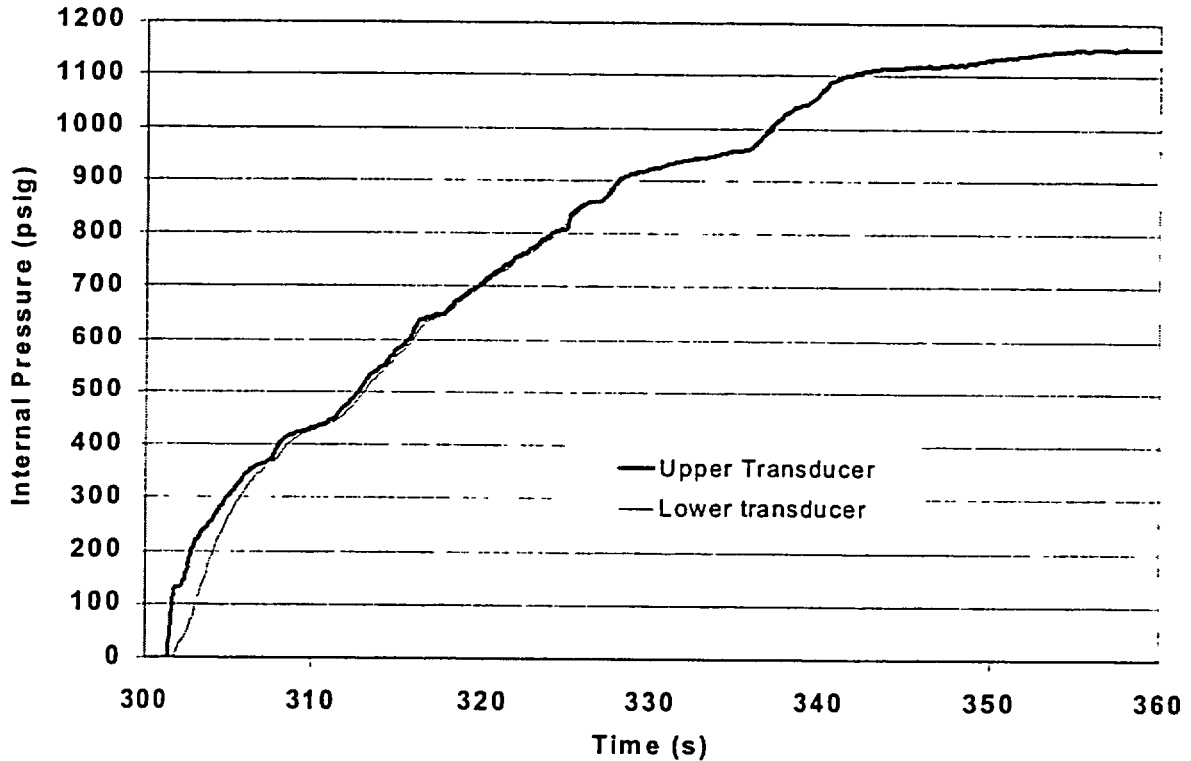


Fig. 15. Responses of the pressure transducers above (upper) and below (lower) the 270-mm-long fuel column during pressurization of the line above the 300°C ICL#1B test specimen. The upper transducer is ≈430 mm above the fuel column; the lower transducer is just below the column. The pressurization line is ≈890-mm-long with a cross-sectional flow area of 7.3 mm<sup>2</sup>.

During the ICL#1B temperature ramp,  $P_g$  peaked at 8.87 MPa ( $T = 728^\circ\text{C}$ ) and burst occurred at  $T \geq 750^\circ\text{C}$  and  $P_g \leq 8$  MPa. Figure 16 shows the  $P_g$  and  $T$  histories during the ramp for the upper pressure transducer and the control TC (36 mm above burst center), respectively. The pressure decrease following burst is also comparable to the ICL#1A test results with a rapid pressure decrease down to  $\approx 3$  MPa, followed by a slow decrease to  $P_g = 0$ . The lower pressure transducer output is not shown in Fig. 16 because it became unreliable after steam was introduced and the temperature was ramped. This transducer goes out of calibration as it heats up, whereas the upper transducer is far enough away from the heated zone to remain cool. Also, the second TC located  $180^\circ$  from the control TC gave unreliably high readings and may have been damaged during assembly.

The ICL#1B specimen burst characteristics are illustrated in Fig. 17 and compared to the results of the out-of-cell companion test (OCL#11) specimen. The results are summarized in Table 2. Cladding outer-diameter strains in the burst region are comparable. As with tests ICL#1A vs. OCL#5, the burst shape for ICL#1B (oval) is significantly different from that of the OCL#11 specimen (dog bone). The ICL#1B specimen has less fuel in the burst region than observed in the ICL#1A specimen (Fig. 12a). The profilometry results for the ICL#1B specimen are given in Fig. 18. A side view of the ICL#1B specimen is shown in Fig. 19. The peak ballooning strain for ICL#1B specimen is comparable to that of ICL#1A and slightly smaller than that for OCL#5 and OCL#11 specimens. Also, the axial extent of ballooning is less for the irradiated specimens.

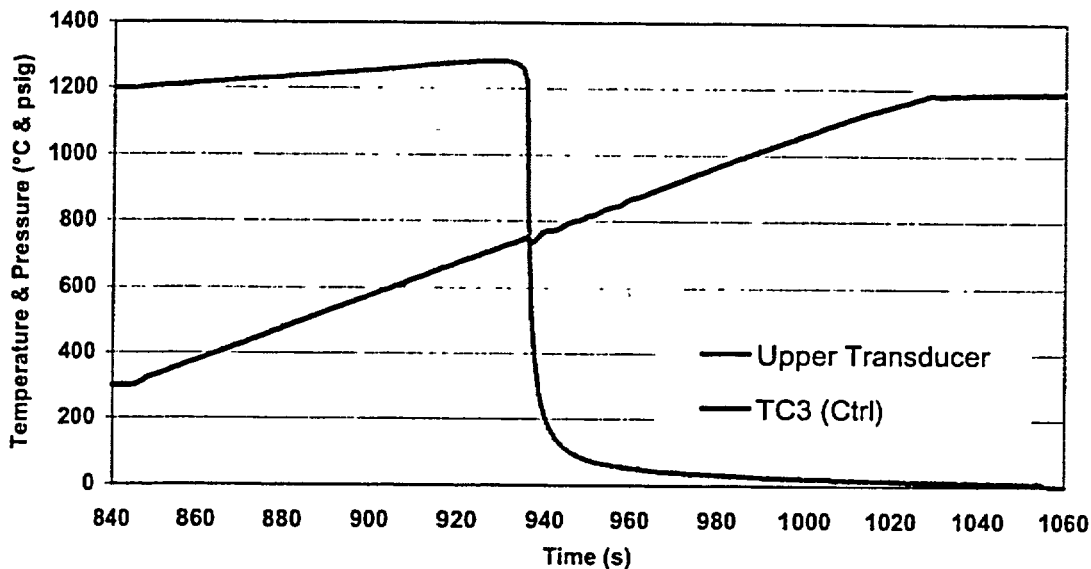
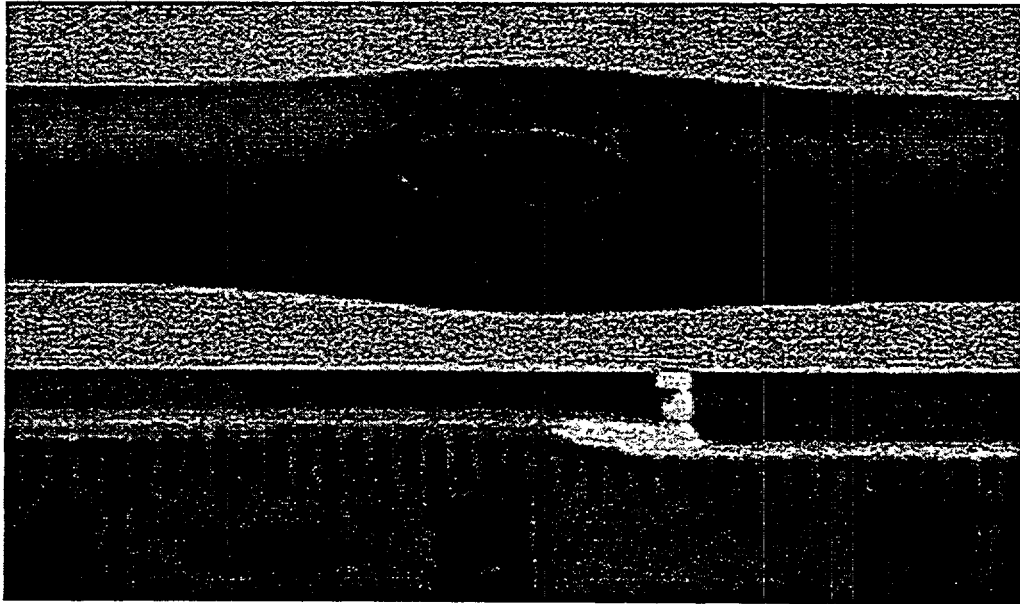
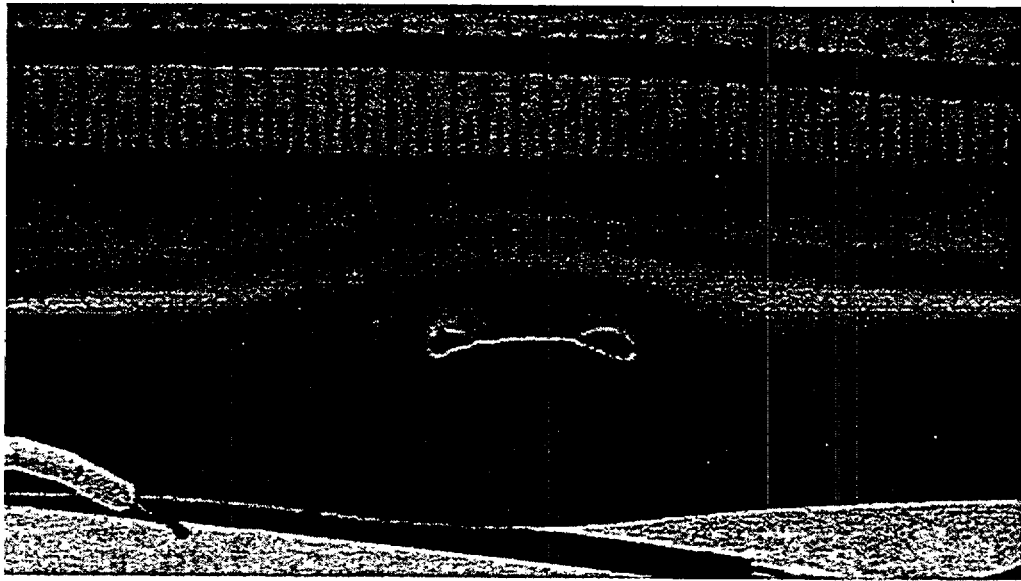


Fig. 16. Temperature and pressure histories during ramp for high-burnup BWR LOCA Integral Test #1: Phase B (ICL#1B).



(a)



(b)

Fig. 17. Comparison of burst openings for (a) high-burnup BWR ICL#1B specimen; and (b) unirradiated Zry-2 sample after 5 minutes in saturated steam at 1204°C.

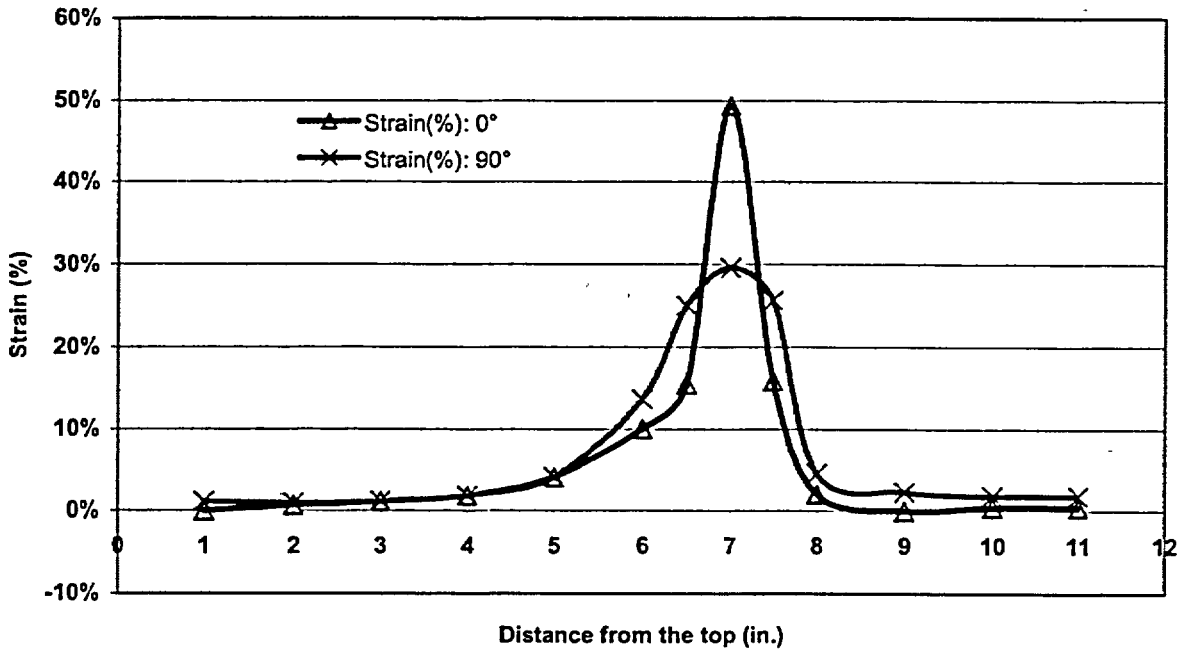


Fig. 18. Cladding outer-diameter strain for high-burnup BWR ICL#1B specimen following 5 minutes in saturated steam at 1204°C. Orientation is relative to burst opening.

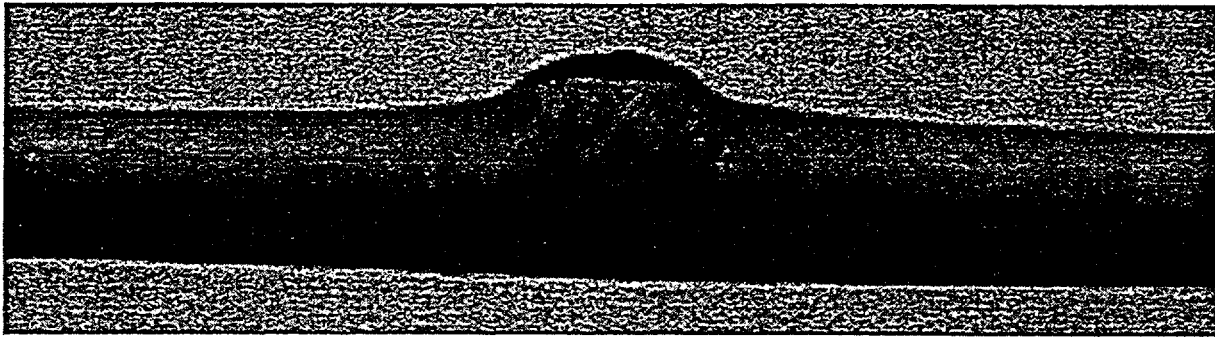


Fig. 19. Side view of the high-burnup BWR ICL#1B specimen after 5 minutes in steam at 1204°C.

## Discussion

A series of out-of-cell LOCA Integral Tests (OCL) have been conducted using archival, unirradiated Limerick BWR Zry-2 cladding filled with undersized (0.1-mm radial gap) zirconia pellets and internally pressurized to 8.3-8.6 MPa (gauge). Peak pressures during the temperature ramp (5°C/s) ranged from 8.6-10.3 MPa. With these internal pressures, burst occurred in the alpha phase at 750±20°C. A few of these tests were ramped to burst in argon and stopped in order to obtain a clear picture of ballooning and burst characteristics. Most tests were ramped to 1204°C in steam, held for 5-10 minutes, slow-cooled at 3°C/s to 800°C and water quenched at 800°C. Based on detailed metallographic analyses, oxygen determination (LECO) and hydrogen determination (LECO), tests conducted for 10 minutes in steam result in high enough oxygen pickup to give a "measured" maximum ECR ≈ 30% (vs. 33% calculated using the Cathcart-Pawel model and 43% calculated using the Baker-Just correlation). Although the oxidation kinetics is the same for these tests, the ECR varies with the reference wall thickness determined after ballooning and burst and prior to steam oxidation. This reference wall thickness decreases with the as the ballooning circumferential strain (≤50±10%) increases. Based on the results of the OCL#4 test (Fig. 9), which failed in the furnace shortly after quench, the 10-minute hold time at 1204°C embrittles the cladding such that it barely survives the water quench. Test results are summarized in Table 1. It was also confirmed that the unirradiated cladding picks up significant hydrogen (1200-3000 wppm) generated from the oxidation of the cladding inner surface. This region of enhanced hydrogen pickup extends at least 60 mm beyond the burst center. Based on the results of the 10-minute tests, the first series of In-Cell LOCA Integral Tests (ICL) were designed for a 5-minute hold time in steam at 1204°C to give a maximum ECR ≈ 20%.

Two in-cell tests (ICL#1A and ICL#1B) with specimens prepared from 56-GWd/MTU Limerick BWR Rod F9 have been conducted, along with several companion tests. Test ICL#1A was designed to reveal information about high-burnup fuel permeability (at room temperature and 300°C), ballooning strain and axial extent and burst characteristics. The specimen was internally pressurized to 8.62 MPa (gauge) at room temperature (RT) and depressurized. The specimen was stabilized at 300°C, repressurized to 8.28 MPa (gauge) and ramped to burst. A similar initial procedure was used for test ICL#1B. However, this sample was ramped through burst in steam to 1204°C, held at 1204°C for 5 minutes, slow-cooled at 3°C/s to 800°C and then furnace-cooled to RT. A 3<sup>rd</sup> test (ICL#1C) is planned to follow the ICL#1B history up to the point of the cool-down to 800°C, at which point water-quench flow will be initiated.

The results from the ICL#1A and ICL#1B tests indicate that high-burnup BWR fuel has adequate permeability to initiate and sustain ballooning and to generate a significant burst opening. Burst occurs at about the same temperature (≈750°C) and pressure (≈8 MPa gauge) as for the OCL unirradiated Zry-2 specimens. Peak outer-surface diametral strains (≈40%) are somewhat less, but comparable, to those measured (40-60%) for OCL cladding specimens. Burst lengths and maximum openings are also comparable. The major differences observed in the data obtained to date for high-burnup BWR specimens exposed to the LOCA Integral Test sequence are:

Pressurization: The pressure increase at the bottom of the 270-mm-long fuel column lags the pressure at the top of fuel column by ≤1 MPa for ≤4 s. The pressure transducers equilibrate at higher pressures, indicating very good fuel permeability for the high-burnup fuel at RT and 300°C.

- Depressurization:** Depressurization following valve opening and/or burst is as rapid for high-burnup fuel as for the unirradiated specimens down to  $\approx 4$  MPa. Below that, the depressurization rate for the high-burnup specimens is much slower.
- Ballooning:** The axial extent (region over which  $\Delta D/D_o > 2\%$ ) of ballooning (70-90 mm) is less than for unirradiated specimens (100-140 mm).
- Burst Shape:** The high-burnup cladding burst opening is oval in shape, as compared to the dog-bone shape observed for unirradiated Zry-2 cladding specimens.
- Fuel Behavior:** For the high-burnup specimens, volatile fission products and/or fine fuel particles form a dark deposit on the quartz tube following burst. It is anticipated that this film contains cesium compounds, but this needs to be verified through gamma scanning. The dark deposit, initially covering axial and circumferential dimensions of  $>50$  mm and  $>90^\circ$ , respectively, fades with time. Some fuel particles ( $<1$  g) are blown through the burst opening following burst. There is significant fuel fallout ( $>4$  g) during test train transport, handling and post-test examinations. The amount collected to date represents less than one BWR pellet ( $\approx 7$  g). The particles have a maximum effective diameter  $<3$  mm, based on the burst opening. This particle size is consistent with the size of fuel macro-cracks observed from metallography of the Limerick BWR fuel cross-section at several axial locations.

It is anticipated that high-burnup fuel cladding may experience less inner-surface oxidation and hydrogen pickup than measured for unirradiated specimens. Detailed metallographic and oxygen-determinator analyses will be performed on the ICL#1B cladding within the axial region between the burst center and 60 mm above the burst center. The results will be compared to those for out-of-cell companion test OCL#11. Based on previous OCL test results, significant double-sided oxidation is observed throughout the ballooned region, peaking at the center of the burst and decreasing towards the neck of the balloon. This profile is opposite to the profile observed for hydrogen pickup.

A significant goal of the current research is to determine the adequacy of the ECCS acceptance criteria for high-burnup fuel in terms of protecting fuel rods from fragmentation both during quench and following quench (i.e., ensuring post-quench ductility). Following water quench (Test ICL#1C), the high-burnup samples will be exposed to four-point bend tests to determine the failure bending moment, the failure mode and the degree of cladding fragmentations vs. ECR and hydrogen content. Previous experience with post-quench LOCA Integral Test specimens from the out-of-cell tests indicates that failure will occur within the burst region at fairly low bending moments. The bending failures for post-quench unirradiated specimens are similar to the failure shown in Fig 9. The failure mode is mixed in that the material is brittle near the burst opening and becomes more ductile approaching  $180^\circ$  from the burst opening. The failure appears to be confined in axial extent to the burst-opening region. It will be interesting to determine the failure mode for post-quench high-burnup specimens vs. ECR and hydrogen content.

As the high-burnup BWR cladding has a thin oxide layer and low hydrogen content, the primary focus of the BWR LOCA Integral testing is the effects of high-burn-up fuel on cladding response during and following the LOCA sequence. Following the BWR tests, high-burnup PWR specimens, with thicker (50-100  $\mu\text{m}$ ) oxide layers and higher (400-800 wppm) hydrogen contents, will be tested to determine their effects on cladding oxidation and response to quench and post-quench loading.

## Conclusions and Future Work

Steam oxidation tests have been completed for unirradiated (archival) and high-burnup (56 GWd/MTU) BWR cladding samples at 1200, 1100 and 1000°C. For the 1200°C samples, which have been analyzed in detail, the weight gain determined from oxygen concentrations in the oxide, alpha and beta layers is in excellent agreement with the Cathcart-Pawel model predictions. The in-reactor-formed oxide layer ( $\approx 10$   $\mu\text{m}$ ) on the high-burnup cladding appears to be nonprotective for high-temperature steam. The primary difference observed is the highly non-uniform alpha-beta interface seen in high-burnup Zircaloy-2. Comparison of the ANL data with data and correlations for Zircaloy-4 and data for Zr-1Nb and Zr-1Sn-1Nb alloys indicates essentially the same weight-gain kinetics for all cladding alloys at 1100-1500°C.

Two In-Cell LOCA Integral Tests have been completed using high-burnup BWR fueled samples from Limerick Rod F9. The Phase A test focused on fuel and cladding behavior during a 5°C/s temperature ramp-to-burst without steam oxidation. The Phase B test was ramped in steam through burst to 1204°C, held for 5 minutes at 1204°C and slow-cooled to provide data on oxygen and hydrogen pickup for high burnup fuel. Based on the Cathcart-Pawel-predicted oxygen pickup and the calculated wall thinning for this test, the estimated maximum ECR is  $\approx 20\%$ . The permeability of high-burnup fuel, as well as the plastic expansion of the cladding away from the fuel, is sufficient to sustain ballooning out to a maximum circumferential strain of  $\approx 40\%$  and to induce burst at  $\approx 750^\circ\text{C}$  and  $\approx 8.3$  MPa internal pressure. These values are consistent with those obtained from companion out-of-cell tests using unirradiated Zircaloy-2 specimens. Significant differences in the behavior of high-burnup test specimens are: axial extent of the ballooned region ( $\approx 80$  mm vs.  $\approx 125$  mm for unirradiated Zry-2), burst-opening shape (oval vs. dog bone for unirradiated Zry-2), ejection of volatile fission products and/or fuel fines that form a dark film on the quartz tube surrounding the specimen (as compared to no dark film from the dense zirconia pellets in the out-of-cell tests), emission of  $<1$  g of fuel particles from the burst opening following burst, and fuel fallout ( $\approx 4$  g) during post-test transport, handling and nondestructive testing.

In future work, the Phase C test will be conducted with quench-water flow initiated at 800°C following 3°C/s cool-down from 1204°C to 800°C. Fuel particles released during the test will be quantified. Also, the isotopic composition of the dark deposit on the quartz tube will be investigated by gamma spectroscopy. Post-quench ductility tests (4-point-bend and ring-compression) will be conducted on this sample if it survives quench without fragmentation. Based on these results, LOCA Integral Tests will be conducted at lower and/or higher ECR values to determine the ECR and hydrogen content corresponding to the post-quench fragmentation threshold. For the two LOCA Integral Tests already conducted, the Phase A test specimen will be examined metallographically to determine the condition of the fuel column near the ends of the sample. The Phase B test sample will be evaluated using metallography, LECO oxygen determination and LECO hydrogen determination to map out the axial variation of ECR and hydrogen content. These results will be compared to those for the companion, unirradiated specimen to determine if there are indeed differences in inner-surface oxygen and hydrogen pickup for high-burnup fuel.

Following the BWR tests, high-burnup PWR specimens with high hydrogen content will be tested to determine the effects of 400-800 wppm hydrogen on oxidation kinetics, quench and post-quench fragmentation thresholds.

## References

1. Y. Yan, R. V. Strain, T. S. Bray, and M. C. Billone, "High Temperature Oxidation of Irradiated Limerick BWR Cladding," Proceedings of the 29<sup>th</sup> Nuclear Safety Research Conference NSRC-2001), Washington, DC, October 22-24, 2001, NUREG/CP-0172 (2002) 239-250.
2. J. V. Cathcart, R. E. Pawel, R. A. McKee, R. E. Druscel, G. J. Yurek, J. J. Cambell, and S. H. Jury, "Zirconium Metal-Water Oxidation Kinetics IV. Reaction Rate Studies", ORNL/NUREG-17, Aug. 1977.
3. W. J. Leech, "Ductility Testing of Zircaloy-4 and ZIRLO<sup>TM</sup> Cladding after High Temperature Oxidation in Steam," Proceedings of the Topical Meeting on LOCA Fuel Safety Criteria, Aix-en-Provence, 22-23 March, 2001, pp 135-143.
4. L. Baker and L. C. Just, "Studies of Metal-Water Reactions at High Temperatures; III. Experimental and Theoretical Studies of the Zirconium-Water Reaction," ANL-6548, May 1962.
5. S. Leistikow and G. Schanz, "The Oxidation Behavior of Zircaloy-4 in Steam between 600 and 1600°C," Werkstoffe und Korrosion 36 (1985) 105-116.
6. V. F. Urbanic, "Oxidation of Zirconium Alloys in Steam at 1000 to 1850°C," Zirconium in the Nuclear Industry, ASTM STP 633, A. L. Lowe, Jr. and G. W. Parry, Eds., American Society for Testing and Materials, 1977, pp. 168-181.
7. N. Waeckel and P. Jacques, EdF, personal communication, July 19-20, 2001.
8. A. Le Bourhis, "Justification of the M5<sup>TM</sup> Behavior in LOCA," Proceedings of the Topical Meeting on LOCA Fuel Safety Criteria, Aix-en-Provence, 22-23 March, 2001, pp 105-133.
9. L. Yegorova, E. Kaplar, A. Shestopalov, K. Lioutov, and A. Konobeyev, "Overview of Test Data on the Mechanical Behavior of Zr-1%Nb Claddings under the LOCA Conditions and Comparison with other Zirconium Alloy Claddings, NSI-RRC "Kurchatov Institute," December 2001 (unpublished progress report submitted to NRC-RES; available upon request).
10. H.C. Tsai and M.C. Billone, "Characterization of High-Burnup PWR and BWR Rods and PWR Rods after Extended Dry-Cask Storage," presented by H.C. Tsai at the 30<sup>th</sup> Nuclear Safety Research Conference, Washington, DC, October 28-30, 2002; published in these proceedings.

This page left intentionally blank

## Characterization of High-Burnup PWR and BWR Rods, and PWR Rods after Extended Dry-Cask Storage

H. Tsai and M. C. Billone

Argonne National Laboratory  
Argonne, Illinois 60439 U.S.A.

### Abstract

In support of ongoing research programs on fuel performance under Loss-of-Coolant Accident (LOCA) and dry storage conditions, pretest fuel and cladding characterization has been performed. The fuels include H. B. Robinson PWR rods at 67 GWd/MTU, Limerick BWR rods at 56 GWd/MTU, and Surry PWR rods at 36 GWd/MTU after 15-y storage in a dry cask.

The condition of all rods examined appears to be sound. The H. B. Robinson rods have a relatively thick cladding oxide layer (up to  $\approx 110$   $\mu\text{m}$ ) and a hydrogen content up to  $\approx 750$  wppm. Hydrides precipitates in the cladding, mostly circumferentially oriented, form a dense band adjacent to the OD oxide layer. Away from the OD, the density diminishes with distance. Fission gas release is low and normal,  $\leq 5\%$ . The fuel/cladding gap is closed with little corrosion of the cladding ID. The thickness of the fuel high-fission "rim" is  $\approx 600$   $\mu\text{m}$ .

For the high-burnup Limerick rods, both oxide layer thickness and hydrogen uptake are small. ID cladding corrosion is minimal. The fission-gas release ( $\approx 17\%$  max.) is relatively high; the cause may be the numerous microtears seen in the gassy region of the fuel that provided long-range connectivity.

For the post-storage Surry rods, there appears to be little or no incremental cladding deformation (creep), fission-gas release, cladding corrosion, hydrogen uptake, or fuel microstructure evolution during the 15-y dry-cask storage.

### Introduction

High-burnup PWR and BWR rods and dry-cask-stored PWR rods were acquired by Argonne National Laboratory (ANL) under the sponsorship of the U.S. Nuclear Regulatory Commission, the U.S. Department of Energy, and the Electric Power Research Institute to conduct a range of research programs on fuel rod performance. These programs include Loss-of-Coolant Accident (LOCA) relevant tests [1], thermal creep tests [2] of as-irradiated and post-dry-storage cladding, and cladding mechanical properties tests relevant to both LOCA and Reactivity-Initiated Accidents. Since the as-irradiated condition of the fuel rods is the prerequisite for test planning and data evaluation, characterization of these fuel rods was undertaken. The characterization data will also be valuable for burnup extension assessment and dry-cask licensing renewal.

During reactor operation, the chemical reaction between the Zircaloy cladding and water coolant causes a corrosion layer to form on the cladding. In addition to the reduction of the load-bearing cladding thickness, the absorption of some of the released hydrogen from the reaction may further affect the cladding performance. If hydrogen were absorbed in sufficient quantities, precipitates of zirconium hydride would form. Due to the significant differences in strength and ductility between the hydrides and the Zircaloy, the morphology of the hydride precipitates may become important – radially-oriented hydrides are potentially more harmful than circumferentially-oriented ones [3]. As cladding behavior is central to fuel rod performance, the determination of oxide thickness, hydrogen content, and hydride morphology is a focal point of the characterization effort.

Fission-gas release, as affected by fuel microstructure evolution during irradiation, will impact the rod's internal pressure, which could influence cladding creep in dry-cask storage and cladding burst rupture in a LOCA. Furthermore, the degree of connectivity between the high-pressure plenum and the fuel column region, via either fuel cracks or the fuel/cladding gap, plays an important role in cladding rupture in a LOCA event. For these reasons, investigating those factors that impact fission-gas release are also important.

### **High-Burnup H. B. Robinson PWR Rods**

#### **Description**

The high-burnup PWR rods examined were from a 15 x 15 assembly of the H. B. Robinson plant Unit 2 [4]. They operated for seven cycles and reached a rod-average burnup of 67 GWd/MTU (73 GWd/MTU peak pellet). The fuel enrichment is 2.90%. The nominal fuel pellet dimensions are 9.06 mm dia. x 9.93 mm height and the active fuel height is 3.66 m. The cladding is cold-worked/stress-relieved Zircaloy-4, 10.77 mm OD x 9.25 mm ID, with a nominal tin content of 1.42%. The rods were pressurized with helium to 2.0 MPa during fabrication.

The rods began operation at a peak linear power of  $\approx 26$  kW/m; the linear power decreased to  $\approx 11$  kW/m at end-of-life.

#### **Results**

Extensive poolside nondestructive examination (NDE) was performed by the plant operator and fuel vendor. The results [4] showed peak cladding oxide thickness of 87 - 110  $\mu\text{m}$ ; axial rod growth of 0.95 - 1.15%; cladding creep-down of 0.6 - 1.1%; and fission-gas release of 1.4 - 2.4%.

At ANL, the condition of the fuel column and axial fission product migration were evaluated with scanning gamma spectroscopy for selected rods. The results are shown in Fig. 1 for one of the rods, B01. The gross distribution, which mimics the core power profile, shows no unusual features such as fuel-column disruption or excessive fission product migration. Slight dips were noted at the grid spacer locations owing to flux depression. In expanded scale, pellet configuration can be readily identified. Isotopic scans show axial migration of volatile fission products to be minor and localized.

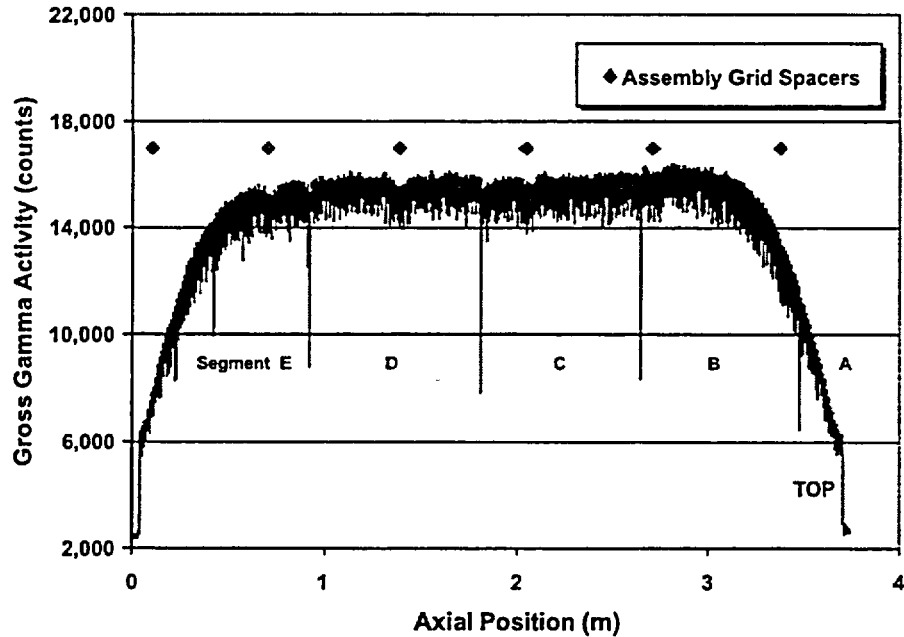


Fig. 1. Gross gamma scan profile for H. B. Robinson Rod B01. The profile is the composite of five scans as the rod was pre-sectioned into five segments (A through E).

The condition of the H. B. Robinson fuel was evaluated with ceramography. The cross-section of the fuel, shown in Fig. 2 for Rod A02, reveals the typical network of start-up and shut-down cracks. Also apparent are modest fuel restructuring in the center, a gassy “rim” on the fuel periphery, and a closed fuel-cladding gap. These features are typical for high-burnup fuel[5,6]. Thickness of high-fission rim is  $\approx 600 \mu\text{m}$ , based on optical data. Figure 3 shows the structure of the fuel in the rim region and the fission-product deposit that filled the fuel/cladding gap. As can be seen, fuel-cladding chemical interaction is minimal.

Typical morphology of the cladding oxide layer is shown in Fig. 4 for a location 0.7 m above the midplane. The thickness at this axial elevation is  $\approx 100 \mu\text{m}$ , in good agreement with the poolside NDE data. Within the layer, circumferentially-oriented microvoids as well as occasional radial cracks can be seen. Oxide spallation, however, is not prevalent.

Hydrogen contents in the cladding were analyzed using a fusion/thermal conductivity technique. The results show hydrogen contents of  $\approx 580 \text{ wppm}$  at axial midplane and  $\approx 750 \text{ wppm}$  at 0.7 m above the midplane. While these concentrations are substantial, they are consistent with the observed oxide layer thickness, corresponding to a hydrogen uptake ratio of  $\approx 23\%$ . With the cladding in etched condition, as shown in Fig. 5 for the 0.7-m-above-midplane elevation, a dense hydride band adjacent to the OD oxide layer can be seen. The density of hydrides, as expected, diminishes towards the cladding ID. Orientation

of the precipitates is mostly circumferential. Since the terminal solubility of hydrogen [7] in the cladding is  $\approx 200$  wppm at the operating temperature, some of the precipitates existed in the cladding during operation. In the on-going mechanical properties tests, determination of the effect of hydrides on cladding properties is a key objective.

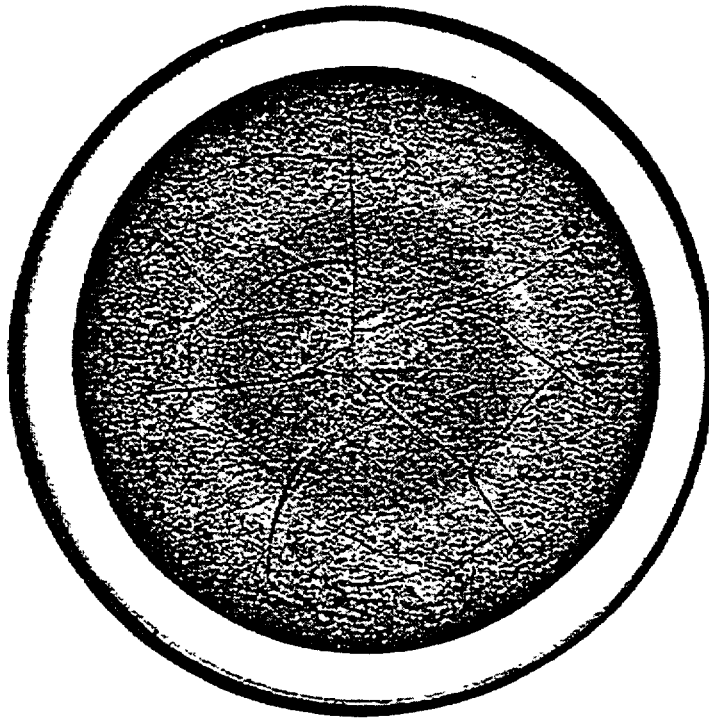


Fig. 2.  
Cross-sectional photocomposite  
of H. B. Robinson Rod A02 at an  
elevation 0.7 m above the fuel  
axial midplane.

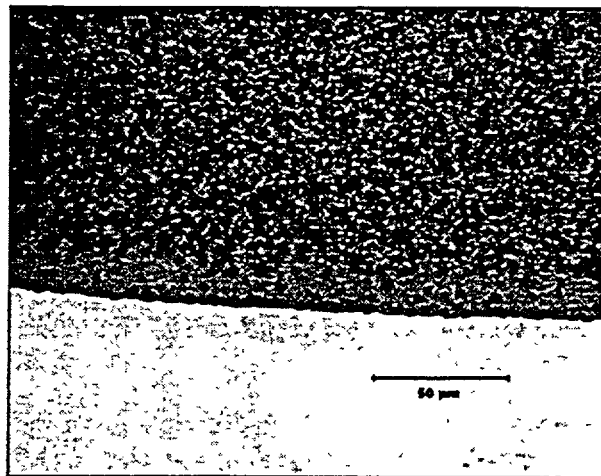


Fig. 3. H. B. Robinson Rod A02 fuel showing the "rim" and the fission product deposit (gray phase) in the fuel/cladding interface.

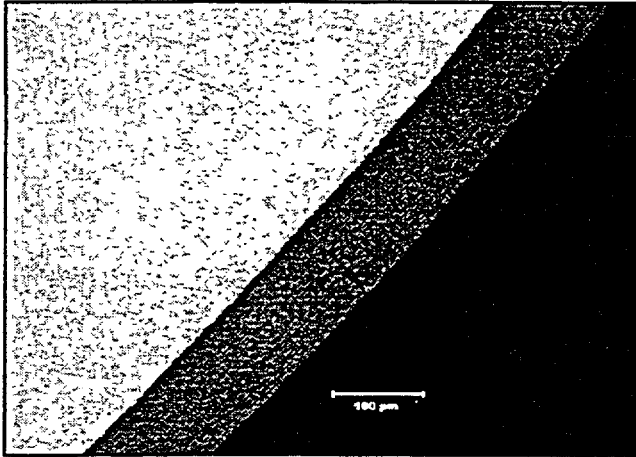


Fig. 4.  
Oxide layer on H. B. Robinson Rod A02  
cladding at an elevation 0.7 m above the fuel  
axial midplane.

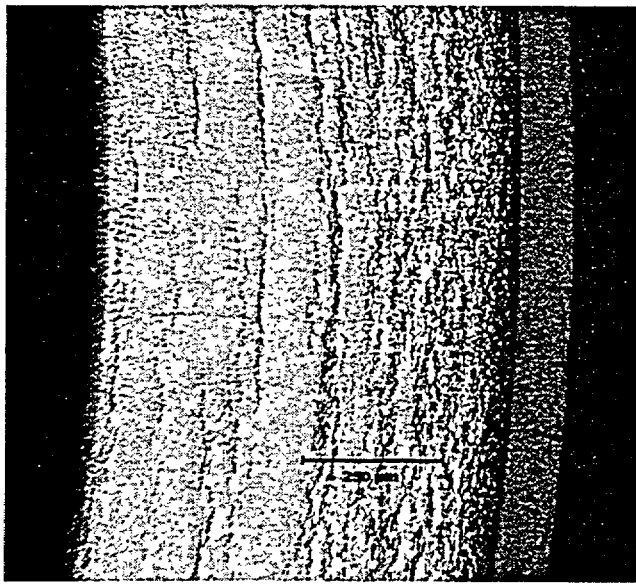


Fig. 5.  
Hydride precipitates in H. B. Robinson Rod  
A02 cladding at an elevation 0.7 m above the  
fuel axial midplane. The OD oxide layer is at  
the right.

## High-Burnup Limerick BWR Rods

### Description

The high-burnup BWR rods examined were from a 9x9 assembly of the Limerick-1 plant. The rods were exposed for three cycles and reached rod average burnup of 56 GWd/MTU burnup (64 GWd/MTU peak pellet). The nominal active fuel height is 3.71 m, of which 3.35 m is enriched. The cladding was Zr-lined Zicaloy-2, recrystallized-annealed, with an OD of 11.18 mm and an ID of 9.75 mm. The rods were pressurized with helium during fabrication. The peak linear power is estimated to be  $\approx 22$  kW/m over life.

### Results

Limited poolside inspection was performed on the Limerick rods. The results show the rods to be in good condition with only minor cladding creep-down and oxide/crud corrosion.

Seven of the rods were punctured for fission-gas release measurements. The release fractions, ranging from 5 to 17%, are slightly higher than the published BWR database [8], as shown in Fig. 6. The reason may be related to the irradiated fuel microstructure, to be discussed later.

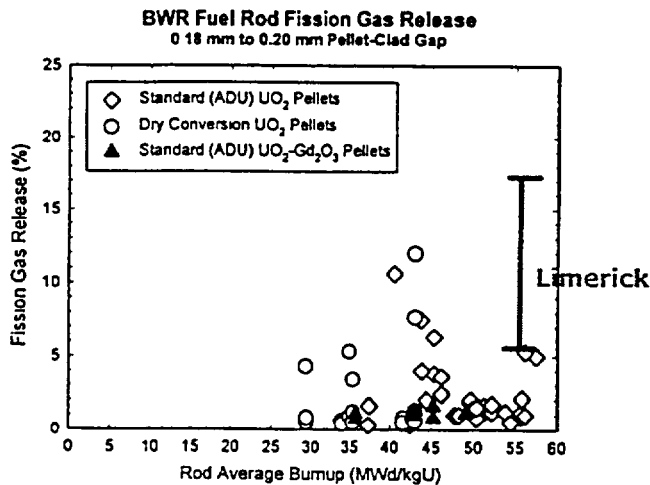


Fig. 6.  
Comparison of fission gas release in Limerick rods with published database (Van Swan et al. 1997 Portland).

Axial gamma scans were performed to evaluate the condition of the Limerick fuel column. The result is shown in Fig. 7 for Rod F9. The gross distribution of the fission products, mimicking that of the power profile, shows no disruptions in the fuel column or other unusual behavior. Slight dips were noted at the grid spacer locations due to flux depression. Isotopic scans show that there was negligible axial migration of fission products, including the volatile cesium.

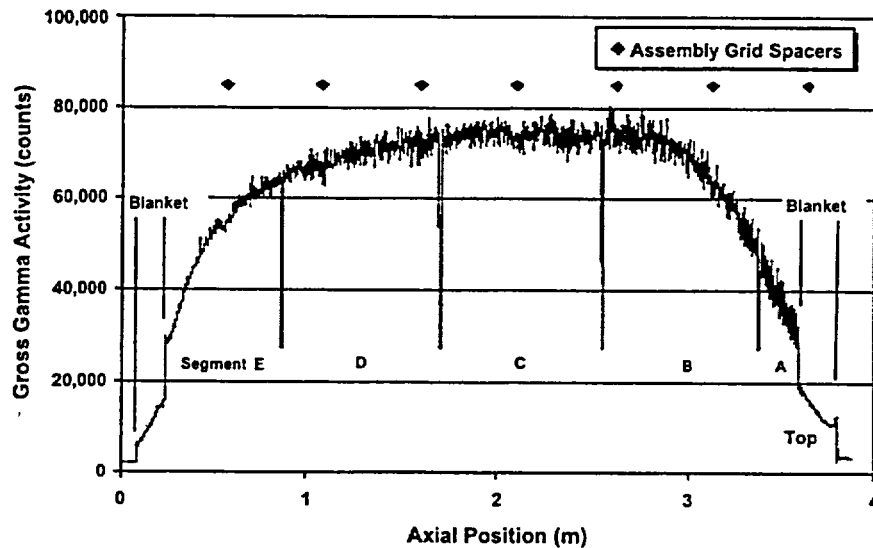


Fig. 7. Gross gamma scan profile for Limerick Rod F9. The profile is a composite of five scans as the rod was pre-sectioned into five segments.

The cross-section of the F9 fuel at an axial elevation of  $\approx 0.8$  m above the midplane, shown in Fig. 8, reveals modest restructuring with discontinuous and off-centered temperature-related features. The off-center restructuring may be partially due to the edge location of the F9 rod in the assembly. Figure 9 shows the typical fuel-cladding interfacial condition in the F9 rod at a higher magnification. The fuel-cladding gap is closed and a fission product phase can be seen in the interface. Also observed is a fission-product deposit at the tip of a radial fuel crack. Microprobe analysis of the deposit confirmed the presence of cesium and lanthanides fission products. Transport of the species down the temperature gradient via the radial crack appears to be the mechanism for forming the crack-tip deposit. Reaction between fission product phase and the cladding liner, however, is negligible.

Numerous microtears can be seen in the gassy outer region of the Limerick fuel, as shown in Fig. 9. These microtears developed along the fuel grain boundaries weakened by fission-gas bubbles and can extend long-range connectivity between fuel pellets. This may be the cause for the observed high fission-gas release in the rods. Limerick fuel contains a well-defined "rim" with varying thickness along the circumference; the fuel grains in the rim are small and laden with fine fission-gas bubbles.

The oxide layer on the Limerick cladding surface is thin,  $\approx 10$   $\mu\text{m}$  average, with a circumferential variation of  $\approx 5$  to  $25$   $\mu\text{m}$ . This thickness is within the published database [8] for BWR fuel. Oxide spallation is not evident. At locations where the oxide thickness is low, a thin tenacious crud ( $\approx 5$ - $10$   $\mu\text{m}$ ) can occasionally be found over the oxide. The crud contains zinc, apparently related to the zinc injection procedure used in Limerick plant for dose-buildup control [9].

Measured hydrogen content in the cladding is low,  $\approx 70$  wppm, and consistent with the observed oxide thickness. Figure 10 shows the typical distribution of the hydride precipitates in the cladding. Due

to the difference in terminal solubility [10] in the low-oxygen zirconium liner and high-oxygen Zircaloy, hydrogen preferentially precipitated in the liner. The precipitates in the Zircaloy are small and relatively uniformly distributed across the thickness. Overall, the Limerick cladding appears to be in excellent condition with no apparent deleterious effects of the high-burnup operation.

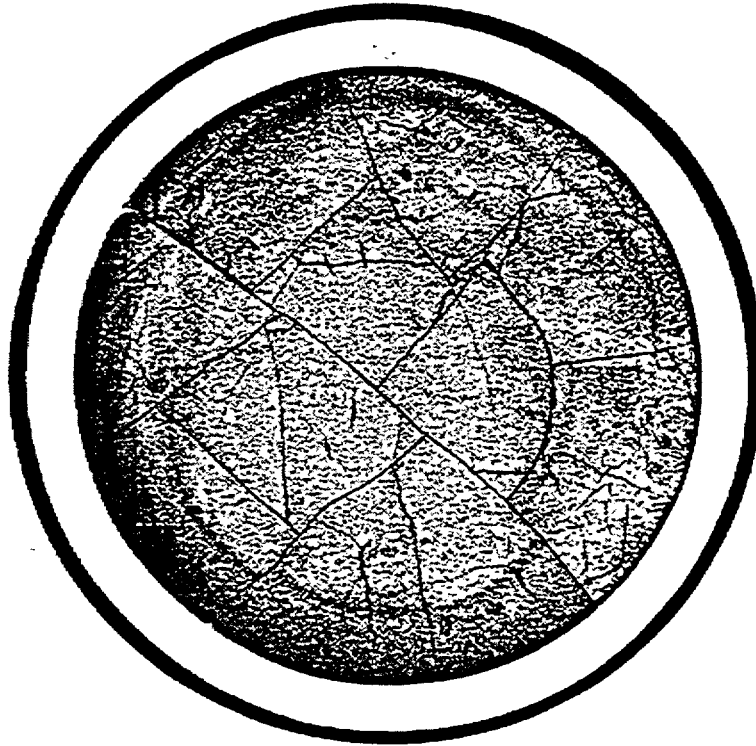


Fig. 8  
Cross-sectional photocomposite of Limerick Rod F9 at an elevation  $\approx 0.8$  m above the fuel axial midplane. Not all restructuring features are symmetric to fuel center.

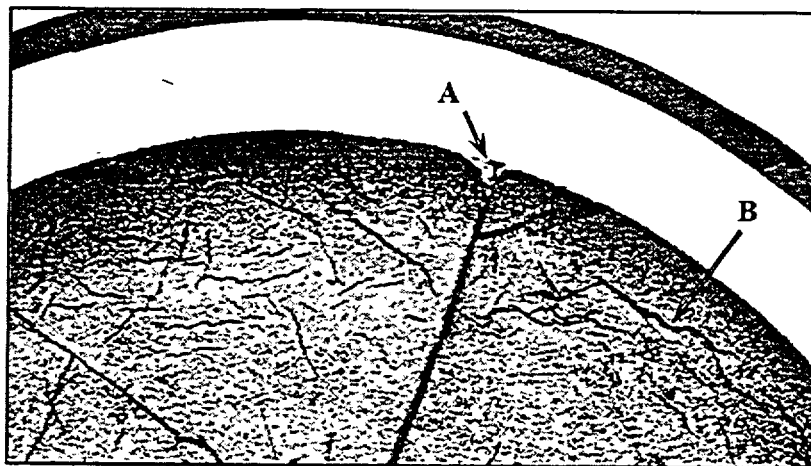


Fig. 9 Photomicrograph of Limerick Rod F9 showing fission product deposit (A) at a crack tip and numerous fuel microtears (B) in the gassy region of the fuel.

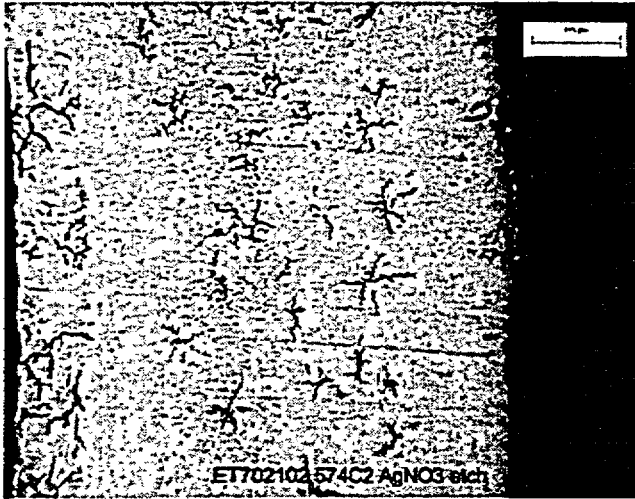


Fig. 10  
Distribution of hydride precipitates in the Limerick cladding. The band on the left side is the zirconium liner.

### Dry-Cask-Stored Surry PWR Rods

#### Description

The Surry rods examined were from one of the fuel assemblies loaded in a Castor-V/21 dry cask in the mid-1980s for benchmarking the thermal and radiological codes for dry-cask storage [11]. After the benchmarking tests, the cask was left undisturbed with an inert atmosphere ( $\text{He}/<1\%$  air) for 15 years until the rod retrieval for the present work. The retrieved rods have an average burnup of 36 GWd/MTU (40 GWd/MTU peak pellet) and attained near the highest cladding temperatures among the rods in the cask during the benchmark tests ( $\approx 415^\circ\text{C}$  peak for several days). The fuel enrichment is 3.1% and the nominal fuel pellet dimensions are 9.29 mm dia. x 15.2 mm height, with an active fuel height of 3.66 m. The cladding is Zircaloy-4, cold-worked and partially annealed, with a dimension of 10.72 mm OD x 9.50 mm ID. The rods were pressurized with helium to 2.9 MPa during fabrication.

#### Results

Profilometry of 12 of the post-storage rods shows the cladding creep-down to be  $\approx 0.6\%$  [12]. As this value is typical of PWR rods at this burnup [13,14], the result suggests no significant outward creep of the cladding during the benchmarking tests or the extended cask storage.

Fission-gas release was measured for four rods and the results show release fractions ranging from 0.39 to 1.08%. These values are within the data band for as-irradiated PWR rods of this type and burnup without a dry-storage history.

The condition of the post-storage fuel is shown in Fig. 11 for Rod H9. All features appear to be normal with no evidence of degradation from the extended storage. As expected for rods of this burnup, fuel restructuring is only minor. The fuel/cladding gap is open and fuel/cladding chemical interaction and fission product deposit in the gap are both insignificant.

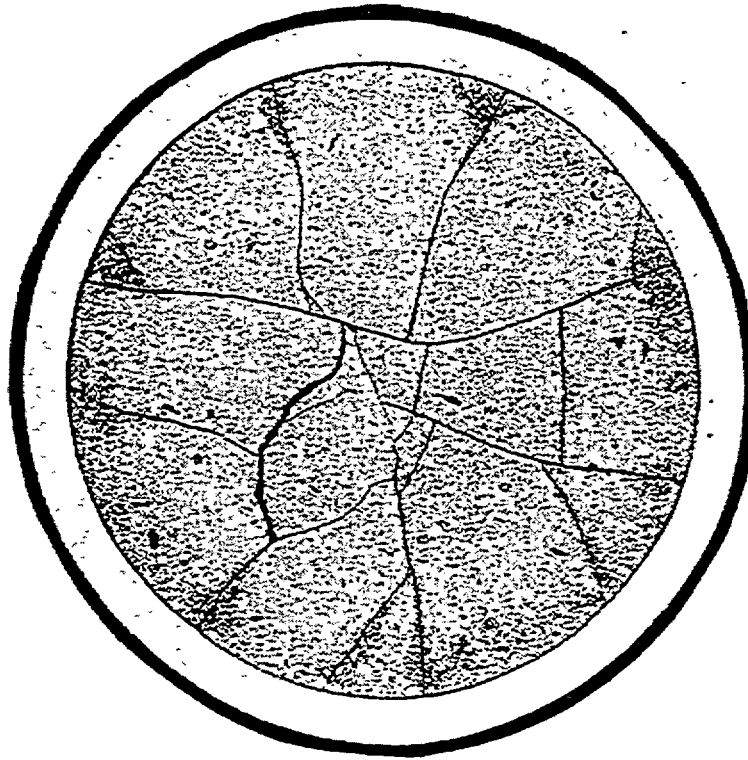


Fig. 11  
Cross-sectional photocomposite of  
post-storage Surry Rod H9 at the  
axial midplane. No storage-induced  
effects are apparent.

Average cladding oxide thickness in the post-storage Surry rods ranged from  $\approx 25 \mu\text{m}$  at the axial midplane to  $\approx 40 \mu\text{m}$  at 1 m above the midplane. These values are within the normal range [13,14] for PWR rods of this burnup and suggest that no additional oxidation during cask loading or storage. Measured hydrogen contents in the cladding are  $\approx 250$  wppm at the axial midplane and  $\approx 300$  wppm at 0.5 m above the midplane. These readings are consistent with the observed oxide thickness.

Hydride morphology in the cladding is illustrated in Fig. 12. In spite of the internal pressure loading and the temperature cycling during the benchmark tests, the precipitated hydrides are aligned mostly in the circumferential direction with no evidence of harmful radial reorientation. Probably because of a lack of strong radial temperature gradient while in the cask, the distribution of the hydrides is fairly uniform across the thickness of the cladding.

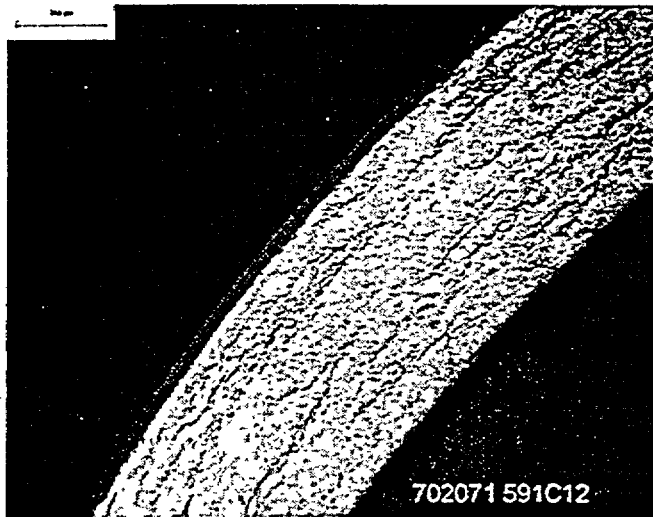


Fig. 12  
Distribution of hydride precipitates in post-storage Surry Rod H9. The axial elevation is 0.5 m above the midplane. The gray band on the left is the OD oxide layer.

### Conclusions

Aside from the relatively high hydrogen content in the cladding, the overall condition of the H. B. Robinson rods examined appears to be sound. Fission-gas release is low and fuel/cladding chemical interaction is minimal. The extended operation resulted in a maximum cladding OD oxide layer of  $\approx 100\text{--}110\ \mu\text{m}$  and a cladding hydrogen content of  $\approx 750\ \text{wppm}$ . Although the oxide contains numerous circumferentially-oriented microvoids, spallation appears to be minimal. Hydrides in the cladding form a dense band adjacent to the OD oxide. Away from the OD, the density of hydrides diminishes with distance. Possible effects of this relatively high hydrogen concentration on the mechanical properties of the cladding will be studied in tensile, bend, and possibly ring compression tests, as well as in thermal creep tests.

Fission gas release fractions in the Limerick rods range from 5 to 17%. The relatively high release may be related to the numerous grain-boundary microtears found in the gassy region of the fuel; such tears promote connectivity with the rod plenum. Fission product deposits can be seen in the now closed fuel/cladding gap as well as at the ends of major radial fuel cracks. In spite of the deposits, reaction between the fission products and the cladding's zirconium liner is minimal. The OD oxide in the Limerick rods is thin,  $\approx 10\ \mu\text{m}$  average. Tenacious crud was found at some locations, but the thickness is only  $\approx 5\text{--}10\ \mu\text{m}$ . Consistent with the thin oxide layer, the density of hydrides in the Limerick cladding is low. The general condition of the Limerick BWR fuel appears to be excellent at the high burnup.

The Surry fuel rods were examined after the 15-y storage in a dry cask. Elevated cladding temperature, up to  $\approx 415^\circ\text{C}$  for several days, resulted from the cask thermal benchmark tests prior to the long-term storage. In the post-storage characterization of the rods, little evidence of deleterious effects, such as additional oxidation, fission gas release, or cladding creep, could be discerned. There is no evidence of hydride reorientation in the cladding.

## Acknowledgments

The authors gratefully acknowledge the support provided by NRC, EPRI, and DOE and the provisions of high-burnup fuel rods by CP&L and Exelon. The authors also gratefully acknowledge the excellent preparatory work performed by Framatome-ANP Richland, Inc. and G.E. Vallecitos Nuclear Center on the H. B. Robinson rods, by G.E. Vallecitos Nuclear Center on the Limerick rods, and by INEEL and ANL-West on the Surry rods.

## References

1. Y. Yan and M. C. Billone, "LOCA Research Results for High-Burnup BWR Fuel," *ibid.*
2. H. Tsai and M. C. Billone, "Thermal Creep of Dry-Cask-Stored Surry PWR Cladding," *ibid.*
3. R. P. Marshall and M. R. Louthan, Jr., "Tensile Properties of Zircaloy with Oriented Hydrides," *Trans. ASM*, 56, 693 (1963).
4. E. J. Ruzauskas and K. N. Fardell, "Design, Operation, and Performance Data for High Burnup PWR Fuel from the H. B. Robinson Plant for Use in the NRC Experimental Program at Argonne National Laboratory," EPRI Report 1001558, May 2001.
5. K. Une, et al., "Effects of Irradiation-induced Microstructural Evolution on High Burnup Fuel Behavior," *Proc. Int. Topical Mtg. on LWR Fuel Perf.*, Portland, Oregon, p. 478 (1997).
6. M. Kinoshita, et al., "High Burnup RIM Project (II) Irradiation and Examination to Investigate Rim-structured Fuel," *Proc. Int. Topical Mtg. on LWR Fuel Perf.*, Park City, Utah, p. 738 (2000).
7. J. J. Kearns, "Terminal Solubility and Partitioning of Hydrogen in the Alpha Phase of Zirconium, Zircaloy-2 and Zircaloy-4," *J. Nucl. Mater.*, 22, 292-303 (1967).
8. L. F. Van Swan, et al., "BWR and PWR Fuel Performance at High Burnup," *Proc. Int. Topical Mtg. on LWR Fuel Perf.*, Portland, Oregon, p. 455 (1997).
9. B. C. Cheng, et al., "Fuel Performance and Water Chemistry Variable in LWRs," *Proc. Int. Topical Mtg. on LWR Fuel Perf.*, Portland, Oregon, p. 379 (1997).
10. S. Yamanaka, et al., "Effects of Oxygen on Hydrogen Solubility in Zirconium," *J. Nucl. Mater.*, 167, 231-237 (1989).
11. M. A. McKinnon and V. A. Deloach, "Spent Nuclear Fuel Storage - Performance Tests and Demonstration," PNL-8451, Pacific Northwest Laboratory, 1993.
12. C. Kimball and M. Billone, "Dry Cask Storage Characterization Project," EPRI Report 1002882, September 2002.
13. R. B. Davis, "Pretest Nondestructive Examination Data Summary Report on Turkey Point Spent Fuel Assemblies D01, D04, and D06 for the Climax - Spent Fuel Tests," HEDL-TME 80-83, UC-70, Hanford Engineering Development Laboratory, January 1981.
14. S. D. Atkin, "Destructive Examination of 3-Cycle LWR Fuel Rods from Turkey Point Unit 3 for the Climax - Spent Fuel Tests," HEDL-TME 80-89, UC-70, Hanford Engineering Development Laboratory, June 1981.